

Copyright
by
Kazuhiro Asakawa
2005

**The Dissertation Committee for Kazuhiro Asakawa Certifies that this is the
approved version of the following dissertation:**

A Generalized Analysis of Partitioning Interwell Tracer Tests

Committee:

Gary A. Pope, Co-Supervisor

Kamy Sepehrnoori, Co-Supervisor

Steven L. Bryant

Mojdeh Delshad

Daene C. McKinney

A Generalized Analysis of Partitioning Interwell Tracer Tests

by

Kazuhiro Asakawa, B.S.; M.S.

Dissertation

Presented to the Faculty of the Graduate School of

The University of Texas at Austin

in Partial Fulfillment

of the Requirements

for the Degree of

Doctor of Philosophy

The University of Texas at Austin

December 2005

Dedication

To Myong-Hee Choi.

Acknowledgements

I would like to express my appreciation to my supervising professors, Dr. Gary A. Pope and Dr. Kamy Sepehrnoori for their encouragement to pursue a doctoral degree in Petroleum Engineering. Without their continuous guidance and support, I cannot imagine I would have been able to perform at this level of research. It is my honor to have them as my supervisors for their systematic knowledge and approach. I would also like to thank my doctoral committee members: Dr. Steven L. Bryant, Dr. Mojdeh Delshad, and Dr. Daene C. McKinney for their valuable suggestions. Dr. Mojdeh Delshad spent lots of precious time to help me to learn how to use reservoir simulators. Joanna Castillo helped me on numerous occasions with computer related issues, which I do appreciate. Esther Barrientes precisely assisted me with all administrative issues. I enjoyed working with Rohit Sinha and Elif Altinay on tracer research. I also appreciate the opportunity to work with Dr. Akhil Datta-Gupta and his student Adedayo Oyerinde on the inverse modeling applications to tracers. I probably came to know more students in this department than most other students do, and I would like to convey my thanks to many of the students, such as Elizabeth, Omar, Siree, Gopi, John, Vishal, Robin, and all of the others who I came to know but cannot write down. Shekhar, Xinglu, Yousef, and Hourshad were helpful on discussing the projects I worked on. Without the love of my

family, I cannot finish my work. Especially Myong extensively encouraged me with carrot and stick.

Financial support for my research was provided by the U.S. Department of Energy, Project # DE-AC26-98BC15109, Development of an Improved Simulator for Chemical and Microbial IOR Methods and Project # 67931, An Integrated Approach to Characterizing Bypassed Oil in Heterogeneous and Fractured Reservoirs Using Partitioning Tracers. Additional support came from the Texaco Centennial Chair held by Professor Pope. I would also like to thank the Center for Petroleum and Geosystems Engineering (CPGE) and the Reservoir Simulation Research Project for providing the computing resources needed for my research, and Schlumberger for providing CPGE with the license for their ECLIPSE software application.

A Generalized Analysis of Partitioning Interwell Tracer Tests

Publication No. _____

Kazuhiro Asakawa, Ph.D.

The University of Texas at Austin, 2005

Co-Supervisors: Gary A Pope and Kamy Sepehrnoori

A partitioning interwell tracer test (PITT) is a method for estimating oil volume and/or oil saturation in the swept zone between a set of injectors and producers in a reservoir. One of the methods for analyzing PITTs is the method of moments, which is based upon calculating the first temporal moment of the tracer concentrations in the produced fluids. PITTs have many advantages over other methods for estimating oil saturation by measuring over a much larger volume than a single well tracer test and a well log. It is especially important to know the remaining oil saturation as accurately as possible before applying enhanced oil recovery methods. PITTs also provide valuable information on swept volumes between wells, flow paths, and breakthrough times. A very general derivation of the method of moments applied to PITT data is presented in this dissertation. This derivation shows that the method of moments can be used for three-dimensional, heterogeneous reservoirs under very general conditions. The general derivation and its verification with numerical simulations shows that the method is not limited to residual oil saturation as generally assumed, but can be extended to mobile oil saturation (or any multiphase flow problem). PITTs in naturally fractured reservoirs are

an extreme example of heterogeneous reservoirs that can be analyzed by the method of moments, although the time to conduct such tests can be generally very long. For this reason, the concept of natural tracers was investigated and analyzed. The technique of using natural tracers is based on the idea of measuring a naturally residing petroleum organic component such as organic alcohols and acids. Since natural tracers originate in the oil itself, its use can be less expensive and more environmentally friendly than the use of injected chemical or radioactive tracers, and can take less time to produce a useful signal. The synthetic tracer data in naturally fractured reservoirs as well as to single-porosity heterogeneous reservoirs are generated using numerical simulators. These data were analyzed under a wide range of reservoir conditions using both the method of moments and inverse modeling using a program developed at TAMU.

Table of Contents

List of Tables	xi
List of Figures	xiii
Chapter 1: Introduction	1
1-1 Research Objectives	2
1-2 Review of Chapters	3
Chapter 2: Literature Review	4
2-1 Partitioning Interwell Tracer Tests	4
2-2 Calculation of Saturations from Partitioning Tracer Data	6
2-3 Chemical Flood Simulator, UTCHEM	9
2-3-1 Formulation	9
2-3-2 Dual Porosity Model	14
2-4 Reservoir Simulator, ECLIPSE	15
Chapter 3: Derivation of the Method of Moments for Analyzing PITTs	16
3-1 Introduction	16
3-2 Derivation of The Method of Moments	17
3-2-1 Derivation for Injected Tracer Slug	19
3-2-2 Derivation with Continuous Tracer Injected	41
3-2-3 Derivation for Dual Porosity Model	53
3-2-4 Application to Natural Tracers	57
3-2-5 Sweep Efficiency from Tracer Slug Injection	59
3-3 Summary of Chapter	63
Chapter 4: Analysis of Partitioning Interwell Tracer Tests	66
4-1 Application of Method of Moments	66
4-1-1 Sweep Efficiency from Tracer Slug Injection	66
4-1-2 Lawyer Canyon Reservoir Simulations	67
4-1-3 South Wasson Clear Fork Reservoir Simulations	70
4-1-4 Tracer Tests with Mobile Oil	72

4-1-5 Natural Tracer Simulations	77
4-2 PITT Analysis with Inverse Modeling Program	79
4-2-1 Sensitivity Study of Inverse Program.....	79
4-2-1-1 Sensitivity to Initial Guess	79
4-2-1-2 Sensitivity to Tracer Concentration Detection Limit.....	81
4-2-2 Inverse Modeling of PITTs with Mobile Oil	83
Chapter 5: Summary, Conclusions, and Recommendations	177
5-1 Summary and Conclusions	177
5-2 Recommendations	180
Appendix A.....	182
Appendix B.....	191
Appendix C.....	197
Appendix D.....	207
References.....	211
Vita	215

List of Tables

Table 4.1: Estimated Oil Saturation for a Waterflood with an End Point Mobility Ratio of 0.5.....	86
Table 4.2: Estimated Oil Saturation for a Waterflood with an End Point Mobility Ratio of 1.2.....	86
Table 4.3: Estimated Oil Saturation for a Waterflood with an End Point Mobility Ratio of 5.2.....	86
Table 4.4: Reservoir Description for Run INV02#4.....	87
Table 4.5: Comparison of Oil Saturation for Run INV02#4	87
Table 4.6: Swept Pore Volume for Run INV02#4.....	87
Table 4.7: Comparison of Oil Saturations for Run INV02#5.....	88
Table 4.8: Swept Pore Volume for Run INV02#5.....	88
Table 4.9: Comparison of Oil Saturations for Run INV02#7.....	88
Table 4.10: Swept Pore Volume for Run INV02#7.....	88
Table 4.11: Comparison of Oil Saturations for Run INV02#8.....	89
Table 4.12: Swept Pore Volume for Run INV02#8.....	89
Table 4.13: Difference between Oil Saturation Calculated from Inverse Model and Actual Oil Saturation for Various Initial Guesses of Oil Satuartion	89
Table 4.14: Difference of Oil Saturation from Inverse Model and Actual Saturation for Various Tracer Detection Limits with an Initial Oil Saturation Guess of 0.26	90
Table 4.15: Difference of Oil Saturation from Inverse Model and Actual Saturation for Various Tracer Detection Limits with an Initial Oil Saturation Guess of 0.30	90

Table 4.16: Description of Two Dimensional Reservoir	90
Table 4.17: Relative Permeability Parameters and Viscosities	91
Table 4.18: Run Summary of Oil Saturation Estimate	91

List of Figures

Figure 4.1: Tracer concentration histories from single phase homogeneous media	92
Figure 4.2: Swept volume calculated from both slug and continuous tracer data	92
Figure 4.3: Sweep efficiency from slug tracer history.....	93
Figure 4.4: Tracer concentration with extrapolation.....	93
Figure 4.5: Swept volume estimate using incomplete data.....	94
Figure 4.6: Swept volume estimate using extrapolated data.....	94
Figure 4.7: Comparison of tracer concentration histories with different Dykstra- Parsons coefficients	95
Figure 4.8: Comparison of sweep efficiency for reservoirs with different Dykstra- Parsons coefficients	95
Figure 4.9: Cross-sectional heterogeneous permeability in md at Lawyer Canyon	96
Figure 4.10: Tracer concentration history from quarter of five-spot well pattern	96
Figure 4.11: Oil volume estimate from tracer response in quarter of five-spot well pattern	97
Figure 4.12: Oil saturation estimate from tracer response in quarter of five-spot well pattern using the method of moments.....	97
Figure 4.13: Swept volume from tracer response in quarter of five-spot well pattern	98
Figure 4.14: Sweep efficiency from tracer response in quarter of five-spot well pattern	98

Figure 4.31: Oil phase tracer concentrations for a PITT at 0.5 PV with an end point mobility ratio of 1.2	107
Figure 4.32: Total tracer concentrations for a PITT at 0.5 PV with an end point mobility ratio of 1.2	107
Figure 4.33: Estimated oil saturation using total tracer concentrations for an end point mobility ratio of 1.2	108
Figure 4.34: Estimated oil saturation using total tracer concentrations for an end point mobility ratio of 0.5	108
Figure 4.35: Estimated oil saturation using total tracer concentrations for an end point mobility ratio of 5.2	109
Figure 4.36: Logarithmic permeability distribution in layer 8 (most permeable layer)	109
Figure 4.37: Permeability distribution in logarithmic scale in layer 5 (least permeable layer)	110
Figure 4.38: Oil production rate.....	110
Figure 4.39: Normalized tracer concentration at PROD-1	111
Figure 4.40: Normalized tracer concentration at PROD-2	111
Figure 4.41: Normalized tracer concentration at PROD-3	112
Figure 4.42: Normalized tracer concentration at PROD-4	112
Figure 4.43: Normalized conservative tracer concentration profile in layer 8 after 35 days of tracer injection.....	113
Figure 4.44: Oil Saturation between well pairs	113
Figure 4.45: Swept pore volume between the injector and the each producer	114
Figure 4.46: Profile of normalized partitioning tracer concentration with a partition coefficient of 2 in layer 1 at the end of PITT.....	114

Figure 4.47: Oil saturation distribution in layer 1 at the end of PITT	115
Figure 4.48: Oil saturation distribution in layer 8 at the end of PITT	115
Figure 4.49: Permeability in the least permeable layer 5.....	116
Figure 4.50: Permeability in the most permeable layer 8	116
Figure 4.51: Oil saturation distribution in layer 5 at the beginning of the tracer injection.....	117
Figure 4.52: Oil saturation distribution in layer 8 at the beginning of the tracer injection.....	117
Figure 4.53: Normalized concentration at PROD-1	118
Figure 4.54: Normalized concentration at PROD-2	118
Figure 4.55: Normalized concentration at PROD-3	119
Figure 4.56: Normalized concentration at PROD-4	119
Figure 4.57: Tracer concentration profile in layer 5 at the end of the PITT.....	120
Figure 4.58: Tracer concentration profile in layer 8 at the end of the PITT.....	120
Figure 4.59: Swept pore volume between the injector and the each producer	121
Figure 4.60: Oil saturation between well pairs	121
Figure 4.61: Oil saturation distribution at the start of tracer injection on layer 5	122
Figure 4.62: Oil saturation distribution at the start of tracer injection on layer 8	122
Figure 4.63: Conservative tracer concentration at 50 days in layer 5.....	123
Figure 4.64: Conservative tracer concentration at 50 days in layer 8.....	123
Figure 4.65: Conservative tracer concentration at end of PITT in layer 5	124
Figure 4.66: Conservative tracer concentration at the end of PITT in layer 8.....	124
Figure 4.67: Tracer concentration history at PROD-1	125

Figure 4.68: Tracer concentration history at PROD-2.....	125
Figure 4.69: Tracer concentration history at PROD-3.....	126
Figure 4.70: Tracer concentration history at PROD-4.....	126
Figure 4.71: Swept pore volume between the injector and the each producer	127
Figure 4.72: Sweep efficiency in the reservoir	127
Figure 4.73: Oil Saturation between well pairs	128
Figure 4.74: Oil saturation distribution in layer 5 at the beginning of the tracer injection.....	128
Figure 4.75: Oil saturation distribution in layer 8 at the beginning of the tracer injection.....	129
Figure 4.76: Normalized tracer concentration at PROD-1	129
Figure 4.77: Normalized tracer concentration at PROD-2	130
Figure 4.78: Normalized tracer concentration at PROD-3	130
Figure 4.79: Normalized tracer concentration at PROD-4	131
Figure 4.80: Partitioning tracer concentration with a partition coefficient of 2 after 25 days of tracer injection in layer 3.....	131
Figure 4.81: Partitioning tracer concentration with a partition coefficient of 2 after 25 days of tracer injection in layer 5.....	132
Figure 4.82: Partitioning tracer concentration with a partition coefficient of 2 at the end of PITT in layer 8.....	132
Figure 4.83: Partitioning tracer concentration with a partition coefficient of 2 at the end of PITT in layer 5.....	133
Figure 4.84: Swept pore volume between the injector and the each producers...	133
Figure 4.85: Oil saturation between well pairs	134
Figure 4.86: Oil saturation distribution in layer 5 at the end of PITT	134

Figure 4.87: Oil saturation distribution in layer 8 at the end of PITT	135
Figure 4.88: Natural tracer history from naturally fractured reservoir	135
Figure 4.89: Oil saturation estimation from natural tracer from naturally fractured reservoir	136
Figure 4.90: Comparison of natural tracers and injected tracers	136
Figure 4.91: Produced tracer data from naturally fractured reservoir	137
Figure 4.92: Comparison of estimated oil saturation in naturally fractured reservoir using the slug and continuous tracer injected	137
Figure 4.93: Comparison of converted tracer slug and continuous tracer	138
Figure 4.94: Comparison of natural tracer concentration with different matrix subgridding for partition coefficient of 0.001	138
Figure 4.95: Comparison of natural tracer concentration with different matrix subgridding for partition coefficient of 1.0.....	139
Figure 4.96: Oil saturation calculated from inverse model for initial guesses between 0.21 and 0.25.....	139
Figure 4.97: Oil saturation calculated from inverse model for initial guesses between 0.26 and 0.30.....	140
Figure 4.98: Oil saturation calculated from inverse model for initial guesses of 0.14, 0.26, and 0.38.....	140
Figure 4.99: RMS error in travel time and amplitude for an initial oil saturation guess of 0.21	141
Figure 4.100: Match of forward and inverse tracer curves from all layers after 4 iterations for an initial oil saturation guess of 0.21	141
Figure 4.101: Match of forward and inverse tracer curves from layer 5 after 4 iterations for an initial oil saturation guess of 0.21	142

Figure 4.102: Match of forward and inverse tracer curves from layer 8 after 4 iterations for an initial oil saturation guess of 0.21	142
Figure 4.103: Oil saturation for layer 5 after 4 iterations for an initial oil saturation guess of 0.21	143
Figure 4.104: Difference in Oil saturation for layer 5 after 4 iterations for an initial oil saturation guess of 0.21	143
Figure 4.105: Oil saturation for layer 8 after 4 iterations for an initial oil saturation guess of 0.21	144
Figure 4.106: Difference in Oil saturation for layer 8 after 4 iterations for an initial oil saturation guess of 0.21	144
Figure 4.107: RMS error in travel time and amplitude for an initial oil saturation guess of 0.28	145
Figure 4.108: Match of forward and inverse tracer curves from all layers after 10 iterations for an initial oil saturation guess of 0.28	145
Figure 4.109: Match of forward and inverse tracer curves from layer 5 after 10 iterations for an initial oil saturation guess of 0.28	146
Figure 4.110: Match of forward and inverse tracer curves from layer 8 after 10 iterations for an initial oil saturation guess of 0.28	146
Figure 4.111: RMS error in travel time and amplitude for an initial oil saturation guess of 0.30	147
Figure 4.112: Match of forward and inverse tracer curves from all layers after 1 iteration for an initial oil saturation guess of 0.30	147
Figure 4.113: Match of forward and inverse tracer curves from layer 5 after 1 iteration for an initial oil saturation guess of 0.30	148

Figure 4.114: Match of forward and inverse tracer curves from layer 8 after 1 iteration for an initial oil saturation guess of 0.30	148
Figure 4.115: RMS error in travel time and amplitude for an initial oil saturation guess of 0.14	149
Figure 4.116: Match of forward and inverse tracer curves from all layers after 4 iterations for an initial oil saturation guess of 0.14.....	149
Figure 4.117: Match of forward and inverse tracer curves from layer 5 after 4 iterations for an initial oil saturation guess of 0.14.....	150
Figure 4.118: Match of forward and inverse tracer curves from layer 8 after 4 iterations for an initial oil saturation guess of 0.14.....	150
Figure 4.119: RMS error in travel time and amplitude for an initial oil saturation guess of 0.38	151
Figure 4.120: Match of forward and inverse tracer curves from all layers after 10 iterations for an initial oil saturation guess of 0.38.....	151
Figure 4.121: Match of forward and inverse tracer curves from layer 5 after 10 iterations for an initial oil saturation guess of 0.38.....	152
Figure 4.122: Match of forward and inverse tracer curves from layer 8 after 10 iterations for an initial oil saturation guess of 0.38.....	152
Figure 4.123: RMS error in travel time and amplitude with an initial oil saturation guess of 0.26 for TDL of 0.0001.....	153
Figure 4.124: Inverse model vertical oil saturation distribution estimates for TDLs 0.0001, 0.001 and 0.01 at initial oil saturation guess 0.26.....	153
Figure 4.125: RMS error in travel time and amplitude with an initial oil saturation guess of 0.26 for TDL of 0.001.....	154

Figure 4.126: RMS error in travel time and amplitude with an initial oil saturation guess of 0.26 for TDL of 0.01.....	154
Figure 4.127: Match of forward and inverse tracer curves from all layers with an initial oil saturation guess of 0.26 for TDLs of 0.0001, 0.001, and 0.01.....	155
Figure 4.128: Match of forward and inverse tracer curves from layer 5 with an initial oil saturation guess of 0.26 for TDLs of 0.0001, 0.001, and 0.01	155
Figure 4.129: Match of forward and inverse tracer curves from layer 8 with an initial oil saturation guess of 0.26 for TDLs of 0.0001, 0.001, and 0.01	156
Figure 4.130: Inverse model vertical oil saturation distribution estimates for TDLs 0.0001, 0.001 and 0.01at initial oil saturations guess 0.30	156
Figure 4.131: RMS error in travel time and amplitude with an initial oil saturation guess of 0.30 for TDL of 0.0001.....	157
Figure 4.132: RMS error in travel time and amplitude with an initial oil saturation guess of 0.30 for TDL of 0.001.....	157
Figure 4.133: RMS error in travel time and amplitude with an initial oil saturation guess of 0.30 for TDL of 0.01.....	158
Figure 4.134: Match of forward and inverse tracer curves from all layers with an initial oil saturation guess of 0.30 for TDLs of 0.0001, 0.001, and 0.01.....	158
Figure 4.135: Match of forward and inverse tracer curves from layer 5 with an initial oil saturation guess of 0.30 for TDLs of 0.0001, 0.001, and 0.01	159

Figure 4.136: Match of forward and inverse tracer curves from layer 8 with an initial oil saturation guess of 0.30 for TDLs of 0.0001, 0.001, and 0.01	159
Figure 4.137: Relative permeability curves in Runs INV07-000 and INV07-600	160
Figure 4.138: Relative permeability curves in Runs INV07-200, INV07-100, and INV07-500	160
Figure 4.139: Fractional flow of water in Run INV07-000	161
Figure 4.140: Fractional flow of water in Runs INV07-600 and INV07-700	161
Figure 4.141: Fractional flow of water in Run INV07-200	162
Figure 4.142: Fractional flow of water in Run INV07-100	162
Figure 4.143: Fractional flow of water in Run INV07-500	163
Figure 4.144: Mean residence time sensitivity to the oil saturation in Run INV07-000 for partition coefficient 10	163
Figure 4.145: Mean residence time sensitivity to the oil saturation in Run INV07-600 for partition coefficient 10	164
Figure 4.146: Mean residence time sensitivity to the oil saturation in Run INV07-200 for partition coefficient 10	164
Figure 4.147: Mean residence time sensitivity to the oil saturation in Run INV07-100 for partition coefficient 10	165
Figure 4.148: Mean residence time sensitivity to the oil saturation in Run INV07-500 for partition coefficient 10	165
Figure 4.149: RMS change on travel time and amplitude in Run INV07-511	166
Figure 4.150: Match of the forward model tracer response from layer 1 by iteration 1 and 6 of inverse model in Run INV07-511	166

Figure 4.151: Match of the forward model tracer response from layer 2 by iteration 1 and 6 of inverse model in Run Inv07-511	167
Figure 4.152: Inverse model oil saturation estimate in layer 1 in Run INV07-511	167
Figure 4.153: Inverse model oil saturation estimate in layer 2 in Run INV07-511	168
Figure 4.154: RMS change on travel time and amplitude in Run INV07-512.....	168
Figure 4.155: Match of the forward model tracer response from layer 1 by iterations 1 and 4 in Run INV07-512.....	169
Figure 4.156: Match of the forward model tracer response from layer 2 by iteration 1 and 4 in Run INV07-512.....	169
Figure 4.157: Oil saturation comparison in layer 1 in Run INV07-512	170
Figure 4.158: Oil saturation comparison in layer 2 in Run INV07-512	170
Figure 4.159: RMS change on travel time and amplitude in Run INV07-513	171
Figure 4.160: Match of the forward model tracer response from layer 1 by iterations 1 and 6 of in Run INV07-513	171
Figure 4.161: Match of the forward model tracer response from layer 1 by iterations 1 and 6 in Run INV07-513.....	172
Figure 4.162: Oil saturation comparison in layer 1 in Run INV07-513	172
Figure 4.163: Oil saturation comparison in layer 2 in Run INV07-513	173
Figure 4.164: RMS change in travel time and amplitude in Run INV07-514.....	173
Figure 4.165: Match of the forward model tracer response from layer 1 by iterations 1 and 6 in Run INV07-514.....	174
Figure 4.166: Match of the forward model tracer response from layer 2 by iterations 1 and 6 in Run INV07-514.....	174

Figure 4.167: Oil saturation comparison in layer 1 in Run INV07-514	175
Figure 4.168: Oil saturation comparison in layer 2 in Run INV07-514	175
Figure 4.169: Injection rate change in Run INV07-513-b	176
Figure 4.170: RMS change on travel time and amplitude in Run INV07-513-b with changing flow rate in each layer	176

Chapter 1: Introduction

Petroleum production always involves uncertainty because the geology of the reservoirs is very complex and cannot be seen physically, and because the acquired data contain noise. The uncertainties include the amount of gas and oil, the distribution of fluid saturations, and the properties of the reservoir and fluids. These uncertain factors become very critical in the development of petroleum reservoirs. Reservoirs are always heterogeneous to various degrees. An extreme example of reservoir heterogeneity is a naturally fractured reservoir, which consists of a network of highly conductive fractures and a rock matrix of high storage capacity. Reservoir simulators are powerful tools for predicting petroleum production provided the appropriate reservoir data are available. Furthermore, the simulators can be very helpful in analyzing the uncertainties of the reservoir data. Many sources of data are available for describing reservoirs. Data types include 3D seismic data, well logs, well tests, tracer tests and cores.

A partitioning interwell tracer test (PITT) is a method for estimating oil volume and/or oil saturation in the swept zone between a set of injectors and producers in a reservoir. One of the methods for analyzing PITTs is the method of moments, which is based upon calculating the first temporal moment of the tracer concentrations in the produced fluids. PITTs have many advantages over other methods for estimating oil saturation. A PITT measures the oil saturation over a much larger volume than a single well tracer test, and a vastly larger volume than a well log. It is especially important to know the remaining oil saturation as accurately as possible before applying enhanced oil recovery methods such as chemical flooding or miscible-gas flooding. PITTs also provide valuable information on swept volumes between wells, flow paths, breakthrough

times, and other important information about the reservoir that can be obtained from the conservative tracer that is always included in such a test.

A very general derivation of the method of moments applied to PITT data is presented in this dissertation. This derivation shows that the method of moments can be used for three-dimensional, heterogeneous reservoirs under very general conditions. Naturally fractured reservoirs can be considered an extreme example of heterogeneous reservoirs. The general derivation shows that the method of moments can be applied even to this extreme case, although the time to conduct such tests can be very long in some cases. For this reason, the concept of natural tracers was investigated and analyzed.

The technique of using natural tracers is based on the idea of measuring a naturally residing petroleum organic component such as organic alcohols and acids. Since this natural tracer originates in the oil itself, the use of natural tracers can be less expensive and more environmentally friendly than the use of injected chemical or radioactive tracers, and can take less time to produce a useful signal.

1-1 RESEARCH OBJECTIVES

The main research objectives are as follows:

1. To derive equations to analyze PITT data in heterogeneous reservoirs including naturally fractured reservoirs under the most general possible conditions and to test these equations under a wide variety of reservoir conditions
2. To introduce and demonstrate the use of natural tracers
3. To demonstrate the advantages and disadvantages of tracer analysis using the inverse modeling approach

The general derivation of the equations for the method of moments in heterogeneous reservoirs was applied to PITTs in naturally fractured reservoirs as well as

to single-porosity, heterogeneous reservoirs. The chemical flood simulator, UTCHEM, and a commercial simulator from Schlumberger, ECLIPSE, were used to simulate the transport of tracers under a wide variety of reservoir conditions to generate synthetic tracer data. These tracer data were then analyzed using both the method of moments and inverse modeling. Inverse modeling was done using a program developed at TAMU coupled with ECLIPSE.

1-2 REVIEW OF CHAPTERS

Chapter 2 reviews tracer analysis from the literature including partitioning interwell tracer tests and tracer tests in naturally fractured reservoirs. Chapter 2 also includes a brief review of the numerical simulators UTCHEM with a description of the dual porosity model and ECLIPSE that were used in this research. Chapter 3 includes the derivation of the method of moments under various conditions with slug and continuous tracer injection. Chapter 4 includes applications of the tracer analysis methods. Chapter 5 includes a summary, conclusions, and recommendations.

Chapter 2: Literature Review

Chapter 2 reviews tracer analysis from the literature including partitioning interwell tracer tests and tracer tests in naturally fractured reservoirs. Chapter 2 also includes a review of UTCHEM with a description of the dual porosity model.

2-1 PARTITIONING INTERWELL TRACER TESTS

Applications of secondary and tertiary oil recovery require information on the reservoir characteristics including flow path of the fluids and swept pore volume. The information obtained from monitoring the flow pattern is based on the assumption that the movement of the tracer reflects the movement of the injected water (Zemel, 1995).

Cooke (1971) patented a method to determine the residual oil saturation in reservoirs from interwell tracer tests based on the separation of the conservative and partitioning tracers. Deans (1978) developed an analytical method for interpreting partitioning tracer data.

Ağca (1987) was added partitioning tracers to the UTCHEM simulator so that it could be used to design and predict the performance of interwell partitioning tracer tests. Allison (1988) and Allison *et al.* (1991) used UTCHEM to history match one of the early multiwell partitioning interwell tracer tests and developed some of the earliest quantitative methods to interpret such field data. Wood *et al.* (1990) and Lichtenberger (1991) presented some of the earliest successful partitioning interwell tracer tests to estimate residual oil saturation. Wood *et al.* compared the results from the interwell test to a single well test and to sponge coring and found excellent agreement in the estimated value of the residual oil saturation.

Tang and Harker (1991b) used interwell tracer tests to determine residual oil saturation from partitioning gas tracers. Tang and Harker (1991a) and Tang (1995) proposed a landmark comparison, which is a form of chromatographic transformation for direct calculation of residual oil saturation from tracer data. Tang and Zhang (2000) analyzed the effect of the mobile oil on oil saturation estimated from chromatographically delay of a partitioning tracer. Tang (2002) shows that chromatographic transformation can be used to estimate layer properties from a single curve. Tang (2003) extended the Brigham model using the chromatographic transformation to estimate residual oil saturation from partitioning tracers.

Maroongroge (1994) used the method of moments to estimate the swept pore volume and residual oil saturation from partitioning tracers. Zemel (1995) presents a comprehensive study of oil field tracers and is a good source of information on how to design and interpret tracer tests in the oil field.

Jin *et al.* (1995) applied the method of moments for the analysis of both swept pore volume and the residual oil saturation in contaminated aquifers and introduced a method for extrapolating the tail of the tracer curve to improve the calculation. Deeds (1999) applied the method of moments to a naturally fractured aquifer and also showed that the method was valid even with rate limited mass transfer partitioning of the tracers between phases. Dwarakanath *et al.* (1999) performed an uncertainty analysis on PITTs. Jayanti (2003) used UTCHEM to investigate the effects of aquifer heterogeneity and tracer detection limit on the accuracy of PITTs and reviewed more than 50 PITTs done in contaminated aquifers.

Sinha (2003) investigated the potential benefits of using downhole sensors to detect tracers at different depths in an oil reservoir to determine the oil saturation for different layers in the reservoir rather than just the average value across the formation.

Altinay (2005) used inverse modeling and the method of moments to analyze PITTs. Lalehrokh (2005) simulated partitioning water tracers in naturally fractured oil reservoirs using both a dual porosity model and a discrete fracture model and compared the results. Garmeh (2005) did a similar study for partitioning gas tracers. Wu *et al.* (2005) studied the use of partitioning tracers in fractured geothermal reservoirs. Cheng *et al.* (2005) used a generalized travel-time inversion to estimate permeability distribution using interwell tracer data from the Ranger field, Texas.

2-2 CALCULATION OF SATURATIONS FROM PARTITIONING TRACER DATA

The method of moments is a simple and robust method to calculate the average value of saturation in a given swept pore volume of a reservoir or aquifer using only tracer production data. Himmelblau and Bischoff (1968) presented a classical derivation of the method of moments theory for single-phase non-reactive flow in packed bed reactors. Maroongroge (1994) presented the calculation of residual oil saturation using the first-moment method. Maroongroge based his derivation for 1D flow on the convection-dispersion equation and for 2D flow on streamline theory. Jin *et al.* (1995) presented the use of the method of moments to calculate saturations from a PITT by using the difference in the mean residence times between two tracers. Deeds *et al.* (1999) gave a derivation of the method of moments that was valid for three phases, included dispersion and diffusion, spatially variable phase saturations and porosity and non-equilibrium partitioning.

Inverse modeling can in principle be used to calculate the entire distribution of oil saturation from partitioning tracer data. Only some of the most recent literature is reviewed for this method. Vasco *et al.* (1998) proposed a technique to generate the sensitivities of reservoir parameters such as saturation. The sensitivities along the

streamlines can be calculated analytically in terms of one-dimensional integrals of analytic functions requiring only a single simulation. Yoon *et al.* (1999) proposed an inversion method using a streamline simulator to estimate the distribution of residual oil saturation from partitioning tracer tests in groundwater. The sensitivities along the streamlines are used to update saturation.

Illiassov and Datta-Gupta (2002) applied this inversion method to oil reservoirs to characterize both the distribution of permeability and oil saturation from partitioning interwell tracer tests. They used Tang's Landmark method as the initial guess for the inverse model. Oyerinde (2004) coupled this inversion approach with a finite-difference simulator. The streamlines are now generated from finite-difference simulations to compute time of flight and the sensitivities of the reservoir properties along streamlines, which are used to update the reservoir parameters in the inverse program. The advantage of using a finite-difference simulator includes a more complete modeling of detailed physics such as compressibility, gravity, viscous and capillary cross flow and cross-streamline mechanisms. Altinay (2005) used the same inverse code from TAMU with the initial guess provided by the average saturation from the method of moments.

The inverse program can estimate reservoir properties such as permeability, porosity and saturations from the production of water and oil and tracer concentrations. The inverse approach can be summarized as follows (Oyerinde, 2004).

1. Sensitivity calculation from a finite-difference simulation

A numerical reservoir simulator such as ECLIPSE can be used to calculate fluid fluxes and pathlines, which coincide with streamlines for steady state flow. The sensitivity of the reservoir parameters along the streamlines can be evaluated from a one-dimensional integration. Note that the sensitivity calculations are required only once from the reservoir simulation, which makes this approach very efficient.

The time of flight along the streamlines can be defined as

$$\tau = \int_{\psi} s(\mathbf{x}) dr \quad (2.1)$$

where the slowness can be expressed as

$$s(\mathbf{x}) = \frac{\phi(\mathbf{x})}{\lambda_t k(\mathbf{x}) |\nabla P|} \left(\frac{S_w + K_o S_o}{f_w + K_o f_o} \right) \quad (2.2)$$

The time of flight sensitivity can be obtained integrating along a streamline.

$$\frac{\partial \tau}{\partial S_w} = \int_{\psi} \frac{\partial s(\mathbf{x})}{\partial S_w} dr \quad (2.3)$$

2. Generalized travel-time computations

For each production well, generalized travel-time is calculated to represent the production data misfit to effectively accomplish amplitude matching while preserving most of the benefits of a travel-time inversion.

The optimal shift will be given by the Δt_j that minimizes the misfit function $J(\Delta t_j)$.

$$J(\Delta t_j) = \sum_{i=1}^{N_{dj}} \left[y^{obj}_j(t_i + \Delta t_j) - y^{cal}_j(t_i) \right]^2 \quad (2.4)$$

Or the optimal shift, $\tilde{\Delta t}_j$, maximizes the coefficient of determination $R^2(\Delta t_j)$.

$$R^2(\Delta t_j) = 1 - \frac{\sum_{i=1}^{N_{dj}} [y^{\text{obj}}_j(t_i + \Delta t_j) - y^{\text{cal}}_j(t_i)]^2}{\sum_{i=1}^{N_{dj}} [y^{\text{obj}}_j(t_i) - \bar{y}^{\text{obj}}_j(t_i)]^2} \quad (2.5)$$

3. Model updating via generalized travel-time inversion

The model parameters are changed using the least-square minimization technique using the sensitivity coefficients derived on streamlines. The penalized misfit function with model norm constraint and model roughness is

$$J = \|\varepsilon - \mathbf{G}\delta\mathbf{S}_w\|^2 + \gamma_1^2 \|\delta\mathbf{S}_w\|^2 + \gamma_2^2 \|\mathbf{L}\delta\mathbf{S}_w\|^2 \quad (2.6)$$

where ε the data misfit vector, \mathbf{G} is the sensitivity matrix, $\delta\mathbf{S}_w$ is the change in saturation update, \mathbf{L} is special difference operator form, and γ_1 and γ_2 are the weighting factors of the model norm and roughness, respectively.

2-3 CHEMICAL FLOOD SIMULATOR, UTCHEM

2-3-1 Formulation

UTCHEM is a three-dimensional, multicomponent, multiphase, compositional model that accounts for surfactant phase behavior, chemical and physical transformations and heterogeneous porous media properties and can be used to simulate chemical flooding and many other chemical processes involving flow and transport in permeable media. To improve the numerical accuracy, a third-order finite-difference method is used to approximate spatial derivatives. The solution scheme is analogous to IMPES, where

pressure is solved for implicitly, but concentrations rather than saturations are then solved for explicitly. Phase saturations and concentrations are then solved in a flash routine. An energy balance equation is solved explicitly for reservoir temperature. The energy balance equation includes heat flow between the reservoir and the over- and underburden rocks.

The flow and transport equations are solved for any number of user-specified chemical components (water, organic contaminants, surfactant, alcohols, polymer, chloride, calcium, other electrolytes, microbiological species, electron acceptors, etc.). These components can form up to four fluid phases (air, water, oil, and microemulsion) and any number of solid minerals depending on the overall composition. The microemulsion forms only above the critical micelle concentration of the surfactant and is a thermodynamically stable mixture of water, surfactant and one or more organic components. The major physical phenomena modeled in the simulator are:

- dispersion
- diffusion
- adsorption of surfactant and polymer
- interfacial tension
- relative permeability
- capillary pressure
- capillary trapping (residual saturations)
- cation exchange
- density
- microemulsion viscosity
- phase behavior (pseudoquaternary)
- aqueous reactions

- partitioning of chemical species between oil and water
- dissolution/precipitation of minerals
- in-situ generation of surfactant from acidic crude oil
- pH dependent surfactant adsorption
- organic biodegradation
- multiple organic species
- equilibrium and non-equilibrium organic dissolution in aqueous phase
- dual porosity
- polymer properties: viscosity, inaccessible pore volume, permeability reduction
- gel properties: viscosity, permeability reduction, adsorption
- tracer properties: partitioning, adsorption, radioactive decay, reaction, dead-end pore (capacitance)
- temperature dependent properties: viscosity, tracer reaction, gel reactions, surfactant phase behavior
- gas mobility reduction due to foam

The assumptions imposed when developing the flow equations are local thermodynamic equilibrium except for tracers and dissolution of organic components, immobile solid phases, slightly compressible soil/rock and fluids, Fickian dispersion, ideal mixing, and Darcy's law. The boundary conditions are no flow and no dispersive flux across impermeable boundaries.

The conservation of mass for component κ is expressed in terms of overall volume of component κ per unit pore volume (\tilde{C}_κ) as

$$\frac{\partial}{\partial t} (\phi \tilde{C}_\kappa \rho_\kappa) + \vec{\nabla} \cdot \left[\sum_{\ell=1}^{n_p} \rho_\kappa \left(C_{\kappa\ell} \bar{u}_\ell - \phi S_\ell \bar{\bar{K}}_{\kappa\ell} \cdot \vec{\nabla} C_{\kappa\ell} \right) \right] = R_\kappa \quad (2.7)$$

where the overall volume of component κ per unit pore volume is the sum over all phases including the adsorbed phases:

$$\tilde{C}_\kappa = \left(1 - \sum_{\kappa=1}^{n_{cv}} \hat{C}_\kappa \right) \sum_{\ell=1}^{n_p} S_\ell C_{\kappa\ell} + \hat{C}_\kappa \quad (2.8)$$

n_{cv} is the total number of volume-occupying components. These components are water, oil, surfactant, and air. n_p is the number of phases; \hat{C}_κ is the adsorbed concentration of species κ ; and ρ_κ is the density of pure component κ at a reference phase pressure P_R relative to its density at reference pressure P_{R0} , usually taken at the surface condition of 1atm. Small and constant compressibilities C_κ^0 are assumed.

$$\rho_\kappa = 1 + C_\kappa^0 (P_R - P_{R0}) \quad (2.9)$$

The dispersion tensor $\bar{\bar{K}}_{\kappa\ell}$ including molecular diffusion ($D_{\kappa\ell}$) is calculated as follows (Bear, 1979):

$$\bar{\bar{K}}_{\kappa\ell ij} \equiv \frac{D_{\kappa\ell}}{\tau} \delta_{ij} + \frac{\alpha_{T\ell}}{\phi S_\ell} |\bar{u}_\ell| \delta_{ij} + \frac{(\alpha_{L\ell} - \alpha_{T\ell}) u_{\ell i} u_{\ell j}}{\phi S_\ell |\bar{u}_\ell|} \quad (2.10)$$

where $\alpha_{L\ell}$ and $\alpha_{T\ell}$ are phase ℓ longitudinal and transverse dispersivities; τ is the tortuosity factor with the definition of being a value greater than one; $u_{\ell i}$ and $u_{\ell j}$ are the

components of Darcy flux of phase ℓ in directions i and j ; and δ_{ij} is the Kronecker delta function. The magnitude of flux vector for each phase is computed as

$$|\bar{u}_\ell| = \sqrt{(u_{x\ell})^2 + (u_{y\ell})^2 + (u_{z\ell})^2} \quad (2.11)$$

The phase flux from Darcy's law is

$$\bar{u}_\ell = -\frac{k_{r\ell} \bar{k}}{\mu_\ell} \cdot (\bar{\nabla} P_\ell - \gamma_\ell \bar{\nabla} D) \quad (2.12)$$

where \bar{k} is the permeability tensor and D is the depth, $k_{r\ell}$ is the relative permeability, μ_ℓ is the viscosity, and γ_ℓ is the specific weight for phase ℓ .

The source terms R_κ are a combination of all rate terms for a particular component and may be expressed as

$$R_\kappa = \phi \sum_{\ell=1}^{n_p} S_\ell r_{\kappa\ell} + (1 - \phi) r_{\kappa s} + Q_\kappa \quad (2.13)$$

where Q_κ is the injection/production rate for component κ , per bulk volume. $r_{\kappa\ell}$ and $r_{\kappa s}$ are the reaction rates for component κ , in phase ℓ and solid phase s respectively.

The description of UTCHEM including mass conservation equations, energy conservation equation, pressure equation, non-equilibrium dissolution, well models, fluid and rock properties, adsorption, cation exchange, phase behavior, phase saturations, interfacial tension, capillary pressure, relative permeability, trapping number and

viscosity can be found in Delshad (1996). UTCHEM version 10.0 was used for the simulations in this dissertation.

2-3-2 Dual Porosity Model

The dual porosity model was developed by adding source and sink terms for the mass transfer between matrix and fractures (Aldejain, 1999). One set of equations is used for flow in the fractures and another set of equations is use for flow in the matrix (rock). In both sets of equations, pressure is first solved for implicitly and then concentrations are solved for explicitly. Note the matrix pressure equation is decoupled from the fracture equations. Once the matrix pressure equation is solved implicitly, the transfer terms are calculated and then added to the fracture pressure equation. Then, the matrix mass conservation equations are solved explicitly, where the transfer terms are calculated and then added to the fracture mass conservation equations.

The matrix gridblocks are divided into nested grids in the horizontal direction and stacked grids in the vertical direction, a modified MINC style gridblocks with the advantage of the reduction in dimensions, from 3 dimensions to 2 dimensions noting the horizontal dimension has just one as showing in the following equation.

$$\begin{aligned}
& \frac{\partial}{\partial t} \left(\phi \tilde{C}_\kappa \left(1 + c^0_\kappa (p_\ell - p_R) \right) \right) \\
&= - \frac{\partial}{\partial h} \left[\sum_{\ell=1}^{n_p} \left(1 + c^0_\kappa (p_\ell - p_R) \right) \left(C_{\kappa\ell} u_{h\ell} - \phi S_\ell K_{hh\kappa\ell} \frac{\partial C_{\kappa\ell}}{\partial h} \right) \right] \\
&- \frac{\partial}{\partial z} \left[\sum_{\ell=1}^{n_p} \left(1 + c^0_\kappa (p_\ell - p_R) \right) \left(C_{\kappa\ell} u_{z\ell} - \phi S_\ell K_{zz\kappa\ell} \frac{\partial C_{\kappa\ell}}{\partial z} \right) \right] \\
&+ Q_\kappa
\end{aligned} \tag{2.14}$$

2-4 RESERVOIR SIMULATOR, ECLIPSE

ECLIPSE 100 is a fully implicit, three-phase, three-dimensional, black oil finite-difference reservoir simulator. Version 2004A was used in this work. The gridblocks can be defined using Cartesian, radial, block-centered geometry, and corner-point geometry. ECLIPSE uses the fully implicit method to provide stability over large time steps. Newton's method is used to solve the non-linear equations. The Jacobian matrix is fully expanded in all variables to ensure quadratic convergence (ECLIPSE Technical Description 2004A, 2004).

The dual porosity/permeability model can be used for simulating naturally fractured reservoirs. Each gridblock consists of a matrix and a fracture. In the dual porosity model, no flow between matrix blocks is allowed. Flow between fractures and flow between a fracture and a matrix are modeled. In the dual permeability model, the flow between matrix blocks is modeled.

Chapter 3: Derivation of the Method of Moments for Analyzing PITTs

3-1 INTRODUCTION

Analysis of a partitioning interwell tracer test (PITT) using the method of moments is a simple and robust tool for estimating oil volume between a set of injectors and producers in a reservoir. However, its theoretical justification for application to 3D heterogeneous reservoirs under general conditions has not until now been fully established. In this dissertation, the first temporal moment is derived for both continuous and tracer slug injection, both residual and mobile oil saturation, and both single porosity and naturally fractured reservoirs. The conditions under which the first temporal moment gives a good approximation to the oil saturation are clearly determined for the first time. The general derivation and its verification with numerical simulations shows that the method is not limited to residual oil saturation as generally assumed, but can be extended to mobile oil saturation (or any multiphase flow problem).

The derivation of the method of moments and its application to PITT data shows that the method of moments can be applicable not only to conventional oil reservoirs but also to naturally fractured reservoirs. An analysis of tracer flood in naturally fractured reservoir shows that subgridding of the matrix in the dual porosity model has a significant effect on the tracer transport because the tracers are transported mostly by the slow process of dispersion, which takes time to retrieve the information from the matrix.

Tracers transport in a permeable medium by both convective and dispersive forces. Typically the dispersion is a much slower process than that of the convection. However, in the matrix of naturally fractured reservoirs, the dispersion may be the tracer's main driving force. To fully obtain the reservoir information from PITT data, especially in naturally fractured reservoirs, a long testing period is required. To

compensate for the lengthy duration of monitoring time in addition to its cost, the use of natural tracers is introduced and demonstrated as well as the derivation of the method of moments for the natural tracers, which is a derivative form of continuous tracer injection. The technique of using natural tracers is based on measuring a naturally residing petroleum organic component such as organic alcohols and acids. Since this natural tracer originates in the petroleum component itself, the use of the natural tracer can be more economical and more environmentally friendly than the use of chemical or radioactive tracers.

3-2 DERIVATION OF THE METHOD OF MOMENTS

In this section, a general version of the method of moments used for analyzing a PITT is derived. The analysis yields (i) the swept pore volume between well pairs of an injector and a producer, (ii) the volume of each phase in the swept pore volume, and (iii) the average phase saturation in the swept pore volume.

The assumptions and conditions for the derivation of the method of moments are as follows:

(1) Saturation can vary with time as well as with space. If the tracers are injected in a slug and the saturation is changing with time, then its value corresponds to the mean residence volume of the tracer test. If the oil production is taken into account, then the saturation can be calculated at the end of the test.

(2) The fluids and porous media do not expand or shrink with time over the duration of a PITT. If pressure stays constant during a PITT, the assumption of constant porosity with time will be satisfied without assuming incompressible media. Note that this assumption as well as statement (1) allows for a general heterogeneity in porosity, permeability and saturation.

(3) The analysis of the method of moments is based on the tracers produced from production or monitoring wells. No mass transfer of tracer at the boundaries of the domain analyzed is allowed except for the open boundaries corresponding to injectors and producers. The volume to be analyzed does not have to be known because it is embedded in the analysis of the method of moments. The tracers sweep only part of the reservoir at finite times and this contacted volume is known as the swept pore volume. The swept pore volume is calculated from the conservative tracer. The volume of oil contacted within the swept pore volume is calculated from the partitioning tracers and does not include oil in parts of the reservoir not swept by the fluid containing the tracers. Any oil not in the swept pore volume is bypassed oil and is not measured by the PITT. The moment analysis may be performed without complete tracer production. However, high recovery of the tracers will give a more accurate result because the uncertainty of the extrapolation of the tracer tail is reduced and because a larger fraction of the reservoir has been swept at longer times.

(4) Tracer partition coefficients are constant. This is a good assumption for PITTs since low tracer concentrations are used. Changes in salinity, temperature and pressure on the partition coefficient of water tracers is almost always very small and were neglected in this study. Tracer decay, adsorption and reaction were also assumed to be zero or negligible. In addition, the presence of the tracers does not change the fluid properties of the water or oil by any means.

(5) The initial tracer concentrations in the reservoir are zero, or their background concentration is below the detection limit. Alternatively, water free of tracers can be injected if the organic components initially distributed in the reservoir are used as the tracers, i.e. natural tracers. If water free of tracers is injected as a slug, then the chase water should include the originally residing tracers with their initial concentration.

(6) At the boundary between the formation and the wells, no diffusion is assumed. This is a very good approximation considering the high flow rates into wells.

(7) Local equilibrium is assumed. For the very long time scales characteristic of PITTs in oil reservoirs, this is a very good assumption. Laboratory tests have shown that only a few hours or even less time is needed for the tracers to partition from water to the oil contacted by the tracers.

These conditions are very general and not at all restrictive with the exception of the need to produce a significant fraction of the tracers. However, in some cases this can take a long time depending on the reservoir conditions. Longer times are needed for large well spacing, low rates, and highly heterogeneous reservoirs.

3-2-1 Derivation for Injected Tracer Slug

The mass conservation equation of a tracer component κ anywhere in the reservoir free of tracer decay, adsorption, and reaction is expressed by

$$\frac{\partial}{\partial t} \left(\phi \sum_{\ell=1}^{n_p} S_{\ell} C_{\kappa\ell} \right) + \nabla \cdot \vec{N}_{\kappa} = 0 \quad (3.1)$$

where $C_{\kappa\ell}$ is the concentration of tracer component κ in the phase ℓ , and \vec{N}_{κ} is the total flux of the tracer component κ , including both the convection and dispersion and

$$\vec{N}_{\kappa} = \sum_{\ell=1}^{n_p} \left(C_{\kappa\ell} \vec{u}_{\ell} - \phi S_{\ell} \vec{K}_{\kappa\ell} \cdot \nabla C_{\kappa\ell} \right) \quad (3.2)$$

The first term in the mass conservation equation, Equation (3.1), is an accumulation term, and the second term is a transport term.

Provided the porosity stays constant over time, Equation (3.1) can be re-written as

$$\phi \frac{\partial C_{\kappa}}{\partial t} + \nabla \cdot \vec{N}_{\kappa} = 0 \quad (3.3)$$

where the overall fluid phase concentration of the tracer component κ , C_{κ} , is defined as follows:

$$C_{\kappa} = \sum_{\ell=1}^{n_p} S_{\ell} C_{\kappa\ell} \quad (3.4)$$

Note that Equation (3.3) is valid for the single porosity model when the tracer is injected either with a slug or continuously. The case with the continuous tracer injection will be discussed in the Section 3-2-2. Also note that, in the case of slug injection of tracers with concentration of $C_{\kappa J}$ with the slug size in time of t_{slug} , the chase water has the initial tracer concentration $C_{\kappa I}$.

$$\begin{cases} C_{\kappa\ell} \Big|_{\text{injector}} = C_{\kappa J} & 0 \leq t \leq t_{\text{slug}} \\ C_{\kappa\ell} \Big|_{\text{injector}} = C_{\kappa I} & t_{\text{slug}} \leq t \end{cases} \quad (3.5)$$

The tracer concentration at the end of the test, or at infinite time, should be equal to the initial concentration in the analyzed domain, since the chase water is injected with the initial concentration given by Equation (3.5). Therefore, the boundary condition at infinite time is as follows:

$$C_{\kappa\ell} \Big|_{t \rightarrow \infty} = C_{\kappa I} \quad (3.6)$$

Now, the notation of the time variables is changed from t to τ for distinguishing integration variables. Equation (3.3) can be written as

$$\phi \frac{\partial C_{\kappa}}{\partial \tau} + \nabla \cdot \vec{N}_{\kappa} = 0 \quad (3.7)$$

Multiplying Equation (3.3) by time τ

$$\tau \phi \frac{\partial C_{\kappa}}{\partial \tau} + \tau \nabla \cdot \vec{N}_{\kappa} = 0 \quad (3.8)$$

Integrating the above equation over time to obtain the first temporal moment

$$\int_0^t \tau \phi \frac{\partial C_{\kappa}}{\partial \tau} d\tau + \int_0^t \tau \nabla \cdot \vec{N}_{\kappa} d\tau = 0 \quad (3.9)$$

Recalling that the porosity is constant with respect to time, and switching the order of the time integration and the del operator in the second term

$$\phi \int_0^t \tau \frac{\partial C_{\kappa}}{\partial \tau} d\tau + \nabla \cdot \int_0^t \tau \vec{N}_{\kappa} d\tau = 0 \quad (3.10)$$

The first term can be integrated by parts as follows:

$$\begin{aligned}
& \int_0^t \tau \frac{\partial C_{\kappa}}{\partial \tau} d\tau \\
&= \int_0^t \left(\frac{\partial}{\partial \tau} [\tau C_{\kappa}] - C_{\kappa} \right) d\tau \\
&= \int_0^t d[\tau C_{\kappa}] - \int_0^t C_{\kappa} d\tau \\
&= [\tau C_{\kappa}]_0^t - \int_0^t C_{\kappa} d\tau
\end{aligned} \tag{3.11}$$

Defining the initial overall concentration

$$C_{\kappa I} = \sum_{\ell=1}^{n_p} S_{\ell I} C_{\kappa \ell I} \tag{3.12}$$

With this definition, the first term in Equation (3.11) can be evaluated as

$$\begin{aligned}
& [\tau C_{\kappa}]_0^t \\
&= [\tau C_{\kappa}]_0^t - [\tau C_{\kappa I}]_0^t + [\tau C_{\kappa I}]_0^t \\
&= [\tau(C_{\kappa} - C_{\kappa I})]_0^t + [\tau C_{\kappa I}]_0^t
\end{aligned} \tag{3.13}$$

Knowing that $C_{\kappa I}$ does not change with time

$$[\tau C_{\kappa I}]_0^t = \int_0^t C_{\kappa I} d\tau \tag{3.14}$$

Therefore, Equation (3.13) becomes

$$\begin{aligned}
& [\tau(C_{\kappa} - C_{\kappa I})]_0^t + [\tau C_{\kappa I}]_0^t \\
&= [\tau(C_{\kappa} - C_{\kappa I})]_{\tau=t} - [\tau(C_{\kappa} - C_{\kappa I})]_{\tau=0} + \int_0^t C_{\kappa I} d\tau \\
&= t(C_{\kappa} - C_{\kappa I}) + \int_0^t C_{\kappa I} d\tau
\end{aligned} \tag{3.15}$$

Now, the first term of Equation (3.10) is evaluated using Equations (3.11), (3.13), and (3.15)

$$\begin{aligned}
& \phi \int_0^t \tau \frac{\partial C_{\kappa}}{\partial \tau} d\tau \\
&= \phi \left[[\tau C_{\kappa}]_0^t - \int_0^t C_{\kappa} d\tau \right] \\
&= \phi \left[[\tau(C_{\kappa} - C_{\kappa I})]_0^t + [\tau C_{\kappa I}]_0^t - \int_0^t C_{\kappa} d\tau \right] \\
&= \phi \left[t(C_{\kappa} - C_{\kappa I}) + \int_0^t C_{\kappa I} d\tau - \int_0^t C_{\kappa} d\tau \right] \\
&= -\phi \left[-t(C_{\kappa} - C_{\kappa I}) + \int_0^t (C_{\kappa} - C_{\kappa I}) d\tau \right]
\end{aligned} \tag{3.16}$$

Therefore, Equation (3.10) can be written as follows:

$$-\phi \left[-t(C_{\kappa} - C_{\kappa I}) + \int_0^t (C_{\kappa} - C_{\kappa I}) d\tau \right] + \nabla \cdot \int_0^t \tau \vec{N}_{\kappa} d\tau = 0 \tag{3.17}$$

Now noting that the integral variable is τ , multiplying Equation (3.3) by time t

$$t\phi \frac{\partial C_{\kappa}}{\partial \tau} + t\nabla \cdot \vec{N}_{\kappa} = 0 \tag{3.18}$$

Integrating the above equation over time from t to the infinity

$$\int_t^\infty t\phi \frac{\partial C_\kappa}{\partial \tau} d\tau + \int_t^\infty t\nabla \cdot \bar{N}_\kappa d\tau = 0 \quad (3.19)$$

Recalling that the porosity is constant with respect to time, and switching the order of the time integration and the del operator in the latter term

$$\phi \int_t^\infty t \frac{\partial C_\kappa}{\partial \tau} d\tau + \nabla \cdot \int_t^\infty t \bar{N}_\kappa d\tau = 0 \quad (3.20)$$

The first term can be integrated as

$$\begin{aligned} & \int_t^\infty t \frac{\partial C_\kappa}{\partial \tau} d\tau \\ &= t \int_t^\infty dC_\kappa \\ &= t[C_\kappa]_t^\infty \\ &= t[C_\kappa]_t^\infty - t[C_{\kappa I}]_t^\infty + t[C_{\kappa I}]_t^\infty \\ &= t[C_\kappa - C_{\kappa I}]_t^\infty + t[C_{\kappa I}]_t^\infty \\ &= t[C_\kappa - C_{\kappa I}]_{\tau \rightarrow \infty} - t[C_\kappa - C_{\kappa I}]_{\tau=t} + t[C_{\kappa I}]_t^\infty \end{aligned} \quad (3.21)$$

From the boundary condition of Equation (3.6)

$$[C_\kappa - C_{\kappa I}]_{\tau \rightarrow \infty} = C_{\kappa I} - C_{\kappa I} = 0 \quad (3.22)$$

Knowing that $C_{\kappa I}$ is constant in time

$$[C_{\kappa I}]_t^\infty = 0 \quad (3.23)$$

Therefore, Equation (3.21) becomes

$$t[C_{\kappa} - C_{\kappa I}]_{\tau \rightarrow \infty} - t[C_{\kappa} - C_{\kappa I}]_{\tau=t} + t[C_{\kappa I}]_t^{\infty} = -t(C_{\kappa} - C_{\kappa I}) \quad (3.24)$$

Now, the first term of Equation (3.20) is evaluated using Equations (3.21) and (3.24)

$$\phi \int_t^{\infty} t \frac{\partial C_{\kappa}}{\partial \tau} d\tau = -\phi t(C_{\kappa} - C_{\kappa I}) \quad (3.25)$$

Therefore, Equation (3.20) can be written as

$$-\phi t(C_{\kappa} - C_{\kappa I}) + \nabla \cdot \int_t^{\infty} t \vec{N}_{\kappa} d\tau = 0 \quad (3.26)$$

From Equations (3.17) and (3.26),

$$\begin{aligned} & -\phi \left[-t(C_{\kappa} - C_{\kappa I}) + \int_0^t (C_{\kappa} - C_{\kappa I}) d\tau \right] - \phi t(C_{\kappa} - C_{\kappa I}) \\ & + \nabla \cdot \int_0^t \tau \vec{N}_{\kappa} d\tau + \nabla \cdot \int_t^{\infty} t \vec{N}_{\kappa} d\tau = 0 \end{aligned} \quad (3.27)$$

Therefore

$$-\phi \int_0^t (C_{\kappa} - C_{\kappa I}) d\tau + \nabla \cdot \int_0^t \tau \vec{N}_{\kappa} d\tau + \nabla \cdot \int_t^{\infty} t \vec{N}_{\kappa} d\tau = 0 \quad (3.28)$$

or

$$-\phi m_{0\kappa} + \nabla \cdot \int_0^t \tau \vec{N}_\kappa d\tau + \nabla \cdot \int_t^\infty t \vec{N}_\kappa d\tau = 0 \quad (3.29)$$

where $m_{0\kappa}$ is the zeroth temporal moment of tracer concentration.

$$m_{0\kappa} = \int_0^t (C_\kappa - C_{\kappa I}) d\tau \quad (3.30)$$

Integrating Equation (3.29) in the domain swept by the tracer:

$$- \iiint \phi m_{0\kappa} dV_R + \iiint \left(\nabla \cdot \int_0^t \tau \vec{N}_\kappa d\tau + \nabla \cdot \int_t^\infty t \vec{N}_\kappa d\tau \right) dV_R = 0 \quad (3.31)$$

Applying the divergence theorem of Gauss to the latter term by changing the volume integration to a surface integration gives

$$- \iiint \phi m_{0\kappa} dV_R + \iint \left(\int_0^t \tau \vec{N}_\kappa d\tau + \int_t^\infty t \vec{N}_\kappa d\tau \right) \cdot \vec{n} dA = 0 \quad (3.32)$$

where \vec{n} is the outer unit normal vector at the boundary. The latter term is evaluated only at the wells since no mass transfer of tracer occurs except at the boundaries with the wells.

$$\begin{aligned}
& \iint \left(\int_0^t \tau \vec{N}_{\kappa} d\tau + \int_t^{\infty} t \vec{N}_{\kappa} d\tau \right) \cdot \vec{n} dA \\
&= \sum_{\text{wells}} \left(\iint \left(\int_0^t \tau \vec{N}_{\kappa} d\tau + \int_t^{\infty} t \vec{N}_{\kappa} d\tau \right) \cdot \vec{n} dA \right) \\
&= \sum_{\text{wells}} \left(\iint \left(\int_0^t \tau \vec{N}_{\kappa} d\tau \right) \cdot \vec{n} dA \right) + \sum_{\text{wells}} \left(\iint \left(\int_t^{\infty} t \vec{N}_{\kappa} d\tau \right) \cdot \vec{n} dA \right) \tag{3.33}
\end{aligned}$$

The first term is evaluated assuming no diffusion at the boundaries with the wells.

$$\begin{aligned}
& \sum_{\text{wells}} \left(\iint \left(\int_0^t \tau \vec{N}_{\kappa} d\tau \right) \cdot \vec{n} dA \right) \\
&= \sum_{\text{wells}} \left(\iint \left(\int_0^t \tau \left(\sum_{\ell=1}^{n_p} \left(C_{\kappa\ell} \vec{u}_{\ell} - \phi S_{\ell} \vec{K}_{\kappa\ell} \cdot \nabla C_{\kappa\ell} \right) \right) d\tau \right) \cdot \vec{n} dA \right) \\
&= \sum_{\text{wells}} \left(\iint \left(\int_0^t \tau \left(\sum_{\ell=1}^{n_p} C_{\kappa\ell} \vec{u}_{\ell} \right) d\tau \right) \cdot \vec{n} dA \right) \tag{3.34}
\end{aligned}$$

Switching the order of summation and integration, and evaluating the flux at the well, allows the equation to be expressed in terms of flow rate

$$\begin{aligned}
& \sum_{\text{wells}} \left(\iint \left(\int_0^t \tau \left(\sum_{\ell=1}^{n_p} C_{\kappa\ell} \bar{u}_\ell \right) d\tau \right) \cdot \bar{n} dA \right) \\
&= \sum_{\text{wells}} \left(\sum_{\ell=1}^{n_p} \left(\iint \left(\int_0^t \tau C_{\kappa\ell} \bar{u}_\ell d\tau \right) \cdot \bar{n} dA \right) \right) \\
&= \sum_{\text{wells}} \left(\sum_{\ell=1}^{n_p} \left(\int_0^t \tau \left(\iint \bar{u}_\ell \cdot \bar{n} dA \right) C_{\kappa\ell} d\tau \right) \right) \\
&= \sum_{\text{wells}} \left(\sum_{\ell=1}^{n_p} \left(\int_0^t \tau q_\ell C_{\kappa\ell} d\tau \right) \right)
\end{aligned} \tag{3.35}$$

where q_ℓ is the flow rate of the phase ℓ at the wells from the well pairs to be considered. Note that the value of q_ℓ is positive if the flow is towards the outward direction, which leads to a positive flow rate in production and a negative flow rate in injection.

Then, switching the order of summation and integration again

$$\begin{aligned}
& \sum_{\text{wells}} \left(\sum_{\ell=1}^{n_p} \left(\int_0^t \tau q_\ell C_{\kappa\ell} d\tau + \int_t^\infty \tau q_\ell C_{\kappa\ell} d\tau \right) \right) \\
&= \sum_{\text{wells}} \left(\int_0^t \tau \left(\sum_{\ell=1}^{n_p} q_\ell C_{\kappa\ell} \right) d\tau + \int_t^\infty \tau \left(\sum_{\ell=1}^{n_p} q_\ell C_{\kappa\ell} \right) d\tau \right)
\end{aligned} \tag{3.36}$$

Knowing that pore volume and fluid volume do not change with time

$$\sum_{\text{wells}} q_\ell = 0 \tag{3.37}$$

Also recognizing that the initial concentration and flow rate do not change with time

$$\sum_{\text{wells}} \left(\int_0^t \tau \left(\sum_{\ell=1}^{n_p} q_{\ell} C_{\kappa\ell I} \right) d\tau \right) = 0 \quad (3.38)$$

Now

$$\begin{aligned} & \sum_{\text{wells}} \left(\int_0^t \tau \left(\sum_{\ell=1}^{n_p} q_{\ell} C_{\kappa\ell} \right) d\tau \right) \\ &= \sum_{\text{wells}} \left(\int_0^t \tau \left(\sum_{\ell=1}^{n_p} q_{\ell} C_{\kappa\ell} \right) d\tau \right) - \sum_{\text{wells}} \left(\int_0^t \tau \left(\sum_{\ell=1}^{n_p} q_{\ell} C_{\kappa\ell I} \right) d\tau \right) \\ &= \sum_{\text{wells}} \left(\int_0^t \tau \left(\sum_{\ell=1}^{n_p} q_{\ell} (C_{\kappa\ell} - C_{\kappa\ell I}) \right) d\tau \right) \\ &= \sum_{\text{wells}} \left(q \int_0^t \tau \left(\sum_{\ell=1}^{n_p} \frac{q_{\ell}}{q} (C_{\kappa\ell} - C_{\kappa\ell I}) \right) d\tau \right) \\ &= \sum_{\text{wells}} (q m_{1\kappa} d\tau) \end{aligned} \quad (3.39)$$

where

$$m_{1\kappa} = \int_0^t \tau \left(\sum_{\ell=1}^{n_p} \frac{q_{\ell}}{q} (C_{\kappa\ell} - C_{\kappa\ell I}) \right) d\tau = \int_0^t \tau \left(\sum_{\ell=1}^{n_p} f_{\ell} (C_{\kappa\ell} - C_{\kappa\ell I}) \right) d\tau \quad (3.40)$$

where f_{ℓ} is the fractional flow of the phase ℓ written as

$$f_\ell = \frac{q_\ell}{q} \quad (3.41)$$

In the same manner, the second term in Equation (3.33) is evaluated as follows:

$$\sum_{\text{wells}} \left(\iint \left(\int_t^\infty t \vec{N}_\kappa d\tau \right) \cdot \vec{n} dA \right) = \sum_{\text{wells}} (q \tilde{m}_{1\kappa} d\tau) \quad (3.42)$$

where

$$\tilde{m}_{1\kappa} = \int_t^\infty t \left(\sum_{\ell=1}^{n_p} f_\ell (C_{\kappa\ell} - C_{\kappa I}) \right) d\tau \quad (3.43)$$

Therefore, Equation (3.32) can be evaluated as

$$- \iiint \phi m_{0\kappa} dV_R + \sum_{\text{wells}} q (m_{1\kappa} + \tilde{m}_{1\kappa}) = 0 \quad (3.44)$$

This equation is very powerful because the data over the entire analyzed domain can be obtained only from that at the wells. The information of the pore volume and the saturation is imbedded in the left hand term. Also note that the above equation applies to general heterogeneity.

Now Equation (3.44) is analyzed for multiphase flow.

$$\begin{aligned}
m_{0\kappa} &= \int_0^t (C_{\kappa} - C_{\kappa I}) d\tau \\
&= \int_0^t \left(\sum_{\ell=1}^{n_p} S_{\ell} C_{\kappa\ell} - \sum_{\ell=1}^{n_p} S_{\ell I} C_{\kappa\ell I} \right) d\tau \\
&= \int_0^t \left(\sum_{\ell=1}^{n_p} (S_{\ell} C_{\kappa\ell} - S_{\ell I} C_{\kappa\ell I}) \right) d\tau
\end{aligned} \tag{3.45}$$

Letting phase 1 be the reference phase:

$$K_{T\kappa\ell} = \frac{C_{\kappa\ell}}{C_{\kappa 1}} \tag{3.46}$$

The concentration of the tracer component κ in the phase ℓ can be expressed by the tracer partition coefficient and by the concentration of the tracer component κ in the reference phase.

$$C_{\kappa\ell} = K_{T\kappa\ell} C_{\kappa 1} \tag{3.47}$$

and

$$C_{\kappa\ell I} = K_{T\ell\kappa} C_{\kappa I} \tag{3.48}$$

The function integrated in Equation (3.45) can be written only with the tracer concentration in the reference phase without that in the other phases.

$$\begin{aligned}
& \sum_{\ell=1}^{n_p} (S_{\ell} C_{\kappa\ell} - S_{\ell I} C_{\kappa\ell I}) \\
&= \sum_{\ell=1}^{n_p} (S_{\ell} K_{T\kappa\ell} C_{\kappa I} - S_{\ell I} K_{T\kappa\ell} C_{\kappa II}) \\
&= \sum_{\ell=1}^{n_p} K_{T\kappa\ell} (S_{\ell} C_{\kappa I} - S_{\ell I} C_{\kappa II})
\end{aligned} \tag{3.49}$$

Assuming constant tracer partition coefficients, Equation (3.45) becomes

$$\begin{aligned}
m_{0\kappa} &= \int_0^t \left(\sum_{\ell=1}^{n_p} (S_{\ell} C_{\kappa\ell} - S_{\ell I} C_{\kappa\ell I}) \right) d\tau \\
&= \int_0^t \left(\sum_{\ell=1}^{n_p} K_{T\kappa\ell} (S_{\ell} C_{\kappa I} - S_{\ell I} C_{\kappa II}) \right) d\tau \\
&= \left(\sum_{\ell=1}^{n_p} K_{T\kappa\ell} \right) \int_0^t (S_{\ell} C_{\kappa I} - S_{\ell I} C_{\kappa II}) d\tau \\
&= \left(\sum_{\ell=1}^{n_p} K_{T\kappa\ell} \hat{S}_{\ell} \right) \int_0^t (C_{\kappa I} - C_{\kappa II}) d\tau \\
&= \left(\sum_{\ell=1}^{n_p} K_{T\kappa\ell} \hat{S}_{\ell} \right) m_{0\kappa I}
\end{aligned} \tag{3.50}$$

where

$$\hat{S}_{\ell} = \frac{\int_0^t (S_{\ell} C_{\kappa I} - S_{\ell I} C_{\kappa II}) d\tau}{\int_0^t (C_{\kappa I} - C_{\kappa II}) d\tau} \tag{3.51}$$

and

$$m_{0\kappa l} = \int_0^t (C_{\kappa l} - C_{\kappa l I}) d\tau \quad (3.52)$$

Equation (3.44) can be written as

$$- \iiint \left(\phi \left(\sum_{\ell=1}^{n_p} K_{T\kappa\ell} \hat{S}_\ell \right) m_{0\kappa l} \right) dV_R + \sum_{\text{wells}} q (m_{1\kappa} + \tilde{m}_{1\kappa}) = 0 \quad (3.53)$$

The use of different tracers for each injector is helpful to analyze the swept pattern. The following discussion is based on an analysis of a single domain between one injector and one of the producers, but the result can be applied to multiple wells. The only adjustment required is to calculate the flow rate, q , as follows:

$$q = \frac{m_n}{M} Q \quad (3.54)$$

where Q and q_{pro} are the injection and production rates respectively and

$$m_n = \int_0^\infty q_{\text{pro}} \left(\sum_{\ell=1}^{n_p} f_\ell (C_{\kappa\ell} - C_{\kappa\ell I}) \right) d\tau \quad (3.55)$$

$$\begin{aligned}
M &= \int_0^{t_{\text{slug}}} Q \left(\sum_{\ell=1}^{n_p} f_{\ell} (C_{\kappa\ell J} - C_{\kappa\ell I}) \right) d\tau \\
&= Qt_{\text{slug}} \left(\sum_{\ell=1}^{n_p} f_{\ell} (C_{\kappa\ell J} - C_{\kappa\ell I}) \right)
\end{aligned} \tag{3.56}$$

Note the mass of tracer produced at the particular production well is m_n , and the total mass of the tracer injected is M .

Now the discussion is based in the domain between an injector and one of the producers. Knowing that pore volume and fluid volume do not change with time, or assuming balanced injection and production,

$$q_{\text{pro}} + q_{\text{inj}} = 0 \tag{3.57}$$

or

$$q_{\text{inj}} = -q_{\text{pro}} \tag{3.58}$$

Equation (3.53) can be further evaluated as

$$\begin{aligned}
& - \iiint \left(\phi \left(\sum_{\ell=1}^{n_p} K_{T\kappa\ell} \hat{S}_{\ell} \right) m_{0\kappa I} \right) dV_R \\
& + q_{\text{pro}} (m_{1\kappa} + \tilde{m}_{1\kappa})_{\text{pro}} + q_{\text{inj}} (m_{1\kappa} + \tilde{m}_{1\kappa})_{\text{inj}} = 0
\end{aligned} \tag{3.59}$$

or

$$\begin{aligned}
& - \iiint \left(\phi \left(\sum_{\ell=1}^{n_p} K_{T\kappa\ell} \hat{S}_\ell \right) \frac{m_{0\kappa l}}{\bar{m}_{0\kappa l}} \right) dV_R \\
& + q_{\text{pro}} \left(\frac{(m_{1\kappa} + \tilde{m}_{1\kappa})_{\text{pro}}}{\bar{m}_{0\kappa l}} - \frac{(m_{1\kappa} + \tilde{m}_{1\kappa})_{\text{inj}}}{\bar{m}_{0\kappa l}} \right) = 0
\end{aligned} \tag{3.60}$$

where

$$\bar{m}_{0\kappa l} = f_l (C_{\kappa l J} - C_{\kappa l I}) t_{\text{slug}} \tag{3.61}$$

Note at $t \geq t_{\text{slug}}$

$$\begin{aligned}
& (m_{1\kappa} + \tilde{m}_{1\kappa})_{\text{inj}} \\
& = \int_0^{t_{\text{slug}}} \tau \left(\sum_{\ell=1}^{n_p} f_\ell (C_{\kappa\ell J} - C_{\kappa\ell I}) \right) d\tau + \int_{t_{\text{slug}}}^t \tau \left(\sum_{\ell=1}^{n_p} f_\ell (C_{\kappa\ell I} - C_{\kappa\ell I}) \right) d\tau \\
& + \int_t^\infty t \left(\sum_{\ell=1}^{n_p} f_\ell (C_{\kappa\ell I} - C_{\kappa\ell I}) \right) d\tau \\
& = \left(\sum_{\ell=1}^{n_p} f_\ell (C_{\kappa\ell J} - C_{\kappa\ell I}) \right) \frac{t_{\text{slug}}^2}{2}
\end{aligned} \tag{3.62}$$

Equation (3.60) can be written as

$$\begin{aligned}
& - \iiint \left(\phi \left(\sum_{\ell=1}^{n_p} K_{T\kappa\ell} \hat{S}_\ell \right) \frac{m_{0\kappa l}}{\bar{m}_{0\kappa l}} \right) dV_R \\
& + q_{\text{pro}} \left(\frac{(m_{1\kappa} + \tilde{m}_{1\kappa})_{\text{pro}}}{\bar{m}_{0\kappa l}} - \frac{t_{\text{slug}}}{2} \right) = 0
\end{aligned} \tag{3.63}$$

Switching the order of the volume integration and the summation

$$\begin{aligned}
& - \sum_{\ell=1}^{n_p} K_{T\kappa\ell} \iiint \left(\phi \hat{S}_\ell \frac{m_{0\kappa l}}{\bar{m}_{0\kappa l}} \right) dV_R \\
& + q_{\text{pro}} \left(\frac{(m_{1\kappa} + \tilde{m}_{1\kappa})_{\text{pro}}}{\bar{m}_{0\kappa l}} - \frac{t_{\text{slug}}}{2} \right) = 0
\end{aligned} \tag{3.64}$$

For simplifying the discussion, two phases, oil and water, are considered in the following discussion. However for multiple phases, Equation (3.64) shows that the volume of phase ℓ seen by the tracer κ , $\iiint \left(\phi \hat{S}_\ell \frac{m_{0\kappa l}}{\bar{m}_{0\kappa l}} \right) dV_R$, can be obtained by solving n_p sets of the linear equations for n_p tracers with different partition coefficients. n_p tracers with different partition coefficients are required for n_p -phases.

Equation (3.64) can be written as follows knowing that the reference phase is water.

$$\begin{aligned}
& - \left[\iiint \left(\phi \hat{S}_w \frac{m_{0\kappa w}}{\bar{m}_{0\kappa l}} \right) dV_R + K_{T\kappa} \iiint \left(\phi \hat{S}_o \frac{m_{0\kappa w}}{\bar{m}_{0\kappa l}} \right) dV_R \right] \\
& + q_{\text{pro}} \left(\frac{(m_{1\kappa} + \tilde{m}_{1\kappa})_{\text{pro}}}{\bar{m}_{0\kappa l}} - \frac{t_{\text{slug}}}{2} \right) = 0
\end{aligned} \tag{3.65}$$

For a conservative tracer, Equation (3.65) becomes

$$- \iiint \left(\phi \hat{S}_w \frac{m_{0\kappa w}}{\bar{m}_{0\kappa l}} \right) dV_R + q_{\text{pro}} \left(\frac{(m_{1\kappa} + \tilde{m}_{1\kappa})_{\text{pro}}}{\bar{m}_{0\kappa l}} - \frac{t_{\text{slug}}}{2} \right) = 0 \quad (3.66)$$

This equation shows that a conservative tracer can be used to tell how much water is contacted at any given time t , which is

$$V_w = \iiint \left(\phi \hat{S}_w \frac{m_{0\kappa w}}{\bar{m}_{0\kappa l}} \right) dV_R = q_{\text{pro}} \left(\frac{(m_{1\kappa} + \tilde{m}_{1\kappa})_{\text{pro}}}{\bar{m}_{0\kappa l}} - \frac{t_{\text{slug}}}{2} \right) \quad (3.67)$$

If a partitioning tracer of partition coefficient $K_{T\kappa l} = 1$ is used, then Equation (3.65) becomes

$$\begin{aligned} & - \left[\iiint \left(\phi \hat{S}_w \frac{m_{0\kappa w}}{\bar{m}_{0\kappa l}} \right) dV_R + \iiint \left(\phi \hat{S}_o \frac{m_{0\kappa w}}{\bar{m}_{0\kappa l}} \right) dV_R \right] \\ & + q_{\text{pro}} \left(\frac{(m_{1\kappa} + \tilde{m}_{1\kappa})_{\text{pro}}}{\bar{m}_{0\kappa l}} - \frac{t_{\text{slug}}}{2} \right) = 0 \end{aligned} \quad (3.68)$$

and knowing $\hat{S}_w + \hat{S}_o = 1$

$$- \iiint \left(\phi \frac{m_{0\kappa w}}{\bar{m}_{0\kappa l}} \right) dV_R + q_{\text{pro}} \left(\frac{(m_{1\kappa} + \tilde{m}_{1\kappa})_{\text{pro}}}{\bar{m}_{0\kappa l}} - \frac{t_{\text{slug}}}{2} \right) = 0 \quad (3.69)$$

This equation indicates that a partitioning tracer with $K_{T\kappa} = 1$ can be used to calculate the pore volume contacted at any given time t , which is

$$V_{\text{swept}} = \iiint \left(\phi \frac{m_{0\kappa w}}{\bar{m}_{0\kappa l}} \right) dV_R = q_{\text{pro}} \left(\frac{(m_{1\kappa} + \tilde{m}_{1\kappa})_{\text{pro}}}{\bar{m}_{0\kappa l}} - \frac{t_{\text{slug}}}{2} \right) \quad (3.70)$$

The mean residence time can be defined as

$$\begin{aligned} \bar{t}_{\kappa} &= \lim_{t \rightarrow \infty} \left(\frac{(m_{1\kappa} + \tilde{m}_{1\kappa})_{\text{pro}}}{\bar{m}_{0\kappa l}} - \frac{t_{\text{slug}}}{2} \right) \\ &= \frac{\lim_{t \rightarrow \infty} \left((m_{1\kappa} + \tilde{m}_{1\kappa})_{\text{pro}} \right)}{\bar{m}_{0\kappa l}} - \frac{t_{\text{slug}}}{2} \\ &= \frac{\int_0^{\infty} \tau \left(\sum_{\ell=1}^{n_p} f_{\ell} (C_{\kappa \ell} - C_{\kappa l}) \right) d\tau}{\bar{m}_{0\kappa l}} - \frac{t_{\text{slug}}}{2} \end{aligned} \quad (3.71)$$

The swept pore volume with a partitioning tracer of $K_{T\kappa} = 1$ is

$$V_p = \lim_{t \rightarrow \infty} V_{\text{swept}} = q_{\text{pro}} \lim_{t \rightarrow \infty} \left(\frac{(m_{1\kappa} + \tilde{m}_{1\kappa})_{\text{pro}}}{\bar{m}_{0\kappa l}} - \frac{t_{\text{slug}}}{2} \right) = q_{\text{pro}} \bar{t}_{\kappa} \quad (3.72)$$

Taking the limit as time approaches infinity, Equation (3.65) for two tracers become

$$\hat{V}_w + K_{T1} \hat{V}_o = q_{\text{pro}} \bar{t}_1 \quad (3.73)$$

$$\hat{V}_w + K_{T2} \hat{V}_o = q_{\text{pro}} \bar{t}_2 \quad (3.74)$$

Now water volume, oil volume, and swept pore volume can be calculated from

$$\hat{V}_w = q_{\text{pro}} \frac{K_{T2}\bar{t}_1 - K_{T1}\bar{t}_2}{K_{T2} - K_{T1}} \quad (3.75)$$

$$\hat{V}_o = q_{\text{pro}} \frac{-\bar{t}_1 + \bar{t}_2}{K_{T2} - K_{T1}} \quad (3.76)$$

$$V_p = \hat{V}_w + \hat{V}_o = q_{\text{pro}} \frac{(K_{T2} - 1)\bar{t}_1 - (K_{T1} - 1)\bar{t}_2}{K_{T2} - K_{T1}} \quad (3.77)$$

The average oil saturation can be calculated from:

$$\hat{S}_o = \frac{-\bar{t}_1 + \bar{t}_2}{(K_{T2} - 1)\bar{t}_1 - (K_{T1} - 1)\bar{t}_2} \quad (3.78)$$

Note that each of these volumes correspond to the mean residence volume of a conservative tracer. The oil volume at the end of the tracer test can be estimated by subtracting the oil volume produced after the mean residence volume. The water volume can be obtained in the same manner. In addition, if there are multiple wells in the reservoir, then the produced volume can be from multiple injectors and the production rate needs to be divided into the rate each injector contributes to apply the moment analysis for each well pair. The production rate is assumed to be proportional to the tracer swept volume. In case that n_s injectors contribute to the producer, the production rate corresponding to each swept volume is given by:

$$q_{\ell} = Q_{\ell} \frac{V_{s_{iinj}}}{\sum_{iinj} V_{s_{iinj}}} \quad (3.79)$$

where Q_{ℓ} is the total production rate and $V_{s_{iinj}}$ is the swept pore volume between the injector $iinj$. The average oil saturation corrected for produced oil within a particular swept volume is then calculated from Equation (3.80) below. Therefore, the oil volume in the analyzed pore volume at the end of the tracer test can be written as follows:

$$\begin{aligned} V_o &= \hat{V}_o - \sum_{wells} \left(q \int_{\bar{t}}^{\infty} f_o d\tau \right) \\ &= q_{pro} \frac{-\bar{t}_1 + \bar{t}_2}{K_{T2} - K_{T1}} - \sum_{wells} \left(q \int_{\bar{t}}^{\infty} f_o d\tau \right) \end{aligned} \quad (3.80)$$

The average oil saturation in the analyzed pore volume at the end of tracer test is:

$$S_o = \frac{-\bar{t}_1 + \bar{t}_2 - \frac{K_{T2} - K_{T1}}{q_{pro}} \sum_{wells} \left(q \int_{\bar{t}}^{\infty} f_o d\tau \right)}{(K_{T2} - 1)\bar{t}_1 - (K_{T1} - 1)\bar{t}_2} \quad (3.81)$$

If tracer 1 is a conservative tracer,

$$\hat{V}_w = q_{pro} \bar{t}_1 \quad (3.82)$$

$$\hat{V}_o = q_{pro} \frac{-\bar{t}_1 + \bar{t}_2}{K_T} \quad (3.83)$$

$$V_p = \hat{V}_w + \hat{V}_o = q_{\text{pro}} \frac{(K_{T2} - 1)\bar{t}_1 + \bar{t}_2}{K_{T2}} \quad (3.84)$$

$$V_o = q_{\text{pro}} \frac{-\bar{t}_1 + \bar{t}_2}{K_T} - \sum_{\text{wells}} \left(q \int_t^{\infty} f_o d\tau \right) \quad (3.85)$$

$$S_o = \frac{-\bar{t}_1 + \bar{t}_2 - \frac{K_T}{q_{\text{pro}}} \sum_{\text{wells}} \left(q \int_t^{\infty} f_o d\tau \right)}{(K_T - 1)\bar{t}_1 + \bar{t}_2} \quad (3.86)$$

3-2-2 Derivation with Continuous Tracer Injected

In Section 3-2-1, the moment analysis was derived for the case of a tracer slug injected in a single porosity reservoir. This section it is derived for the case of continuous tracer injected in a single porosity reservoir. The idea of continuous tracer injection can be applied to the use of natural tracers or to the analysis in the naturally fractured reservoirs, which will be discussed in a later section. Thereafter, the moment analysis using the derived equations will be demonstrated to obtain the pore volume between well pairs of injectors and producers, the volume of each phase and the average phase saturation in the swept pore volume. The derivation of the applied equations in the moment analysis starts from the mass balance equation of tracer components, as starting in the previous section.

All six assumptions and remarks described in the beginning of Section 3-2 will be applied. First, equations for the moment analysis are derived to estimate the reservoir data over the entire analyzed domain, which is obtained only at the wells. As discussed in the Section 3-2-1, the mass conservation equation of Equation (3.3) can be held with either tracers are injected with slug or continuously.

Note that in the case of continuous tracer injection with concentration of $C_{\kappa lJ}$, the initial and boundary conditions are as follows:

$$C_{\kappa l} \Big|_{\text{injector}} = C_{\kappa lJ} \quad t > 0 \quad (3.87)$$

and

$$\begin{cases} C_{\kappa l} = C_{\kappa lI} & t = 0 \\ C_{\kappa l} = C_{\kappa lJ} & t \rightarrow \infty \end{cases} \quad (3.88)$$

Now, Equation (3.7) can be integrated over time noting that the integration valuable is τ .

$$\int_0^t \phi \frac{\partial C_{\kappa}}{\partial \tau} d\tau + \int_0^t \nabla \cdot \vec{N}_{\kappa} d\tau = 0 \quad (3.89)$$

Recalling that the porosity is constant with respect to time, and switching the order of the time integration and the del operator

$$\phi \int_0^t dC_{\kappa} + \nabla \cdot \int_0^t \vec{N}_{\kappa} d\tau = 0 \quad (3.90)$$

With the initial condition from Equation (3.88), Equation (3.90) can be evaluated as

$$\phi(C_{\kappa} - C_{\kappa I}) + \nabla \cdot \int_0^t \vec{N}_{\kappa} d\tau = 0 \quad (3.91)$$

where

$$C_{\kappa I} = C_{\kappa}|_{t=0} = \sum_{\ell=1}^{n_p} S_{\ell I} C_{\kappa \ell I} \quad (3.92)$$

Integrating Equation (3.91) in the domain swept by the tracer:

$$\iiint (\phi(C_{\kappa} - C_{\kappa I})) dV_R + \iiint \nabla \cdot \left(\int_0^t \vec{N}_{\kappa} d\tau \right) dV_R = 0 \quad (3.93)$$

Applying the divergence theorem of Gauss to the latter term to change the volume integration to a surface integration gives

$$\iiint (\phi(C_{\kappa} - C_{\kappa I})) dV_R + \iint \left(\int_0^t \vec{N}_{\kappa} d\tau \right) \cdot \vec{n} dA = 0 \quad (3.94)$$

where \vec{n} is the outer unit normal vector at the boundary.

The second term in Equation (3.94) can be further evaluated only at the wells, since no mass transfer of tracer occurs except at the boundaries with the wells.

$$\iint \left(\int_0^t \vec{N}_{\kappa} d\tau \right) \cdot \vec{n} dA = \sum_{\text{wells}} \left(\iint \left(\int_0^t \vec{N}_{\kappa} d\tau \right) \cdot \vec{n} dA \right) \quad (3.95)$$

Assuming no diffusion at the boundary with the wells

$$\begin{aligned}
& \sum_{\text{wells}} \left(\iint \left(\int_0^t \vec{N}_{\kappa} d\tau \right) \cdot \vec{n} dA \right) \\
&= \sum_{\text{wells}} \left(\iint \left(\int_0^t \left(\sum_{\ell=1}^{n_p} \left(C_{\kappa\ell} \bar{u}_{\ell} - \phi S_{\ell} \vec{K}_{\kappa\ell} \cdot \nabla C_{\kappa\ell} \right) \right) d\tau \right) \cdot \vec{n} dA \right) \\
&= \sum_{\text{wells}} \left(\iint \left(\int_0^t \left(\sum_{\ell=1}^{n_p} C_{\kappa\ell} \bar{u}_{\ell} \right) d\tau \right) \cdot \vec{n} dA \right)
\end{aligned} \tag{3.96}$$

Switching the orders of summation and integrations and evaluating the flux at the wells, allows the equation to be expressed in terms of flow rate

$$\begin{aligned}
& \sum_{\text{wells}} \left(\iint \left(\int_0^t \left(\sum_{\ell=1}^{n_p} C_{\kappa\ell} \bar{u}_{\ell} \right) d\tau \right) \cdot \vec{n} dA \right) \\
&= \sum_{\text{wells}} \left(\sum_{\ell=1}^{n_p} \left(\iint \left(\int_0^t C_{\kappa\ell} \bar{u}_{\ell} d\tau \right) \cdot \vec{n} dA \right) \right) \\
&= \sum_{\text{wells}} \left(\sum_{\ell=1}^{n_p} \left(\int_0^t \left(\iint \bar{u}_{\ell} \cdot \vec{n} dA \right) C_{\kappa\ell} d\tau \right) \right) \\
&= \sum_{\text{wells}} \left(\sum_{\ell=1}^{n_p} \left(\int_0^t q_{\ell} C_{\kappa\ell} d\tau \right) \right)
\end{aligned} \tag{3.97}$$

Then, switching the order of summation and integration again

$$\sum_{\text{wells}} \left(\sum_{\ell=1}^{n_p} \left(\int_0^t q_{\ell} C_{\kappa\ell} d\tau \right) \right) = \sum_{\text{wells}} \left(\int_0^t \left(\sum_{\ell=1}^{n_p} q_{\ell} C_{\kappa\ell} \right) d\tau \right) \tag{3.98}$$

Equation (3.98) can be evaluated knowing that the total flow rate does not change with time

$$\begin{aligned}
& \sum_{\text{wells}} \left(\int_0^t \left(\sum_{\ell=1}^{n_p} q_{\ell} C_{\kappa\ell} \right) d\tau \right) \\
&= \sum_{\text{wells}} \left(q \int_0^t \left(\sum_{\ell=1}^{n_p} \frac{q_{\ell}}{q} C_{\kappa\ell} \right) d\tau \right) \\
&= \sum_{\text{wells}} (q m_{0c\kappa})
\end{aligned} \tag{3.99}$$

With the definition of the tracer partition coefficient in Equation (3.47), the terms containing the tracer concentration in the phase ℓ in Equation (3.99) can be written only with its concentration in the reference phase.

$$C_{\kappa I} = \sum_{\ell=1}^{n_p} S_{\ell I} C_{\kappa\ell I} = \sum_{\ell=1}^{n_p} S_{\ell I} K_{T\kappa\ell} C_{\kappa I} = \left(\sum_{\ell=1}^{n_p} K_{T\kappa\ell} S_{\ell I} \right) C_{\kappa I} \tag{3.100}$$

$$C_{\kappa} = \sum_{\ell=1}^{n_p} S_{\ell} C_{\kappa\ell} = \sum_{\ell=1}^{n_p} S_{\ell} K_{T\kappa\ell} C_{\kappa I} = \left(\sum_{\ell=1}^{n_p} K_{T\kappa\ell} S_{\ell} \right) C_{\kappa I} \tag{3.101}$$

and

$$\int_0^t \left(\sum_{\ell=1}^{n_p} f_{\ell} C_{\kappa\ell} \right) d\tau = \int_0^t \left(\sum_{\ell=1}^{n_p} f_{\ell} K_{T\kappa\ell} C_{\kappa I} \right) d\tau = \sum_{\ell=1}^{n_p} K_{T\kappa\ell} \int_0^t f_{\ell} C_{\kappa I} d\tau \tag{3.102}$$

Therefore, Equation (3.94) can be written as

$$\begin{aligned} & \iiint \left(\phi \left(\left(\sum_{\ell=1}^{n_p} K_{T\kappa\ell} S_{\ell} \right) C_{\kappa l} - \left(\sum_{\ell=1}^{n_p} K_{T\kappa\ell} S_{\ell I} \right) C_{\kappa l I} \right) \right) dV_R \\ & + \sum_{\text{wells}} \left(q \sum_{\ell=1}^{n_p} K_{T\kappa\ell} \int_0^t f_{\ell} C_{\kappa l} d\tau \right) = 0 \end{aligned} \quad (3.103)$$

Switching the order of the integration and the summation in the first term

$$\begin{aligned} & \iiint \left(\phi \left(\left(\sum_{\ell=1}^{n_p} K_{T\kappa\ell} S_{\ell} \right) C_{\kappa l} - \left(\sum_{\ell=1}^{n_p} K_{T\kappa\ell} S_{\ell I} \right) C_{\kappa l I} \right) \right) dV_R \\ & = \sum_{\ell=1}^{n_p} K_{T\kappa\ell} \iiint (\phi S_{\ell} C_{\kappa l}) dV_R - \sum_{\ell=1}^{n_p} K_{T\kappa\ell} \iiint (\phi S_{\ell I} C_{\kappa l I}) dV_R \\ & = \sum_{\ell=1}^{n_p} K_{T\kappa\ell} \iiint (\phi S_{\ell} C_{\kappa l}) dV_R - C_{\kappa l I} \sum_{\ell=1}^{n_p} K_{T\kappa\ell} \iiint (\phi S_{\ell I}) dV_R \end{aligned} \quad (3.104)$$

The volume integration term represents the phase volume in the reservoir, which can be expressed with the initial volume of the phase and with the total fluid amount transported through the boundary, i.e. wells, is

$$\iiint (\phi S_{\ell I}) dV_R = \iiint (\phi S_{\ell}) dV_R + \sum_{\text{wells}} \left(q \int_0^t f_{\ell} d\tau \right) \quad (3.105)$$

Therefore, Equation (3.104) can be written as

$$\begin{aligned}
& \sum_{\ell=1}^{n_p} K_{T\kappa\ell} \iiint (\phi S_\ell C_{\kappa I}) dV_R - C_{\kappa II} \sum_{\ell=1}^{n_p} K_{T\kappa\ell} \iiint (\phi S_{II}) dV_R \\
&= \sum_{\ell=1}^{n_p} K_{T\kappa\ell} \iiint (\phi S_\ell C_{\kappa I}) dV_R \\
&\quad - C_{\kappa II} \sum_{\ell=1}^{n_p} K_{T\kappa\ell} \left[\iiint (\phi S_\ell) dV_R + \sum_{\text{wells}} \left(q \int_0^t f_\ell d\tau \right) \right] \\
&= \sum_{\ell=1}^{n_p} K_{T\kappa\ell} \iiint (\phi S_\ell C_{\kappa I}) dV_R \\
&\quad - C_{\kappa II} \sum_{\ell=1}^{n_p} K_{T\kappa\ell} \iiint (\phi S_\ell) dV_R - C_{\kappa II} \sum_{\ell=1}^{n_p} K_{T\kappa\ell} \sum_{\text{wells}} \left(q \int_0^t f_\ell d\tau \right) \\
&= \sum_{\ell=1}^{n_p} K_{T\kappa\ell} \iiint (\phi S_\ell (C_{\kappa I} - C_{\kappa II})) dV_R \\
&\quad - \sum_{\text{wells}} \left(q \sum_{\ell=1}^{n_p} K_{T\kappa\ell} \int_0^t f_\ell C_{\kappa II} d\tau \right)
\end{aligned} \tag{3.106}$$

Therefore, Equation (3.103) can be written as

$$\begin{aligned}
& \sum_{\ell=1}^{n_p} K_{T\kappa\ell} \iiint (\phi S_\ell (C_{\kappa I} - C_{\kappa II})) dV_R \\
&\quad - \sum_{\text{wells}} \left(q \sum_{\ell=1}^{n_p} K_{T\kappa\ell} \int_0^t f_\ell C_{\kappa II} d\tau \right) + \sum_{\text{wells}} \left(q \sum_{\ell=1}^{n_p} K_{T\kappa\ell} \int_0^t f_\ell C_{\kappa I} d\tau \right) = 0
\end{aligned} \tag{3.107}$$

or

$$\begin{aligned}
& \sum_{\ell=1}^{n_p} K_{T\kappa\ell} \iiint (\phi S_{\ell} (C_{\kappa I} - C_{\kappa II})) dV_R \\
& + \sum_{\text{wells}} \left(q \sum_{\ell=1}^{n_p} K_{T\kappa\ell} \int_0^t f_{\ell} (C_{\kappa I} - C_{\kappa II}) d\tau \right) = 0
\end{aligned} \tag{3.108}$$

Note the total flow rate between an injector and a producer, q , can be estimated as below when multiple wells are employed.

$$q = \frac{m_n}{M} Q \tag{3.109}$$

where Q and q_{pro} are the injection and production rates respectively and

$$m_n = q_{\text{pro}} \sum_{\ell=1}^{n_p} (f_{\ell} (C_{\kappa\ell} - C_{\kappa I}))_{\text{pro}} \Big|_{t \rightarrow \infty} \tag{3.110}$$

$$M = Q \sum_{\ell=1}^{n_p} (f_{\ell} (C_{\kappa\ell} - C_{\kappa I}))_{\text{inj}} \Big|_{t \rightarrow \infty} \tag{3.111}$$

Equation (3.108) shows that the reservoir data can be obtained only at the wells. Also note that the above equation is not restricted by the heterogeneities of the media or the mechanism of the transport.

Evaluating the latter term with one producer and one injector

$$\begin{aligned}
& \sum_{\text{wells}} \left(q \sum_{\ell=1}^{n_p} K_{T\kappa\ell} \int_0^t f_\ell (C_{\kappa I} - C_{\kappa II}) d\tau \right) \\
&= \left(q \sum_{\ell=1}^{n_p} K_{T\kappa\ell} \int_0^t f_\ell (C_{\kappa I} - C_{\kappa II}) d\tau \right) \Big|_{\text{producer}} \\
&+ \left(q \sum_{\ell=1}^{n_p} K_{T\kappa\ell} \int_0^t f_\ell (C_{\kappa I} - C_{\kappa II}) d\tau \right) \Big|_{\text{injector}}
\end{aligned} \tag{3.112}$$

Evaluating the term of the injector knowing the boundary condition given by Equation (3.87), noting $q_{\text{inj}} = -q_{\text{pro}}$

$$\begin{aligned}
& \left(q \sum_{\ell=1}^{n_p} K_{T\kappa\ell} \int_0^t f_\ell (C_{\kappa I} - C_{\kappa II}) d\tau \right) \Big|_{\text{injector}} \\
&= -q_{\text{pro}} \left(\sum_{\ell=1}^{n_p} K_{T\kappa\ell} \int_0^t f_\ell (C_{\kappa I} - C_{\kappa II}) d\tau \right) \Big|_{\text{injector}}
\end{aligned} \tag{3.113}$$

Therefore, Equation (3.108) can be written as

$$\begin{aligned}
& \sum_{\ell=1}^{n_p} K_{T\kappa\ell} \iiint (\phi S_\ell (C_{\kappa I} - C_{\kappa II})) dV_R \\
&+ q_{\text{pro}} \left(\sum_{\ell=1}^{n_p} K_{T\kappa\ell} \int_0^t f_\ell (C_{\kappa I} - C_{\kappa II}) d\tau \right) \Big|_{\text{producer}} \\
&- q_{\text{pro}} \left(\sum_{\ell=1}^{n_p} K_{T\kappa\ell} \int_0^t f_\ell (C_{\kappa I} - C_{\kappa II}) d\tau \right) \Big|_{\text{injector}} = 0
\end{aligned} \tag{3.114}$$

or

$$\sum_{\ell=1}^{n_p} K_{T\kappa\ell} \iiint \left(\phi S_\ell \frac{C_{\kappa I} - C_{\kappa II}}{C_{\kappa IJ} - C_{\kappa II}} \right) dV_R - q_{\text{pro}} m_{0c\kappa} = 0 \quad (3.115)$$

where

$$m_{0c\kappa} = \left(\sum_{\ell=1}^{n_p} K_{T\kappa\ell} \int_0^t f_\ell d\tau \right) \Big|_{\text{injector}} - \left(\sum_{\ell=1}^{n_p} K_{T\kappa\ell} \int_0^t f_\ell \frac{C_{\kappa I} - C_{\kappa II}}{C_{\kappa IJ} - C_{\kappa II}} d\tau \right) \Big|_{\text{producer}} \quad (3.116)$$

For simplifying the discussion, two phases, oil and water, are considered in the following discussion. However for multiple phases, Equation (3.115) indicates that the volume of the phase ℓ seen by the tracer κ , $\iiint \left(\phi S_\ell \frac{C_{\kappa I} - C_{\kappa II}}{C_{\kappa IJ} - C_{\kappa II}} \right) dV_R$, can be obtained with solving n_p sets of the linear equations from n_p tracers with different partition coefficients. n_p kinds of the tracers with different partition coefficients are required in n_p -phase condition.

Equation (3.115) can be written now as follows knowing that the reference phase is water.

$$\iiint \left(\phi S_w \frac{C_{\kappa w} - C_{\kappa wI}}{C_{\kappa wJ} - C_{\kappa wI}} \right) dV_R + K_{T\kappa} \iiint \left(\phi S_o \frac{C_{\kappa w} - C_{\kappa wI}}{C_{\kappa wJ} - C_{\kappa wI}} \right) dV_R - q_{\text{pro}} m_{0c\kappa} = 0 \quad (3.117)$$

If a conservative tracer is used, then Equation (3.117) becomes

$$\iiint \left(\phi S_w \frac{C_{\kappa w} - C_{\kappa w I}}{C_{\kappa w J} - C_{\kappa w I}} \right) dV_R - q_{\text{pro}} m_{0\kappa} = 0 \quad (3.118)$$

This equation shows that a conservative tracer can be used to tell how much water is contacted at any given time t , which is

$$V_{\text{water}} = \iiint \left(\phi S_w \frac{C_{\kappa w} - C_{\kappa w I}}{C_{\kappa w J} - C_{\kappa w I}} \right) dV_R = q_{\text{pro}} m_{0\kappa} \quad (3.119)$$

If a partitioning tracer of partition coefficient $K_{T\kappa} = 1$ is used, then Equation (3.117) becomes

$$\begin{aligned} & \iiint \left(\phi S_w \frac{C_{\kappa w} - C_{\kappa w I}}{C_{\kappa w J} - C_{\kappa w I}} \right) dV_R + \iiint \left(\phi S_o \frac{C_{\kappa w} - C_{\kappa w I}}{C_{\kappa w J} - C_{\kappa w I}} \right) dV_R \\ & - q_{\text{pro}} m_{0\kappa} = 0 \end{aligned} \quad (3.120)$$

and knowing $S_w + S_o = 1$ and $f_w + f_o = 1$

$$\iiint \left(\phi \frac{C_{\kappa w} - C_{\kappa w I}}{C_{\kappa w J} - C_{\kappa w I}} \right) dV_R - q_{\text{pro}} m_{0\kappa} = 0 \quad (3.121)$$

This equation indicates that a partitioning tracer of $K_{T\kappa} = 1$ can tell how much of pore volume is contacted at any given time t , which is

$$V_{\text{swept}} = \iiint \left(\phi \frac{C_{\kappa W} - C_{\kappa WI}}{C_{\kappa WJ} - C_{\kappa WI}} \right) dV_R = q_{\text{pro}} m_{0\kappa} \quad (3.122)$$

The mean residence time can be defined as

$$\bar{t}_{\kappa} = \lim_{t \rightarrow \infty} m_{0\kappa} \quad (3.123)$$

The swept pore volume with a partitioning tracer of $K_{T\kappa} = 1$ is

$$V_p = \lim_{t \rightarrow \infty} V_{\text{swept}} = q_{\text{pro}} \lim_{t \rightarrow \infty} m_{0\kappa} = q_{\text{pro}} \bar{t}_{\kappa} \quad (3.124)$$

Taking the limit with respect to time to infinity, Equations (3.117) for two tracers become

$$V_w + K_{T1} V_o = q_{\text{pro}} \bar{t}_1 \quad (3.125)$$

$$V_w + K_{T2} V_o = q_{\text{pro}} \bar{t}_2 \quad (3.126)$$

Now water volume, oil volume, and swept pore volume can be written as

$$V_w = q_{\text{pro}} \frac{K_{T2} \bar{t}_1 - K_{T1} \bar{t}_2}{K_{T2} - K_{T1}} \quad (3.127)$$

$$V_o = q_{\text{pro}} \frac{-\bar{t}_1 + \bar{t}_2}{K_{T2} - K_{T1}} \quad (3.128)$$

$$V_p = V_w + V_o = q_{\text{pro}} \frac{(K_{T2} - 1)\bar{t}_1 - (K_{T1} - 1)\bar{t}_2}{K_{T2} - K_{T1}} \quad (3.129)$$

The average oil saturation can be written as follows:

$$S_o = \frac{-\bar{t}_1 + \bar{t}_2}{(K_{T2} - 1)\bar{t}_1 - (K_{T1} - 1)\bar{t}_2} \quad (3.130)$$

Equations (3.127) to (3.130) are very similar to Equation (3.75) to (3.78), the equations for the injection of a tracer slug. Note that regardless of the different definition of the mean residence time, the same equations can be obtained with the only difference in when the saturation is calculated.

If tracer 1 is a conservative tracer,

$$V_w = q_{\text{pro}} \bar{t}_1 \quad (3.131)$$

$$V_o = q_{\text{pro}} \frac{-\bar{t}_1 + \bar{t}_2}{K_T} \quad (3.132)$$

$$V_p = V_w + V_o = q_{\text{pro}} \frac{(K_{T2} - 1)\bar{t}_1 + \bar{t}_2}{K_{T2}} \quad (3.133)$$

$$S_o = \frac{-\bar{t}_1 + \bar{t}_2}{(K_T - 1)\bar{t}_1 + \bar{t}_2} \quad (3.134)$$

3-2-3 Derivation for Dual Porosity Model

In Sections 3-2-1 and 3-2-2, the equations for the method of moments were derived for the case of slug and continuous tracer injected in a single porosity reservoir.

Next the equations are derived for the case of tracer injected into a dual porosity reservoir. The derivation starts from the mass balance equations of a tracer component in both fracture and matrix similar to that described in the previous section. All of the assumptions and remarks described in the Section 3-2 will be applied to this section as well.

The mass conservation equations similar to Equation (3.3) can be written for a dual porosity model as follows. The mass conservation equation for flow in fractures is

$$\phi_f \frac{\partial C_{f\kappa}}{\partial t} + \nabla \cdot \vec{N}_{f\kappa} + \tau_{fm} = 0 \quad (3.135)$$

where

$$C_{f\kappa} = \sum_{\ell=1}^{n_p} S_{\ell} C_{f\kappa\ell} \quad (3.136)$$

The mass conservation equation for the rock matrix is

$$\phi_m \frac{\partial C_{m\kappa}}{\partial t} - \tau_{fm} = 0 \quad (3.137)$$

where

$$C_{m\kappa} = \sum_{\ell=1}^{n_p} S_{\ell} C_{m\kappa\ell} \quad (3.138)$$

Note that τ_{fm} is the mass transfer function between fracture and matrix. There is no mass flux between matrix blocks in the dual porosity model.

In the case of slug tracer injection in the dual porosity model, the initial and boundary conditions are as follows:

$$\begin{cases} C_{f\kappa\ell} = C_{m\kappa\ell} = C_{\kappa\ell I} & t = 0 \\ C_{f\kappa\ell} = C_{m\kappa\ell} = C_{\kappa\ell I} & t \rightarrow \infty \end{cases} \quad (3.139)$$

In the case of continuous tracer injection in the dual porosity model, the initial and boundary conditions are as follows:

$$\begin{cases} C_{f\kappa\ell} = C_{m\kappa\ell} = C_{\kappa\ell I} & t = 0 \\ C_{f\kappa\ell} = C_{m\kappa\ell} = C_{\kappa\ell J} & t \rightarrow \infty \end{cases} \quad (3.140)$$

Before tracer test is started, equilibrium is achieved and the concentration in fracture and matrix is the same. At infinite time, the concentration in both fracture and matrix reaches the initial concentration for slug injection and the injected concentration for continuous injection.

Adding Equations (3.135) and (3.136), the mass conservation equation can be written as

$$\phi_f \frac{\partial C_{f\kappa}}{\partial t} + \phi_m \frac{\partial C_{m\kappa}}{\partial t} + \nabla \cdot \vec{N}_{f\kappa} = 0 \quad (3.141)$$

Define total porosity and total concentration:

$$\phi_t = \phi_f + \phi_m \quad (3.142)$$

and

$$C_{t\kappa} = \frac{\phi_f C_{f\kappa} + \phi_m C_{m\kappa}}{\phi_t} \quad (3.143)$$

With these definitions, the mass conservation equation becomes

$$\phi_t \frac{\partial C_{t\kappa}}{\partial t} + \nabla \cdot \vec{N}_{f\kappa} = 0 \quad (3.144)$$

Equation (3.144) is identical to Equation (3.3). The boundary and initial conditions are the same as those discussed in both Sections 3-2-1 and 3-2-2.

$$\begin{aligned} & - \iiint \left(\phi \left(\sum_{\ell=1}^{n_p} K_{T\kappa\ell} \hat{S}_\ell \right) m_{0\kappa l} \right) dV_R \\ & + q_{\text{pro}} (m_{1\kappa} + \tilde{m}_{1\kappa})_{\text{pro}} + q_{\text{inj}} (m_{1\kappa} + \tilde{m}_{1\kappa})_{\text{inj}} = 0 \end{aligned} \quad (3.145)$$

$$\begin{aligned} & \sum_{\ell=1}^{n_p} K_{T\kappa\ell} \iiint (\phi S_\ell (C_{\kappa l} - C_{\kappa l I})) dV_R \\ & + \sum_{\text{wells}} \left(q \sum_{\ell=1}^{n_p} K_{T\kappa\ell} \int_0^t f_\ell (C_{\kappa l} - C_{\kappa l I}) d\tau \right) = 0 \end{aligned} \quad (3.146)$$

Therefore, Equation (3.144) can be evaluated as for tracer slug and continuous tracer injected as Equations (3.145) and (3.146) respectively. Equations (3.145) and

(3.146) show that the information over the entire domain is obtained only at the wells for the dual porosity model just like it is for the case of the single porosity model.

Because the governing equations are identical and the initial and boundary conditions are the same, the results obtained in the Sections 3-2-1 and 3-2-2 can be directly applied to the results of the dual porosity model with mobile phases under the assumptions discussed earlier. In conclusion, the following three results can be obtained from the tracer test: (i) the swept pore volume between a well pair of an injector and a producer, (ii) the volume of each phase in the swept pore volume, and (iii) the average phase saturation in the swept pore volume.

3-2-4 Application to Natural Tracers

In this section, the equations are derived for the method of moments for the case of natural tracers. The natural tracers are organic components initially distributed in the reservoir fluids, which can be used as tracers by measuring these component concentrations during a waterflood. The following discussion illustrates the case of water flowing at residual oil saturation.

Note that saturation can vary with time as well as with space. However, it is assumed that the reservoir is at equilibrium before the waterflood so that the organic component concentrations in each phase are uniform over the reservoir.

Since only water without the organic components is injected

$$C_{\kappa\ell}|_{\text{injector}} = 0 \quad t > 0 \quad (3.147)$$

and

$$\begin{cases} C_{\kappa l} = C_{\kappa l I} & t = 0 \\ C_{\kappa l} = 0 & t \rightarrow \infty \end{cases} \quad (3.148)$$

Then, Equation (3.123) for the mean residence time can be written as

$$\bar{t}_{\kappa} = \lim_{t \rightarrow \infty} m_{0c\kappa} \quad (3.149)$$

where

$$\begin{aligned} m_{0c\kappa} &= \left(\int_0^t (f_w + K_{TK} f_o) d\tau \right) \Big|_{\text{injector}} \\ &\quad - \left(\int_0^t \left((f_w + K_{TK} f_o) \frac{C_{\kappa w} - C_{\kappa w I}}{C_{\kappa w J} - C_{\kappa w I}} \right) d\tau \right) \Big|_{\text{producer}} \\ &= \left(\int_0^t d\tau \right) \Big|_{\text{injector}} \\ &\quad - \left(\int_0^t \left((f_w + K_{TK} f_o) \frac{C_{\kappa w} - C_{\kappa w I}}{-C_{\kappa w I}} \right) d\tau \right) \Big|_{\text{producer}} \\ &= \left(\int_0^t d\tau \right) \Big|_{\text{producer}} \\ &\quad - \left(\int_0^t \left((f_w + K_{TK} f_o) \frac{C_{\kappa w} - C_{\kappa w I}}{-C_{\kappa w I}} \right) d\tau \right) \Big|_{\text{producer}} \\ &= \left(\int_0^t \left(1 - (f_w + K_{TK} f_o) \frac{C_{\kappa w I} - C_{\kappa w}}{C_{\kappa w I}} \right) d\tau \right) \Big|_{\text{producer}} \end{aligned} \quad (3.150)$$

The initial water and oil volumes as well as pore volume can be obtained from Equations (3.131) through (3.134) at the initial time before the waterflood. The oil

volume at the end of the tracer test can be estimated by subtracting the oil volume produced from the initial oil volume.

3-2-5 Sweep Efficiency from Tracer Slug Injection

In this section, tracer slug injection and continuous tracer injection are shown to be equivalent. The sweep efficiency can then be calculated from tracer slug injection data. For simplifying the discussion, no tracer is initially in the reservoir and single-phase flow is assumed.

The swept volume at any given time t can be calculated from Equation (3.70):

$$V_{\text{swept}} = q_{\text{pro}} \left(\frac{(m_{1K} + \tilde{m}_{1K})_{\text{pro}}}{\bar{m}_{0Kw}} - \frac{t_{\text{slug}}}{2} \right) \quad (3.151)$$

where

$$\bar{m}_{0Kw} = C_{Kw} J t_{\text{slug}} = \int_0^{\infty} C_{Kw} d\tau \quad (3.152)$$

$$m_{1K} = \int_0^t \tau C_{Kw} d\tau \quad (3.153)$$

and

$$\tilde{m}_{1K} = \int_t^{\infty} t C_{Kw} d\tau \quad (3.154)$$

Note the tracer is injected during time period $0 \leq t \leq t_{\text{slug}}$. Equation (3.153) can be expressed as a double integral and then the integration order changed to:

$$\int_0^t \tau C_{\kappa w} d\tau = \int_0^t \left(\int_0^\tau dt' \right) C_{\kappa w} d\tau = \int_0^t \left(\int_{t'}^t C_{\kappa w} d\tau \right) dt' \quad (3.155)$$

and

$$\int_t^\infty t C_{\kappa w} d\tau = \int_t^\infty \left(\int_0^t dt' \right) C_{\kappa w} d\tau = \int_0^t \left(\int_t^\infty C_{\kappa w} d\tau \right) dt' \quad (3.156)$$

Using this equation, the first term of the swept volume can be evaluated as follows:

$$\begin{aligned} \frac{(m_{1\kappa} + \tilde{m}_{1\kappa})_{\text{pro}}}{\bar{m}_{0\kappa w}} &= \frac{\int_0^t \left(\int_{t'}^t C_{\kappa w} d\tau \right) dt' + \int_t^\infty t C_{\kappa w} d\tau}{C_{\kappa w J} t_{\text{slug}}} \\ &= \int_0^t \left(\frac{\int_{t'}^t C_{\kappa w} d\tau + \int_t^\infty C_{\kappa w} d\tau}{\int_0^\infty C_{\kappa w} d\tau} \right) dt' \\ &= \int_0^t \left(\frac{\int_{t'}^\infty C_{\kappa w} d\tau}{\int_0^\infty C_{\kappa w} d\tau} \right) dt' \\ &= \int_0^t \left(\frac{\int_0^\infty C_{\kappa w} d\tau - \int_0^{t'} C_{\kappa w} d\tau}{\int_0^\infty C_{\kappa w} d\tau} \right) dt' \\ &= \int_0^t \left(1 - \frac{\int_0^{t'} C_{\kappa w} d\tau}{\int_0^\infty C_{\kappa w} d\tau} \right) dt' \end{aligned} \quad (3.157)$$

Now the swept volume can be written as

$$V_{\text{swept}} = q_{\text{pro}} \left(\int_0^t \left(1 - \frac{\int_0^{t'} C_{\text{kw}} d\tau}{\int_0^{\infty} C_{\text{kw}} d\tau} \right) dt' - \frac{t_{\text{slug}}}{2} \right) \quad (3.158)$$

The pore volume can be estimated by taking the limit to infinity.

$$\begin{aligned} V_p &= \lim_{t \rightarrow \infty} V_{\text{swept}} \\ &= \lim_{t \rightarrow \infty} \left(q_{\text{pro}} \left(\int_0^t \left(1 - \frac{\int_0^{t'} C_{\text{kw}} d\tau}{\int_0^{\infty} C_{\text{kw}} d\tau} \right) dt' - \frac{t_{\text{slug}}}{2} \right) \right) \\ &= q_{\text{pro}} \left(\int_0^{\infty} \left(1 - \frac{\int_0^{t'} C_{\text{kw}} d\tau}{\int_0^{\infty} C_{\text{kw}} d\tau} \right) dt' - \frac{t_{\text{slug}}}{2} \right) \end{aligned} \quad (3.159)$$

The mean residence time can be expressed as

$$\bar{t} = \frac{V_p}{q_{\text{pro}}} = \int_0^{\infty} \left(1 - \frac{\int_0^{t'} C_{\text{kw}} d\tau}{\int_0^{\infty} C_{\text{kw}} d\tau} \right) dt' - \frac{t_{\text{slug}}}{2} \quad (3.160)$$

Note that the mean residence time can be also written as

$$\bar{t} = \frac{\int_0^{\infty} \tau C_{\text{kw}} d\tau}{\int_0^{\infty} C_{\text{kw}} d\tau} - \frac{t_{\text{slug}}}{2} \quad (3.161)$$

Note both equations give the same value of the mean residence time.

Defining the time be origin shifted to the center of the slug,

$$\hat{t} = t - \frac{t_{\text{slug}}}{2} \quad (3.162)$$

when the tracer is injected $-\frac{t_{\text{slug}}}{2} \leq \hat{t} \leq \frac{t_{\text{slug}}}{2}$. Then the mean residence time can be written as

$$\bar{\hat{t}} = \int_0^{\infty} \left(1 - \frac{\int_0^{\hat{t}'} C_{\text{kw}} d\hat{t}}{\int_0^{\infty} C_{\text{kw}} d\hat{t}} \right) d\hat{t}' \quad (3.163)$$

This implies that tracer slug injection can mimic continuous tracer injection by

$$C_D = \frac{\int_0^{\hat{t}'} C_{\text{kw}} d\hat{t}}{\int_0^{\infty} C_{\text{kw}} d\hat{t}} \quad (3.164)$$

which satisfies

$$\bar{\hat{t}} = \int_0^{\infty} (1 - C_D) d\hat{t}' \quad (3.165)$$

and

$$c_D|_{\hat{t}'=0} = \frac{\int_0^0 C_{\text{kw}} d\hat{t}}{\int_0^{\infty} C_{\text{kw}} d\hat{t}} = 0 \quad (3.166)$$

$$c_D|_{\hat{t}'=0} = \frac{\int_0^{\infty} C_{kw} d\hat{t}}{\int_0^{\infty} C_{kw} d\hat{t}} = 1 \quad (3.167)$$

Thus, the tracer slug injection has been converted to an equivalent continuous tracer injection. The sweep efficiency has been calculated using these equations and is illustrated in Chapter 4.

3-3 SUMMARY OF CHAPTER

The following section is the summary of the method of moments.

The pore volume, the volume of oil, and the oil saturation can be estimated with the tracers injected with slug as following:

$$V_p = q_{pro} \frac{(K_T - 1)\bar{t}_1 + \bar{t}_2}{K_T} \quad (3.168)$$

$$V_o = q_{pro} \frac{-\bar{t}_1 + \bar{t}_2}{K_T} - \sum_{wells} \left(q \int_t^{\infty} f_o d\tau \right) \quad (3.169)$$

$$S_o = \frac{-\bar{t}_1 + \bar{t}_2 - \frac{K_T}{q_{pro}} \sum_{wells} \left(q \int_t^{\infty} f_o d\tau \right)}{(K_T - 1)\bar{t}_1 + \bar{t}_2} \quad (3.170)$$

where

$$\bar{t}_\kappa = \frac{\int_0^\infty \tau \left(\sum_{\ell=1}^{n_p} f_\ell (C_{\kappa\ell} - C_{\kappa\ell I}) \right) d\tau}{f_1 (C_{\kappa 1 J} - C_{\kappa 1 I}) t_{\text{slug}}} - \frac{t_{\text{slug}}}{2} \quad (3.171)$$

The pore volume, the volume of oil, and the oil saturation can be estimated with the tracers injected continuously and with natural tracer as following:

$$V_p = q_{\text{pro}} \frac{(K_{T2} - 1)\bar{t}_1 + \bar{t}_2}{K_{T2}} \quad (3.172)$$

$$V_o = q_{\text{pro}} \frac{-\bar{t}_1 + \bar{t}_2}{K_T} \quad (3.173)$$

$$S_o = \frac{-\bar{t}_1 + \bar{t}_2}{(K_T - 1)\bar{t}_1 + \bar{t}_2} \quad (3.174)$$

where the mean residence time for continuously injected tracer and natural tracer are given by respectively

$$\begin{aligned} \bar{t}_\kappa &= \left(\sum_{\ell=1}^{n_p} K_{T\kappa\ell} \int_0^\infty f_\ell d\tau \right)_{\text{injector}} \\ &\quad - \left(\sum_{\ell=1}^{n_p} K_{T\kappa\ell} \int_0^\infty f_\ell \frac{C_{\kappa\ell} - C_{\kappa\ell I}}{C_{\kappa 1 J} - C_{\kappa 1 I}} d\tau \right)_{\text{producer}} \\ &= \sum_{\ell=1}^{n_p} K_{T\kappa\ell} \left[\left(\int_0^\infty f_\ell d\tau \right)_{\text{injector}} - \left(\int_0^\infty f_\ell \frac{C_{\kappa\ell} - C_{\kappa\ell I}}{C_{\kappa 1 J} - C_{\kappa 1 I}} d\tau \right)_{\text{producer}} \right] \quad (3.175) \end{aligned}$$

$$\bar{t}_K = \left(\int_0^\infty \left(1 - (f_w + K_{TK} f_o) \frac{C_{KwI} - C_{Kw}}{C_{KwI}} \right) d\tau \right) \Big|_{\text{producer}} \quad (3.176)$$

Chapter 4: Analysis of Partitioning Interwell Tracer Tests

4-1 APPLICATION OF METHOD OF MOMENTS

The method of moments was tested with synthetic tracer data generated with numerical simulations of tracer floods under a variety of reservoir conditions. These results are presented and discussed in this chapter.

4-1-1 Sweep Efficiency from Tracer Slug Injection

This case, run number of 2D-TRA06, illustrates the calculation of swept pore volume for single-phase flow. Tracer was injected into a homogeneous reservoir with a quarter five-spot well pattern with dimensions of 165 ft x 165 ft x 5 ft. A 30x30x1 grid was used to simulate the tracer flood. The porosity is 0.25 and the permeability is 200 md. The pore volume is 34,031 ft³. The tracer slug was injected for 1.815 days with 375 ft³/day of water. The slug size is 0.02 PV. In addition to the tracer slug, another tracer was injected continuously. The flow rate is 375 ft³/day. The simulations were performed with UTCHEM.

Figure 4.1 shows the produced tracer concentrations for both slug and continuous tracers. Figure 4.2 shows the swept pore volume calculated from the produced tracer concentrations injected in the tracer slug using the method of moments. The swept pore volume was also obtained directly from the concentration profiles of the continuous tracer at several times, specifically at 42 days, 82 days, 122 days, 162 days, and 202 days. Figure 4.2 shows very good agreement between these two values of swept pore volume. Both curves reach the total pore volume after about 200 days when the normalized tracer concentration from the slug has declined to about 0.001, which implies a detection limit of 10 ppm would be needed if 1000 ppm were injected and the goal were to measure the

entire pore volume. In this case, the swept pore volume can be divided by the total pore volume to convert it to a sweep efficiency, as shown in Figure 4.3.

Figure 4.4 shows the same case but with less complete tracer data used for the analysis due to an assumed higher detection limit for the measured tracer concentration. When tracer concentration data are plotted on a semi log scale as shown in Figure 4.1, the data sometimes follow a linear decline that can be extrapolated. This is illustrated in Figure 4.4 starting at 152 days when the normalized concentration is 0.003. Using the extrapolated curve will often improve the estimate of swept pore volume. Figure 4.5 shows the calculated swept pore volume without extrapolation of the data past 152 days and Figure 4.6 shows it with extrapolation. Although the extrapolation underestimates the tracer concentration in this example, the estimated swept pore volume of 33,734 ft³ is only 1% less than the true value of 34,031 ft³. This is a significant improvement over the value without extrapolation.

A heterogeneous permeability field was stochastically generated using the FFT software for Dykstra-Parsons coefficients of 0.6 and 0.8 for run numbers 2DHT02 and 2DHT04, respectively. The input file for Run 2DHT04 is in Appendix A. The same reservoir but with different permeability distributions was simulated to generate the produced tracer history as shown in Figure 4.7. For higher heterogeneity, earlier tracer breakthrough and a longer tail are observed. Figure 4.8 shows the sweep efficiency calculated from Figure 4.7. Low sweep efficiency for high heterogeneity is observed.

4-1-2 Lawyer Canyon Reservoir Simulations

The derivation of the method of moments was first tested with a three-dimensional stochastic reservoir model for both tracer injected as a slug and tracer injected continuously. This case tests the method for single-phase flow of water at residual oil saturation. The reservoir data used for this example was obtained from a

study of Lawyer Canyon area located in New Mexico and West Texas done by the Bureau of Economic Geology of the University of Texas (Jennings *et al.*, 2000). Measurements were made on the San Andres carbonate outcrop along a 17 mile continuous exposure of the Algerita Escarpment in the Guadalupe Mountains.

The size of the model reservoir simulated to evaluate a PITT is 150 ft x 150 ft x 15 ft. The geological model represents one of the cycles in the formation. The grid was 300x30x30 with 300 gridblocks in the x-direction, 30 gridblocks in the y-direction and 30 gridblocks in the vertical z-direction. The porosity is 0.15. Figure 4.9 shows the permeability distribution for a vertical cross section of the reservoir at $J=1$. The log mean permeability is 13.7 md and the Dykstra-Parsons coefficient is 0.87. The simulations were performed with ECLIPSE.

The well is located at the corners of the reservoir, making a quarter of five-spot well pattern. Both injector and producer are controlled by bottomhole pressure of 4000 psia and 1000 psia, respectively. The tracers are injected for 10 days. The input file run number KVTR48 is in Appendix B. Figure 4.10 shows the tracer concentration history. Tracers with partition coefficients of 0, 0.5, 1, and 2 were used. The partitioning tracers are retarded by the residual oil in the reservoir, so later breakthrough and lower peak concentrations compared to the conservative tracer are observed. The tracer data shown in Figure 4.10 were used to calculate the oil volume, oil saturation, and swept pore volume in the reservoir (Figures 4.11 through 4.13). Swept volume is obtained from the conservative tracer. Note that the oil volume in the reservoir is 2705 bbl, the average oil saturation is 0.30, and the pore volume that can be contacted by a conservative tracer is 6311 bbl. Also note that 1 PV injection takes 93.7 days. All of the estimated quantities approach the true reservoir values at long times. Figures 4.14 and 15 show sweep efficiency calculated from the conservative tracer data by dividing the swept water

volume by the total volume of water. Even though the reservoir is heterogeneous, the tracer sweeps most of the pore volume at 1.5 PV of water injection.

Tang and Harker (1991b) proposed the technique to analyze PITT to estimate residual oil saturation, which is called landmark comparison technique. The theory is based on the chromatographic transformation of produced tracer concentration. From the analytical solution of tracer transport equation, the partitioning tracer response is retarded as a factor of $1 + \frac{K_T S_o}{1 - S_o}$, or

$$t_{p,r} = t_{c,r} \left(1 + \frac{K_T S_o}{1 - S_o} \right) \quad (4.1)$$

where $t_{c,r}$ is the tracer production time for a conservative tracer and $t_{p,r}$ is the tracer production time for a partitioning tracers. The set of produced times are obtained to solve for S_o ,

$$S_o = \frac{t_{p,r} - t_{c,r}}{t_{p,r} - (K_T - 1)t_{c,r}} \quad (4.2)$$

Tang (1995) showed that the landmark comparison and equal recovery is equivalent, by which the tracer recovery curves for a conservative and a partitioning tracer are compared. For given values of tracer recovery, the production time can be read from Figure 4.16, and then used in Equation (4.2) to calculate the average oil saturation as shown in Figure 4.17. The estimate is in the range of 0.27 and 0.29, which is close to the reservoir value of 0.30. In comparing with Figure 4.11, which is estimated from the method of moments, the Landmark method approaches to the reservoir oil saturation

value more quickly, but it does not reach it. Note that this Tang's method is not estimating oil volume, swept pore volume, and sweep efficiency. Very low oil saturation seen in ground water applications does not give a separation in the peak concentration as seen in Jayanti (2003), where the Tang's method is not applicable.

Another case, run number KVTR47, was simulated for the same reservoir, but with a spatially variable residual oil saturation distribution rather than a uniform value. The residual oil saturation was correlated to the permeability as follows (Sinha, 2003):

$$S_{or} = \exp(-0.8k_x^{0.1}) \quad (4.3)$$

The average residual oil saturation is 0.354 and the oil volume in the reservoir is 3193 bbl. The reservoir with this residual oil saturation distribution and a heterogeneous permeability was simulated to generate a tracer response, which is shown in Figure 4.18. From the tracer data, the oil volume and oil saturation were calculated using the method of moments Figures 4.19 and 4.20. The swept pore volume and sweep efficiency calculated from a conservative tracer are shown in Figure 4.21 through 4.23. Most of the reservoir is swept even though it is heterogeneous. Figure 4. 24 shows the tracer recovery, which can be used to estimate oil saturation using the Landmark method shown in Figure 4. 25. The Landmark method gives an average oil saturation of about 0.35, which is close to the reservoir average oil saturation of 0.354. The oil saturation calculated from the Landmark method approaches the reservoir oil saturation much sooner than the value calculated from the method of moments.

4-1-3 South Wasson Clear Fork Reservoir Simulations

The method of moments was next tested with a three-dimensional heterogeneous reservoir with multiple wells using a reservoir model obtained from the study of the

South Wason Clear Fork field located in Yoakum County, Texas. The reservoir model is based on the porosity and permeability data measured from the outcrop of this formation. There are two thick oil-producing reservoirs—the middle and lower Clear Fork. The middle Clear Fork reservoir has a thickness of about 700 ft (Lucia *et al.*, 2001). The geological model includes large-scale heterogeneity comprised of a series of rock-fabric flow layers and geologic layering architecture (Jennings *et al.*, 2002, Lucia *et al.*, 2003).

The well pattern is shown in Figure 4.26. There are 5 injectors and 15 producers. The area between wells SW8502 and SW8536 was simulated for this demonstration. The total area is 2924 ft x 3096 ft. The average thickness in this model of the middle Clear Fork is 584 ft and the average porosity is 0.0366. 17x18x96 gridblocks were used. Water was injected at residual oil saturation. The simulation was made with ECLIPSE.

Figure 4.27 shows the tracer response at production well SW8536 for the tracer injected from injection well SW8502. The average oil saturation in the reservoir is 0.30. Figure 4.28 shows the oil saturation calculated from the tracer response. The oil saturation is still increasing but has reached a value of only 0.23 after 15,000 days. It would not be practical to conduct a PITT under these conditions of low permeability, large well spacing and low production rates, so additional studies of this case were not pursued. However, this example could be used to show how a water flood in such a reservoir does not completely sweep the reservoir due to the high heterogeneity. Thus, tracers could in principle be used to locate unswept oil, but infill drilling, horizontal wells, hydraulic fractures or other methods would be needed to do so in a reasonable time.

4-1-4 Tracer Tests with Mobile Oil

The 3D simulation domain is a quarter of a five-spot well pattern with dimensions of 660 ft long, 660 ft wide and 50 ft thick (Sinha *et al.*, 2004). A heterogeneous permeability field was stochastically generated using the FFT software. The permeability field has a log mean permeability of 344 md and a Dykstra-Parsons coefficient of 0.81. The correlation lengths are 100 ft in the horizontal direction and 10 ft in the vertical direction. A uniform residual oil saturation of 0.25 was used. The reservoir has a uniform porosity of 0.2. A tracer slug consisting of a conservative tracer and three partitioning tracers with partition coefficients of 0.5, 1.0 and 2.0 was injected for 0.1 PV during the waterflood while there was still mobile oil present in the reservoir. The simulations were performed with UTCHEM.

To simulate tracer tests with different volumes of mobile oil initially in the reservoir, tracer tests were started at different stages of the waterflood. The tracer tests were started after 0.5, 1.0, 1.5, 2.0, 2.5 and 3.0 PV of water injection. The oil saturation is estimated after 7.0 PV of chase water injection using the method of moments. In practice, shorter times could be used with some extrapolation of the tracer concentration data. A sensitivity study was carried out with waterflood end point mobility ratios of 0.5, 1.2, and 5.2.

Figure 4.29 shows the oil production rate for the waterflood simulation with an end point mobility ratio of 1.2. Since oil is being produced and partitioning tracers are used, some of the tracer is in the oil as well as in the water. Figures 4.30 and 4.31 show the tracer concentration curves for water and oil for a simulation with tracer injection starting 0.5 PV after the waterflood starts. Equations (3.71) and (3.86) were used to calculate the oil saturation using the total tracer concentration rather than the aqueous values as in previous examples. The total tracer concentration can be obtained by either

directly measuring the tracer concentrations in both the produced water and oil, or by measuring only the concentrations in the water and then calculating the oil concentration from the measured partition coefficient, but this would mean more uncertainty in the estimate.

Figure 4.32 shows the total tracer concentrations for the same case. Figure 4.33 shows a comparison between the estimated oil saturation and the oil saturation using total tracer concentrations. Figures 4.34 and 35 shows oil saturation comparison with an end point mobility ratio of 0.5 and 5.2, respectively. Tables 4.1 through 4.3 summarize the results for the different cases. The maximum difference between the average oil saturation during the PITT and the oil saturation estimated from the PITT is 0.01. Some adjustment in the oil saturation would be needed to estimate the oil saturation at the end of the PITT rather than an average value during the PITT. In these examples, the differences are small. One approach would be to use the PITT estimates to condition a simulation and then predict the oil saturation at other times using the simulator, ideally incorporating other conditioning data at the same time.

In example INV02#4, a PITT was simulated in an inverted, confined, 40 acre five-spot well pattern (Table 4.4). ECLIPSE was used in this and subsequent examples. A constant injection rate of 6000 bbl/day was used. The producer was constrained to produce at a constant bottom hole pressure of 2000 psia. A stochastic permeability field with the properties shown in Table 4.4 was generated using the FFT method. The simulations were performed with ECLIPSE.

Figures 4.36 and 4.37 show the permeability distribution of the most and the least permeable layers with a Dykstra-Parsons coefficient of 0.81. The reservoir was water flooded for 2000 days before the tracer injection (99% water cut). The oil production rate from the start of tracer injection is shown in Figure 4.38. Total simulation time is 6000

days (12 PV). Four tracers were injected as a slug for 50 days (0.1 PV) with partition coefficients of 0, 0.5, 1, and 2. The results illustrated below were calculated using the tracer with a partition coefficient of 2.

Tracer concentration plots for each production well are given in Figures 4.39 through 4.42. In Figures 4.39 and 41, tracer breakthrough is quite early and the tracer curves have sharp peaks. This can be explained as due to the high permeable channels around production PROD-1 and PROD-3. Early breakthrough of the tracers in these production wells is clearly seen in Figure 4.43, which show the tracer concentration profiles at 35 days after the tracer injection in layer 8, the most permeable layer.

Figure 4.44 shows the oil saturation calculated between the injector and each producer using the method of moments. Table 4.5 shows the difference between these results and the reservoir oil saturation values in each quadrant at the end of the simulation. In the first row of Table 4.5, the residual oil saturation in the reservoir is given as 0.234. This value is calculated by subtracting the amount of oil produced (ECLIPSE output) from the initial oil saturation and is smaller than the input value of 0.25, which implies there is some numerical error in this result.

The difference between the method of moment results and the reservoir values vary between -0.035 and -0.001. The biggest difference is seen in the oil saturation between the injector and PROD-1. Tracer concentrations at the end of the flood are higher in the region between production PROD-1 and PROD-3 than between PROD-2 and PROD-4 (Figure 4.46). Figure 4.45 and Table 4.6 show the swept pore volumes between the injector and each producer. After 4000 days from the start of the PITT, 98.4% of the reservoir is swept and oil saturations for each quadrant were estimated within acceptable errors. Figures 4.47 and 4.48 show the oil saturation distribution profiles in the 1st and the 2nd layers at the end of the simulation.

In example INV02#5, all parameters were kept the same as the previous full five-spot example except the Dykstra-Parsons coefficient was increased to 0.90 to see how this would affect the PITT results. Figures 4.49 and 4.50 show the permeability distribution of the most and the least permeable layers. The reservoir was water flooded for 2000 days (99% water cut) before the PITT. A slug with four tracers was injected for 50 days (0.1 PV). The oil saturation distribution at the beginning of the PITT is shown in Figures 4.51 and 4.52. Tracer production curves are shown in Figures 4.53 through 4.56. Figures 4.57 and 4.58 show the tracer concentration profiles for layers 5 and 8 for the tracer with a partition coefficient of 2.

Figure 4.59 shows the swept pore volume between the injector and each producer. Not all of the reservoir has been swept after 5000 days since the swept pore volume is still increasing. Figure 4.60 shows the average oil saturation calculated in the swept pore volume. The values calculated from the first temporal moment are approaching the true values after about 3500 days although they are still low because of incomplete sweep at this time. Table 4.7 compares the average oil saturations for each swept pore volume at the end of the simulation. The results are still good even though the reservoir is much more heterogeneous than the first case. Table 4.8 shows the swept pore volumes and sweep efficiency at the end of the PITT.

In example INV02#7, an unconfined, inverted 20-acre five-spot well pattern was simulated with the same reservoir parameters used in the confined five-spot well pattern with a Dykstra-Parsons coefficient of 0.81. The reservoir was water flooded for 1000 days (99% water cut) and then a tracer slug was injected for 50 days (0.1 PV). Total simulation time was 6000 days.

Figures 4.61 and 4.62 show the oil saturation in the least and most permeable layers (layers 5 and 8) at the beginning of the tracer injection. Figures 4.63 and 4.64

show the conservative tracer concentration in those 2 layers at 50 days. Figures 4.65 and 4.66 show the conservative tracer concentration at 6000 days.

Figures 4.67 through 4.70 show the tracer concentration histories for tracers with partition coefficients of 0, 0.5, 1, and 2 and all four producers. There is almost no separation in the tracer peaks in this example although the tracer with a partition coefficient of 2 does show a small lag compared to the conservative tracer. Almost all of the separation between the partitioning tracers and the conservative tracer is in the tails i.e. almost all of the signal is in the long tails. Any attempt to calculate oil saturation from the separation of the peaks would be futile and subject to very large errors. The method of moments is able to capture the signal in the tails but only if accurate concentration data are available at long times.

Figure 4.71 shows the swept pore volumes, and the swept pore volume is still increasing even after 3500 days. Figure 4.72 shows the sweep efficiency.

The oil saturation values in each swept pore volume are shown in Figure 4.67 and Table 4.9. The largest error in the estimated oil saturation is for the swept pore volume between the injector and production well 2, which has a very low permeability region. Table 4.10 summarizes the swept pore volumes.

In example INV02#8, tracer injection began after 250 days of water flooding (0.5 PV and 77% water cut). The purpose of this example was to test the method of moments for a case with more mobile oil to verify that the generalized method as derived in this dissertation can be used to give a good approximation to the oil saturation even if it is far above residual oil saturation.

Figures 4.74 and 4.75 show the oil saturation in the reservoir at the beginning of the tracer flood. Figures 4.76 through 4.79 show the tracer concentrations for each production well. In Figures 4.77 through 4.79, early tracer breakthrough is observed.

Figures 4.80 and 4.81 show the tracer concentration in layers 8 and 5 after 25 days of tracer flooding and also shows the early breakthrough at production wells 2, 3 and 4. Figures 4.82 and 4.83 show the tracer concentration in layers 8 and 5 at the end of the simulation. Most of the tracer was recovered except past the four production wells.

Figures 4.84 and 4.85 show the swept pore volumes and the oil saturations calculated from the method of moments. Table 4.11 summarizes the oil saturation values. Table 4.12 shows the swept pore volumes. Although the tracer injection started at 77% water cut, mobile oil in the reservoir didn't increase the error in the estimated oil saturations compared to the previous example with the PITT starting at 99% water cut. However, the oil saturation in the reservoir is close to the residual oil saturation at the end of simulation as shown in Figures 4.86 and 4.87.

4-1-5 Natural Tracer Simulations

Natural tracers from the crude oil in a naturally fractured reservoir were simulated for the first test case. The reservoir size is 500 ft x 500 ft x 50 ft. The fracture permeability is 100 md and the matrix permeability is 1 md. The porosity of fracture and matrix are 0.01 and 0.24, respectively. The oil saturation in fracture and matrix are 0.001 and 0.301, respectively. The average oil saturation is 0.289. The simulations were performed with UTCHEM. The input file for Run TZ9857 is in Appendix C.

In this example, two organic components that partition from the crude oil to the water are used as the partitioning tracers. The solubility can be transformed to partition coefficient, and the partition coefficients are 0.1 and 1, which are a unique property of the component.

Figure 4.88 shows the oil component concentration normalized with the initial concentration. Figure 4.89 shows the oil saturation calculated from the oil component

concentration plotted in Figure 4.88. The average oil saturation is 0.289, so the estimate value from the natural tracers is very accurate even in this naturally fractured reservoir.

Figure 4.90 shows that natural tracers and injected tracers behave the same. This observation is beneficial since numerical simulations using commercial simulators can be performed with injected tracers whereas natural tracers, i.e. dissolved oil components in water, cannot be simulated with most of these reservoir simulators (UTCHEM is an exception).

Figure 4.91 shows the produced tracer data for a tracer slug injected for 10 days with partition coefficients of 0 and 1. The oil saturation is estimated with the tracer data shown in Figure 4.92 for both the continuous tracer and the natural tracer. Both estimates approach the reservoir average oil saturation of 0.289, but the tracer injected in a slug takes longer to reach to the plateau. For example, the oil saturation estimate to 0.28, 1% saturation difference from reservoir saturation, can be reached by 2400 days with continuous tracers but by 3500 days with slug tracers. Therefore, the natural tracer is more useful than the injected tracer with slug especially for very heterogeneous reservoirs such as naturally fractured reservoirs, since it generally takes time to produce enough tracer data to analyze. Even though the approaching oil saturation is the same, but the convergence is not. Therefore, the idea of converting the slug tracer data to a conservative tracer data becomes useful using Equation (3.167) as shown in Figure 4.93. Note that the converted slug tracer and the continuous tracer coincide almost perfectly for both tracers. Once the slug tracers are converted into continuous tracers, then the oil saturation can be estimated from equations for continuous tracers, which converges quicker as seen in Figure 4.92.

The sensitivity to subgridding of the matrix blocks was studied for a fractured reservoir similar to the previous case. The only difference is porosity. The fracture

porosity is 0.009975 and the matrix porosity is 0.237606. Figure 4.94 shows the normalized natural tracer concentration with a partition coefficient of 0.001. Figure 4.95 shows the normalized natural tracer concentration with a partition coefficient of 1.0. Four subgridding schemes were compared (1) no subgridding 1x1, (2) 4x1, (3) 4x8, and (4) 32x1. These figures show that the tracer concentrations are not sensitive to the subgridding for this particular problem.

4-2 PITT ANALYSIS WITH INVERSE MODELING PROGRAM

4-2-1 Sensitivity Study of Inverse Program

4-2-1-1 Sensitivity to Initial Guess

The inverse modeling program from TAMU was with synthetic tracer data from a layered reservoir with a quarter of a five-spot well pattern (Altinay, 2005). The reservoir dimensions are 660 ft x 660 ft x 50 ft. The log mean permeability of the reservoir is 256 md and the porosity is 0.20. A 22 x 22 x 10 grid was used for the forward simulations with ECLIPSE. The residual oil saturation was correlated to the permeability in Equation (4.3) and the average oil saturation was 0.2585. A partition coefficient of 2 was used in this sensitivity study.

The inverse modeling program was tested with various guesses of initial oil saturation. The initial oil saturation guesses from 0.14 to 0.38 were selected to evaluate convergence of the inverse modeling program with the initial guesses far from the true average value. Figures 4.96 through 4.98 show the vertical oil saturation calculated from the inverse code. Figure 4.96 is for the case that the initial oil saturation guess is less than the true saturation. Figure 4.97 is for the case that the initial oil saturation guess is more than the true saturation. Figure 4.98 is for the case that the initial oil saturation

guess is far away from the true saturation. Table 4.13 shows the oil saturation calculated using the inverse model for each of these initial guesses and the differences between the forward and inverse model values. The input file for Run INV04UP2#10 is in Appendix D.

The Root Mean Square (RMS) error in the travel time and amplitude for each iteration is shown in Figure 4.99 for the run with an initial oil saturation guess of 0.21. The calculation converges after 4 iterations. The computational time for this and other similar runs done using a PC with a 3 GHz processor was about 15 minutes. The match between the inverse and forward model tracer curves is shown in Figure 4.100 for all layers and for the least and most permeable layers in Figures 4.101 and 4.102. There is only a small difference in the tail of the curves shown in Figures 4.100 and 4.101 for all layers and for the least permeable layer, respectively. The estimated oil saturation distribution in layer 5 is shown in Figure 4.103. Figure 4.104 shows the difference in oil saturation from the forward model. The oil saturation is correctly estimated where the tracer is flowing, but is not accurately estimated along the edges of the reservoir where there is no tracer in the pathlines. Therefore, if the initial guess of oil saturation is lower than the reservoir value, the estimate from the inverse model tends to give lower saturation. Figures 4.105 and 106 show the oil saturation and the difference in oil saturation in layer 8. The reservoir saturation in this layer is 0.201, which is close to the initial guess of 0.21. The difference in oil saturation in this layer is very small.

The RMS error for an initial oil saturation guess of 0.28 is shown in Figure 4.107. The tracer curve matches are all very good as shown in Figures 4.108 through 4.110. Figure 4.111 shows the RMS error for an initial oil saturation guess of 0.30 showing that the errors are not decreasing with iterations. Tracer curve matches for the 1st iteration are shown in Figures 4.112 to 4.114.

The results of RMS errors and the tracer curve matches are shown in Figures 4.115-4.122 and Table 4.13. The general trend of the vertical oil saturation distribution is captured, but the RMS error in the oil saturation of 4% is much larger than with better initial guesses. Matches of the tracer concentration curves for the 4th iteration are shown in Figures 4.116 through 4.118. The poor tracer concentration match for the 5th layer, is noticeable, as shown in Figure 4.117. Figure 4.119 shows the RMS error for an initial oil saturation guess of 0.38. The smallest RMS error is at iteration 10. Figures 4.120 through 4.122 show the matches of the tracer curves. Again a poor curve match is noticeable for the least permeable layer 5, as shown in Figure 4.121.

These results show the importance of a good initial guess for the oil saturation. When the initial guess is sufficiently close to the true value, the calculation converges very fast after only a few iterations to values that are close to the true values in each layer and the match between the forward and inverse curves is close. An important conclusion is that using the method of moments to provide the initial guess of the average oil saturation is very beneficial in terms of getting satisfactory results from the inverse model.

4-2-1-2 Sensitivity to Tracer Concentration Detection Limit

The tracer concentration detection limit is an important design variable for any tracer flood and is highly variable depending on the tracers, the analytical measurement method, the duration of the sampling or logging and other factors. Some tracers can be detected down to parts per billion, but this may be expensive or require sampling for long periods of time. Thus, there is a big economic incentive to determine the accuracy of a PITT to the tracer detection limit (TDL). Also, the effect of the TDL needs to be determined for different methods of interpretation. For example, most of the tracer curve data must be accurately measured for the method of moments to yield accurate estimates

of oil saturation. Extrapolation of the tracer tails helps, but the uncertainty of the estimates increases since an exponential extrapolation may not always be appropriate and the noise in the data at low concentrations where the extrapolation is started is often higher than desired. Simulation of the tracer tails with parameters fit to the higher concentration tracer data using an inverse model is in principle a better way to extrapolate such tails. In this section, this idea is tested using the TAMU inverse modeling program. The same reservoir case with a partition coefficient of 2 used to study the sensitivity of the guess of the initial oil saturation was used for the study with the inverse model.

Figure 4.123 shows the calculated vertical oil saturation distribution for normalized tracer concentration detection limits of 0.0001, 0.001 and 0.01 for the cases with the initial oil saturation guess of 0.26. If 1000 ppm of tracer were injected, then a normalized TDL of 0.0001 would correspond to 0.1 ppm. TDLs are typically anywhere from 0.01 to 10 ppm.

The results for TDLs of 0.0001 and 0.001 are equally good, but the error starts to increase at 0.01 (Table 4.14). The calculation for a TDL of 0.0001 converges in 5 iterations as shown in Figure 4.124. For a TDL 0.001, six iterations are needed as shown in Figure 4.125. For a TDL of 0.01, the calculation does not converge as shown in Figure 4.126, so iteration 4 was used in this case. Tracer curve matches are very good as shown in Figures 4.127 through 4.129.

Figure 4.130 and Table 4.15 shows the calculated vertical oil saturation distribution for normalized tracer concentration detection limits of 0.0001, 0.001 and 0.01 for the case with an initial oil saturation guess of 0.30. The RMS errors are shown in Figures 4.131 through 4.133 for TDLs of 0.0001, 0.001 and 0.01. Figures 4.134 through 4.136 show the tracer curve matches.

The inverse model extrapolates the tracer concentration data very well even at the high detection limit of 0.01 although the oil saturation at this TDL is poor compared to the estimates at the smaller TDLs.

4-2-2 Inverse Modeling of PITTs with Mobile Oil

Next the inverse program was used to model PITTs with mobile oil (two-phase flow in the reservoir). A very simple reservoir with a uniform permeability (100 md) and porosity was model as the first test case. The reservoir parameters are tabulated in Table 4.16. There are two layers with different oil saturations and each layer is 25 ft thick. The reservoir dimensions are 660 ft x 330 ft x 50 ft (5 acres). The porosity is 0.2 and the pore volume is 387,900 bbl. 500 Bbl/day of water were injected into each layer. The vertical permeability was zero so there would be no cross flow between layers. A partitioning tracer with a partition coefficient of 10 was injected for 50 days (0.129 PV) as a slug followed by chase water. Table 4.17 is a summary of the runs made for this study.

First, five simulations were done to evaluate the sensitivity of the tracer response to relative permeability and viscosity. Figures 4.139 and 4.140 show the two relative permeability curves Figures 4.141 through 4.143 show the fractional flow curves. Second, four simulations (Table 4.18) were made to evaluate the sensitivity to the initial guess of oil saturation in the reservoir using the data set from Run 500. Run 511 was made with the total injection rate specified rather than specifying it for each layer.

The mobile phase affects the velocity of the tracer. The retardation is locally proportional to $\frac{S_w + K_T S_o}{f_w + K_T f_o}$ as shown in Figures 4.144 through 4.148. Each figure shows how the oil saturation is sensitive to the tracer production data for both single-phase flow and two-phase flow. For single phase flow, the degree of the retardation increases monotonically, but for two-phase flow it does not. In Run 000 in Figure 4.144,

the tracers are not sensitive when the oil saturation is low or high, i.e. $0.3 < S_o < 0.35$ or $0.6 < S_o < 0.7$. This insensitivity implies that the inverse code may fail to converge to the true saturation. In other words, the inverse code may work in the oil saturation is between 0.35 and 0.6. In Run 600 shown in Figure 4.145, the inverse code may work in the range of $0.4 < S_o < 0.7$. Figures 4.146 and 4.147 show the sensitivity for Runs 200 and 100. Under these specific relative permeability curves and viscosities, the sensitivity is monotonically decreasing with oil saturation, as seen for single-phase flow. In Run 500 shown in Figure 4.148, the tracer sensitivity is monotonically changing in the range of $0.3 < S_o < 0.45$ and $0.5 < S_o < 0.7$, where the inverse code may work. This sensitivity study shows that there is a possibility that the inverse code may work well for some particular conditions, but not in general.

After seeing the sensitivity to oil saturation and the initial oil saturation guess, the relative permeability and the viscosity were chosen for further inverse modeling simulations. For Run 500, the oil saturation in layer 1 is 0.4 and in layer 2 it is 0.6. The initial guesses of the oil saturation are tabulated in Table 4.17 for Runs 511, 512, 513, and 514.

Figure 4.149 shows that 6 iterations are enough to reduce the error in this case. Figures 4.150 and 4.151 show the tracer response matches in both layers after the 6th iteration. The inverse code performs well to match the curve in both layers. In layer 1, the tracer response from the inverse model is merging to that from the forward model. In layer 2, the initial guess brings good enough tracer response that no significant changes in tracer response are seen. Figures 4.152 and 4.153 show the oil saturation match in each layer. The saturation in layer 1 is estimated very well, while that in layer 2 is estimated not as good as in layer 1. However, the estimation is going towards the right direction, or the oil saturation is increased from the low initial guess, which is supposed to be. Recall

that Figure 4.151 shows that the initial guess gives good response in the produced concentration.

Figures 4.154 through 4.158 are the results from Run 512 with initial guesses different from that of Run 511. The results from Runs 513 and 514 are shown in Figures 4.159 to 4.163 and Figures 4.164 through 4.168, respectively. The results from these runs with the different initial guesses show that the inverse code works well regardless of the initial guess in reducing the matching error, in matching the tracer response, and in matching oil saturation.

Finally the inverse code was run without controlling flow rate in each layer. The total injection rate is kept the same as in Run 511 of 1000 bbl/day, but the flow rate in each layer is changing with time in layers by not controlling flow rate for each layer as shown in Figure 4.169. Figure 4.170 shows the error with iterations. The inverse code does not offer converging result and the errors are much larger than the previous cases that converged.

The study of the PITT with mobile oil using the inverse program concludes that:

1. For two-phase flow, the velocities of the tracers are not monotonic to oil saturation whereas it is for single-phase flow.
2. The tracer response is not really sensitive to the oil saturation in the reservoir because most of the tracer is in the water behind the oil bank.
3. The flow rate change seems to affect the inverse calculation more seriously than the initial oil saturation in the reservoir does.

Table 4.1: Estimated Oil Saturation for a Waterflood with an End Point Mobility Ratio of 0.5

PV of Water Injected Before Initiating Tracer Test	Average Oil Saturation During Tracer Test	Estimated Oil Saturation from PITT	Difference in Oil Saturation
0.5	0.262	0.259	0.003
1.0	0.259	0.257	0.002
1.5	0.259	0.254	0.005
2.0	0.257	0.254	0.003
2.5	0.257	0.253	0.004
3.0	0.256	0.252	0.004

Table 4.2: Estimated Oil Saturation for a Waterflood with an End Point Mobility Ratio of 1.2

PV of Water Injected Before Initiating Tracer Test	Average Oil Saturation During Tracer Test	Estimated Oil Saturation from PITT	Difference in Oil Saturation
0.5	0.286	0.285	0.001
1.0	0.280	0.279	0.001
1.5	0.276	0.274	0.002
2.0	0.273	0.270	0.003
2.5	0.271	0.267	0.004
3.0	0.269	0.265	0.004

Table 4.3: Estimated Oil Saturation for a Waterflood with an End Point Mobility Ratio of 5.2

PV of Water Injected Before Initiating Tracer Test	Average Oil Saturation During Tracer Test	Estimated Oil Saturation from PITT	Difference in Oil Saturation
0.5	0.326	0.347	-0.011
1.0	0.326	0.333	-0.007
1.5	0.318	0.322	0.004
2.0	0.315	0.315	0.000
2.5	0.310	0.308	0.002
3.0	0.306	0.303	0.003

Table 4.4: Reservoir Description for Run INV02#4

Grid	44x44x10
Gridblock Size, ft x ft x ft	30x30x5
Reservoir Dimensions, ft x ft x ft	1320x1320x50
Drainage Area, acres	40
Porosity	0.2
Reservoir Pore Volume, bbl	3,103,117
Horizontal Correlation Length, ft	100
Vertical Correlation Length, ft	10
Dykstra-Parsons Coefficient	0.81
Log Mean of Permeability, md	312
Initial Oil Saturation	0.7
Residual Water Saturation	0.3
Residual Oil Saturation	0.25

Table 4.5: Comparison of Oil Saturation for Run INV02#4

Quadrant	PROD-1	PROD-2	PROD-3	PROD-4
Average Oil Saturation	0.258	0.261	0.254	0.254
Estimated Oil Saturation	0.223	0.247	0.240	0.253
Difference	-0.035	-0.014	-0.014	-0.001

Table 4.6: Swept Pore Volume for Run INV02#4

Quadrant	PROD-1	PROD-2	PROD-3	PROD-4	Entire Reservoir
Swept Pore Volume, bbl	1,052,168	555,314	886,385	558,286	3,052,153
Ratio of Swept Pore Volume to Entire Reservoir	0.339	0.179	0.286	0.180	0.984

Table 4.7: Comparison of Oil Saturations for Run INV02#5

Quadrant	PROD-1	PROD-2	PROD-3	PROD-4
Average Oil Saturation	0.254	0.253	0.253	0.255
Estimated Oil Saturation	0.230	0.240	0.240	0.237
Difference	-0.024	-0.013	-0.013	-0.018

Table 4.8: Swept Pore Volume for Run INV02#5

Quadrant	PROD-1	PROD-2	PROD-3	PROD-4	Entire Reservoir
Swept Pore Volume, bbl	589,444	818,921	888,288	735,376	3,032,029
Ratio of Swept Pore Volume to Entire Reservoir	0.190	0.264	0.286	0.237	0.977

Table 4.9: Comparison of Oil Saturations for Run INV02#7

Quadrant	PROD-1	PROD-2	PROD-3	PROD-4
Average Oil Saturation	0.269	0.276	0.263	0.261
Estimated Oil Saturation	0.210	0.202	0.234	0.225
Difference	-0.059	-0.074	-0.029	-0.036

Table 4.10: Swept Pore Volume for Run INV02#7

Quadrant	PROD-1	PROD-2	PROD-3	PROD-4	Entire Reservoir
Swept Pore Volume, bbl	780,465	663,622	736,652	674,832	2,855,570
Ratio of Swept Pore Volume to Entire Reservoir	0.25	0.21	0.24	0.22	0.92

Table 4.11: Comparison of Oil Saturations for Run INV02#8

Quadrant	PROD-1	PROD-2	PROD-3	PROD-4
Average Oil Saturation	0.269	0.276	0.263	0.261
Estimated Oil Saturation	0.226	0.197	0.251	0.226
Difference	-0.044	-0.079	-0.012	-0.036

Table 4.12: Swept Pore Volume for Run INV02#8

Quadrant	PROD-1	PROD-2	PROD-3	PROD-4	Entire Reservoir
Swept Pore Volume, bbl	781,780	659,269	727,266	671,643	2,839,958
Ratio of Swept Pore Volume to Entire Reservoir	0.252	0.212	0.234	0.216	0.915

Table 4.13: Difference between Oil Saturation Calculated from Inverse Model and Actual Oil Saturation for Various Initial Guesses of Oil Saturation

Initial Guess of Oil Saturation	Depth, ft										RMS error
	5	10	15	20	25	30	35	40	45	50	
0.14	-0.035	-0.037	-0.049	-0.060	-0.065	-0.049	-0.050	-0.024	-0.022	-0.035	4.48 %
0.21	-0.009	-0.013	-0.029	-0.039	-0.040	-0.015	-0.006	0.009	0.004	-0.008	2.14 %
0.22	-0.014	-0.006	-0.013	-0.030	-0.035	-0.008	0.028	0.007	0.004	-0.013	1.89 %
0.23	0.001	-0.009	-0.014	-0.021	-0.021	-0.008	0.023	0.016	0.013	0.006	1.50 %
0.24	0.015	-0.003	-0.006	-0.015	-0.019	0.003	0.037	0.015	0.013	0.020	1.75 %
0.25	0.019	-0.001	-0.008	-0.017	-0.016	-0.004	0.013	0.015	0.014	0.028	1.54 %
0.26	0.014	0.000	-0.009	-0.015	-0.016	-0.004	0.017	0.000	0.021	0.017	1.34 %
0.27	0.019	0.007	0.000	-0.008	-0.011	0.003	0.045	0.002	0.022	0.023	1.90 %
0.28	0.029	0.009	0.000	-0.005	-0.008	0.000	-0.019	-0.020	0.011	0.033	1.72 %
0.29	0.024	0.015	-0.002	-0.014	-0.018	0.007	0.030	0.017	0.041	0.023	2.20 %
0.30	0.030	0.021	0.004	-0.010	-0.014	0.014	0.040	0.006	0.041	0.029	2.44 %
0.38	0.013	0.045	0.043	0.028	0.030	0.046	0.061	0.016	0.058	0.058	4.30 %

Table 4.14: Difference of Oil Saturation from Inverse Model and Actual Saturation for Various Tracer Detection Limits with an Initial Oil Saturation Guess of 0.26

Tracer Detecion Limits	Depth, ft										RMS error
	5	10	15	20	25	30	35	40	45	50	
0.0001	0.014	0.000	-0.009	-0.015	-0.016	-0.004	0.017	0.000	0.021	0.017	1.34 %
0.001	0.014	0.001	-0.008	-0.014	-0.016	-0.004	0.017	0.000	0.022	0.018	1.35 %
0.01	0.011	-0.002	-0.009	-0.018	-0.027	0.004	0.076	0.015	0.013	0.017	2.78 %

Table 4.15: Difference of Oil Saturation from Inverse Model and Actual Saturation for Various Tracer Detection Limits with an Initial Oil Saturation Guess of 0.30

Tracer Detecion Limits	Depth, ft										RMS error
	5	10	15	20	25	30	35	40	45	50	
0.0001	0.030	0.021	0.004	-0.010	-0.014	0.014	0.040	0.006	0.041	0.029	2.44 %
0.001	0.030	0.021	0.004	-0.010	-0.014	0.014	0.040	0.006	0.041	0.029	2.44 %
0.01	0.025	0.016	0.001	-0.016	-0.021	0.011	0.040	0.006	0.041	0.023	2.35 %

Table 4.16: Description of Two Dimensional Reservoir

Number of Gridblocks	66 x 1 x 2
Size of Gridblocks, ft x ft x ft	10 x 330 x 25
Drainage Area, acres	5
Reservoir Pore Volume, bbl	387,890
Porosity	0.2
Lateral Permeability, md	100
Residual Oil Saturation	0.3
Residual Water Saturation	0.3

Table 4.17: Relative Permeability Parameters and Viscosities

Run Number	Endpoint Relative Permeability		Exponent of Relative Permeability		Viscosity, cp	
	Water	Oil	Water	Oil	Water	Oil
INV07-000	0.15	0.85	1.5	2	0.7	5
INV07-600	0.15	0.85	1.5	2	0.7	20
INV07-100	1	1	1	1	0.7	5
INV07-200	1	1	1	1	0.7	0.7
INV07-500	1	1	1	1	0.7	20

Table 4.18: Run Summary of Oil Saturation Estimate

Run Number	Initial Saturation		Initial Guess of Saturation		Estimated Saturation	
	Layer1	Layer2	Layer1	Layer2	Layer1	Layer2
INV07-511	0.4	0.6	0.35	0.55	0.4	0.561
INV07-512	0.4	0.6	0.35	0.65	0.399	0.644
INV07-513	0.4	0.6	0.45	0.55	0.4	0.561
INV07-514	0.4	0.6	0.45	0.65	0.4	0.644

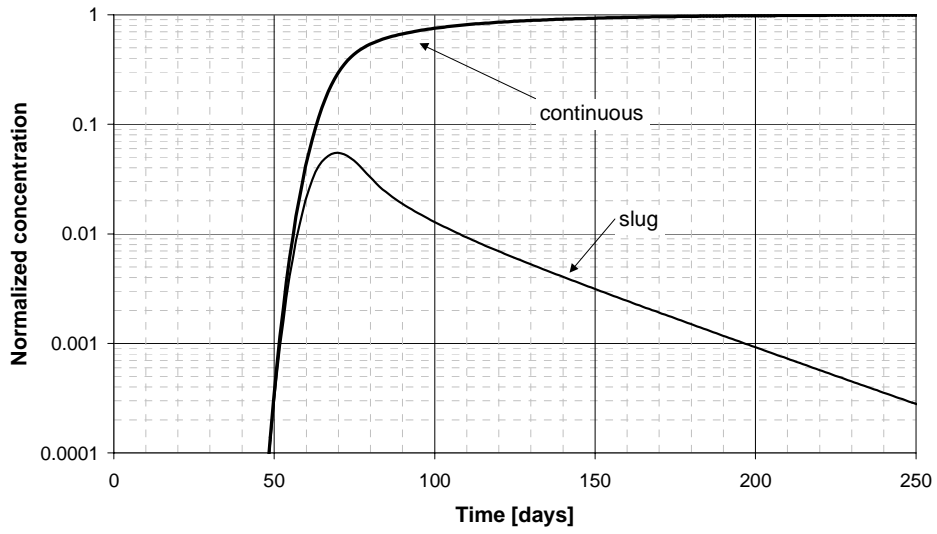


Figure 4.1: Tracer concentration histories from single phase homogeneous media

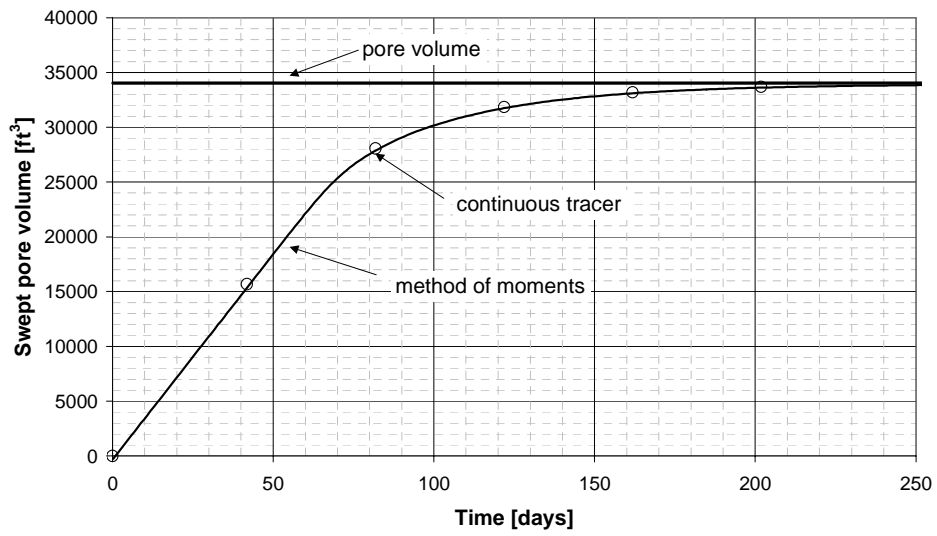


Figure 4.2: Swept volume calculated from both slug and continuous tracer data

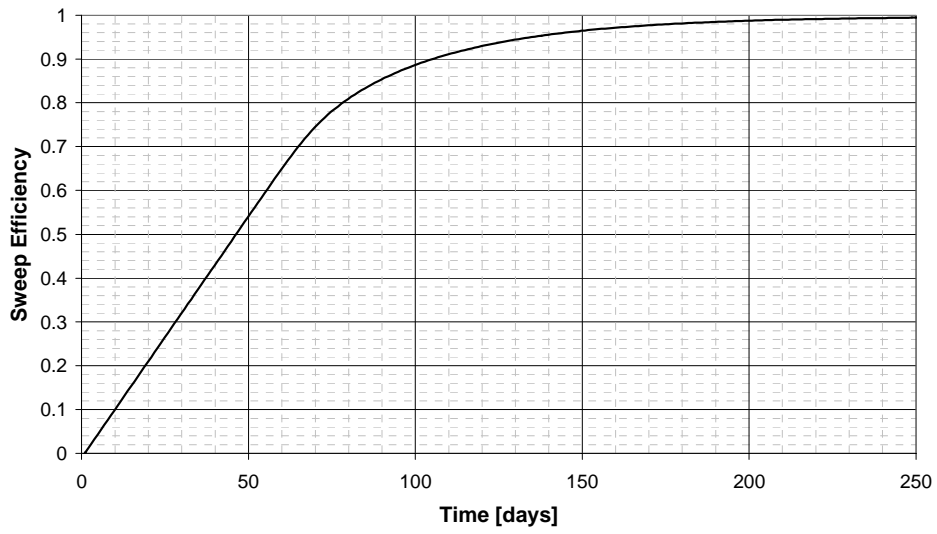


Figure 4.3: Sweep efficiency from slug tracer history

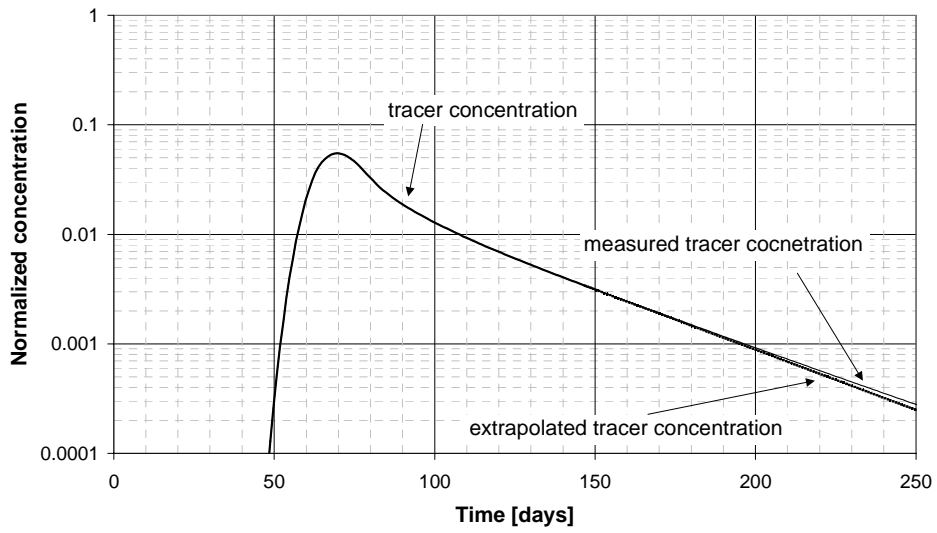


Figure 4.4: Tracer concentration with extrapolation

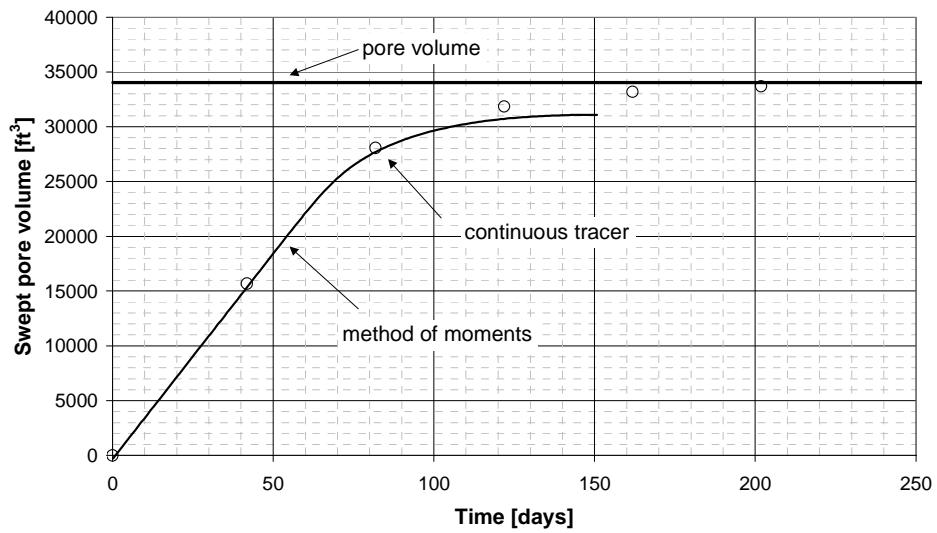


Figure 4.5: Swept volume estimate using incomplete data

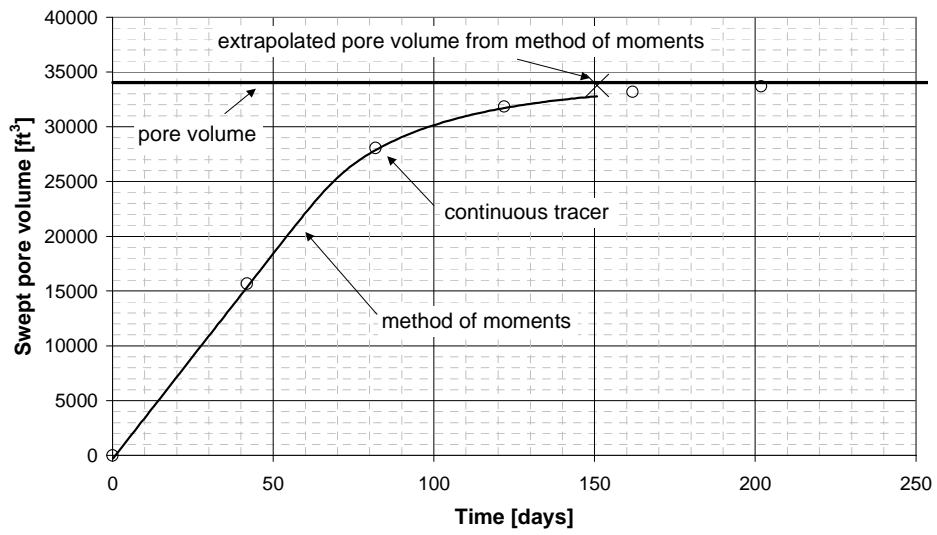


Figure 4.6: Swept volume estimate using extrapolated data

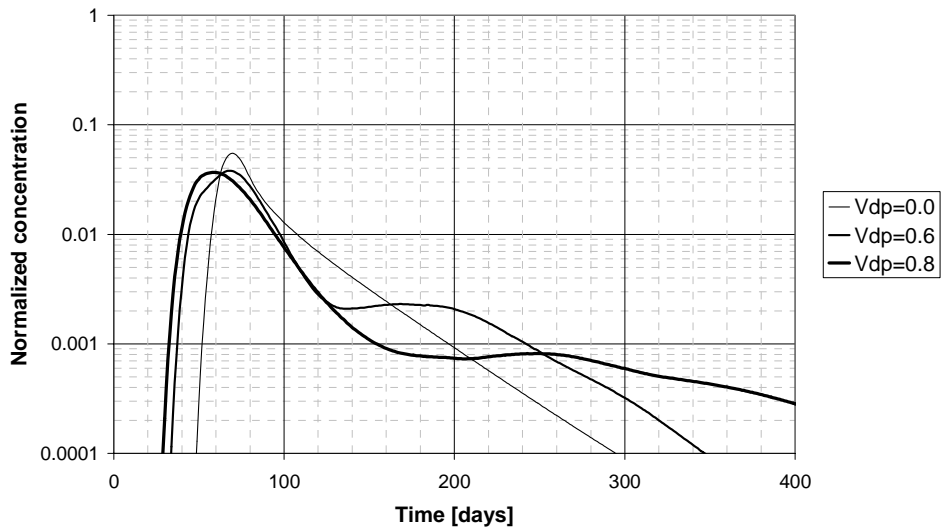


Figure 4.7: Comparison of tracer concentration histories with different Dykstra-Parsons coefficients

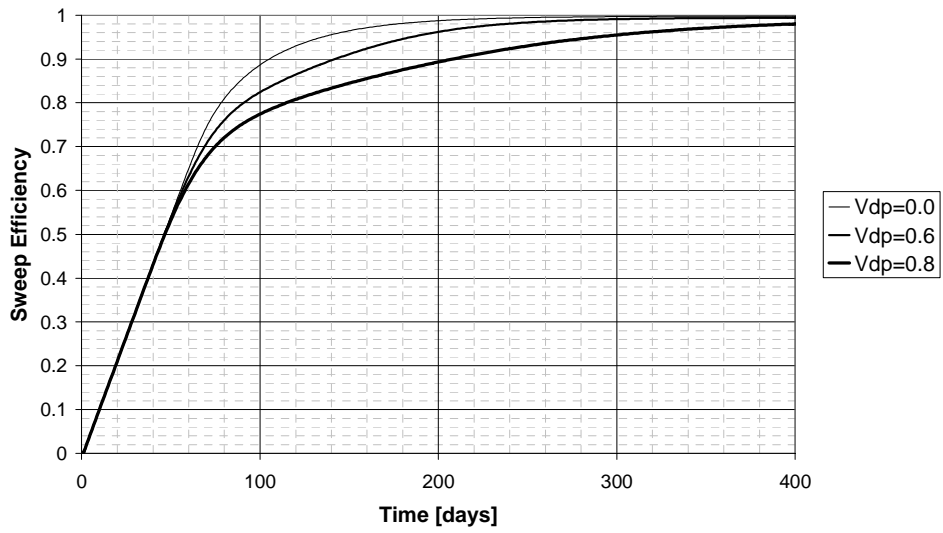


Figure 4.8: Comparison of sweep efficiency for reservoirs with different Dykstra-Parsons coefficients

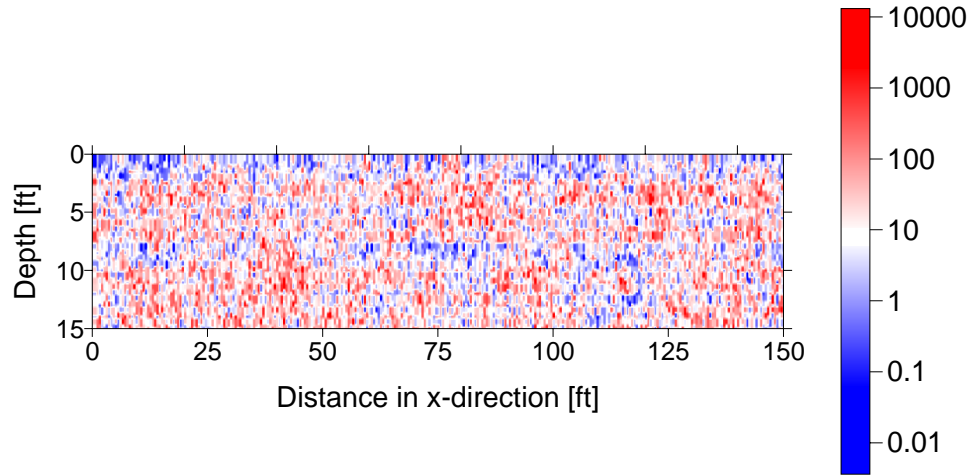


Figure 4.9: Cross-sectional heterogeneous permeability in md at Lawyer Canyon

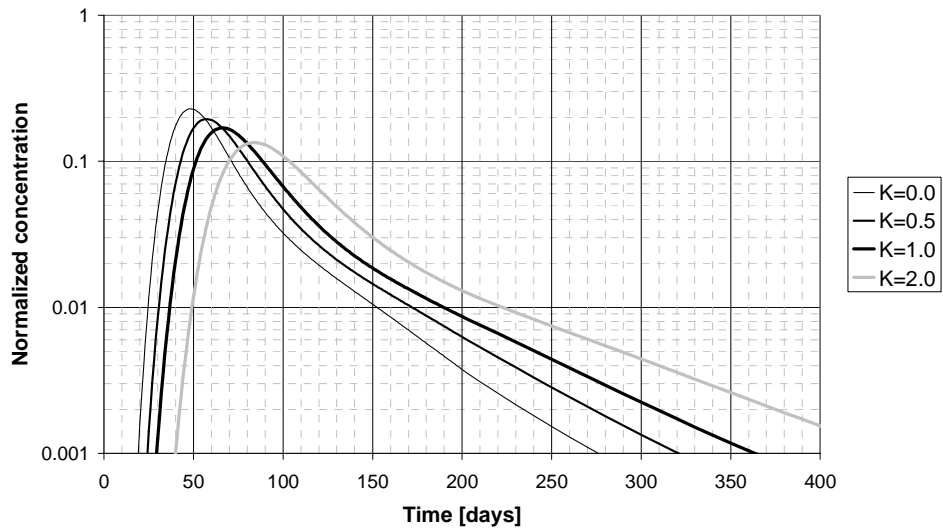


Figure 4.10: Tracer concentration history from quarter of five-spot well pattern

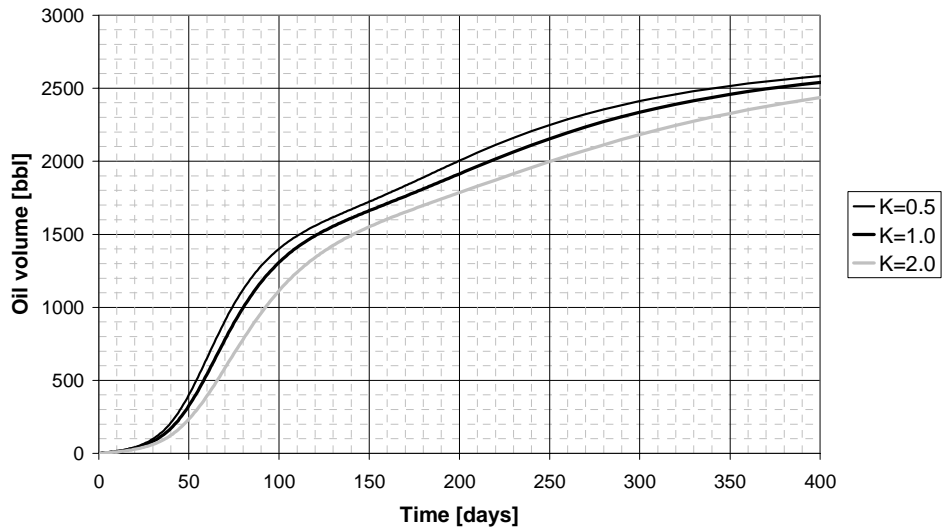


Figure 4.11: Oil volume estimate from tracer response in quarter of five-spot well pattern

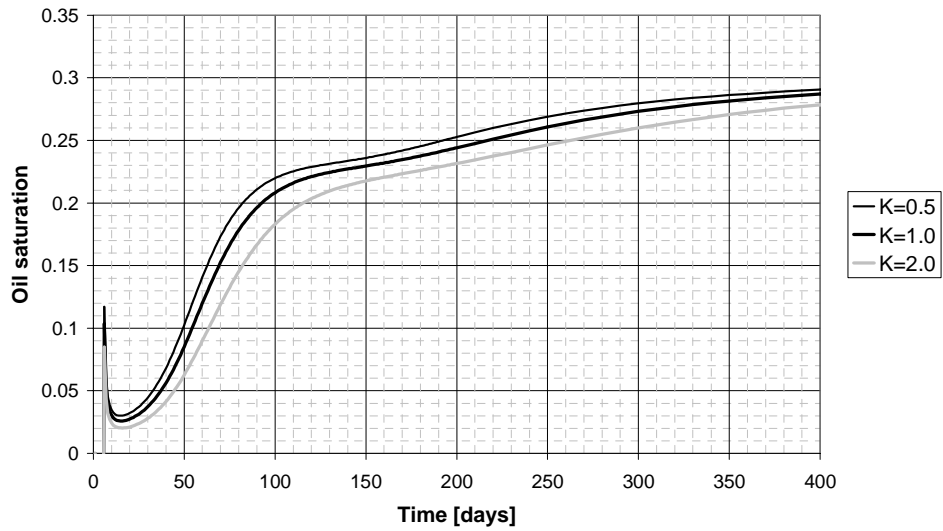


Figure 4.12: Oil saturation estimate from tracer response in quarter of five-spot well pattern using the method of moments

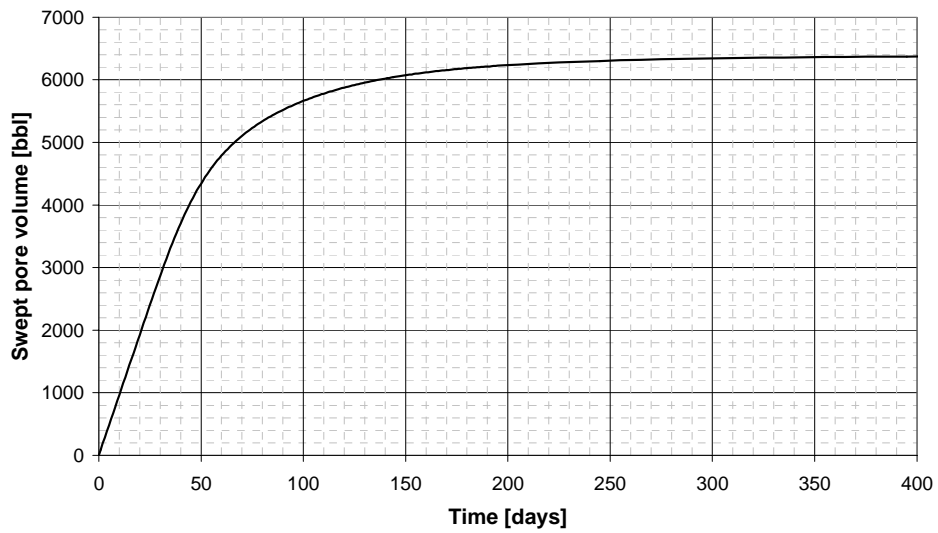


Figure 4.13: Swept volume from tracer response in quarter of five-spot well pattern

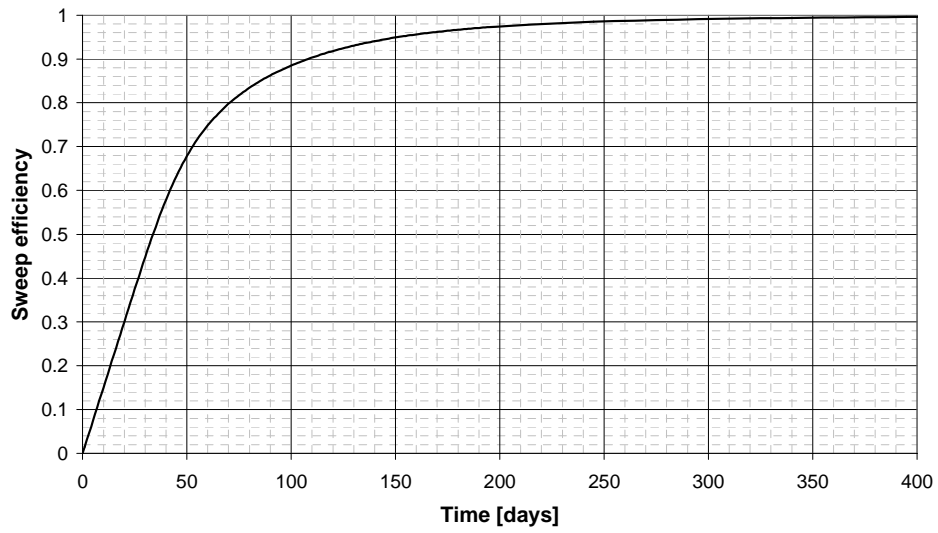


Figure 4.14: Sweep efficiency from tracer response in quarter of five-spot well pattern

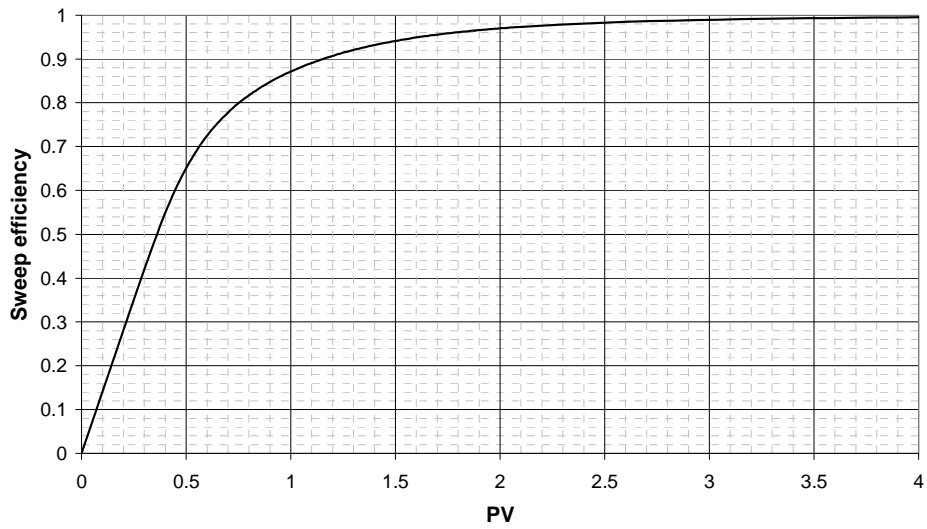


Figure 4.15: Sweep efficiency from tracer response in quarter of five-spot well pattern

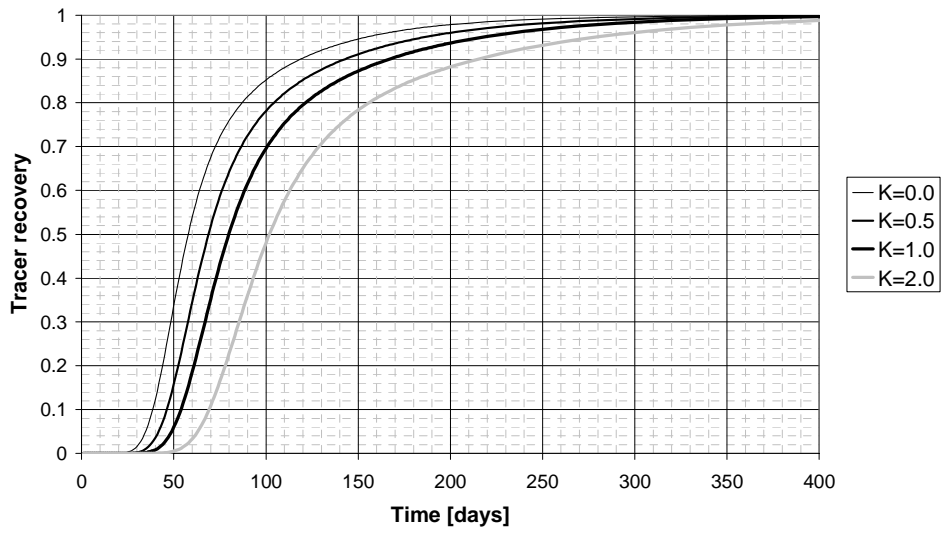


Figure 4.16: Tracer recovery in quarter of five-spot well pattern

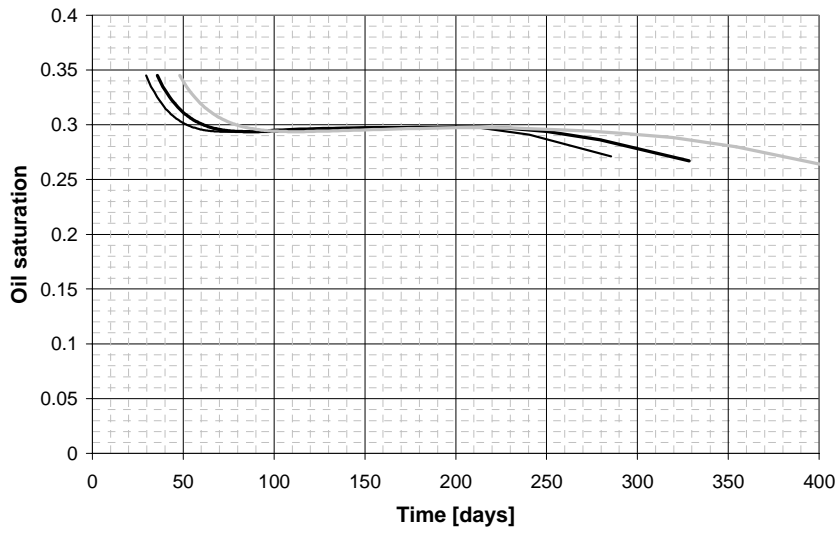


Figure 4.17: Oil saturation estimated from Landmark method

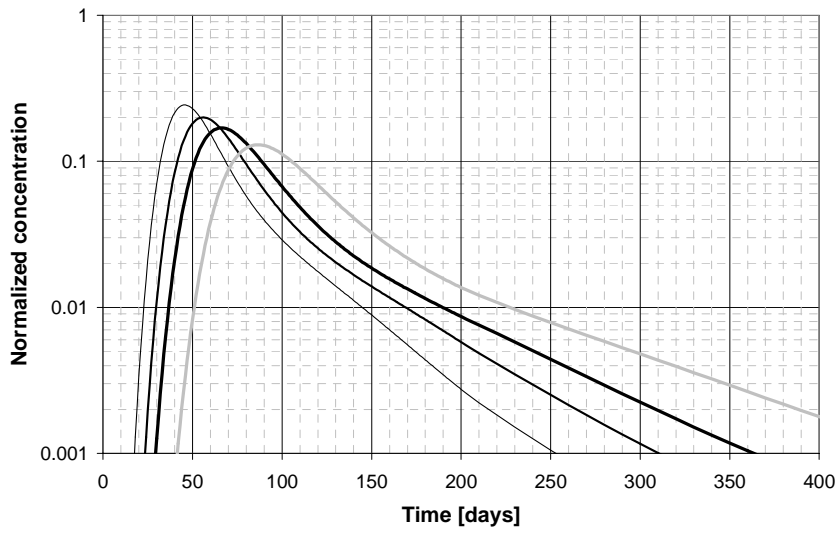


Figure 4.18: Tracer concentration history from quarter of five-spot well pattern

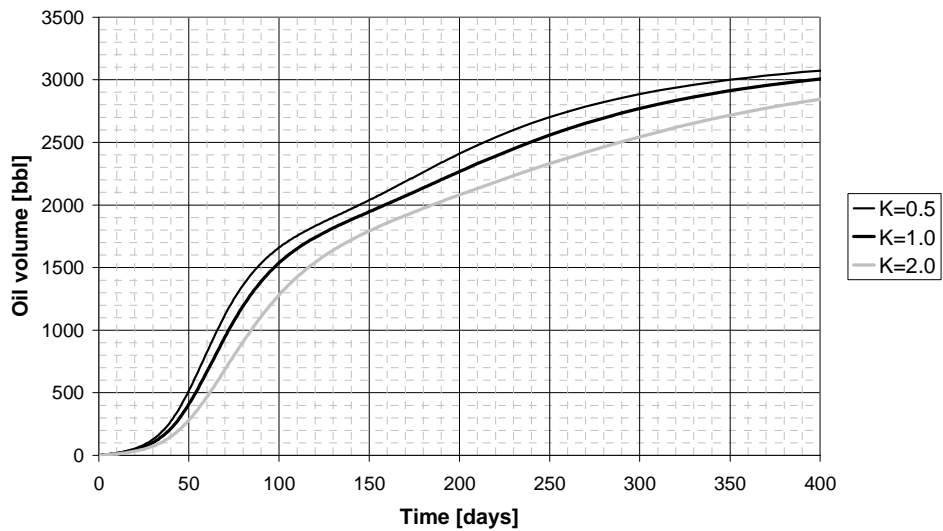


Figure 4.19: Oil volume estimate from tracer response in quarter of five-spot well pattern

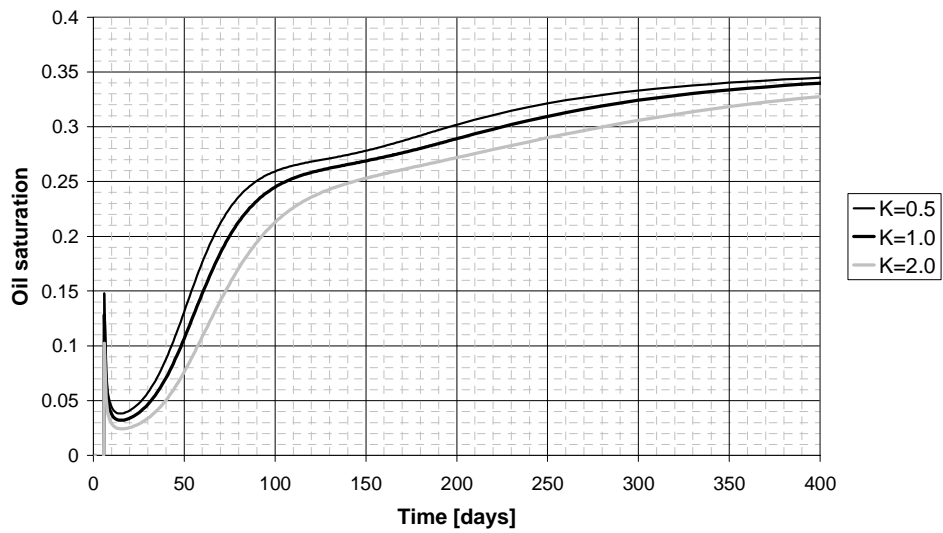


Figure 4.20: Oil saturation estimate from tracer response in quarter of five-spot well pattern using the method of moments

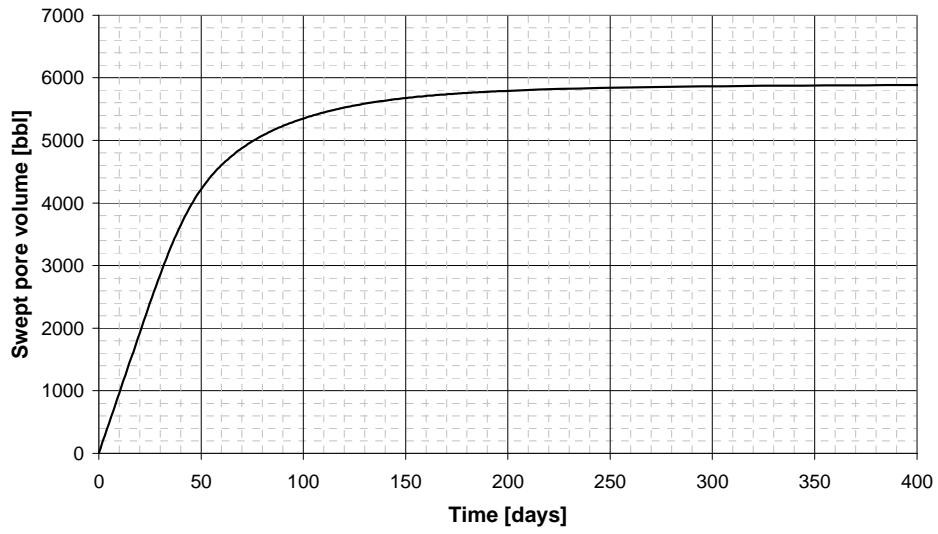


Figure 4.21: Swept volume from tracer response in quarter of five-spot well pattern

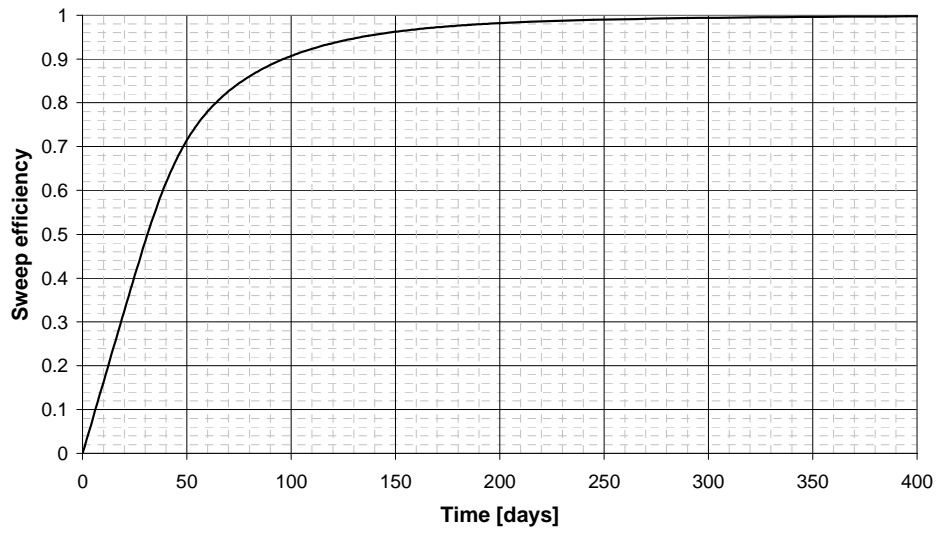


Figure 4.22: Sweep efficiency from tracer response in quarter of five-spot well pattern

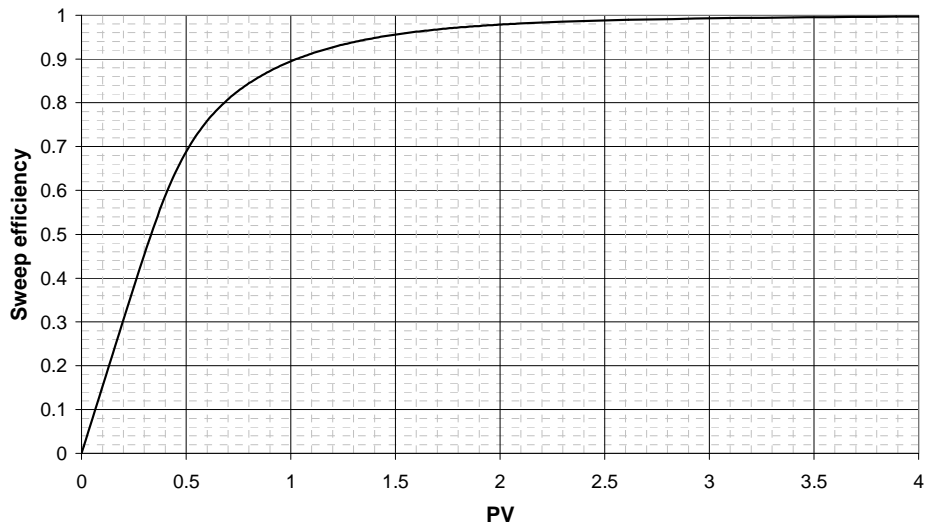


Figure 4.23: Sweep efficiency from tracer response in quarter of five-spot well pattern

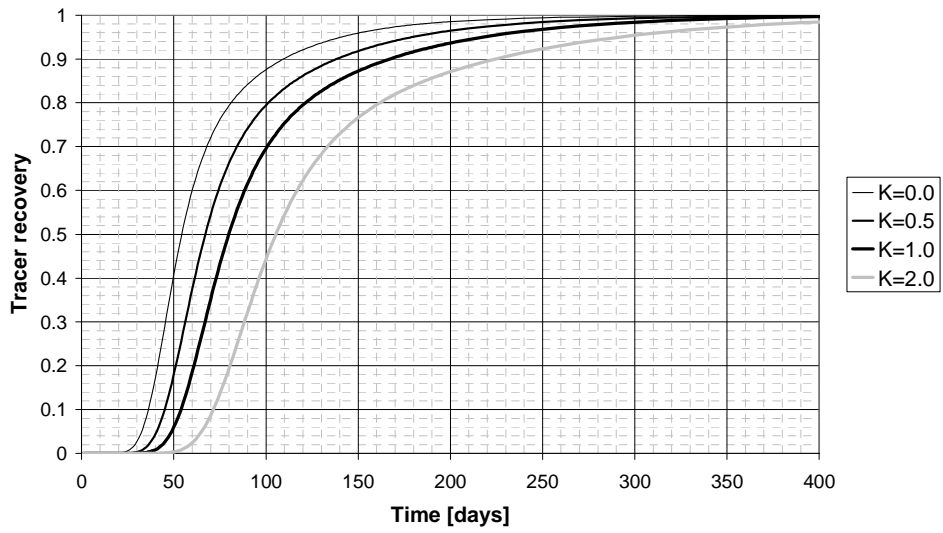


Figure 4.24: Tracer recovery in quarter of five-spot well pattern

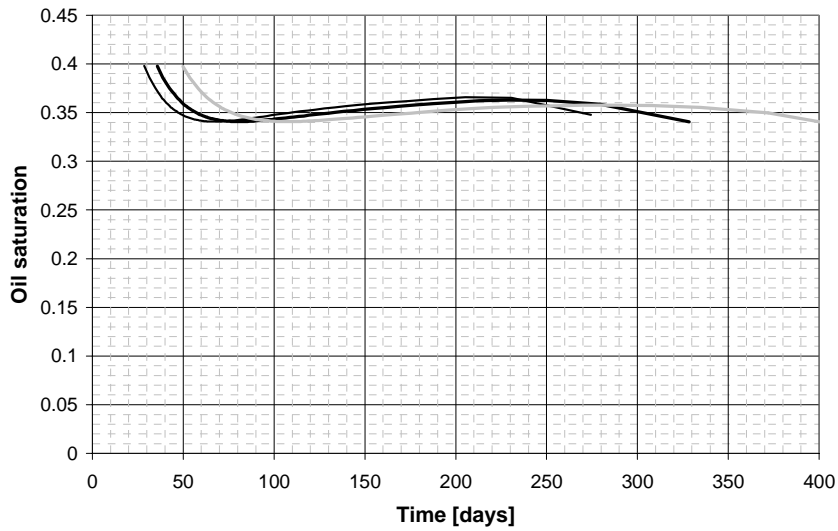


Figure 4.25: Oil saturation estimated from Landmark method

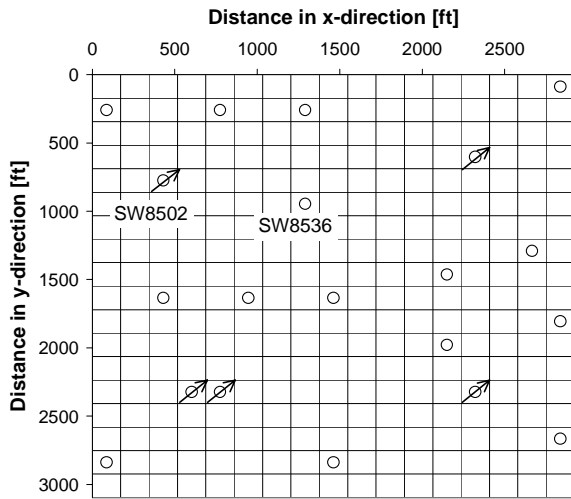


Figure 4.26: Well pattern in the reservoir at South Wasson Clear Fork field

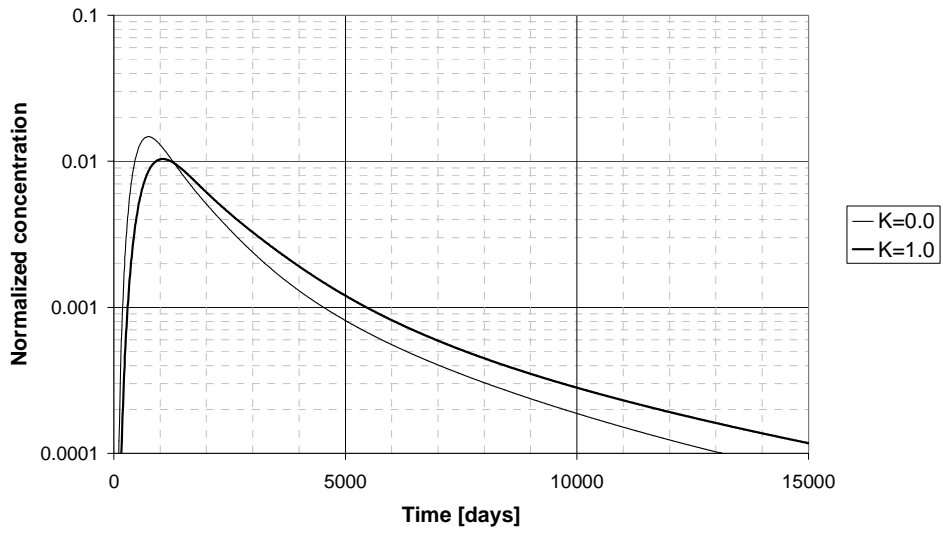


Figure 4.27: Tracer concentration history from SW8536

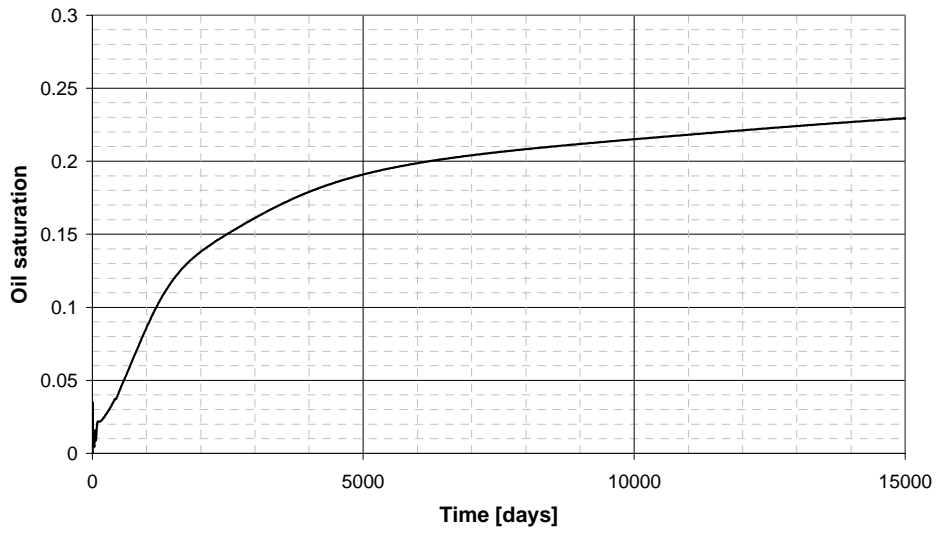


Figure 4.28: Oil volume estimate from tracer response between SW8502 and SW8536

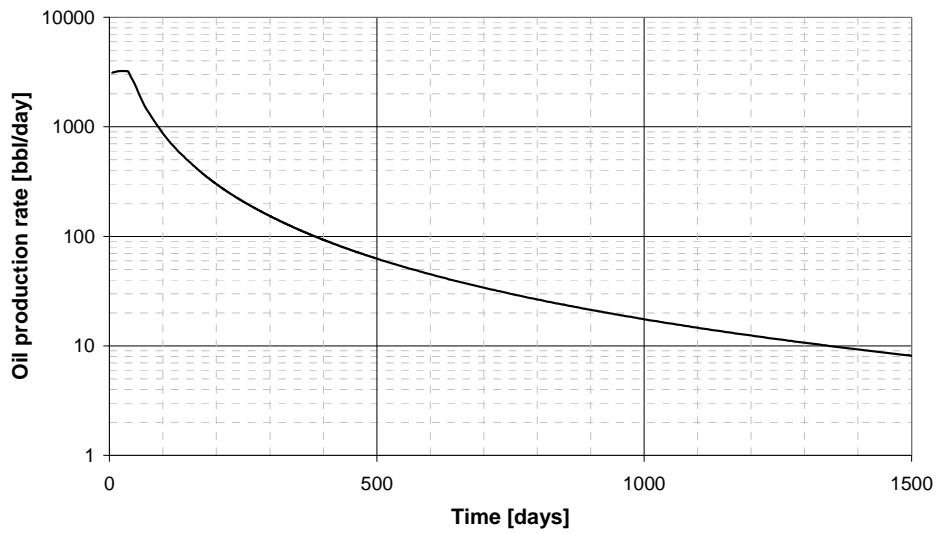


Figure 4.29: Oil production rate for the simulation with a mobility ratio of 1.2

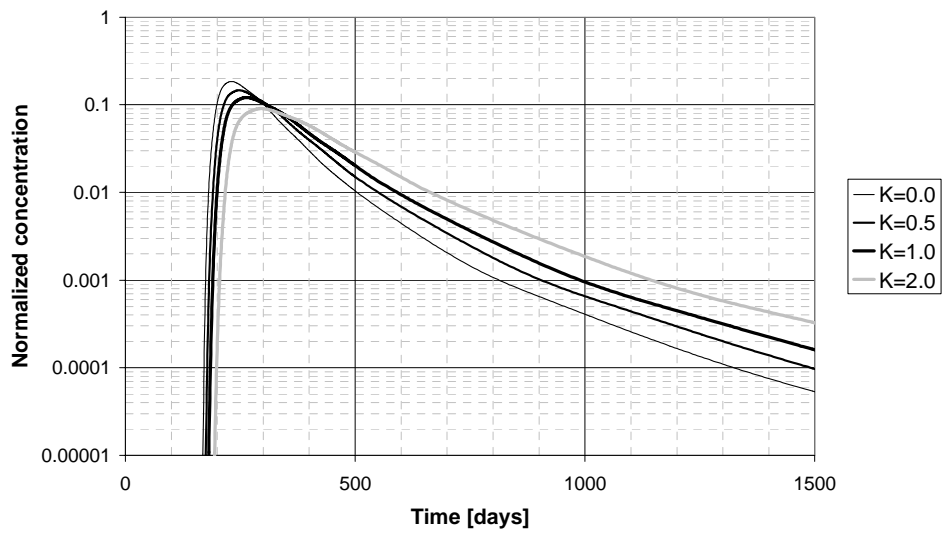


Figure 4.30: Water phase tracer concentrations for a PITT at 0.5 PV with an end point mobility ratio of 1.2

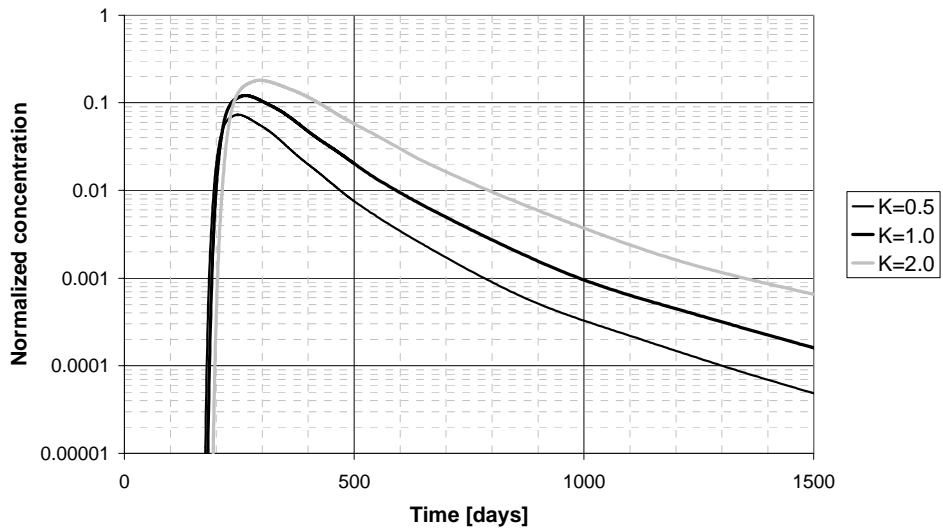


Figure 4.31: Oil phase tracer concentrations for a PITT at 0.5 PV with an end point mobility ratio of 1.2

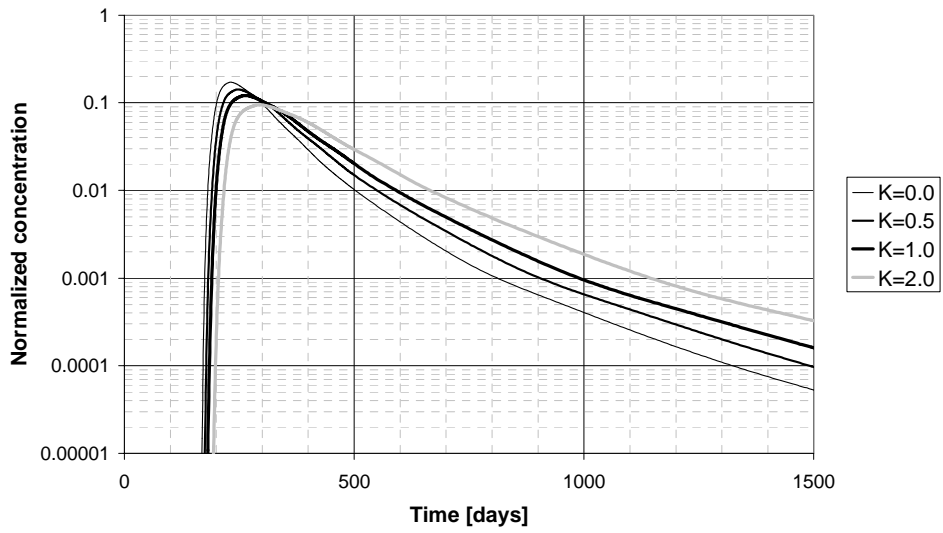


Figure 4.32: Total tracer concentrations for a PITT at 0.5 PV with an end point mobility ratio of 1.2

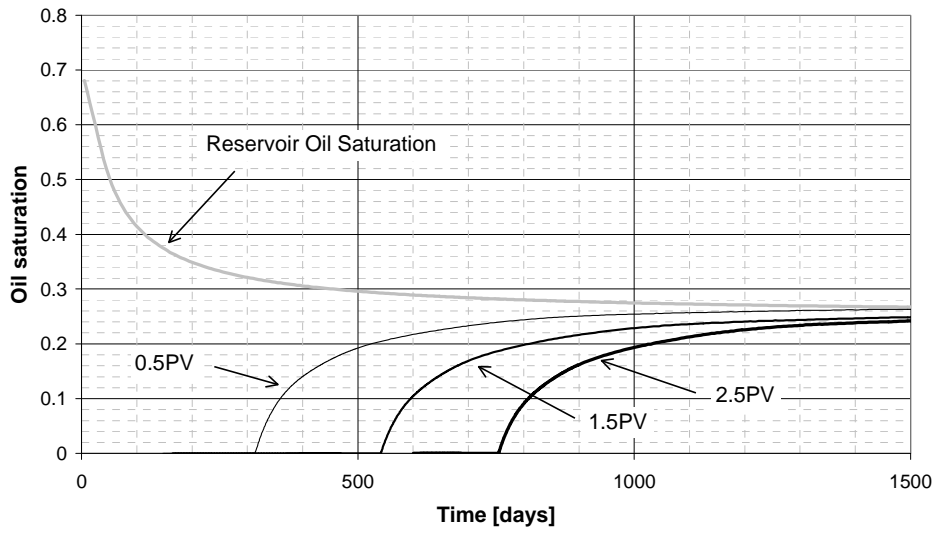


Figure 4.33: Estimated oil saturation using total tracer concentrations for an end point mobility ratio of 1.2

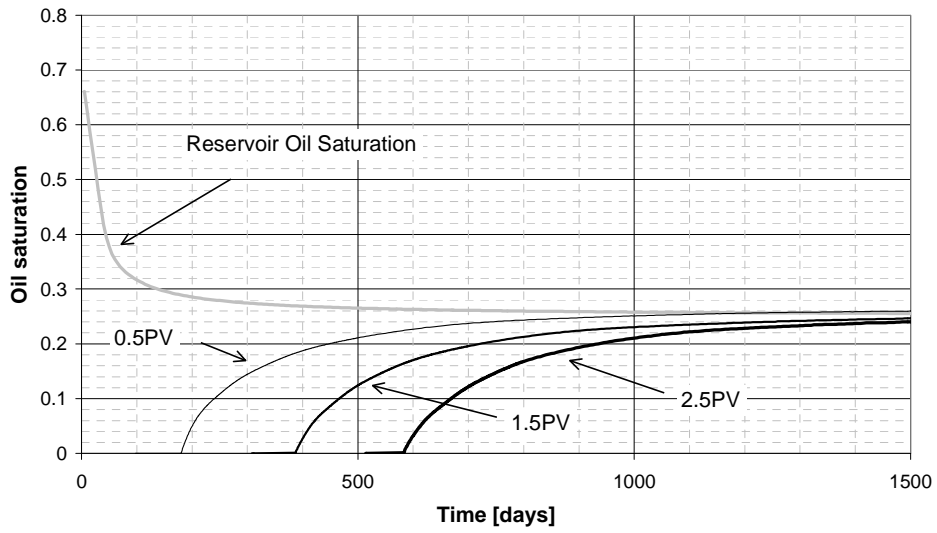


Figure 4.34: Estimated oil saturation using total tracer concentrations for an end point mobility ratio of 0.5

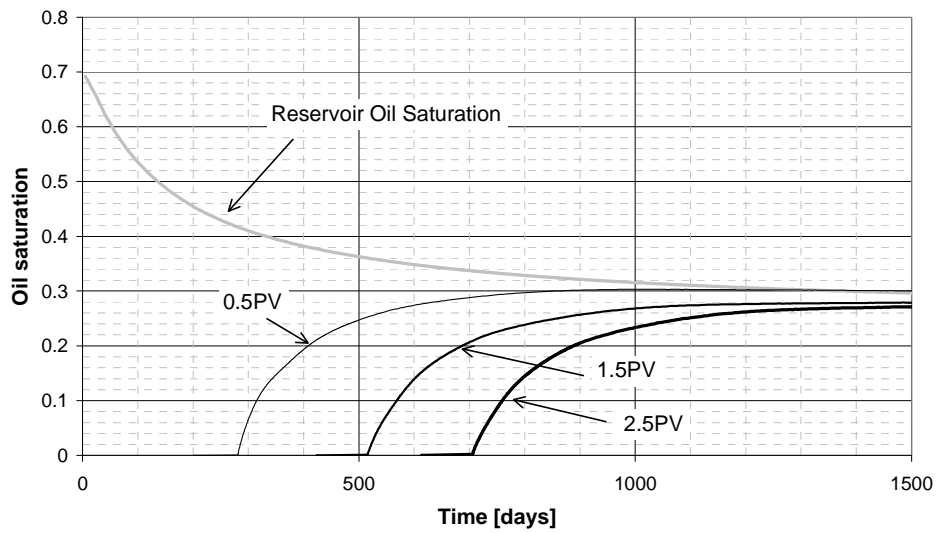


Figure 4.35: Estimated oil saturation using total tracer concentrations for an end point mobility ratio of 5.2

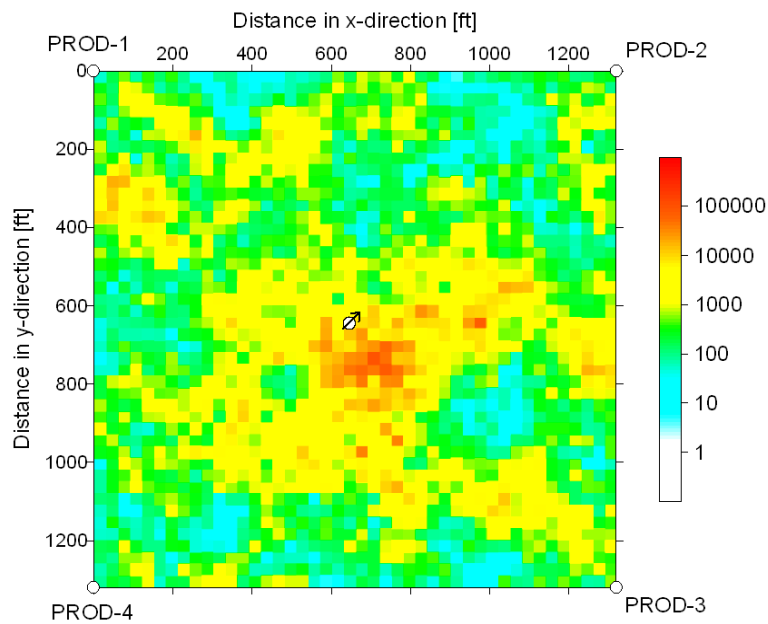


Figure 4.36: Logarithmic permeability distribution in layer 8 (most permeable layer)

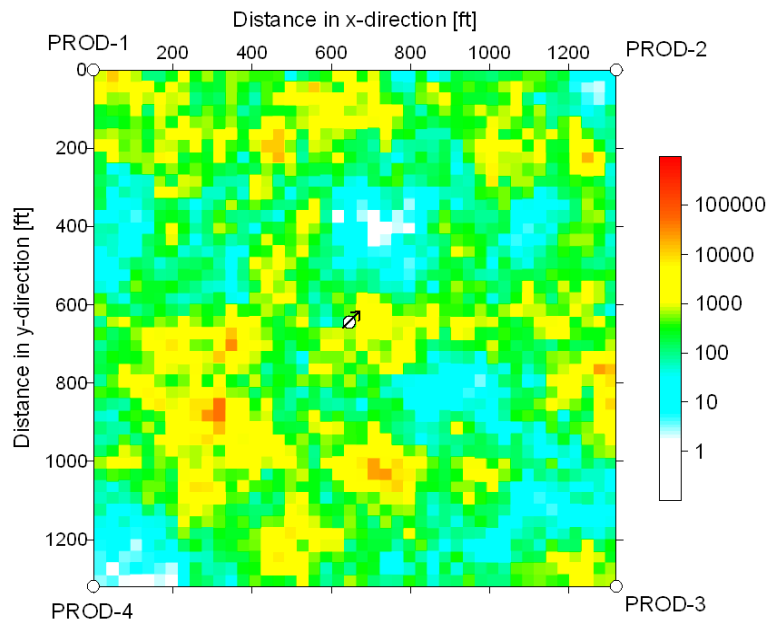


Figure 4.37: Permeability distribution in logarithmic scale in layer 5 (least permeable layer)

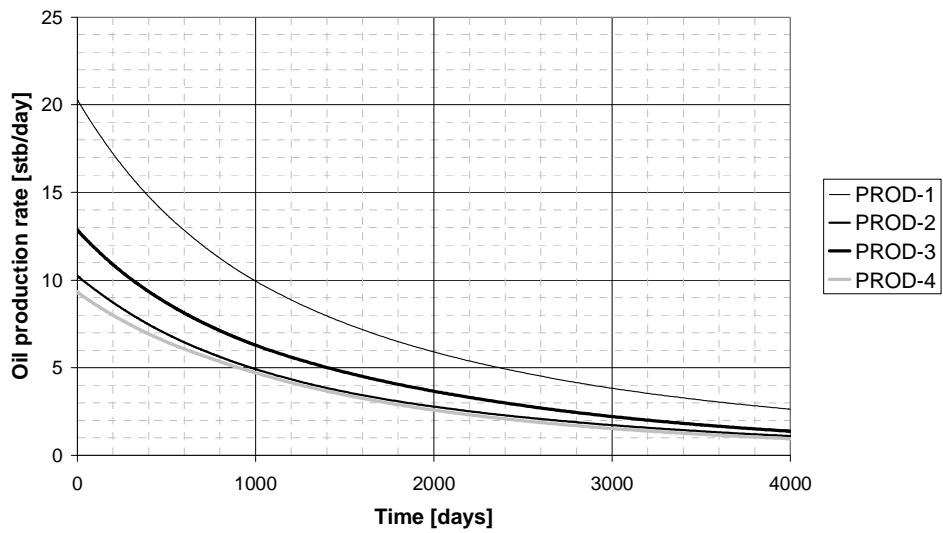


Figure 4.38: Oil production rate

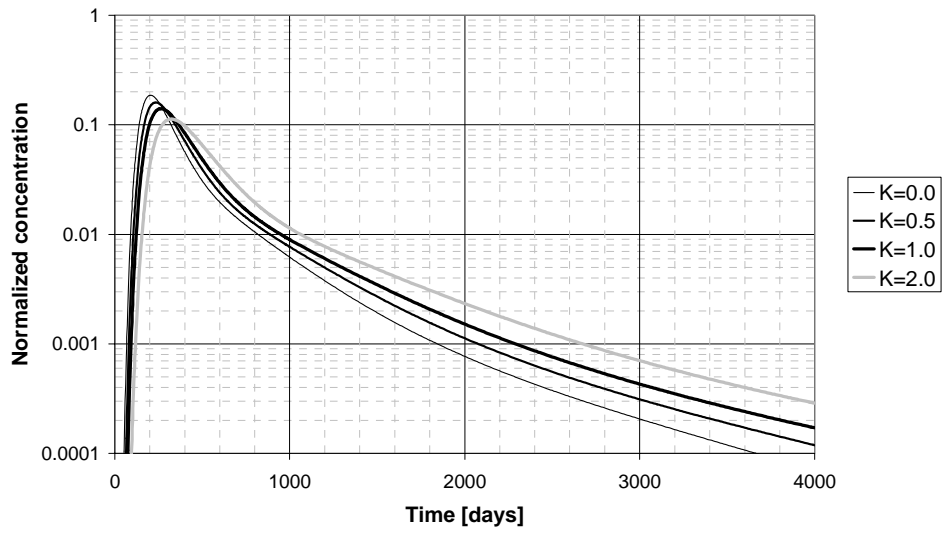


Figure 4.39: Normalized tracer concentration at PROD-1

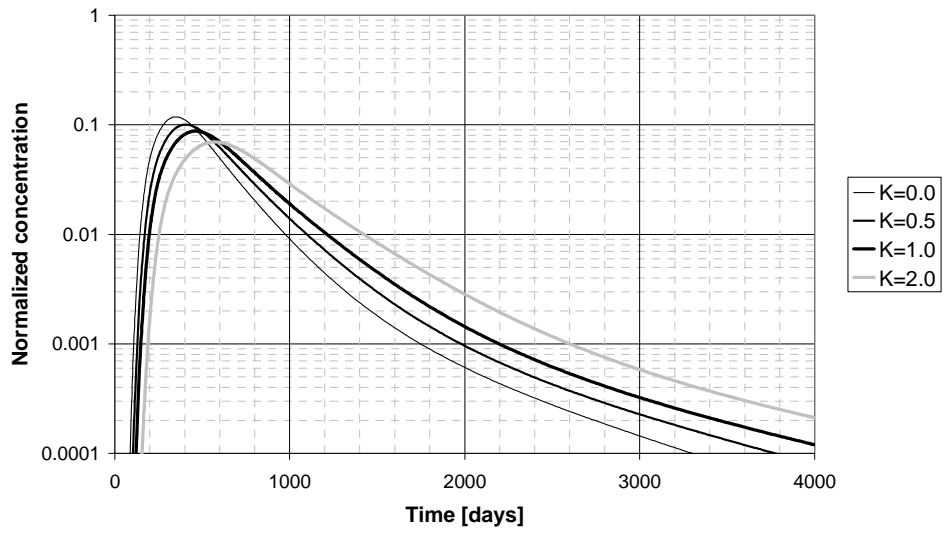


Figure 4.40: Normalized tracer concentration at PROD-2

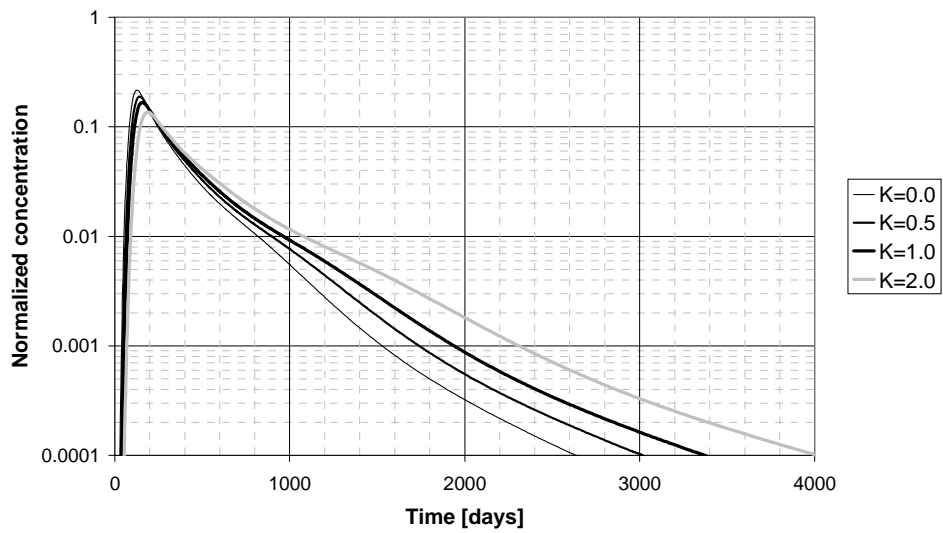


Figure 4.41: Normalized tracer concentration at PROD-3

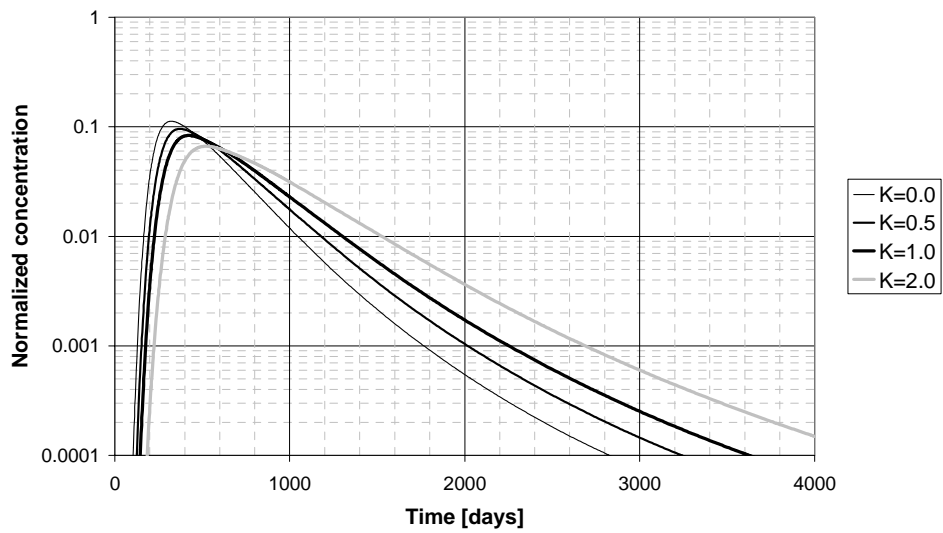


Figure 4.42: Normalized tracer concentration at PROD-4

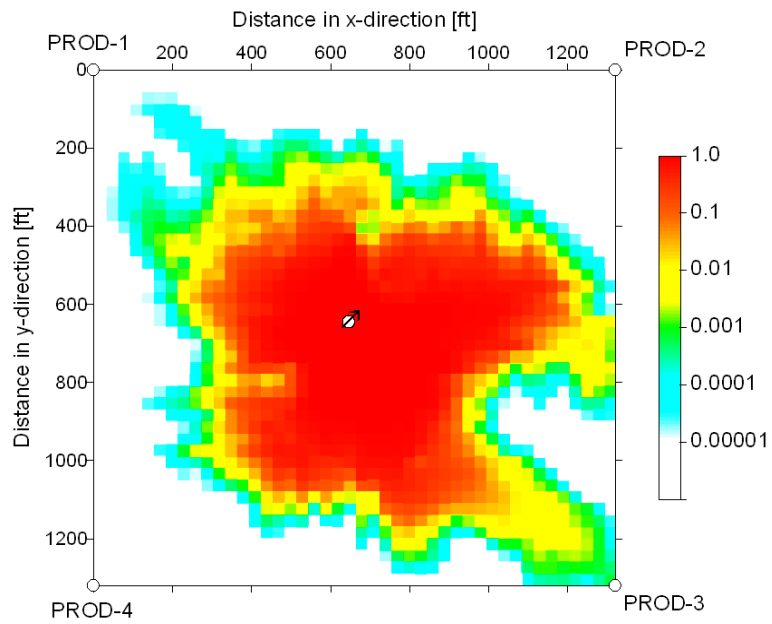


Figure 4.43: Normalized conservative tracer concentration profile in layer 8 after 35 days of tracer injection

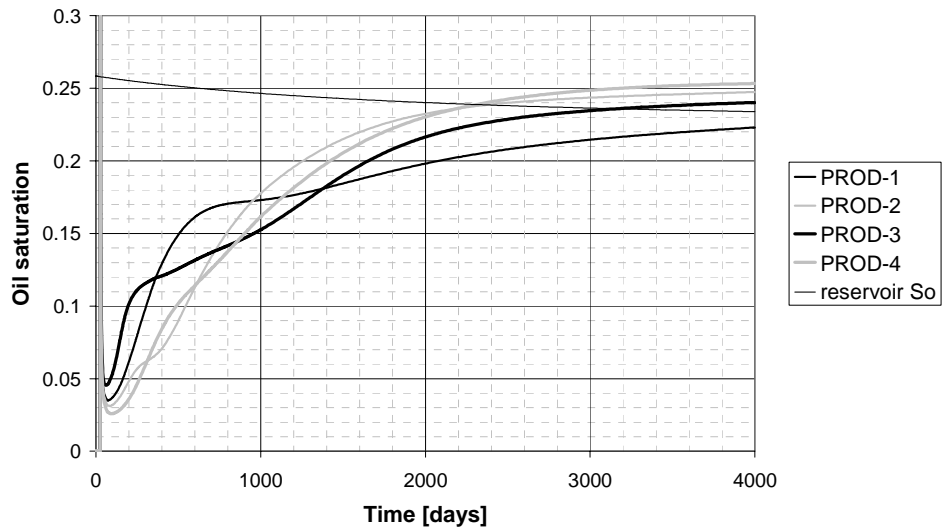


Figure 4.44: Oil Saturation between well pairs

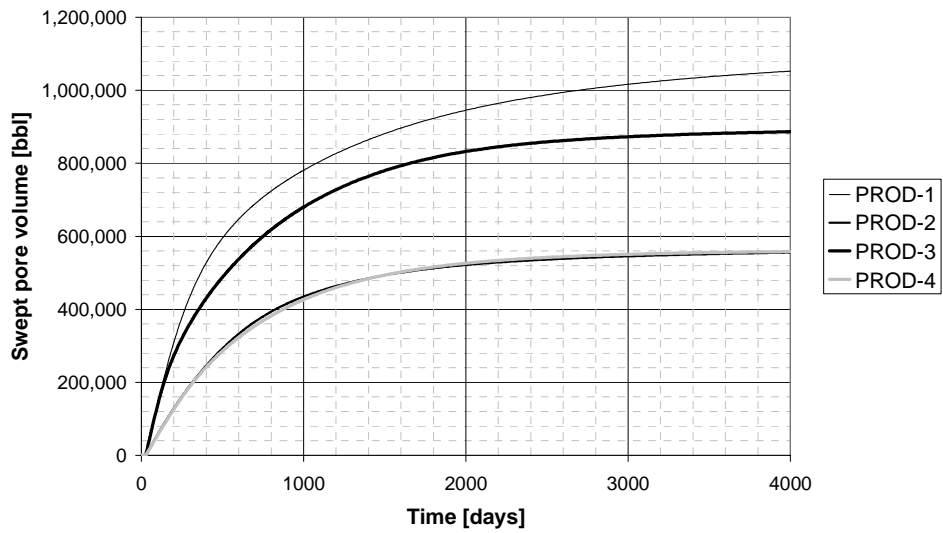


Figure 4.45: Swept pore volume between the injector and the each producer

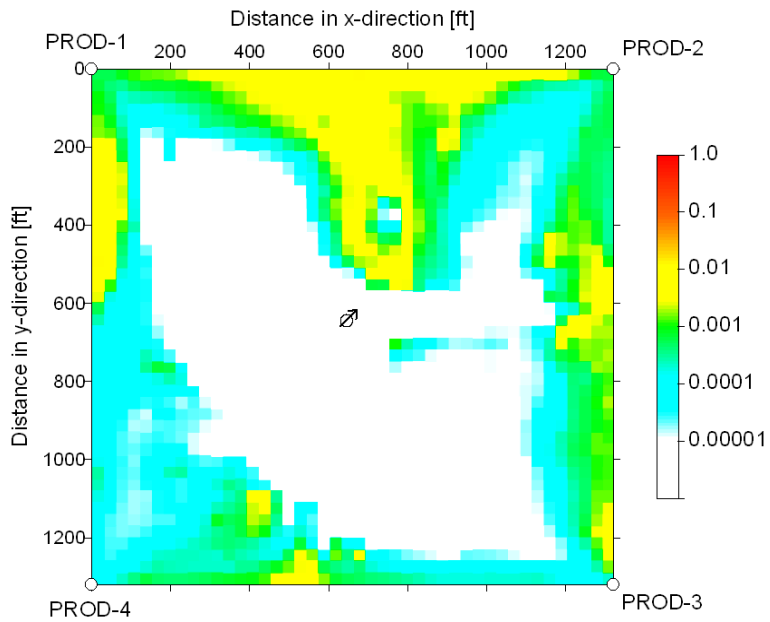


Figure 4.46: Profile of normalized partitioning tracer concentration with a partition coefficient of 2 in layer 1 at the end of PITT

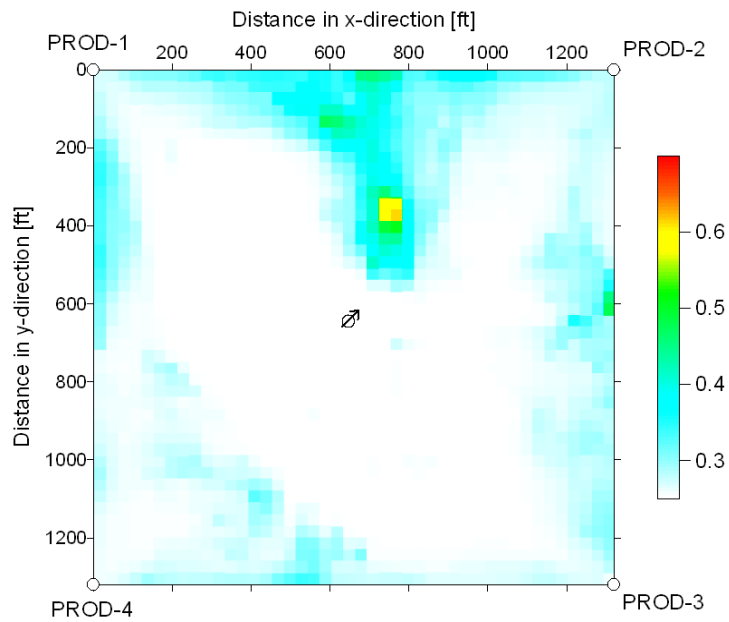


Figure 4.47: Oil saturation distribution in layer 1 at the end of PITT

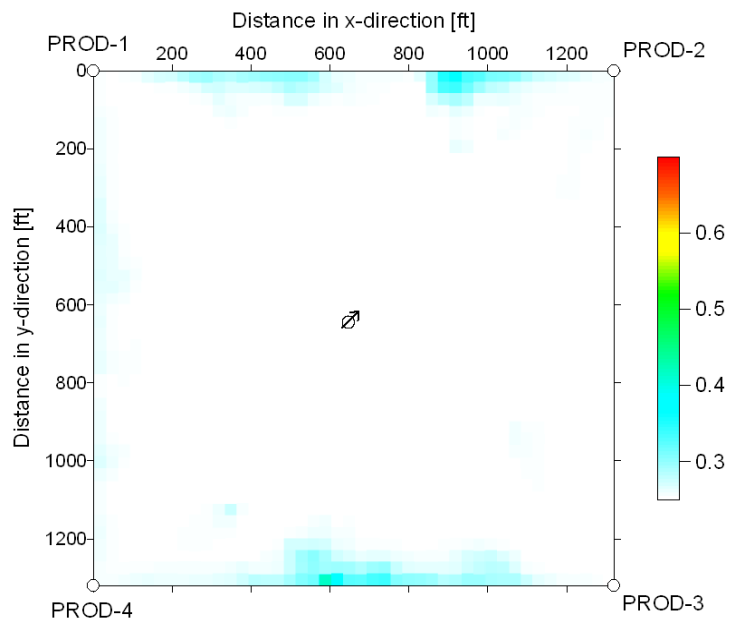


Figure 4.48: Oil saturation distribution in layer 8 at the end of PITT

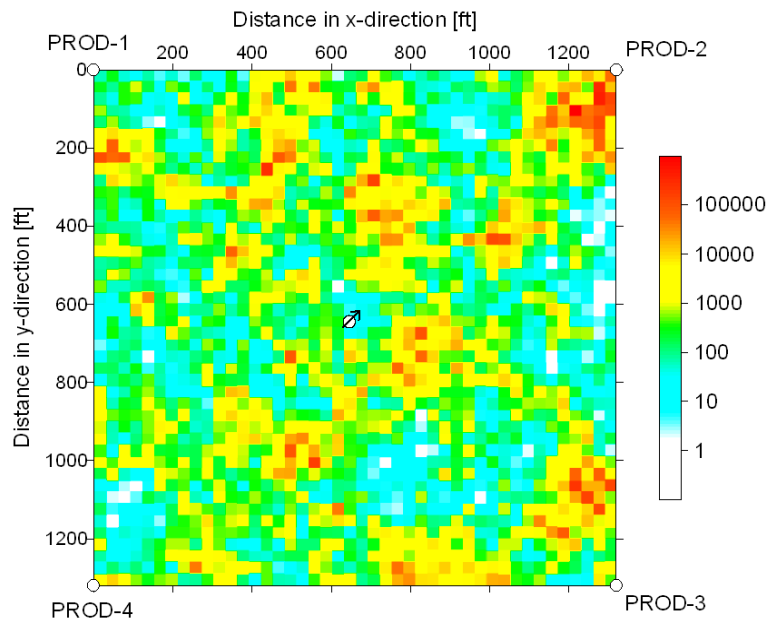


Figure 4.49: Permeability in the least permeable layer 5

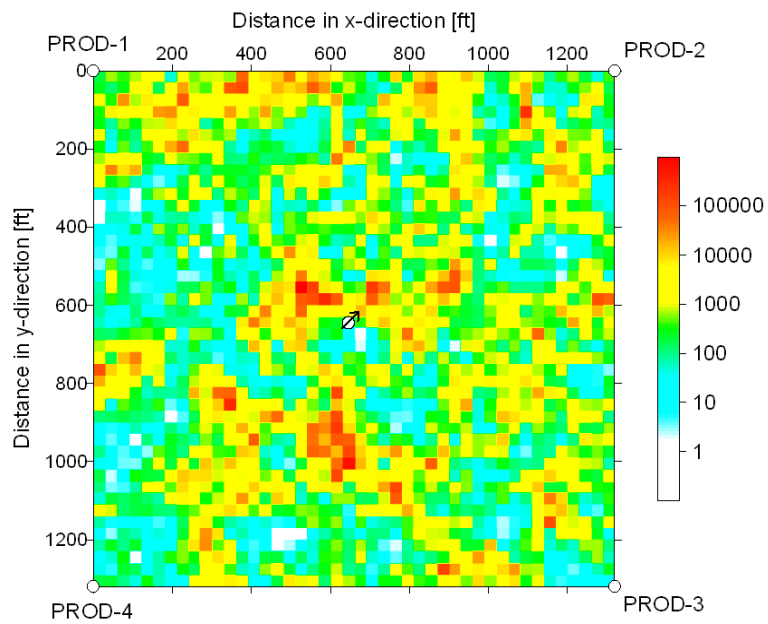


Figure 4.50: Permeability in the most permeable layer 8

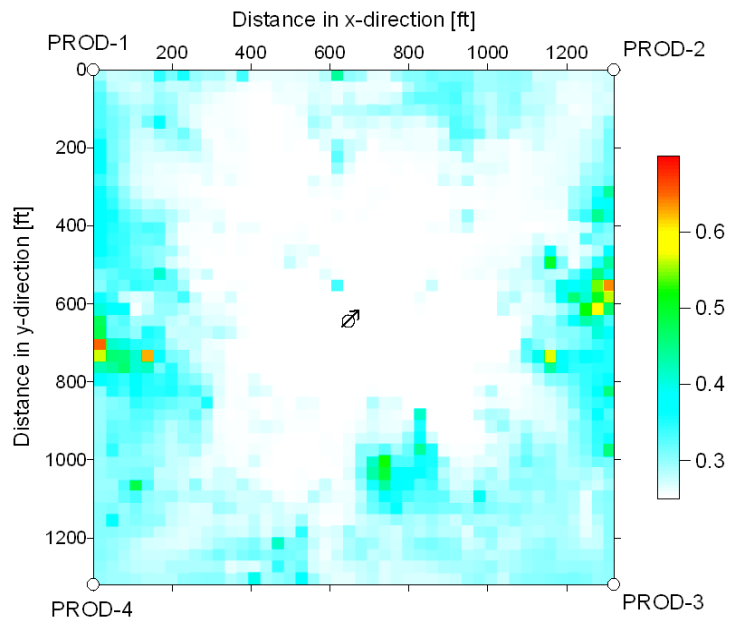


Figure 4.51: Oil saturation distribution in layer 5 at the beginning of the tracer injection

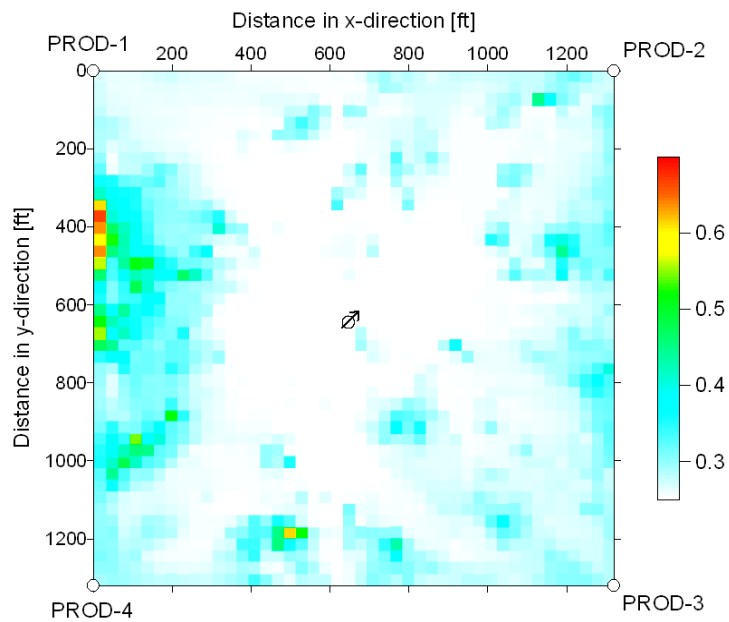


Figure 4.52: Oil saturation distribution in layer 8 at the beginning of the tracer injection

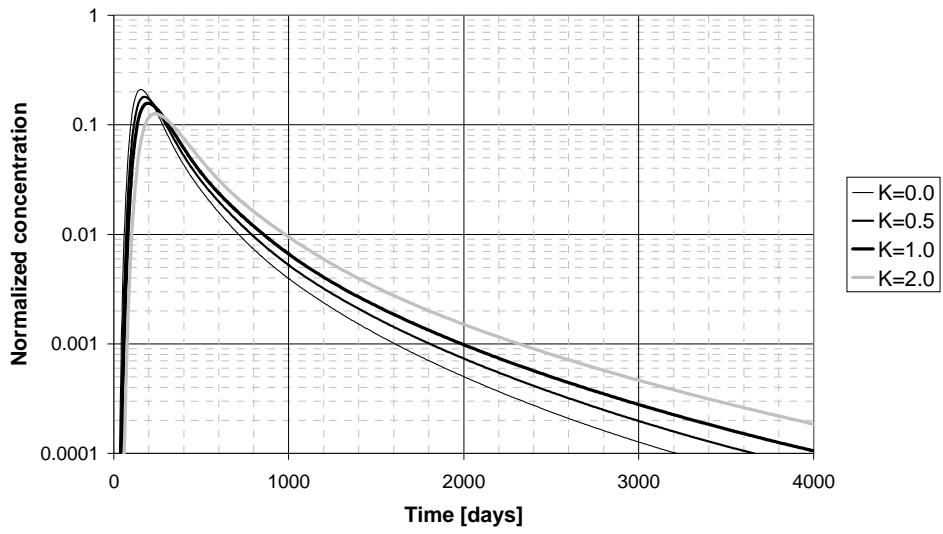


Figure 4.53: Normalized concentration at PROD-1

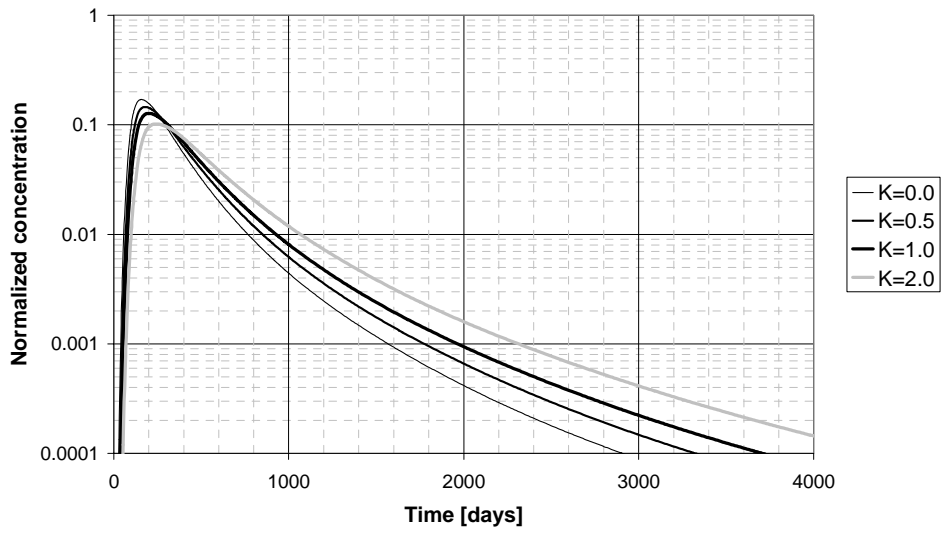


Figure 4.54: Normalized concentration at PROD-2

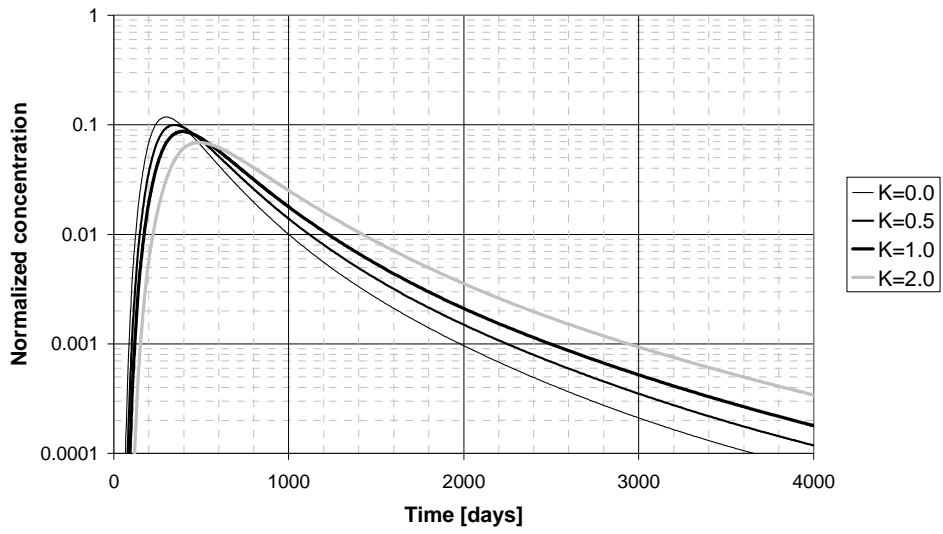


Figure 4.55: Normalized concentration at PROD-3

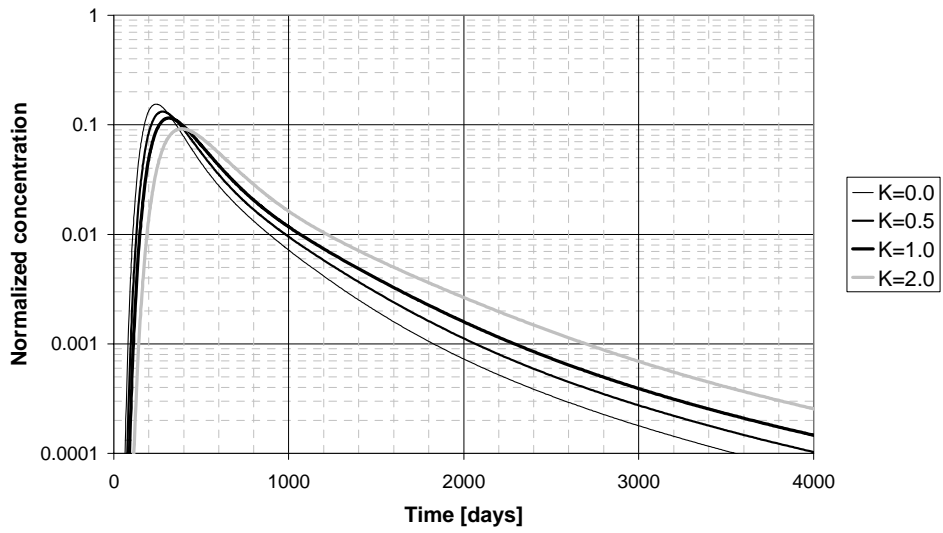


Figure 4.56: Normalized concentration at PROD-4

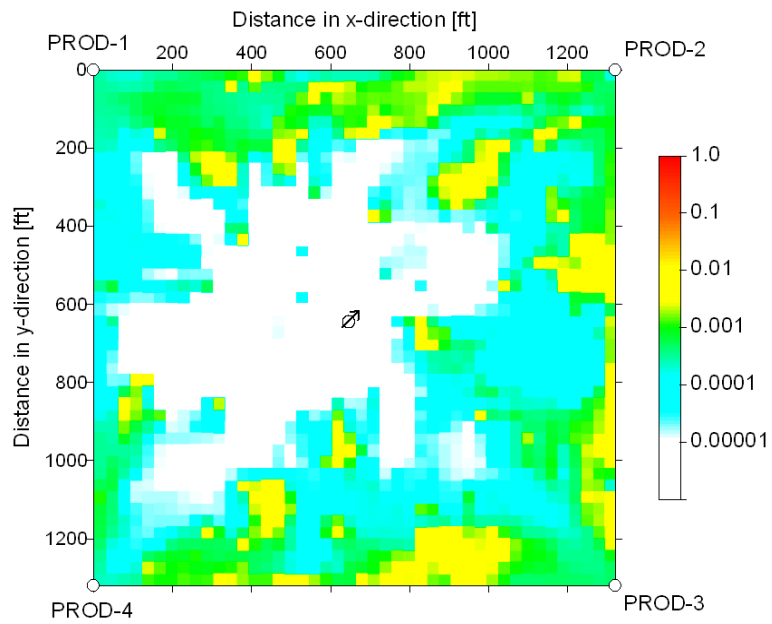


Figure 4.57: Tracer concentration profile in layer 5 at the end of the PITT

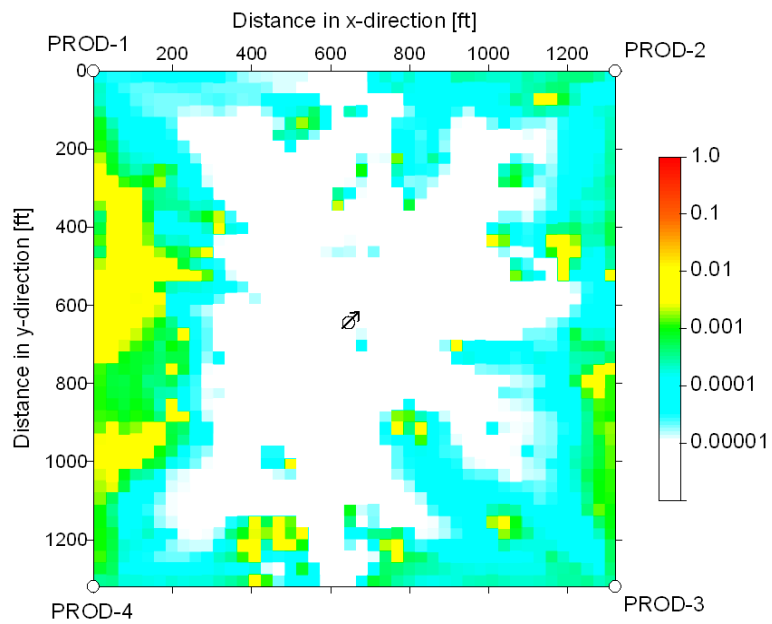


Figure 4.58: Tracer concentration profile in layer 8 at the end of the PITT

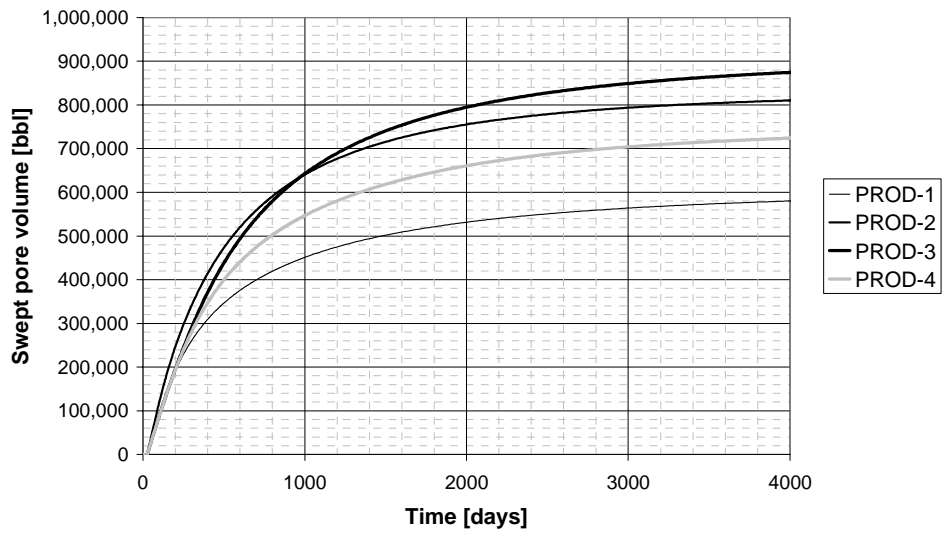


Figure 4.59: Swept pore volume between the injector and the each producer

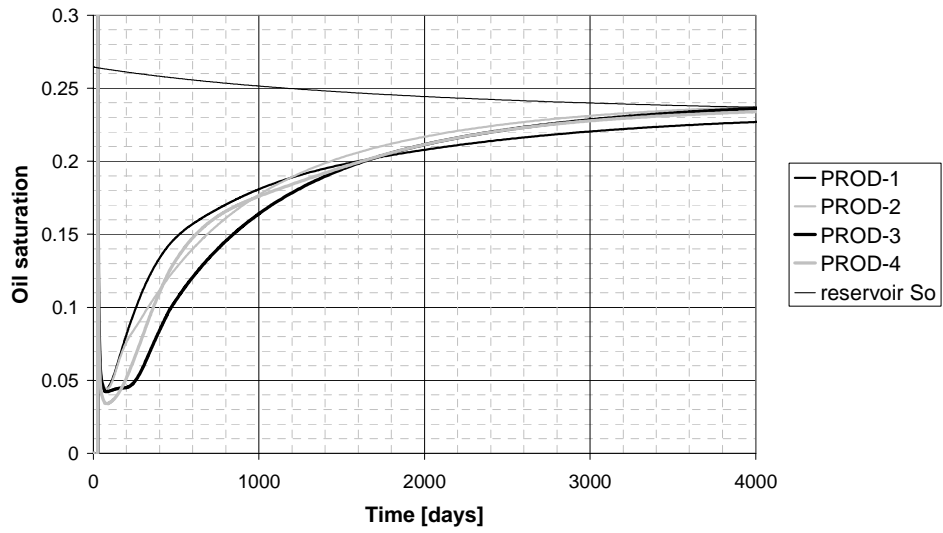


Figure 4.60: Oil saturation between well pairs

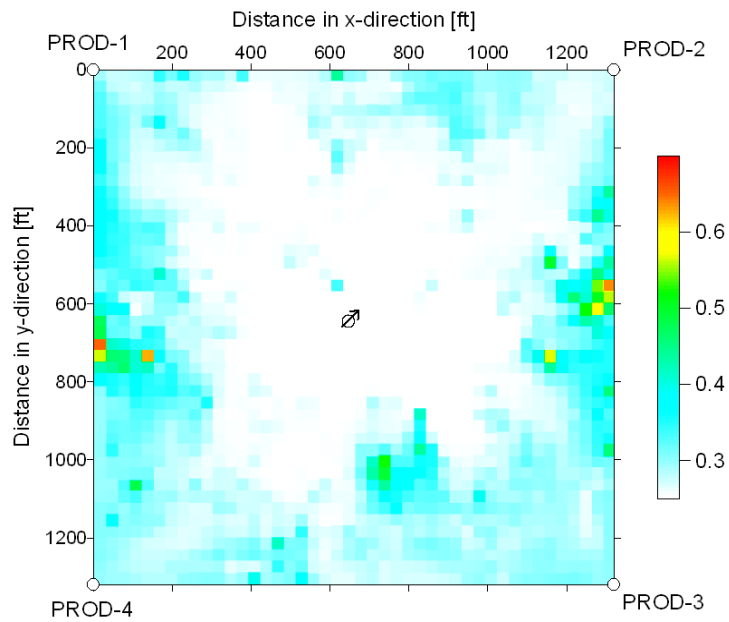


Figure 4.61: Oil saturation distribution at the start of tracer injection on layer 5

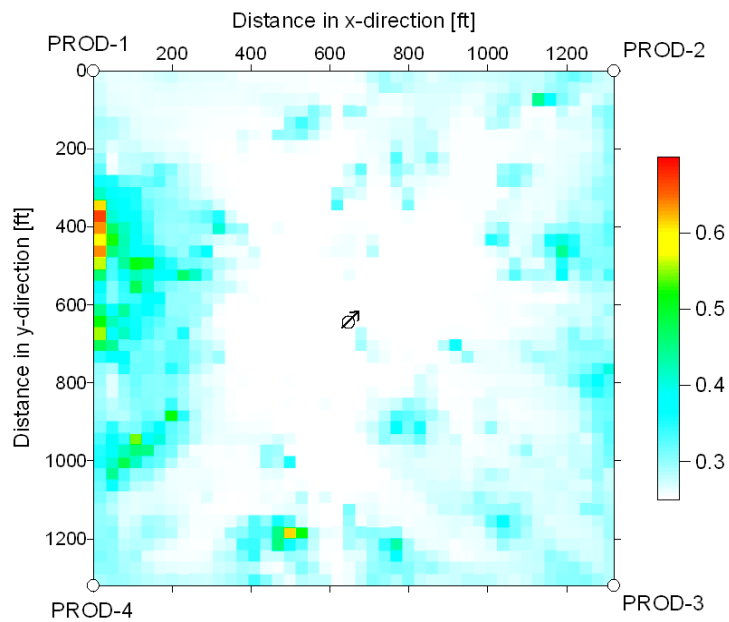


Figure 4.62: Oil saturation distribution at the start of tracer injection on layer 8

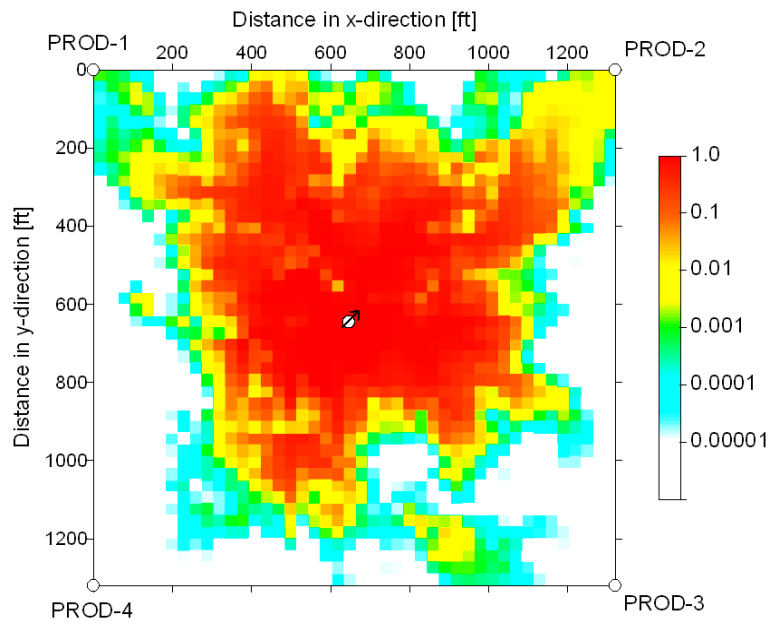


Figure 4.63: Conservative tracer concentration at 50 days in layer 5

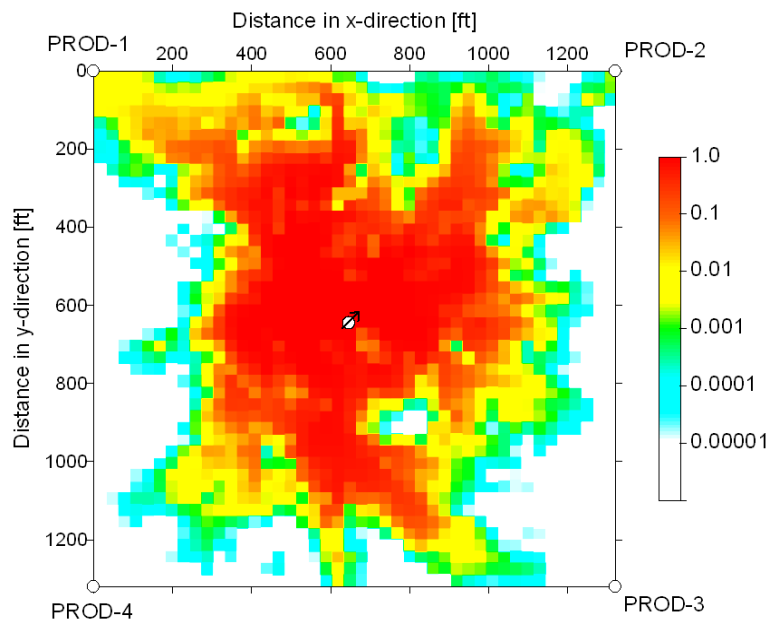


Figure 4.64: Conservative tracer concentration at 50 days in layer 8

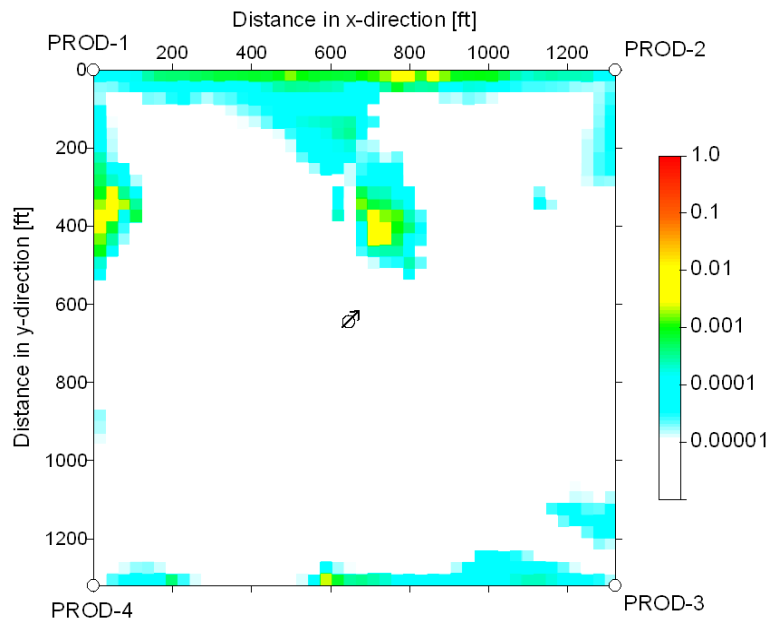


Figure 4.65: Conservative tracer concentration at end of PITT in layer 5

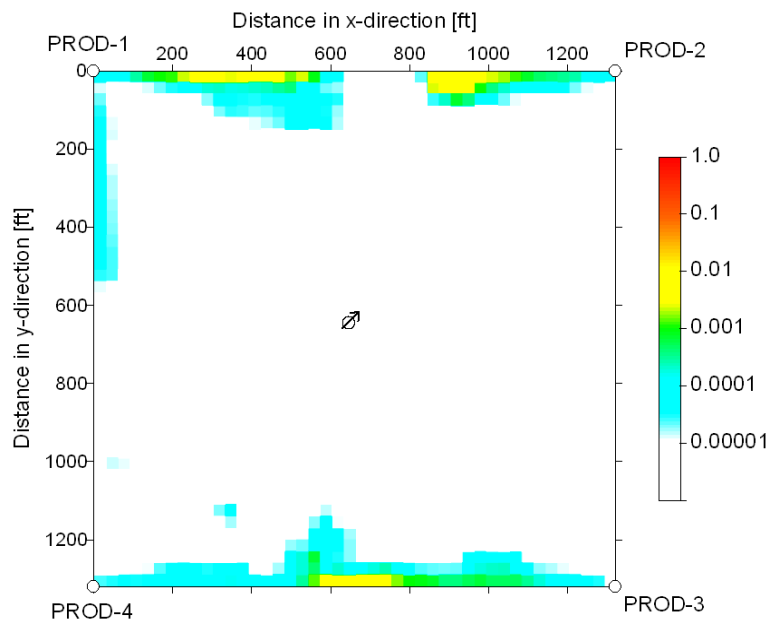


Figure 4.66: Conservative tracer concentration at the end of PITT in layer 8

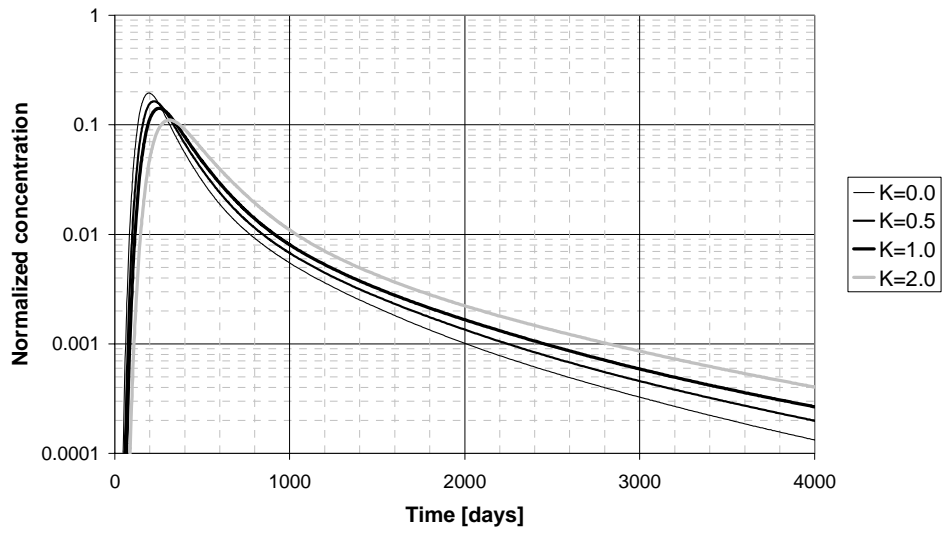


Figure 4.67: Tracer concentration history at PROD-1

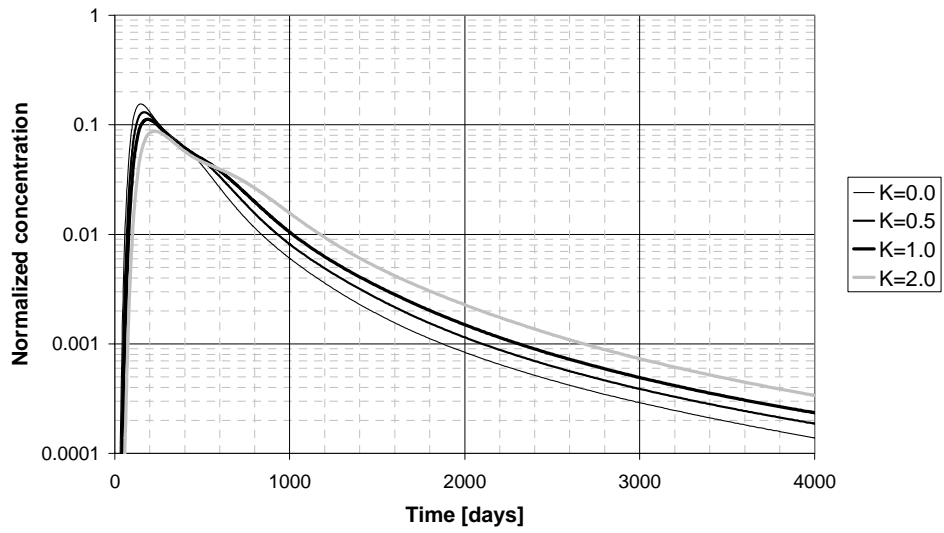


Figure 4.68: Tracer concentration history at PROD-2

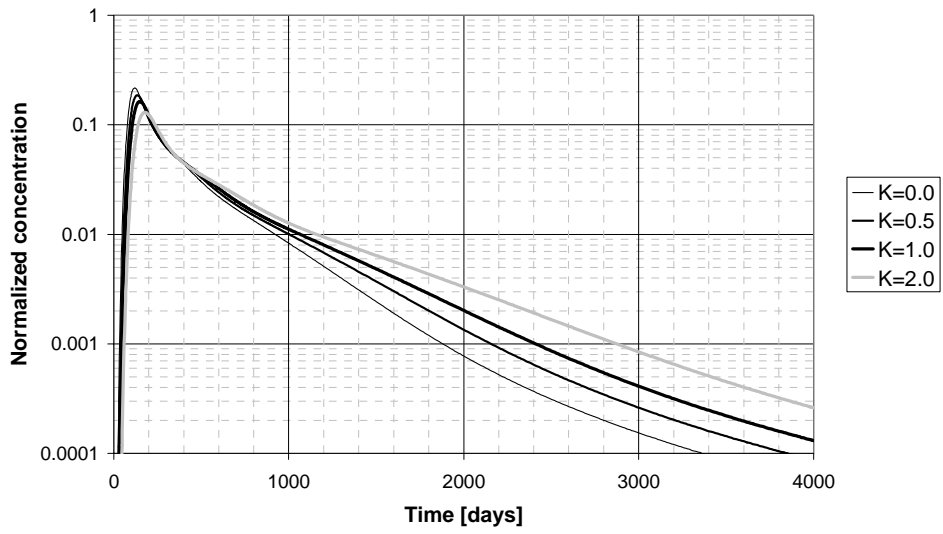


Figure 4.69: Tracer concentration history at PROD-3

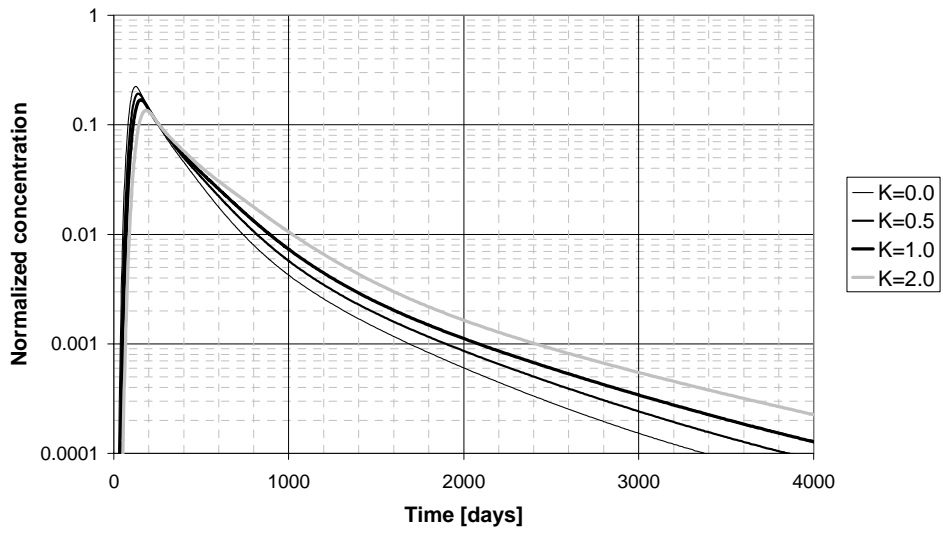


Figure 4.70: Tracer concentration history at PROD-4

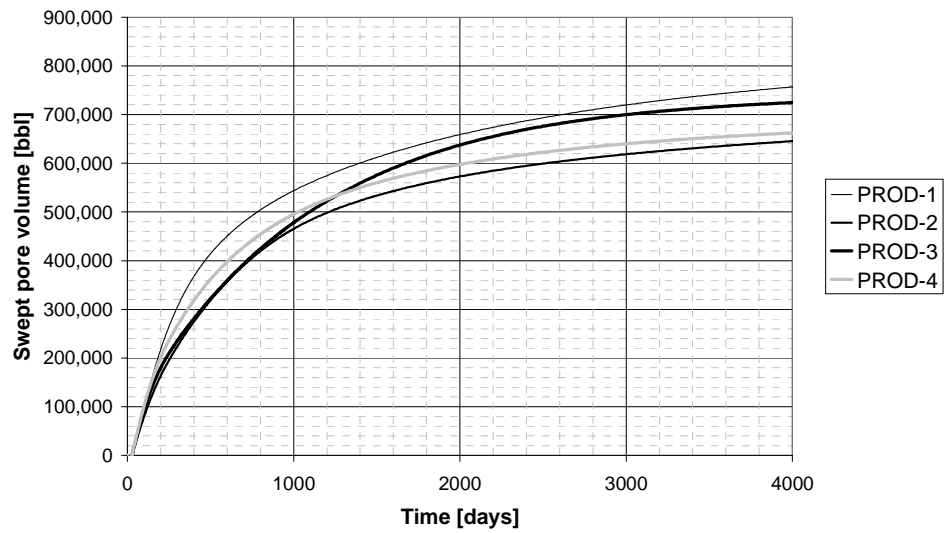


Figure 4.71: Swept pore volume between the injector and the each producer

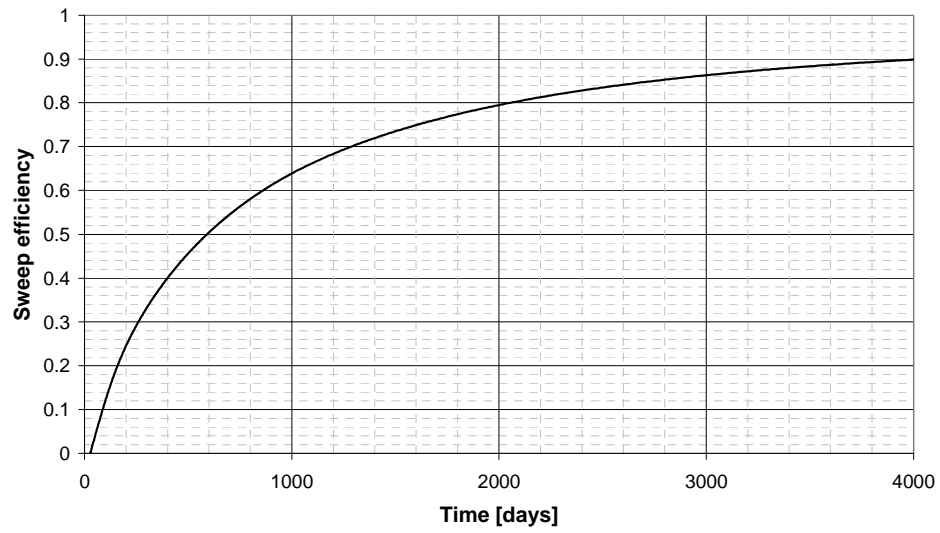


Figure 4.72: Sweep efficiency in the reservoir

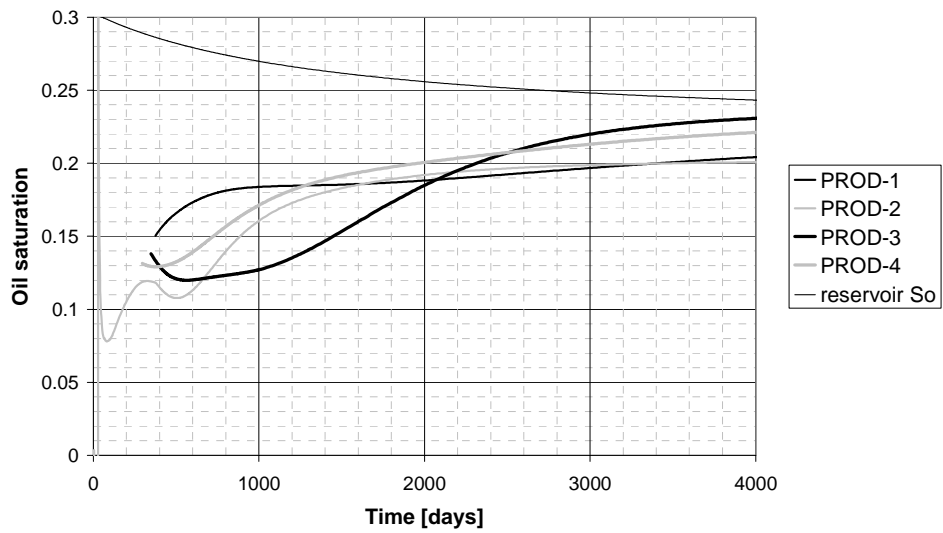


Figure 4.73: Oil Saturation between well pairs

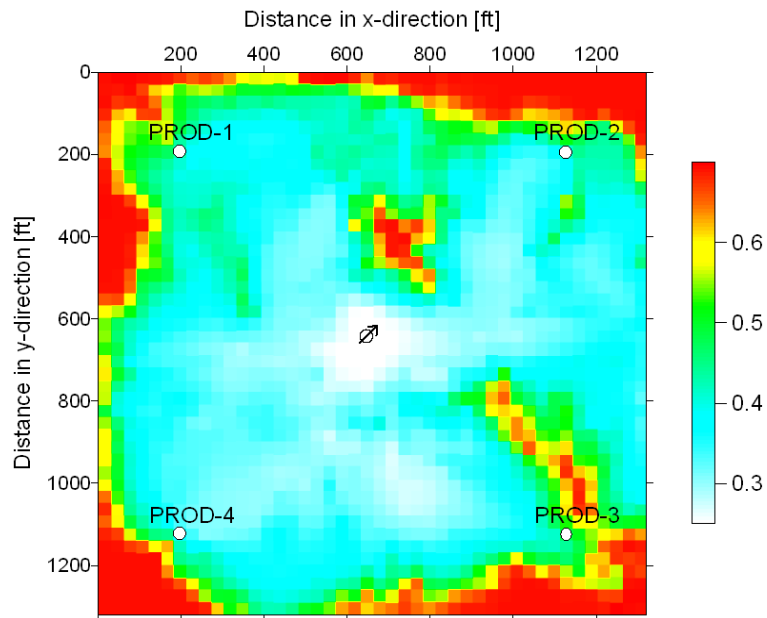


Figure 4.74: Oil saturation distribution in layer 5 at the beginning of the tracer injection

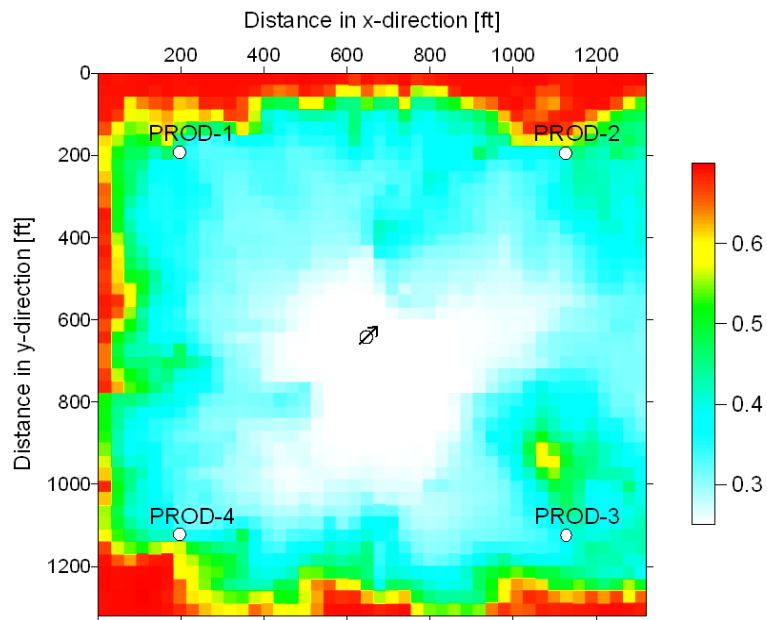


Figure 4.75: Oil saturation distribution in layer 8 at the beginning of the tracer injection

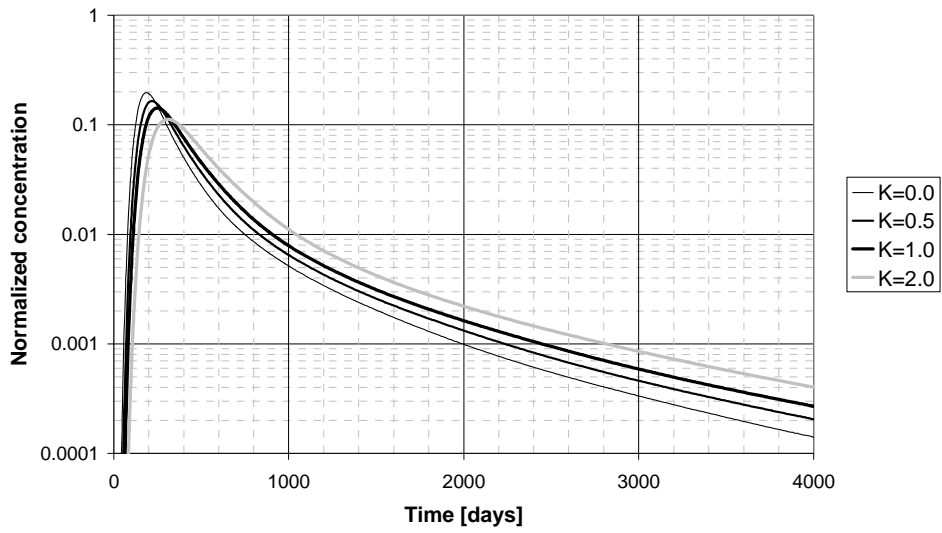


Figure 4.76: Normalized tracer concentration at PROD-1

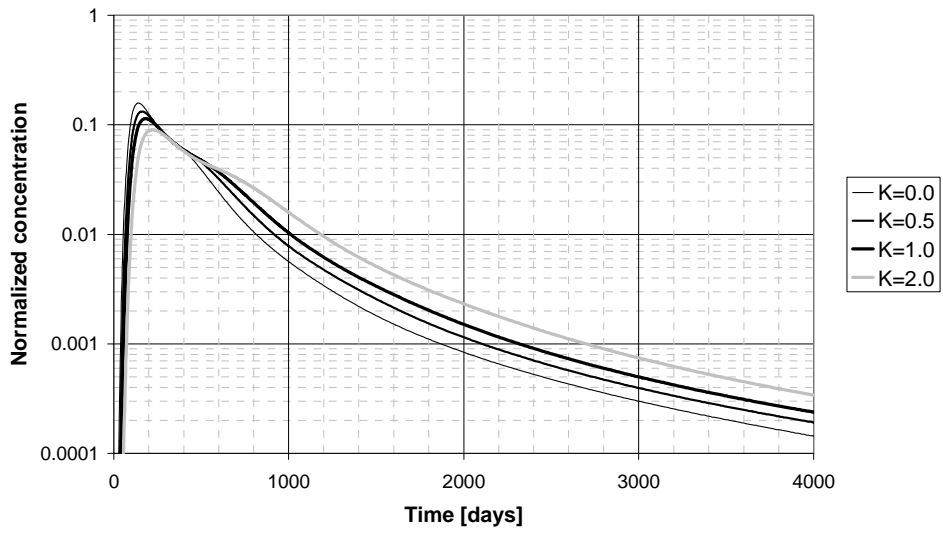


Figure 4.77: Normalized tracer concentration at PROD-2

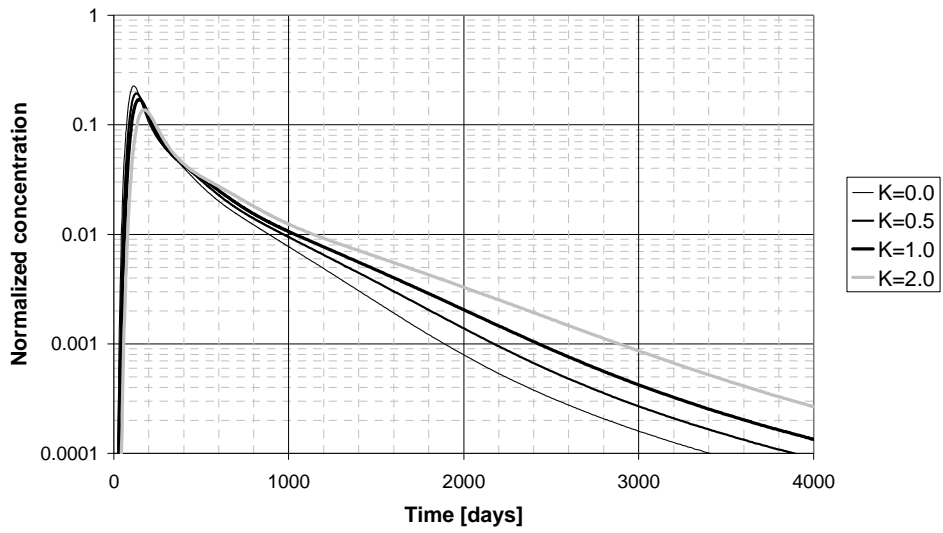


Figure 4.78: Normalized tracer concentration at PROD-3

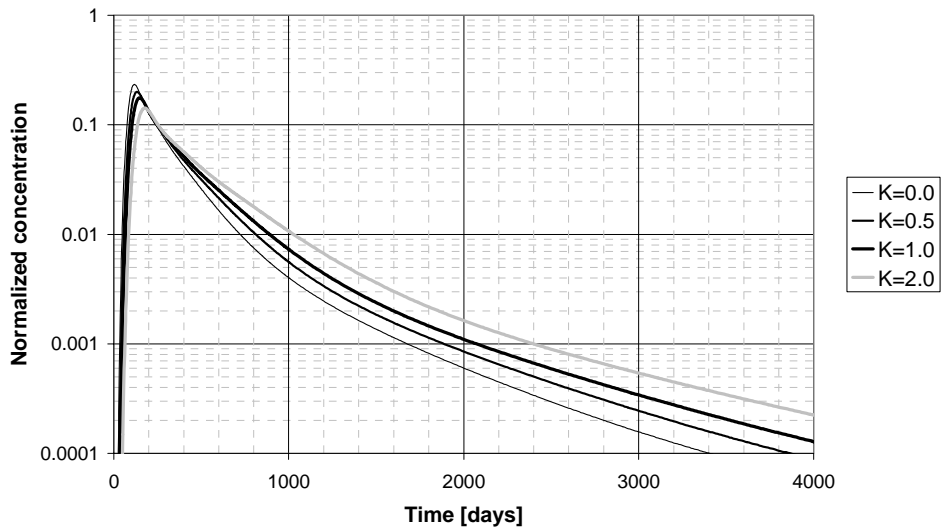


Figure 4.79: Normalized tracer concentration at PROD-4

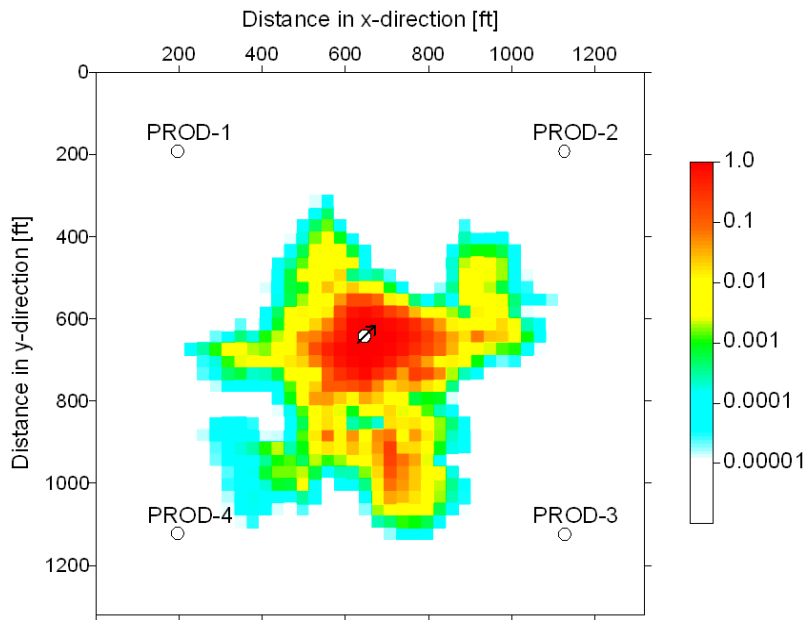


Figure 4.80: Partitioning tracer concentration with a partition coefficient of 2 after 25 days of tracer injection in layer 3

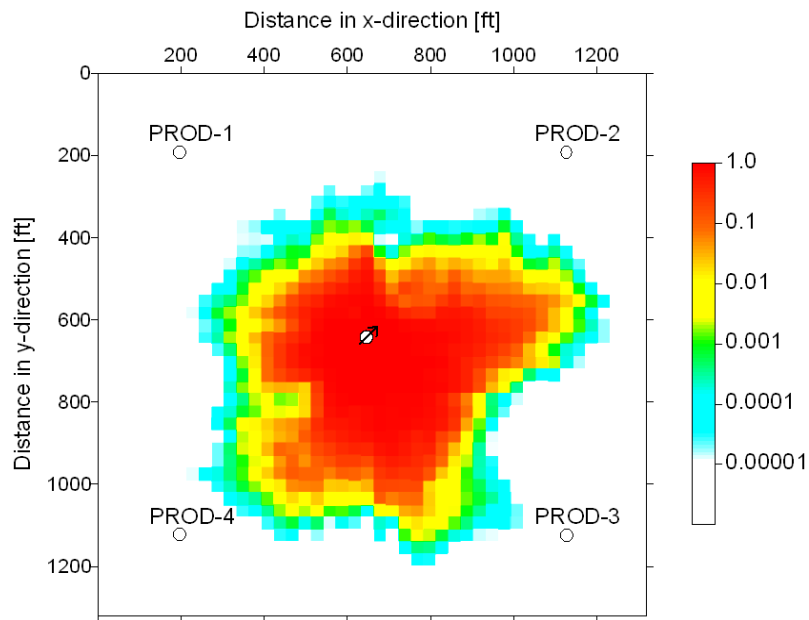


Figure 4.81: Partitioning tracer concentration with a partition coefficient of 2 after 25 days of tracer injection in layer 5

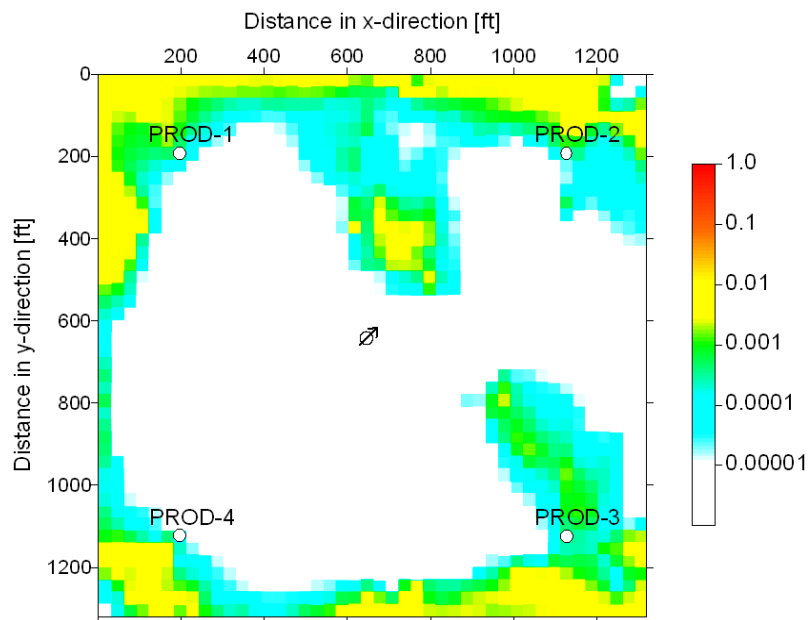


Figure 4.82: Partitioning tracer concentration with a partition coefficient of 2 at the end of PITT in layer 8

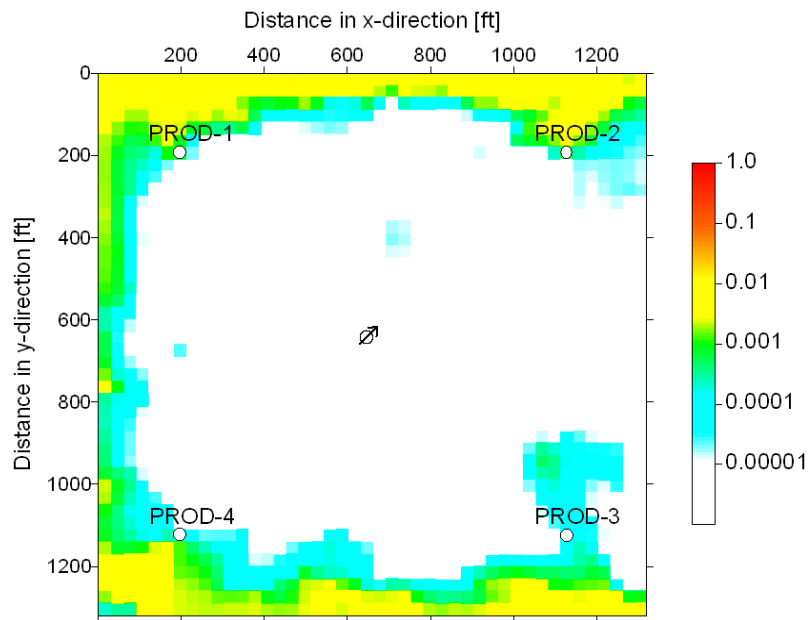


Figure 4.83: Partitioning tracer concentration with a partition coefficient of 2 at the end of PITT in layer 5

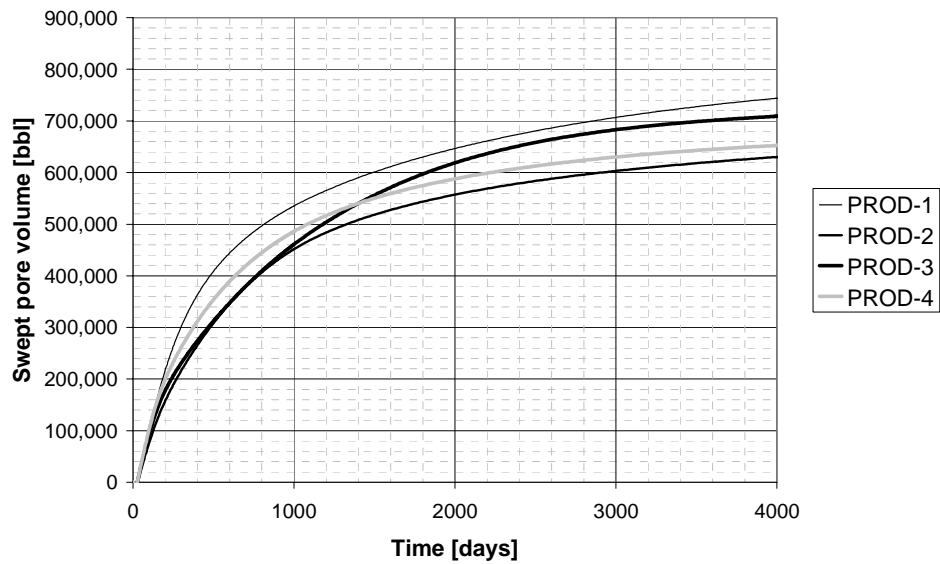


Figure 4.84: Swept pore volume between the injector and the each producers

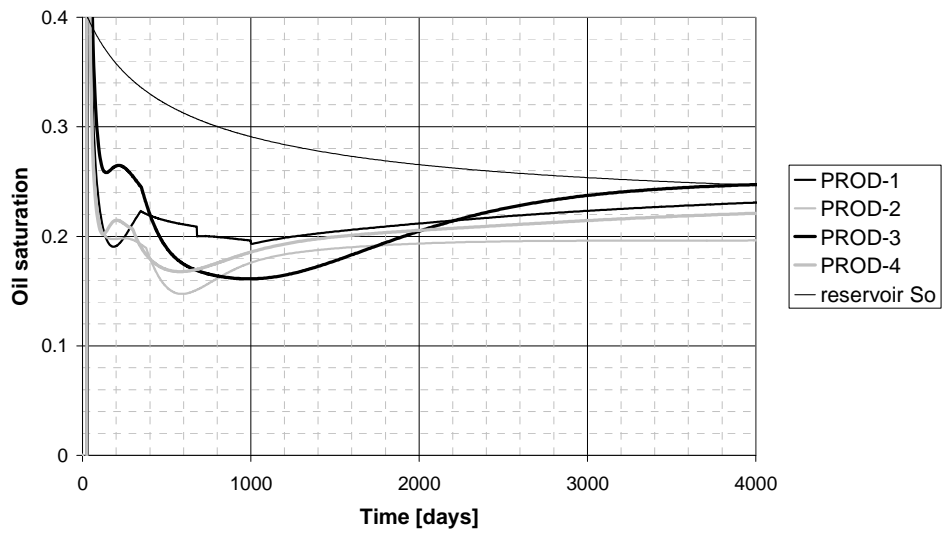


Figure 4.85: Oil saturation between well pairs

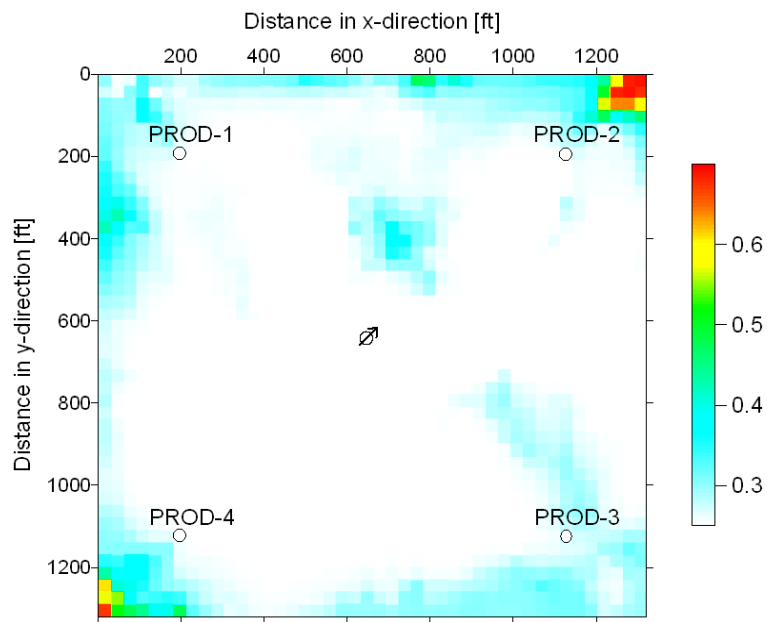


Figure 4.86: Oil saturation distribution in layer 5 at the end of PITT

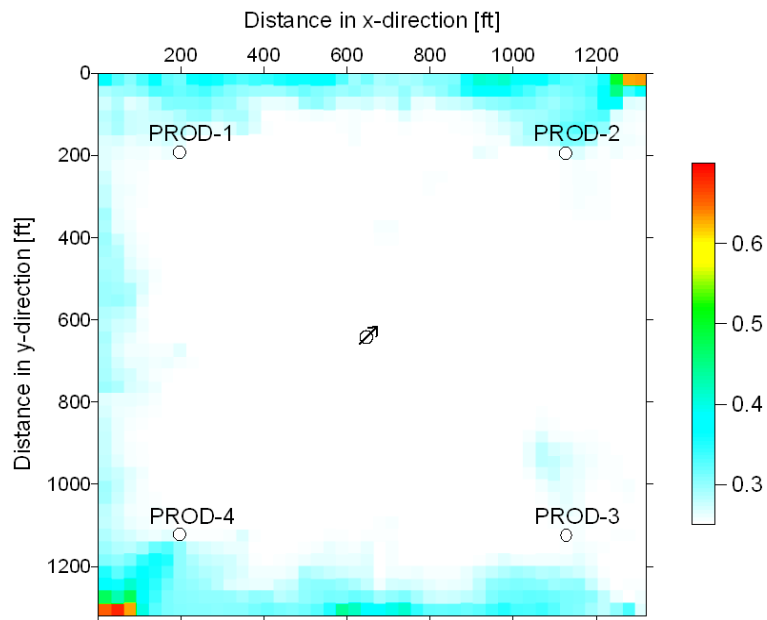


Figure 4.87: Oil saturation distribution in layer 8 at the end of PITT

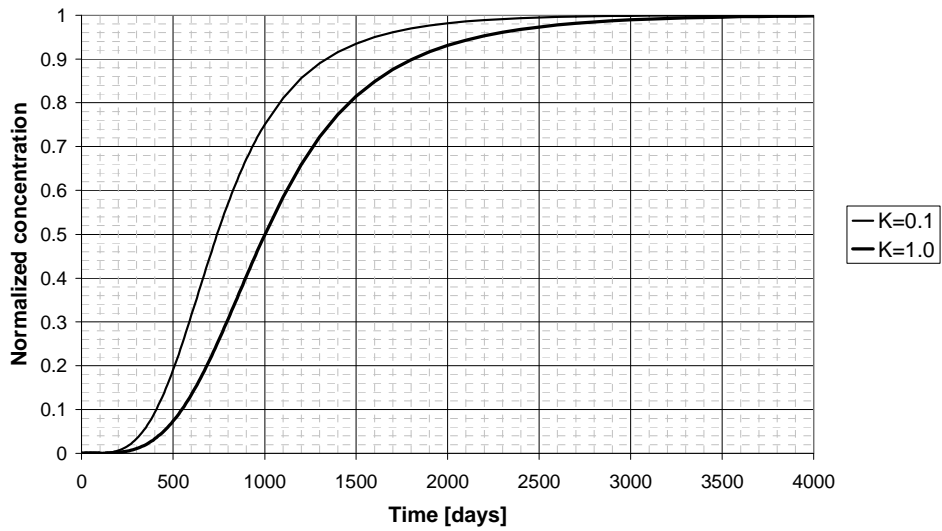


Figure 4.88: Natural tracer history from naturally fractured reservoir

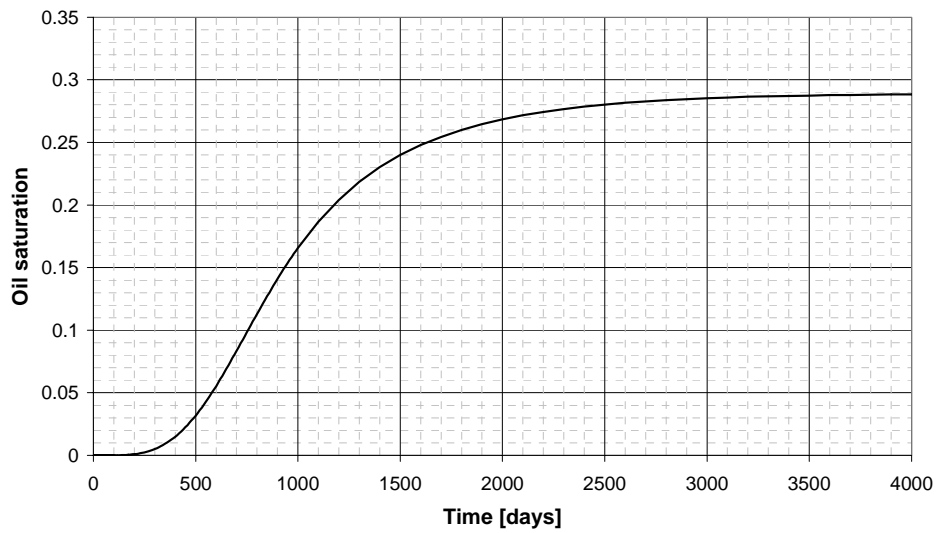


Figure 4.89: Oil saturation estimation from natural tracer from naturally fractured reservoir

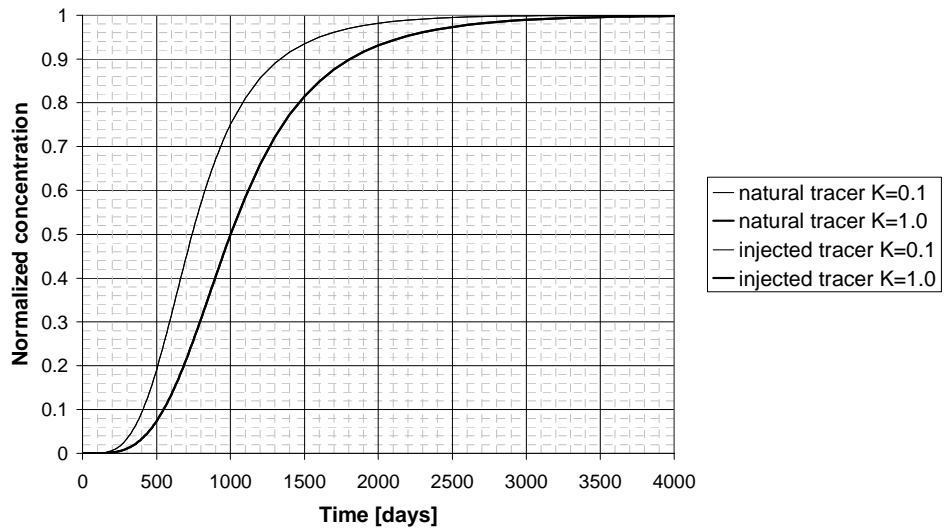


Figure 4.90: Comparison of natural tracers and injected tracers

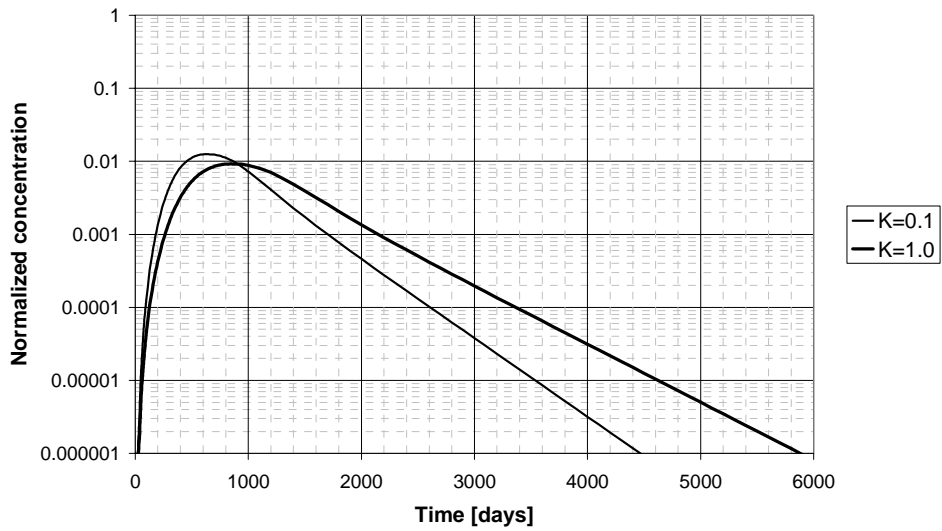


Figure 4.91: Produced tracer data from naturally fractured reservoir

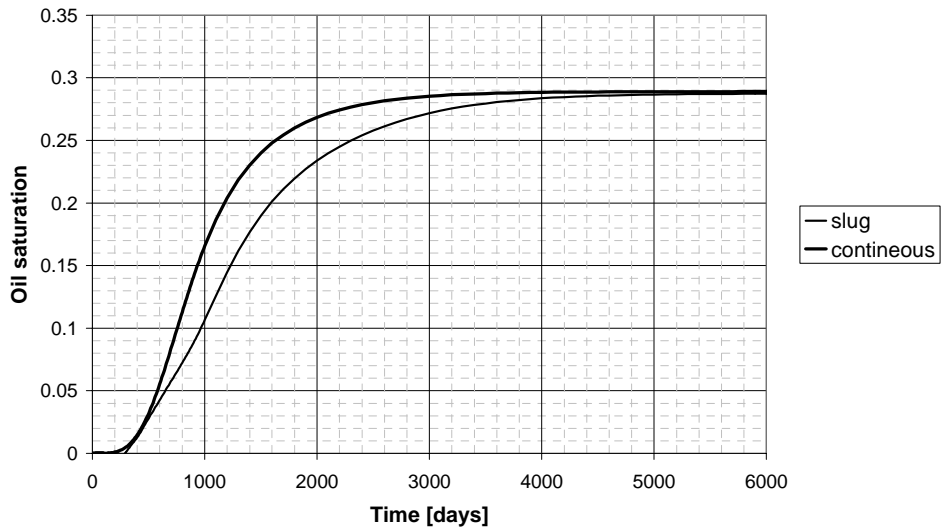


Figure 4.92: Comparison of estimated oil saturation in naturally fractured reservoir using the slug and continuous tracer injected

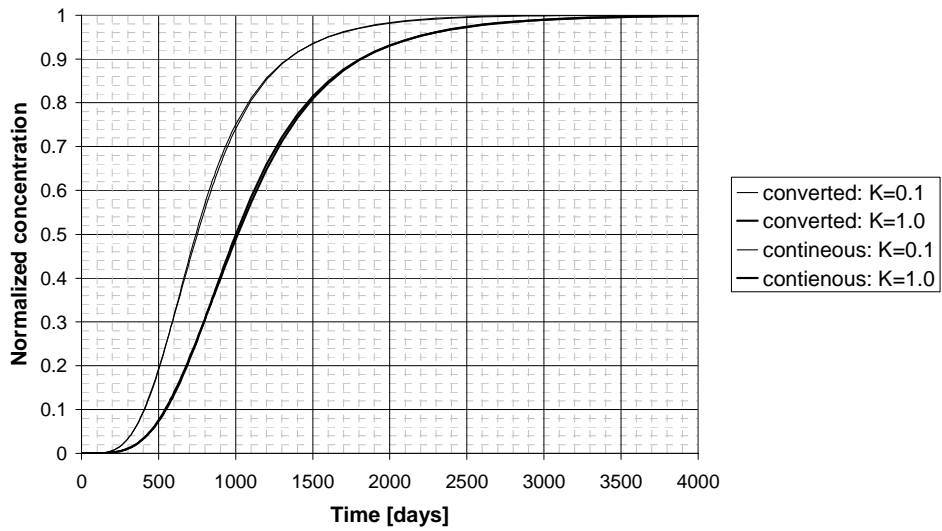


Figure 4.93: Comparison of converted tracer slug and continuous tracer

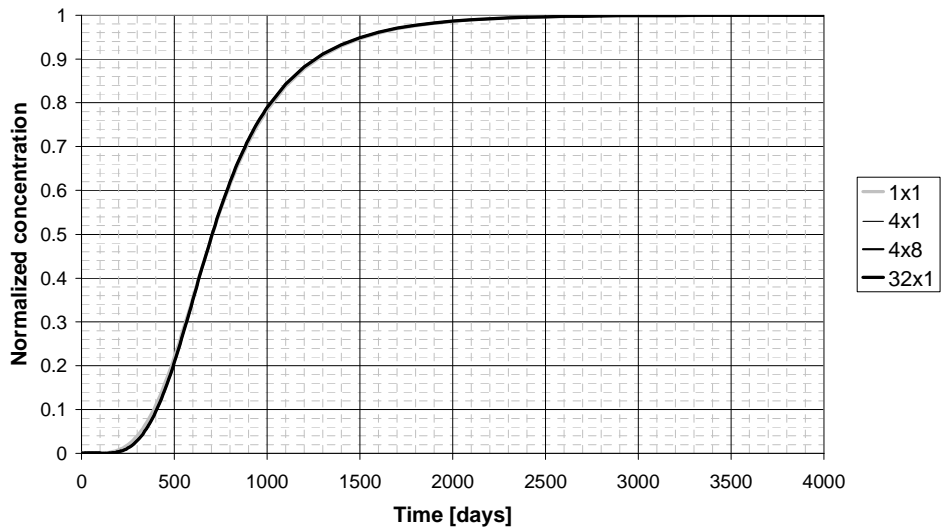


Figure 4.94: Comparison of natural tracer concentration with different matrix subgridding for partition coefficient of 0.001

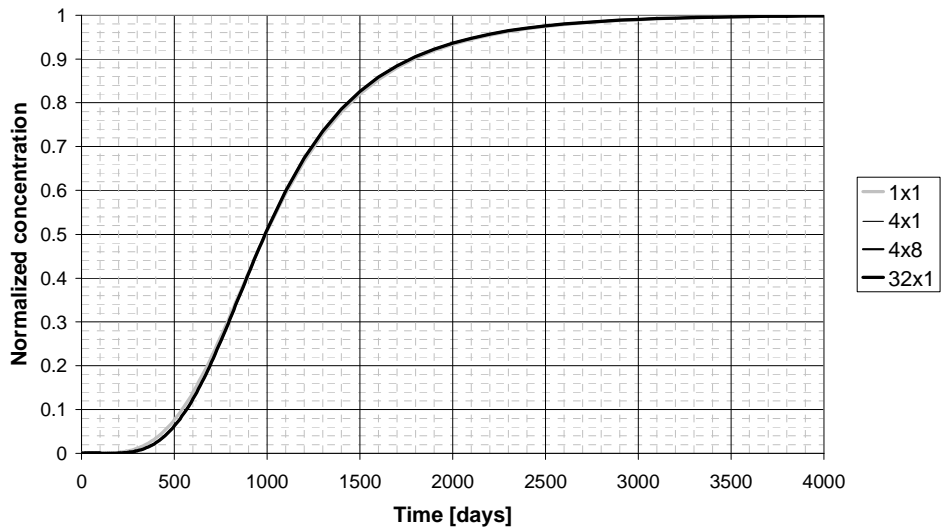


Figure 4.95: Comparison of natural tracer concentration with different matrix subgridding for partition coefficient of 1.0

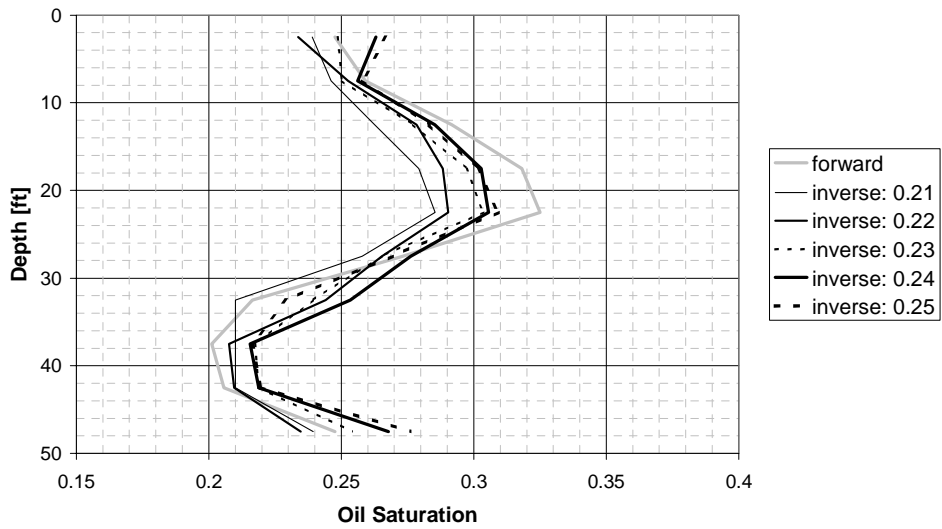


Figure 4.96: Oil saturation calculated from inverse model for initial guesses between 0.21 and 0.25

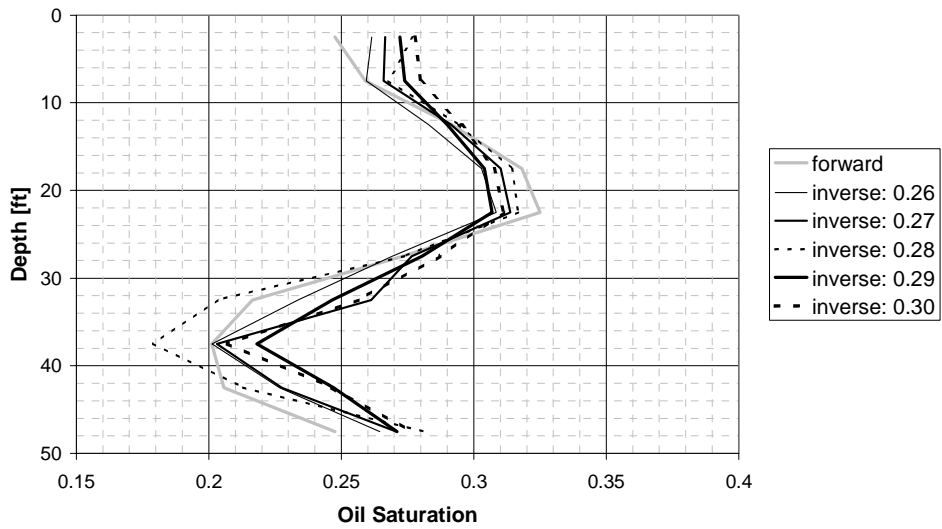


Figure 4.97: Oil saturation calculated from inverse model for initial guesses between 0.26 and 0.30

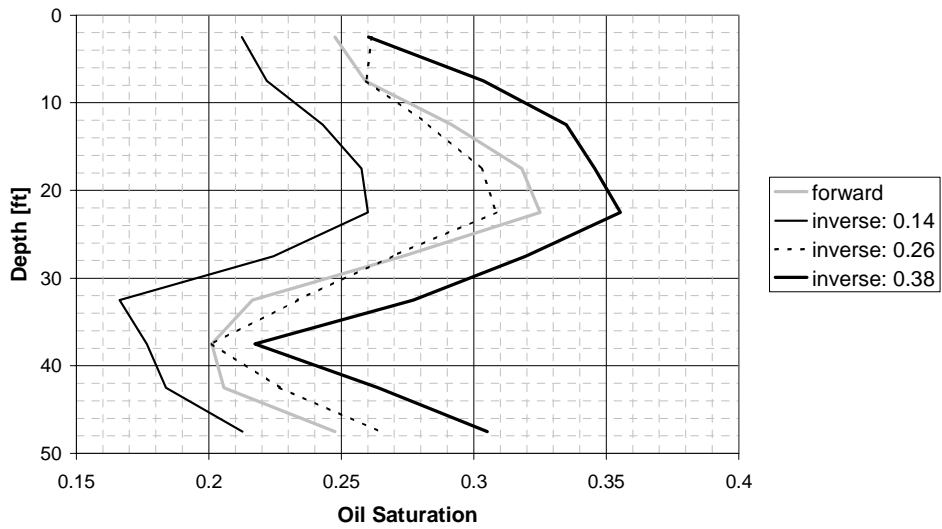


Figure 4.98: Oil saturation calculated from inverse model for initial guesses of 0.14, 0.26, and 0.38

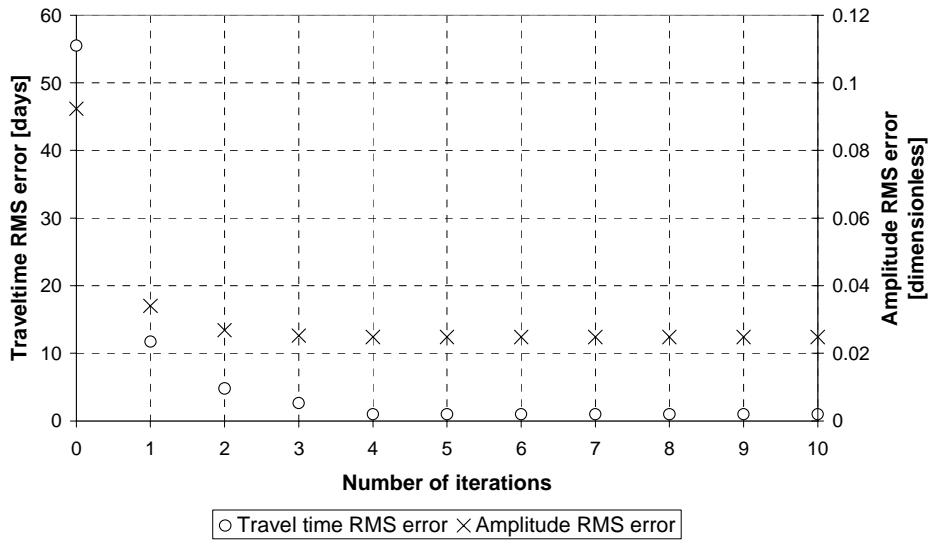


Figure 4.99: RMS error in travel time and amplitude for an initial oil saturation guess of 0.21

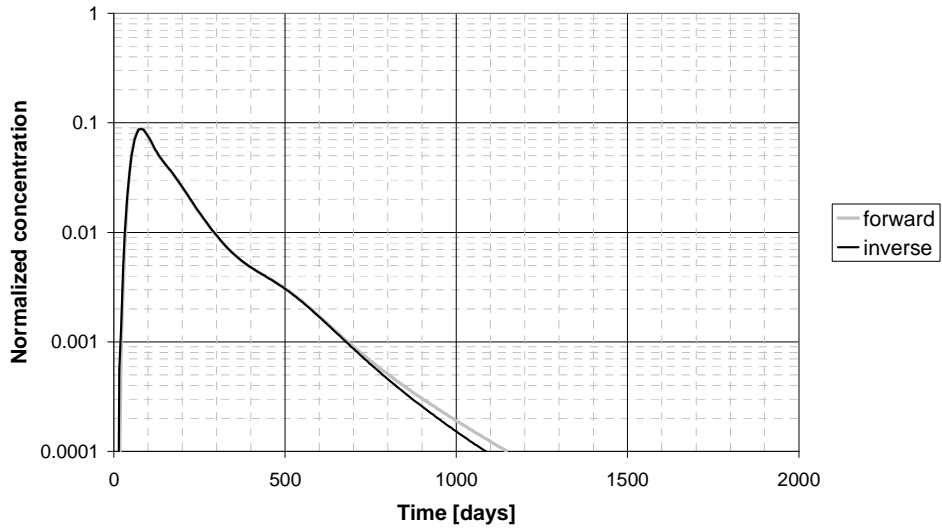


Figure 4.100: Match of forward and inverse tracer curves from all layers after 4 iterations for an initial oil saturation guess of 0.21

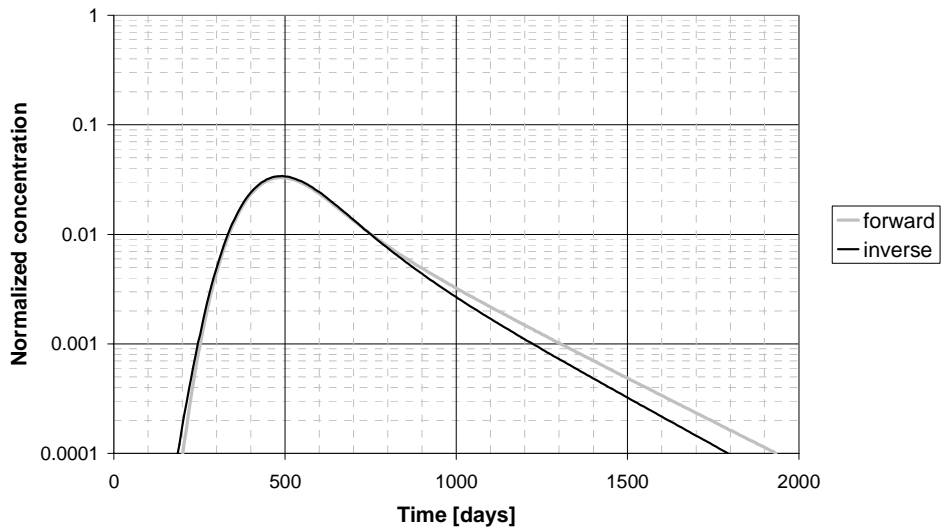


Figure 4.101: Match of forward and inverse tracer curves from layer 5 after 4 iterations for an initial oil saturation guess of 0.21

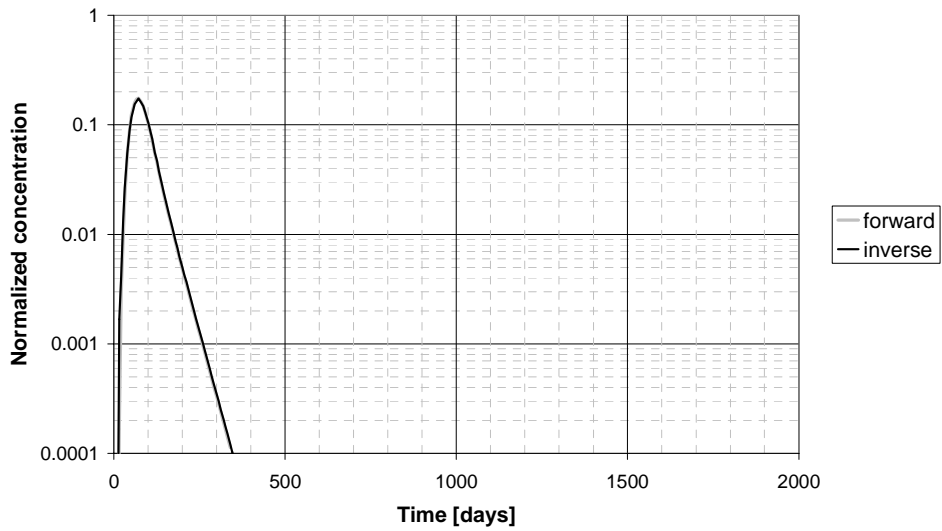


Figure 4.102: Match of forward and inverse tracer curves from layer 8 after 4 iterations for an initial oil saturation guess of 0.21

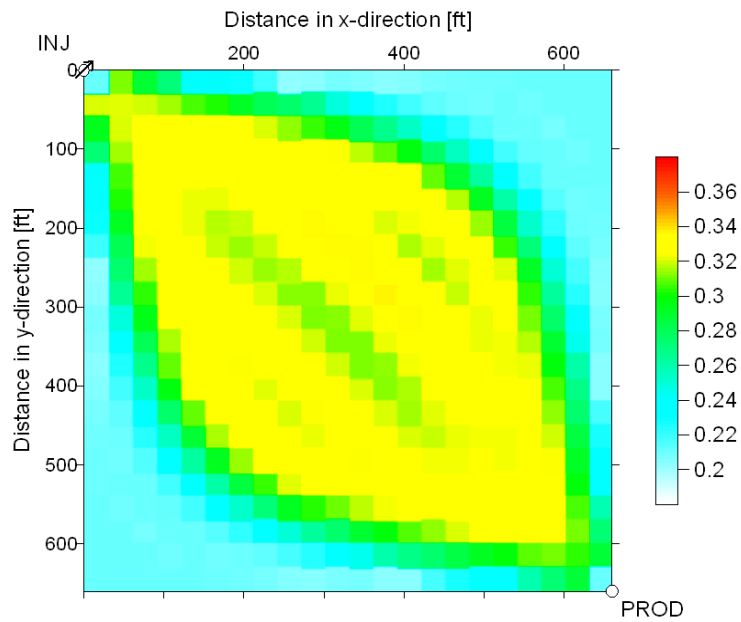


Figure 4.103: Oil saturation for layer 5 after 4 iterations for an initial oil saturation guess of 0.21

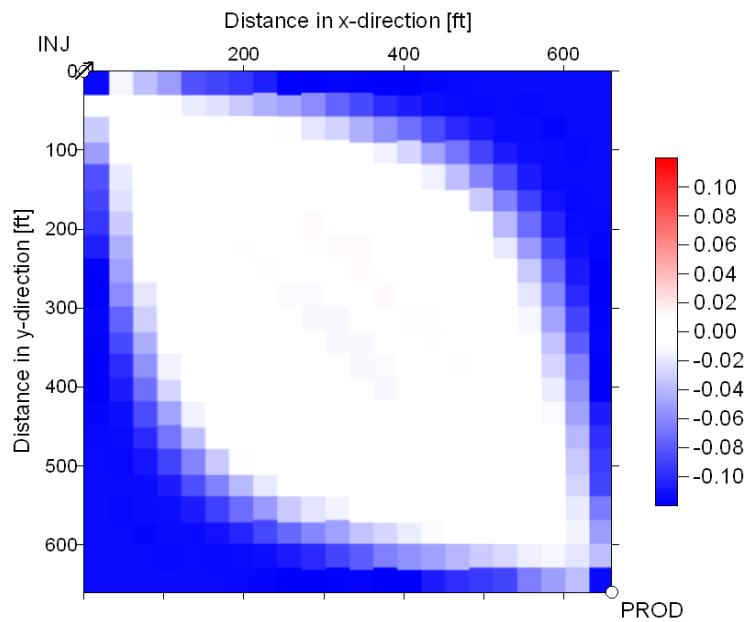


Figure 4.104: Difference in Oil saturation for layer 5 after 4 iterations for an initial oil saturation guess of 0.21

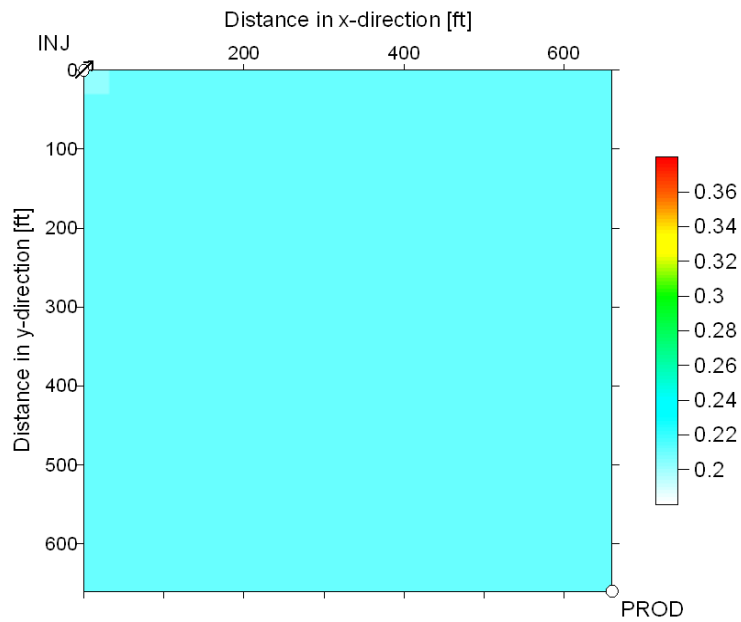


Figure 4.105: Oil saturation for layer 8 after 4 iterations for an initial oil saturation guess of 0.21

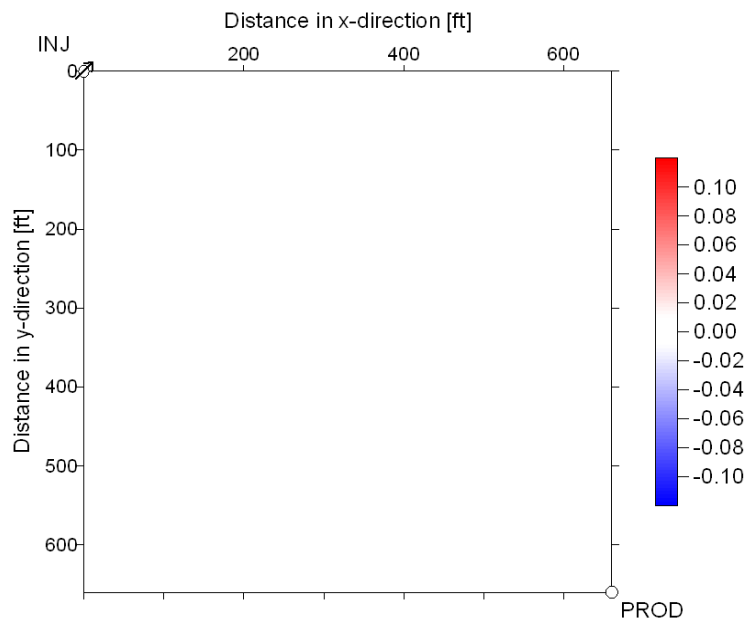


Figure 4.106: Difference in Oil saturation for layer 8 after 4 iterations for an initial oil saturation guess of 0.21

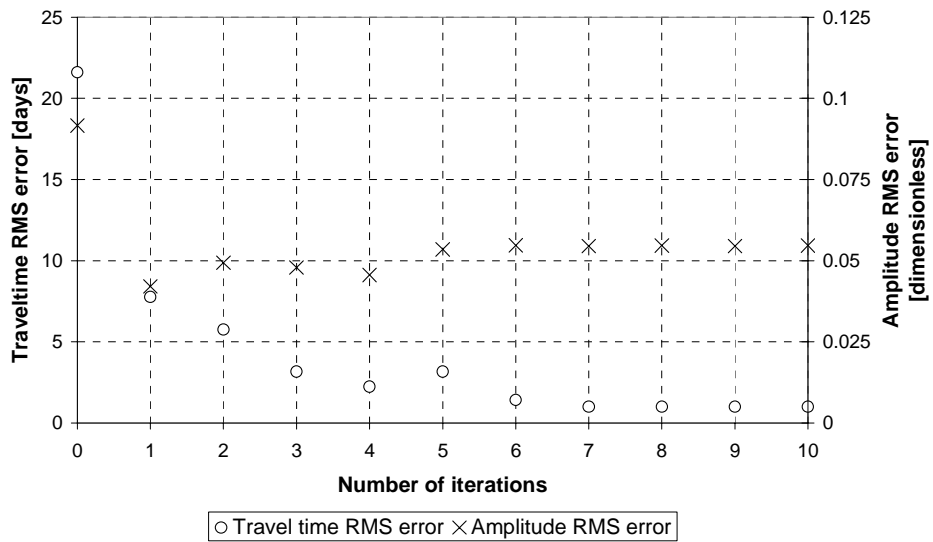


Figure 4.107: RMS error in travel time and amplitude for an initial oil saturation guess of 0.28

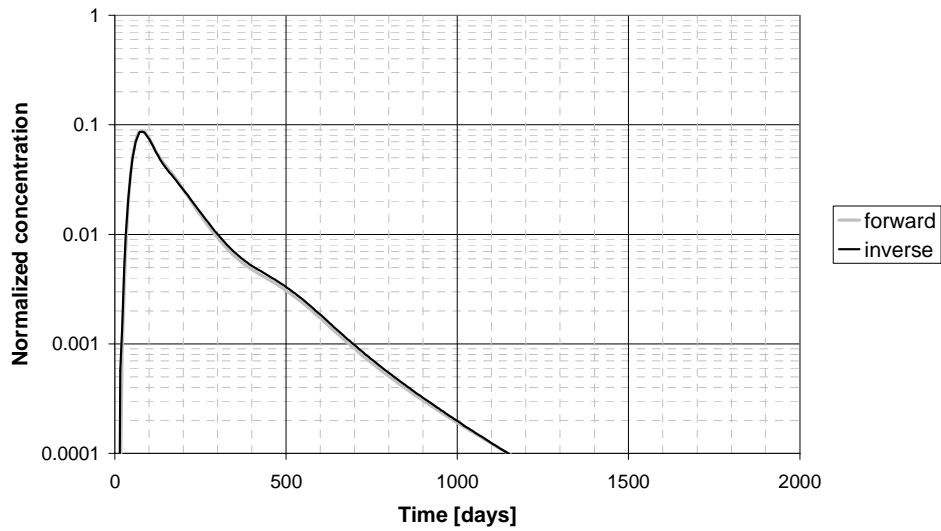


Figure 4.108: Match of forward and inverse tracer curves from all layers after 10 iterations for an initial oil saturation guess of 0.28

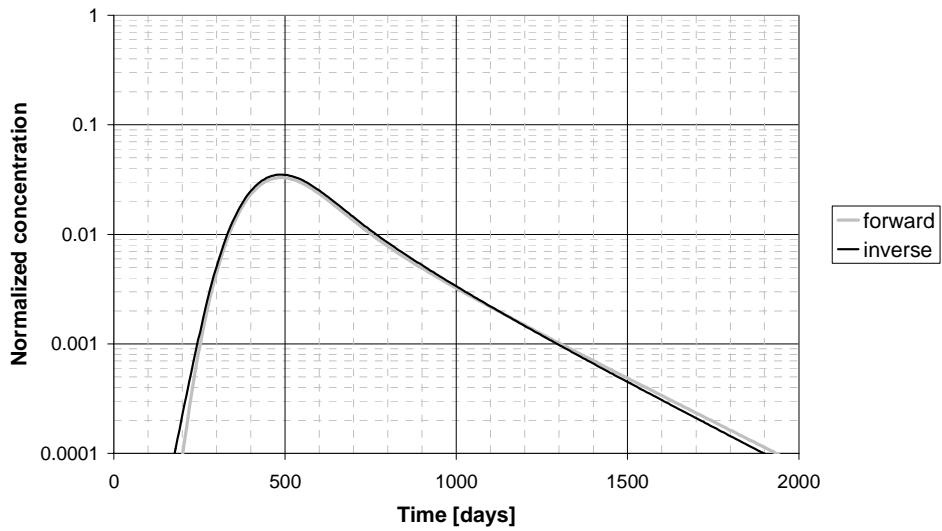


Figure 4.109: Match of forward and inverse tracer curves from layer 5 after 10 iterations for an initial oil saturation guess of 0.28

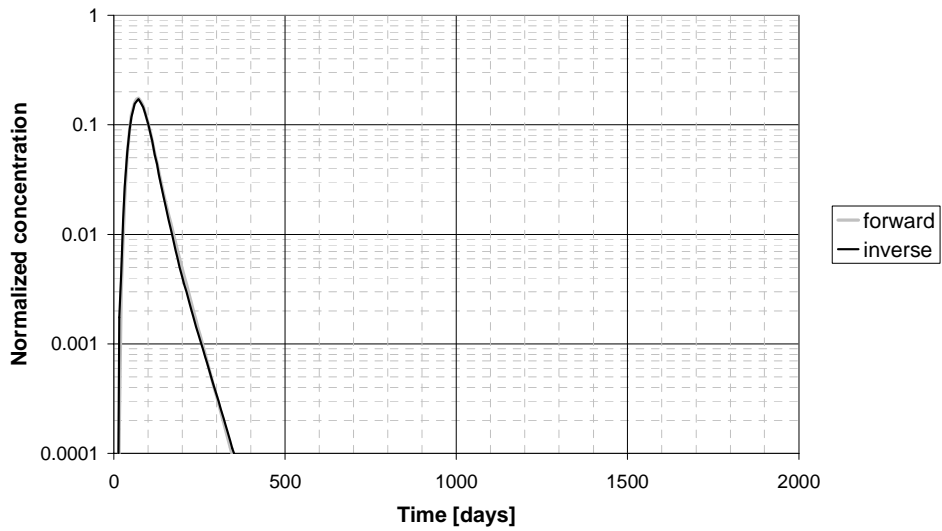


Figure 4.110: Match of forward and inverse tracer curves from layer 8 after 10 iterations for an initial oil saturation guess of 0.28

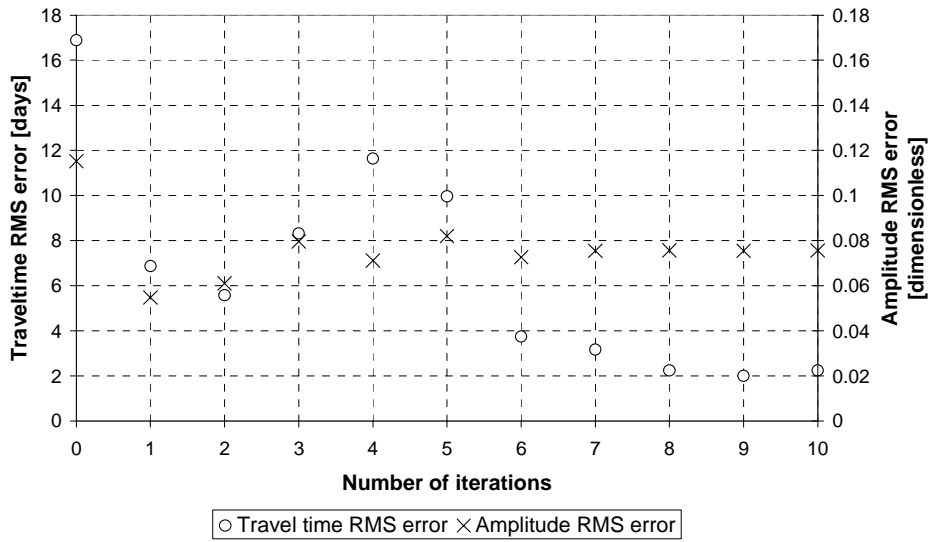


Figure 4.111: RMS error in travel time and amplitude for an initial oil saturation guess of 0.30

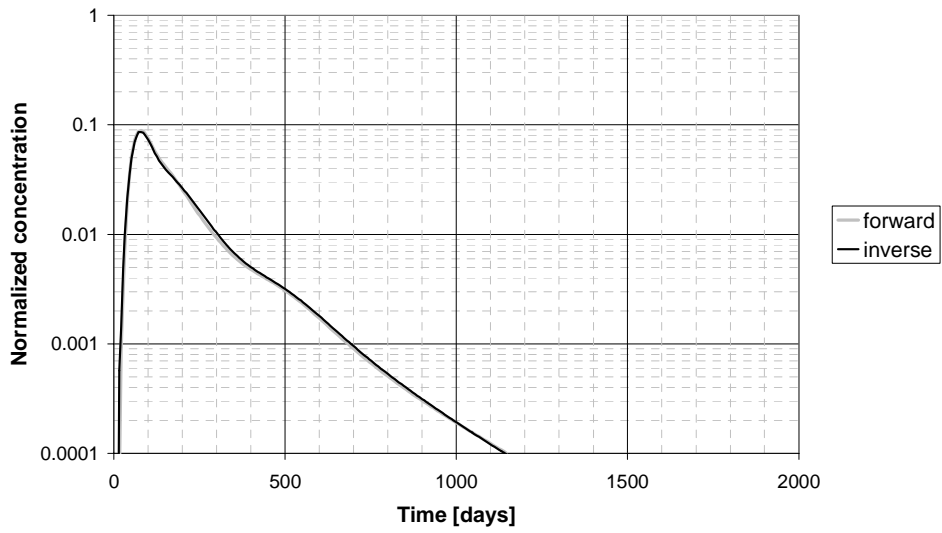


Figure 4.112: Match of forward and inverse tracer curves from all layers after 1 iteration for an initial oil saturation guess of 0.30

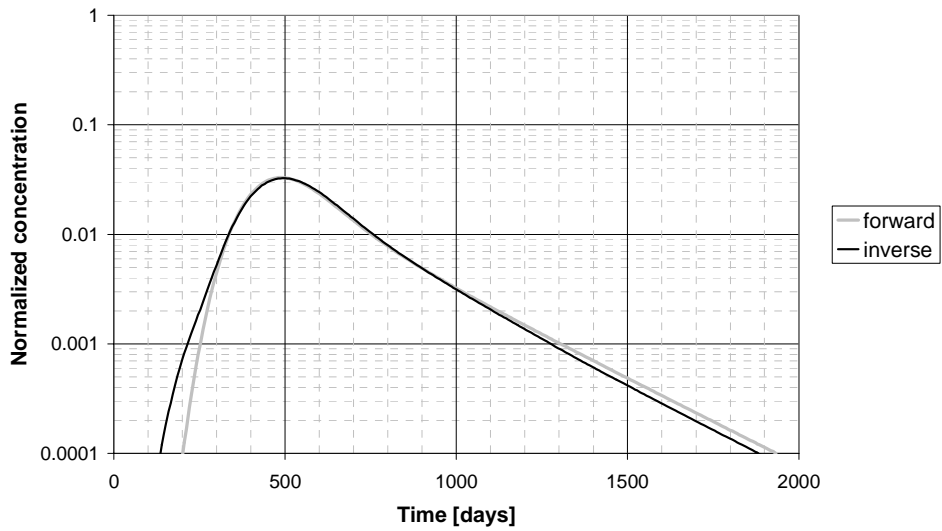


Figure 4.113: Match of forward and inverse tracer curves from layer 5 after 1 iteration for an initial oil saturation guess of 0.30

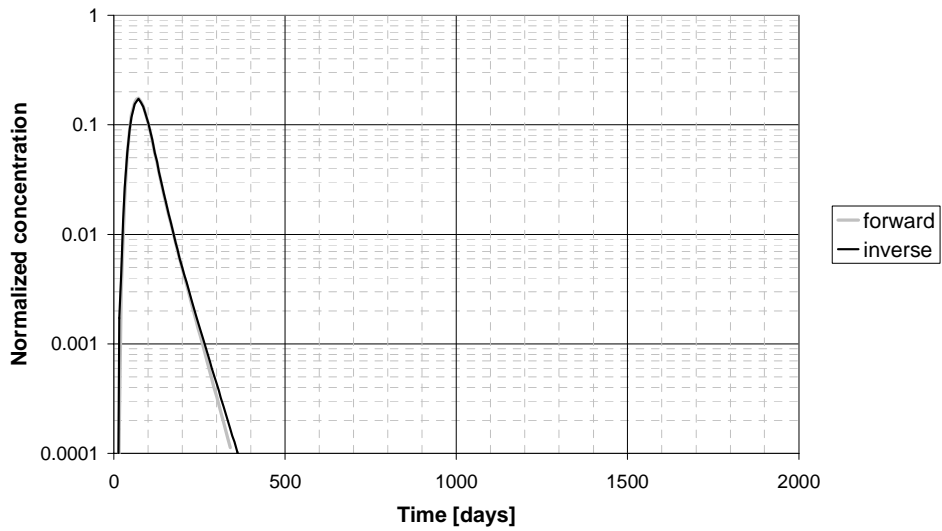


Figure 4.114: Match of forward and inverse tracer curves from layer 8 after 1 iteration for an initial oil saturation guess of 0.30

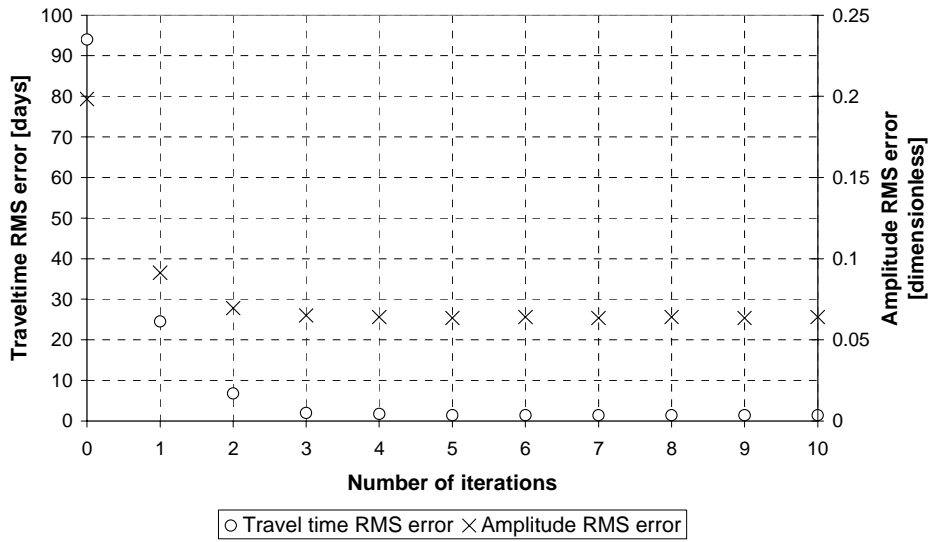


Figure 4.115: RMS error in travel time and amplitude for an initial oil saturation guess of 0.14

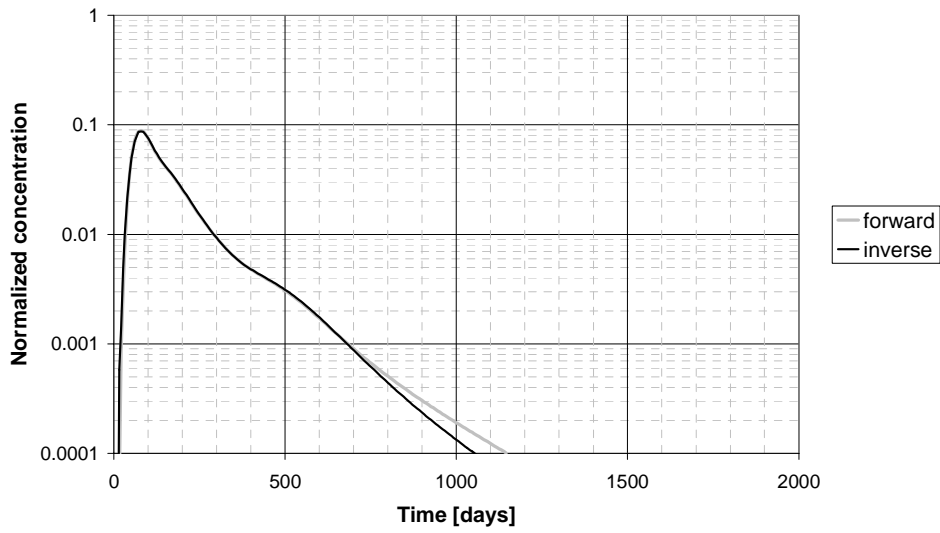


Figure 4.116: Match of forward and inverse tracer curves from all layers after 4 iterations for an initial oil saturation guess of 0.14

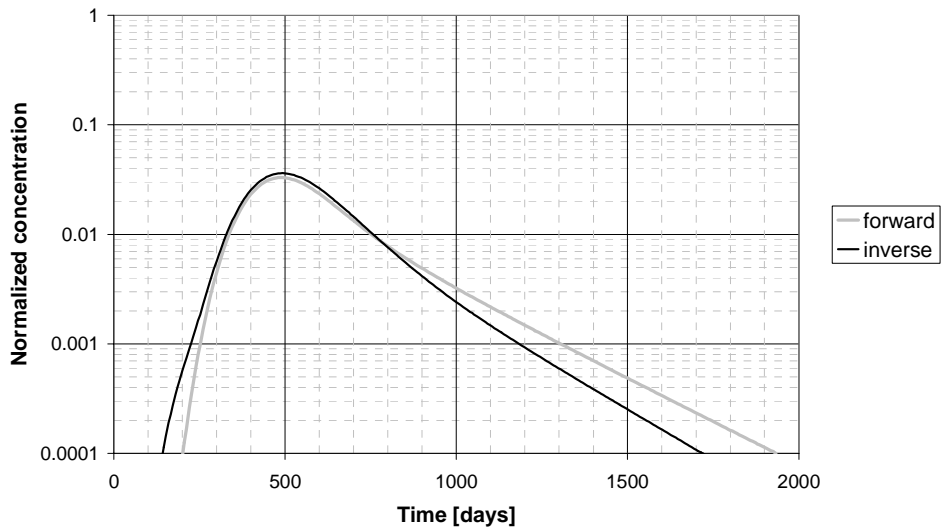


Figure 4.117: Match of forward and inverse tracer curves from layer 5 after 4 iterations for an initial oil saturation guess of 0.14

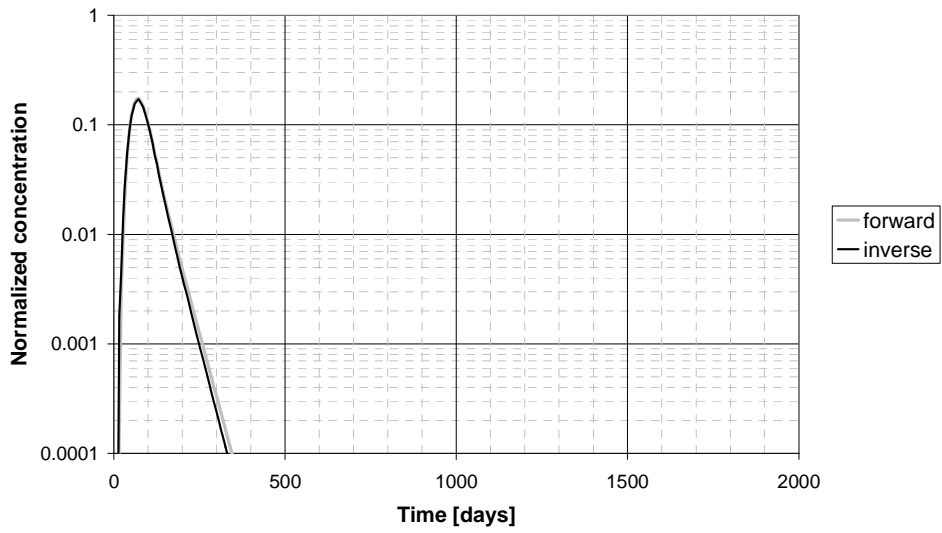


Figure 4.118: Match of forward and inverse tracer curves from layer 8 after 4 iterations for an initial oil saturation guess of 0.14

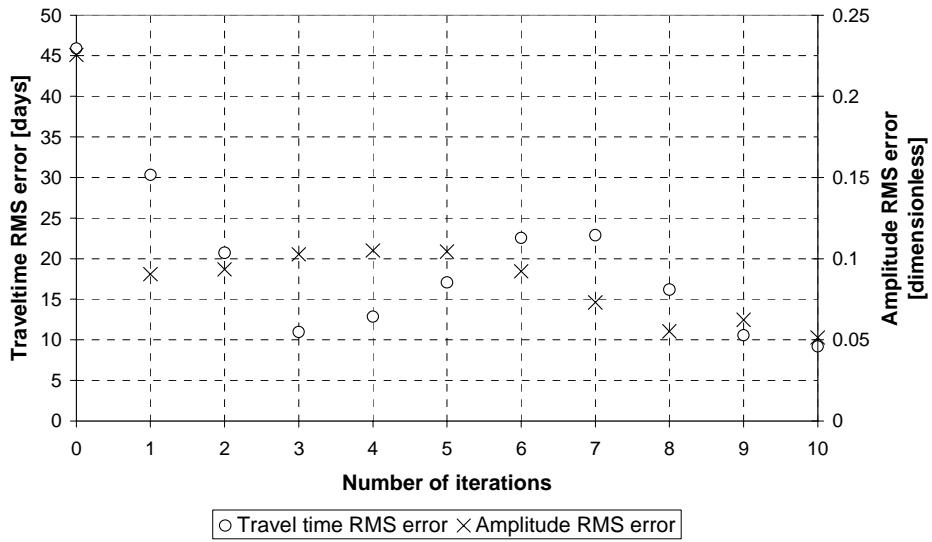


Figure 4.119: RMS error in travel time and amplitude for an initial oil saturation guess of 0.38

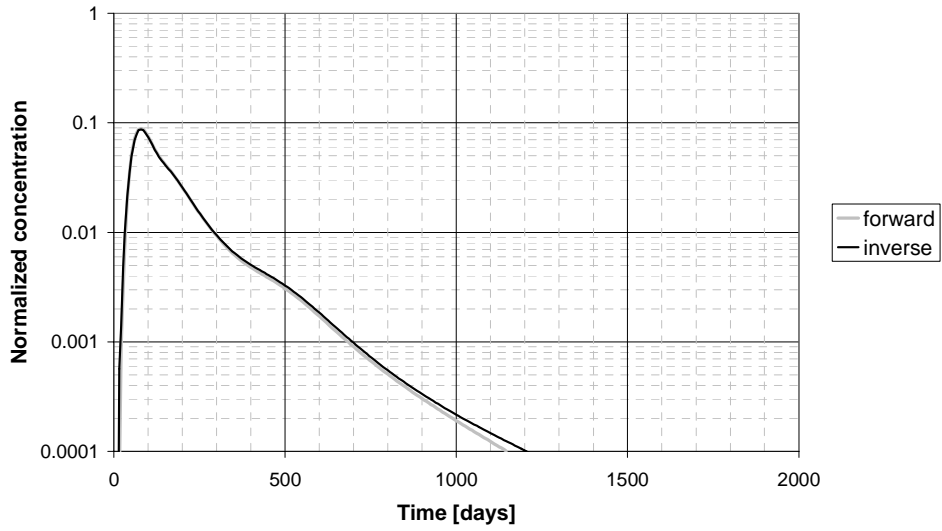


Figure 4.120: Match of forward and inverse tracer curves from all layers after 10 iterations for an initial oil saturation guess of 0.38

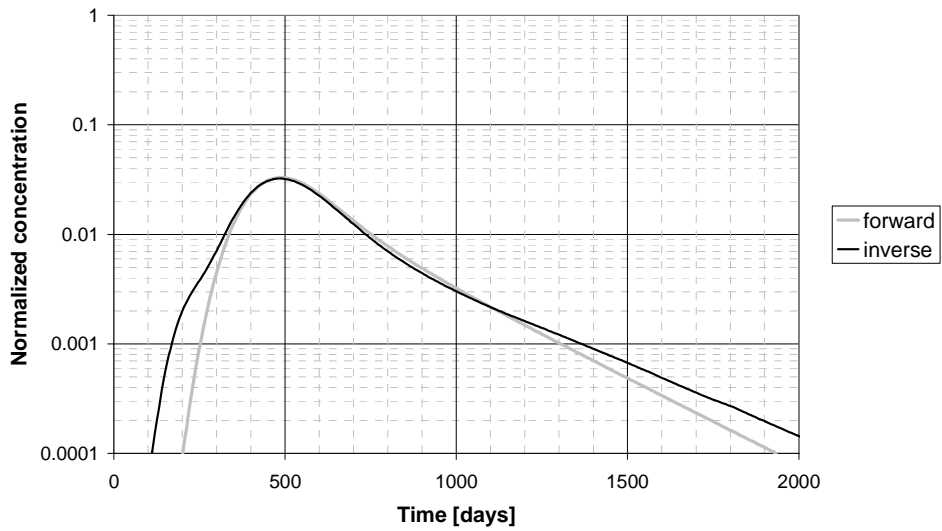


Figure 4.121: Match of forward and inverse tracer curves from layer 5 after 10 iterations for an initial oil saturation guess of 0.38

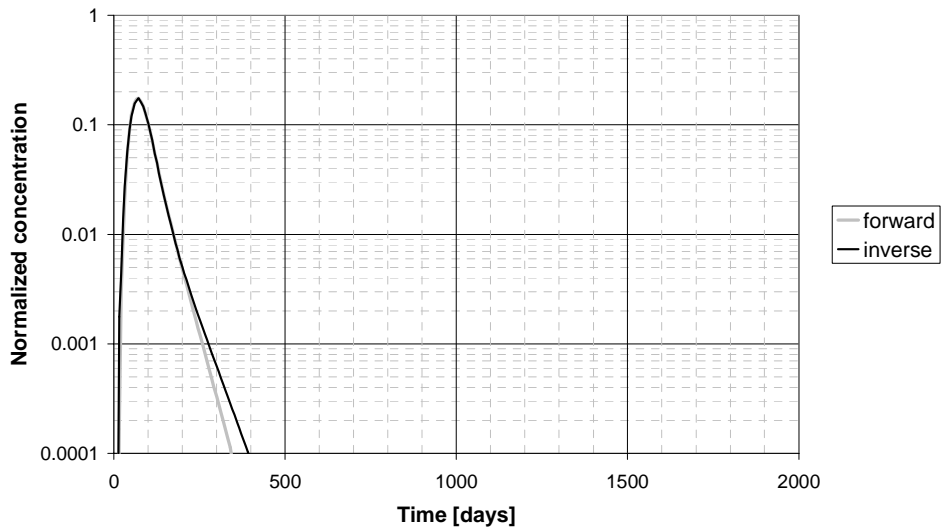


Figure 4.122: Match of forward and inverse tracer curves from layer 8 after 10 iterations for an initial oil saturation guess of 0.38

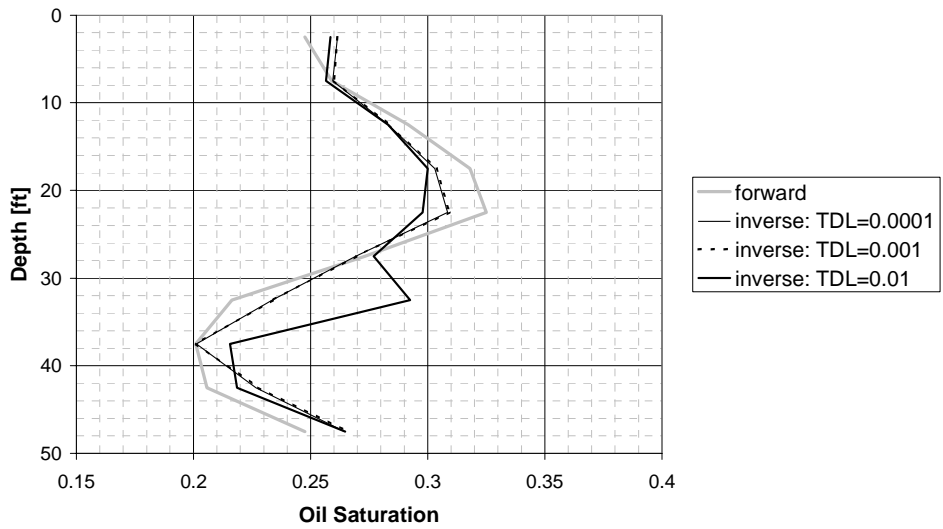


Figure 4.123: RMS error in travel time and amplitude with an initial oil saturation guess of 0.26 for TDL of 0.0001

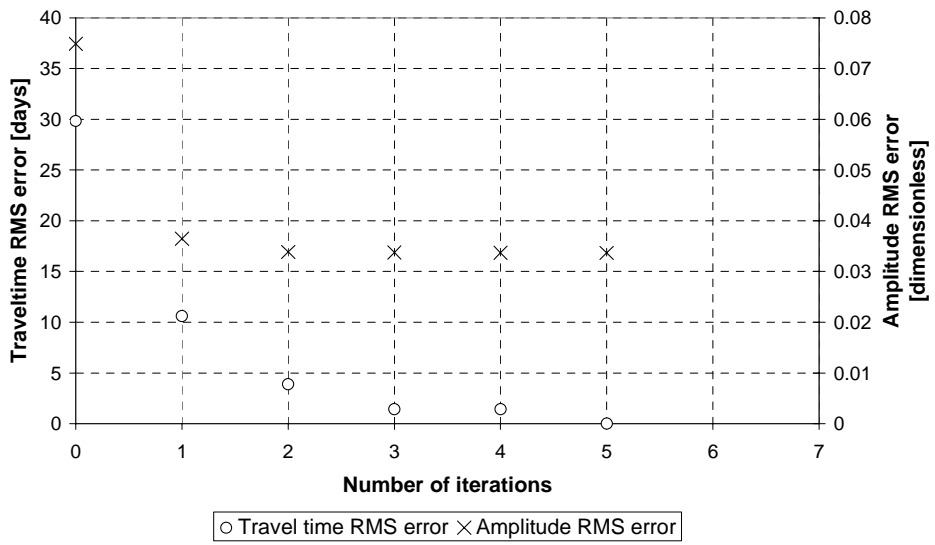


Figure 4.124: Inverse model vertical oil saturation distribution estimates for TDLs 0.0001, 0.001 and 0.01 at initial oil saturation guess 0.26

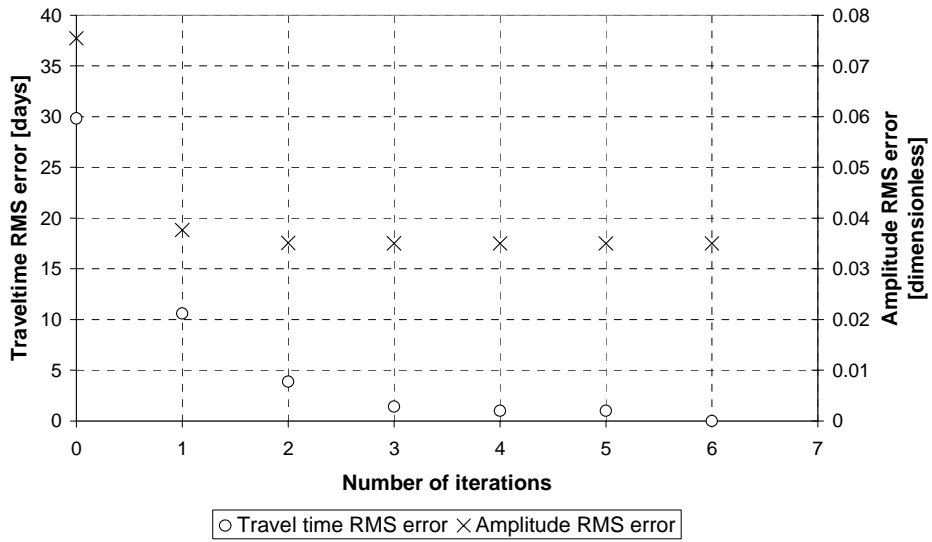


Figure 4.125: RMS error in travel time and amplitude with an initial oil saturation guess of 0.26 for TDL of 0.001

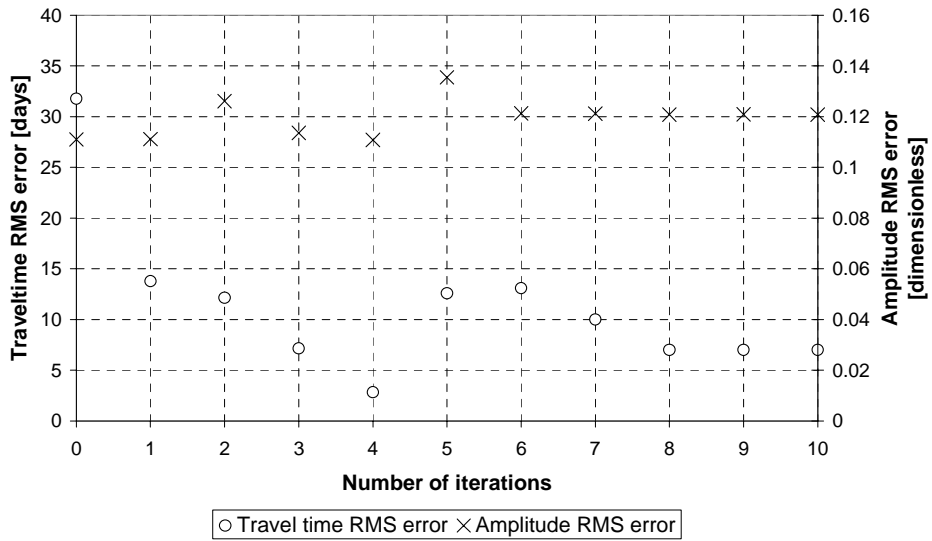


Figure 4.126: RMS error in travel time and amplitude with an initial oil saturation guess of 0.26 for TDL of 0.01

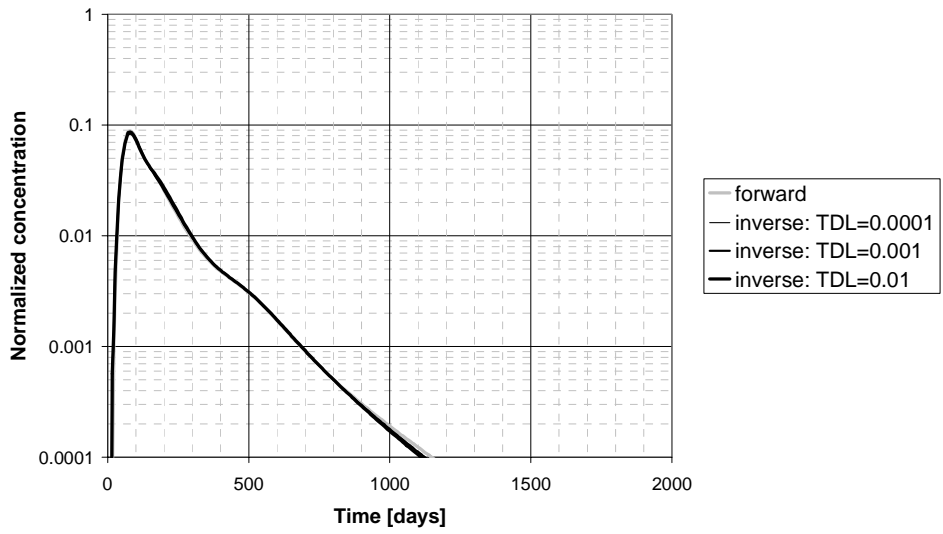


Figure 4.127: Match of forward and inverse tracer curves from all layers with an initial oil saturation guess of 0.26 for TDLs of 0.0001, 0.001, and 0.01

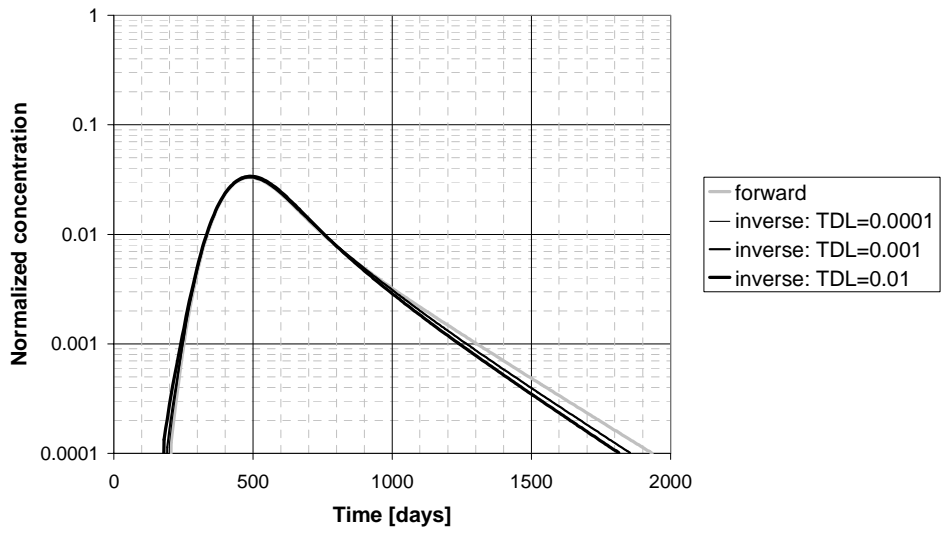


Figure 4.128: Match of forward and inverse tracer curves from layer 5 with an initial oil saturation guess of 0.26 for TDLs of 0.0001, 0.001, and 0.01

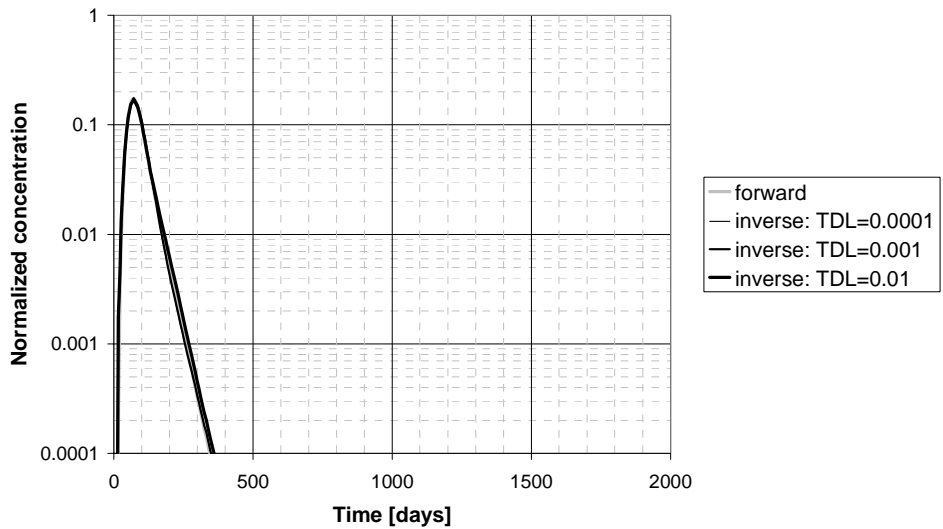


Figure 4.129: Match of forward and inverse tracer curves from layer 8 with an initial oil saturation guess of 0.26 for TDLs of 0.0001, 0.001, and 0.01

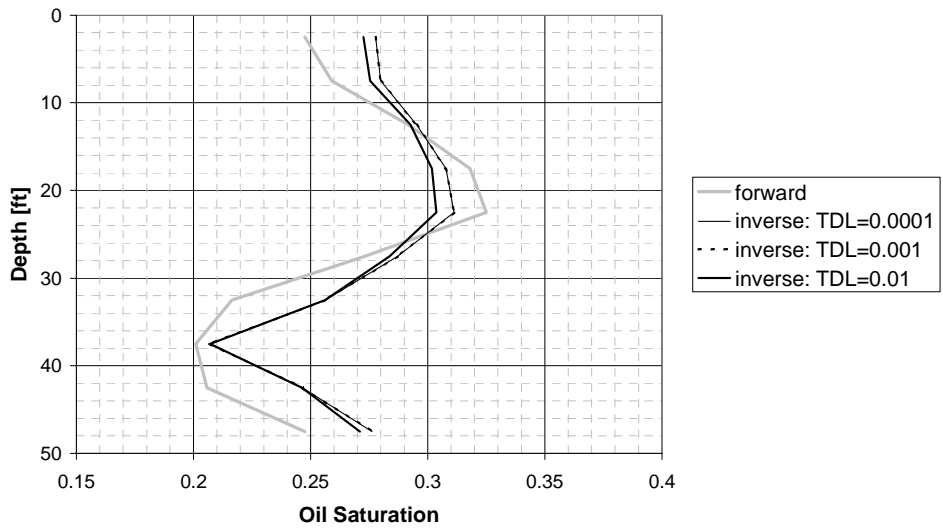


Figure 4.130: Inverse model vertical oil saturation distribution estimates for TDLs 0.0001, 0.001 and 0.01 at initial oil saturations guess 0.30

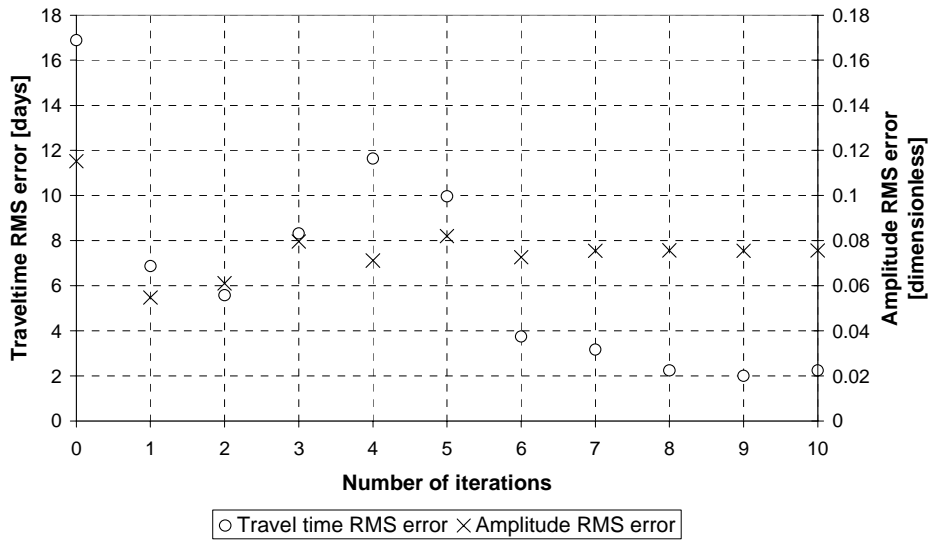


Figure 4.131: RMS error in travel time and amplitude with an initial oil saturation guess of 0.30 for TDL of 0.0001

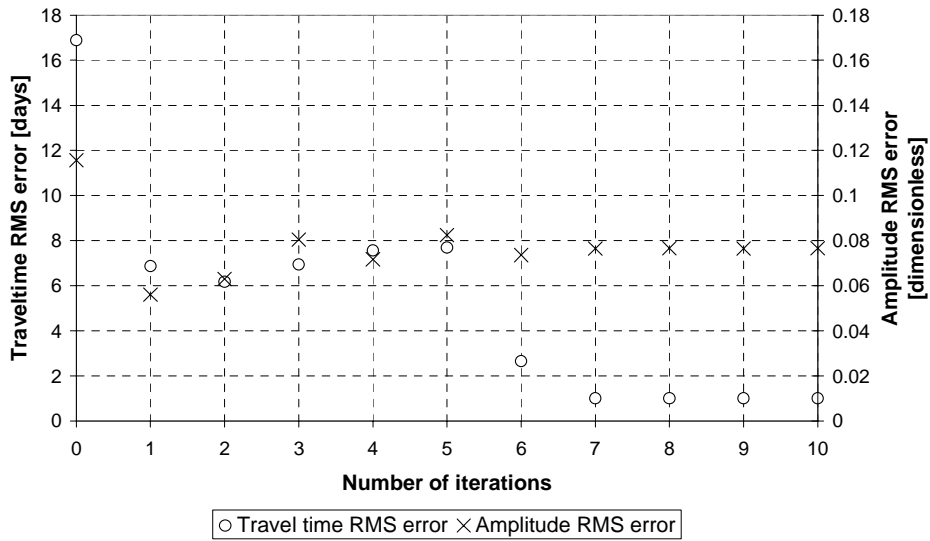


Figure 4.132: RMS error in travel time and amplitude with an initial oil saturation guess of 0.30 for TDL of 0.001

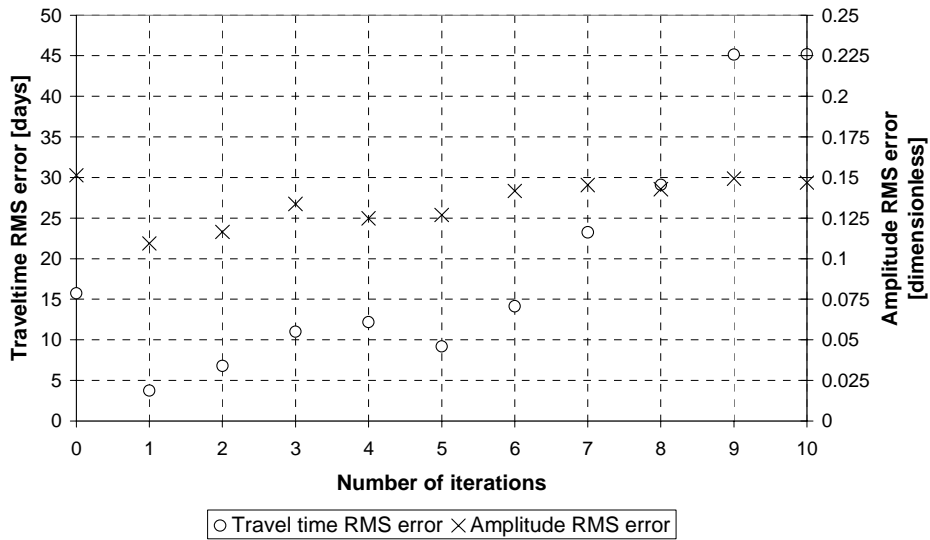


Figure 4.133: RMS error in travel time and amplitude with an initial oil saturation guess of 0.30 for TDL of 0.01

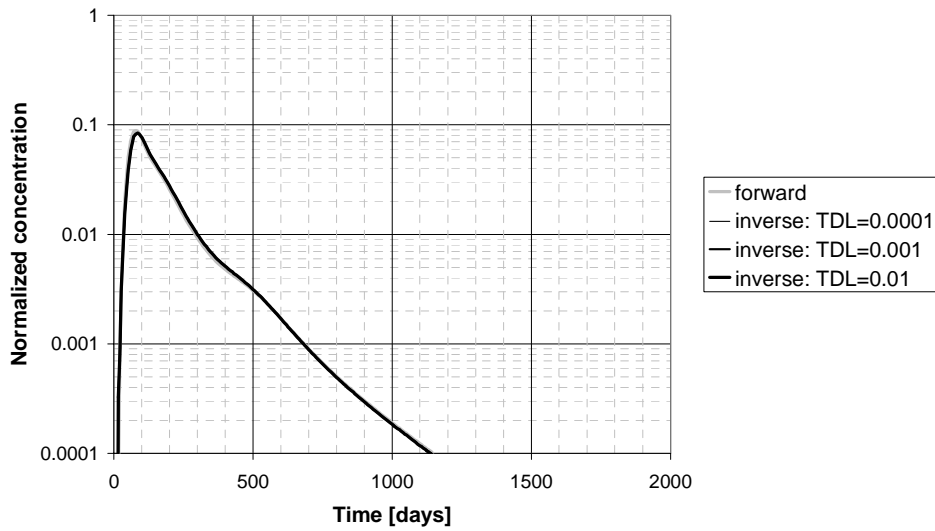


Figure 4.134: Match of forward and inverse tracer curves from all layers with an initial oil saturation guess of 0.30 for TDLs of 0.0001, 0.001, and 0.01

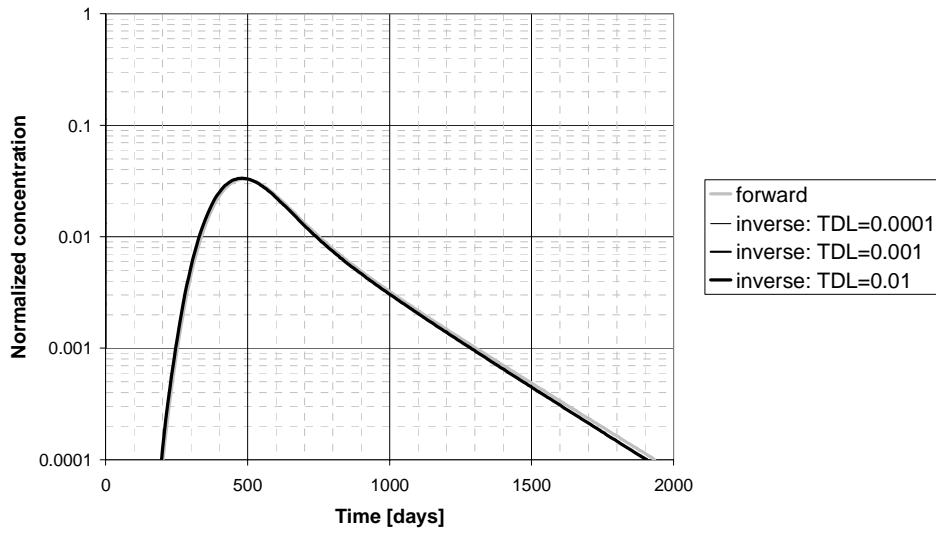


Figure 4.135: Match of forward and inverse tracer curves from layer 5 with an initial oil saturation guess of 0.30 for TDLs of 0.0001, 0.001, and 0.01

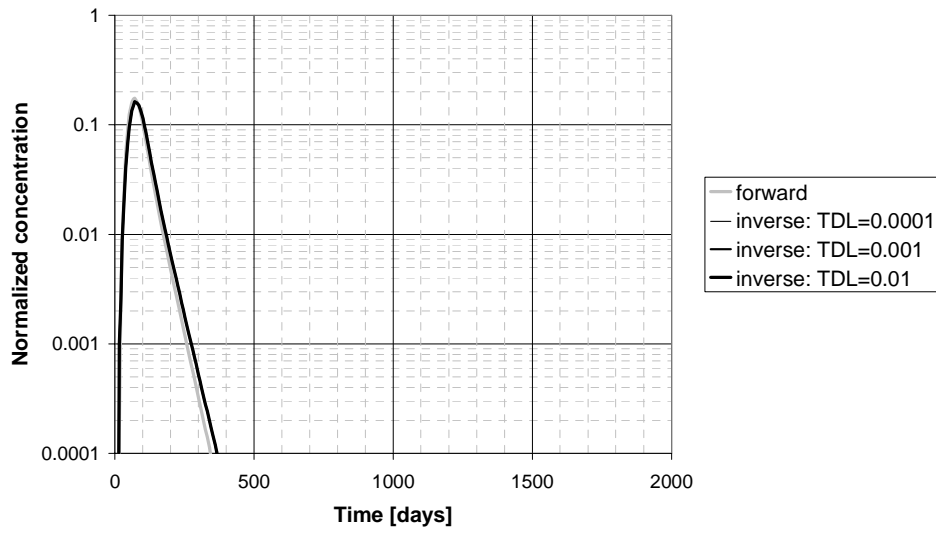


Figure 4.136: Match of forward and inverse tracer curves from layer 8 with an initial oil saturation guess of 0.30 for TDLs of 0.0001, 0.001, and 0.01

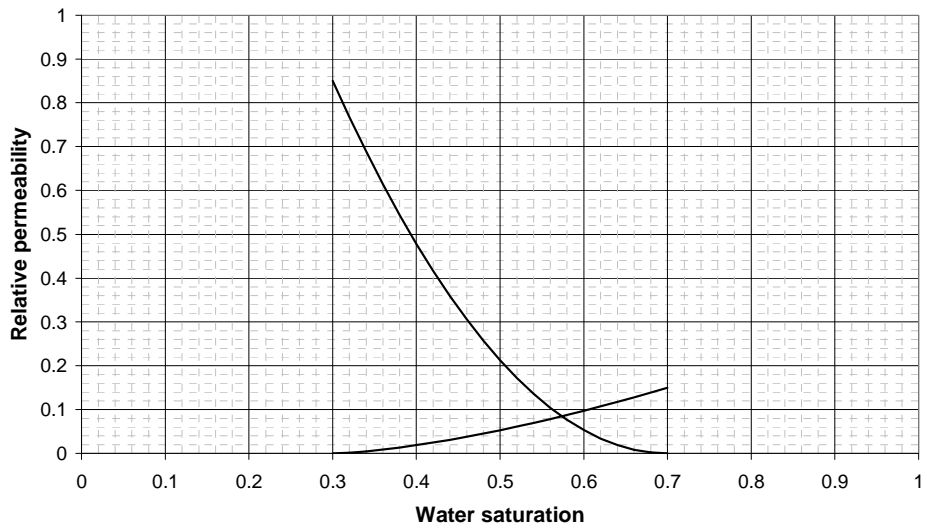


Figure 4.137: Relative permeability curves in Runs INV07-000 and INV07-600

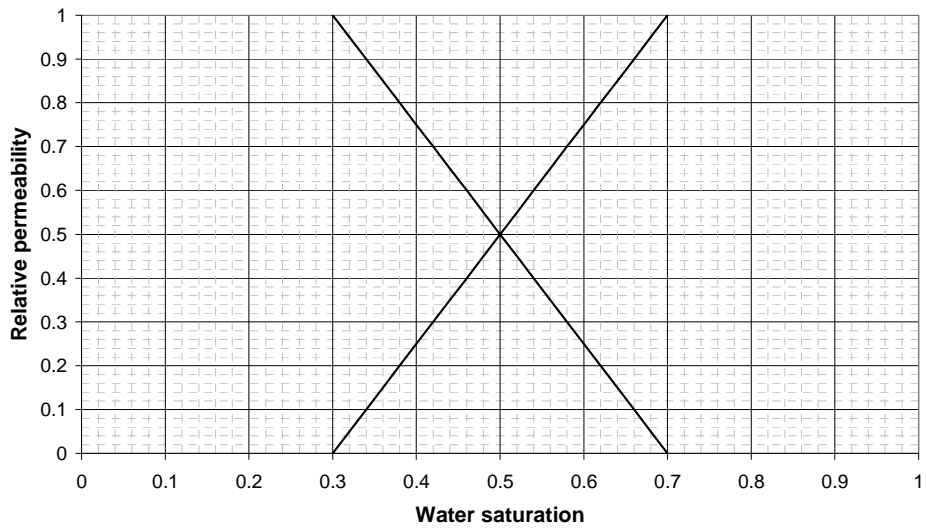


Figure 4.138: Relative permeability curves in Runs INV07-200, INV07-100, and INV07-500

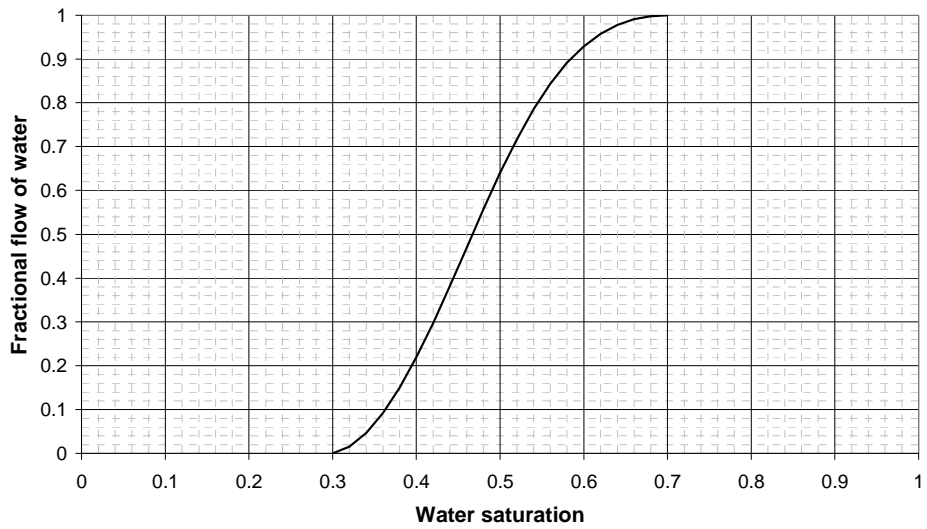


Figure 4.139: Fractional flow of water in Run INV07-000

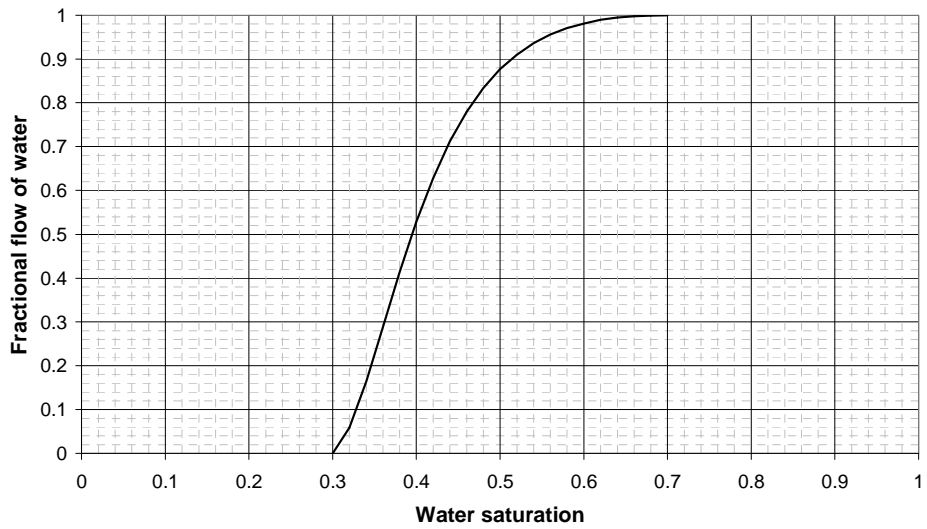


Figure 4.140: Fractional flow of water in Runs INV07-600 and INV07-700

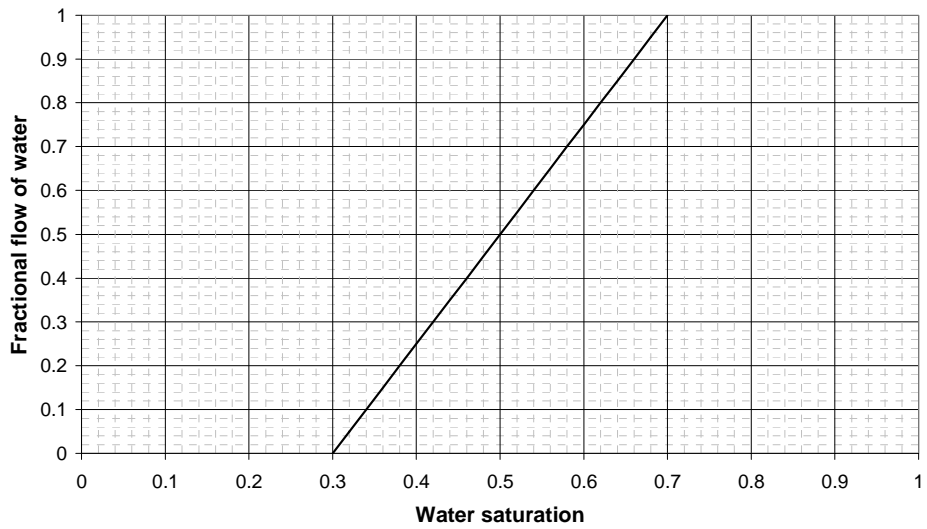


Figure 4.141: Fractional flow of water in Run INV07-200

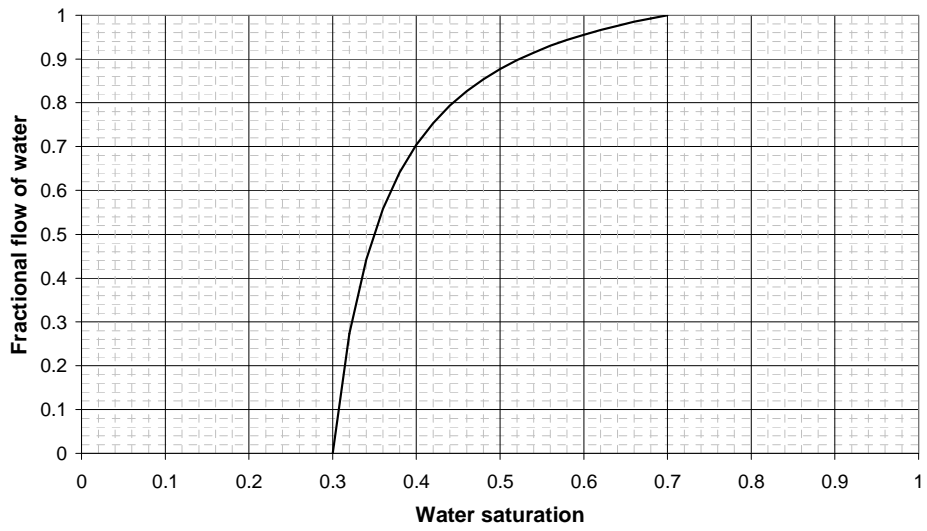


Figure 4.142: Fractional flow of water in Run INV07-100

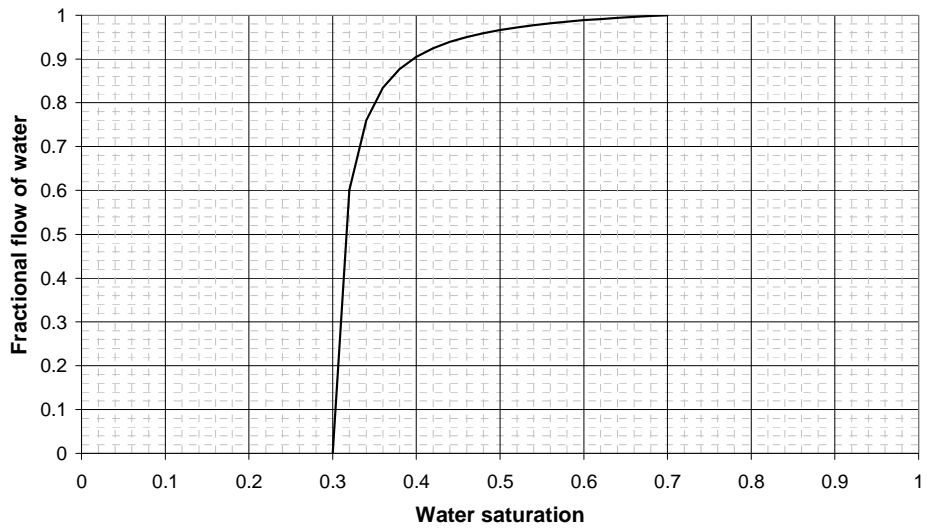


Figure 4.143: Fractional flow of water in Run INV07-500

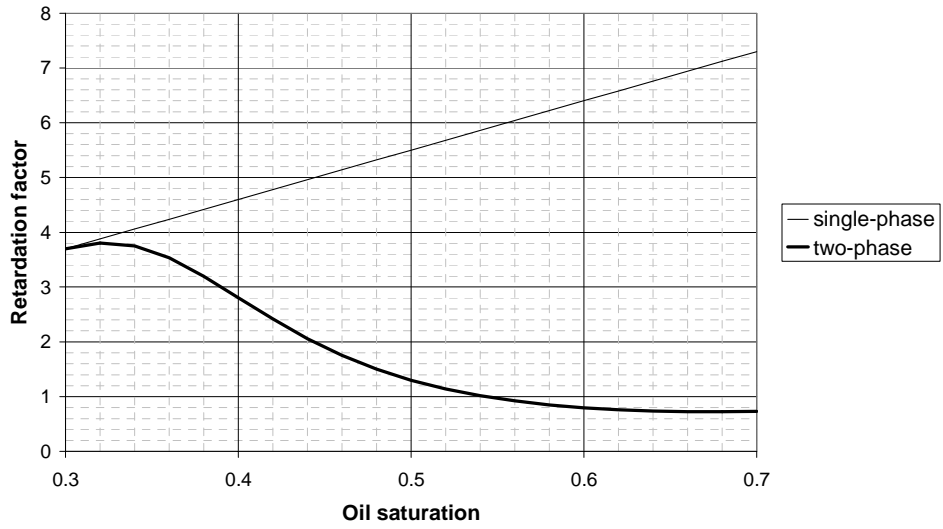


Figure 4.144: Mean residence time sensitivity to the oil saturation in Run INV07-000 for partition coefficient 10

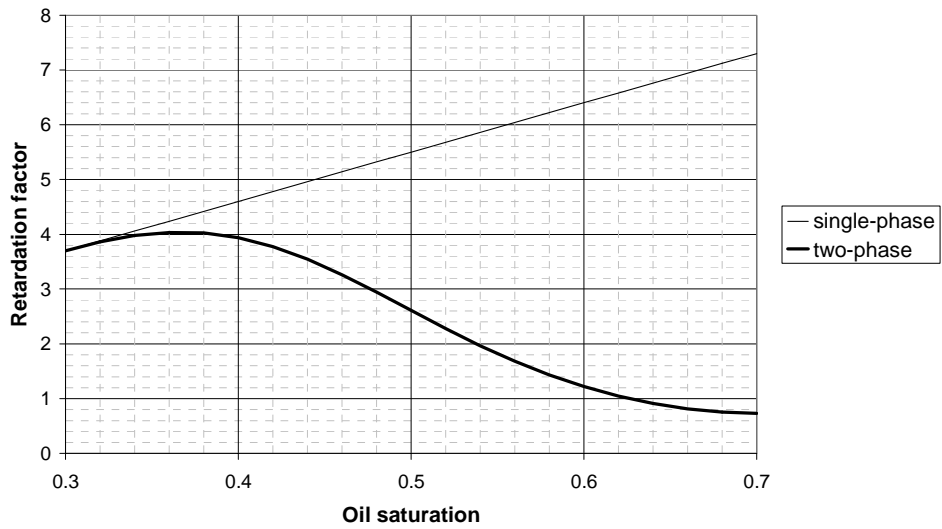


Figure 4.145: Mean residence time sensitivity to the oil saturation in Run INV07-600 for partition coefficient 10

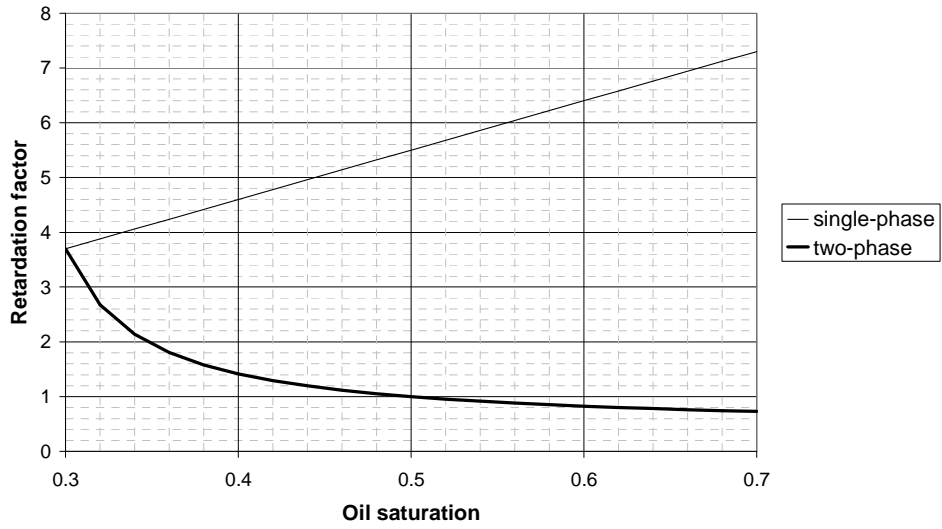


Figure 4.146: Mean residence time sensitivity to the oil saturation in Run INV07-200 for partition coefficient 10

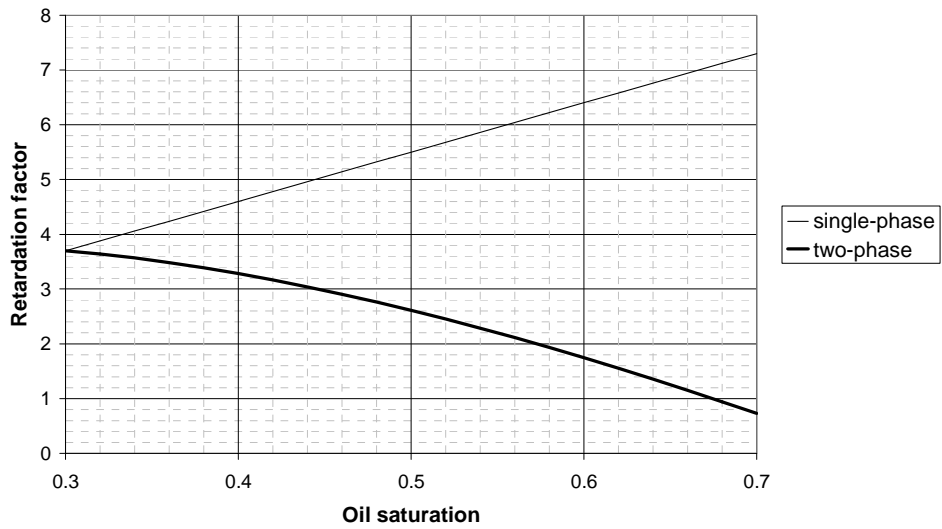


Figure 4.147: Mean residence time sensitivity to the oil saturation in Run INV07-100 for partition coefficient 10

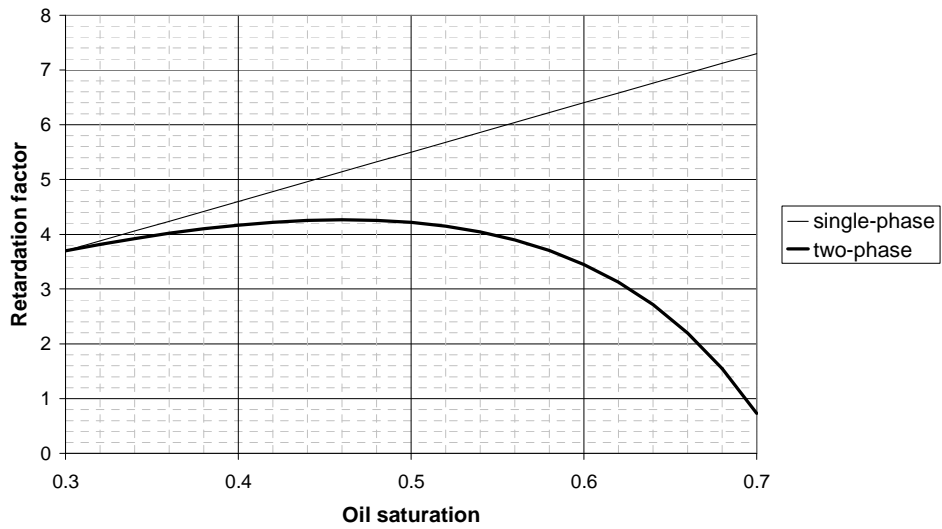


Figure 4.148: Mean residence time sensitivity to the oil saturation in Run INV07-500 for partition coefficient 10

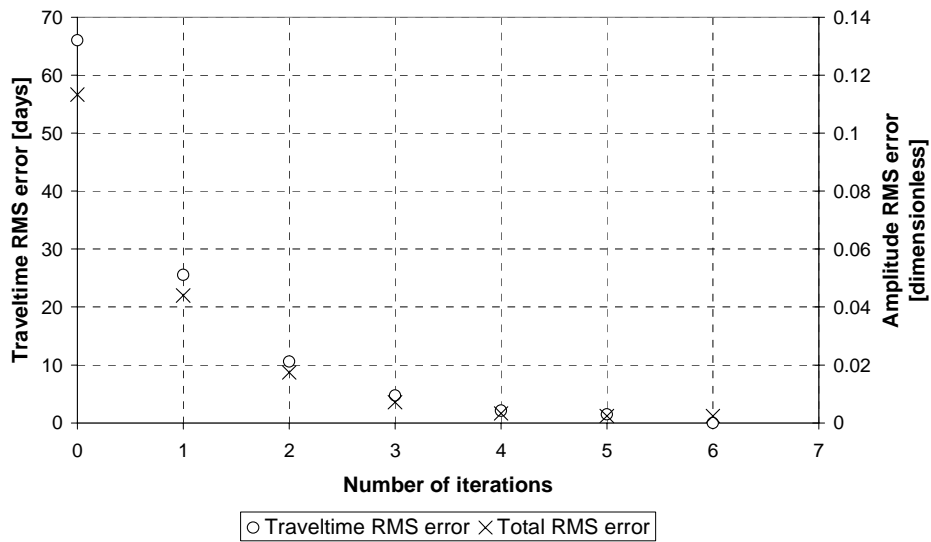


Figure 4.149: RMS change on travel time and amplitude in Run INV07-511

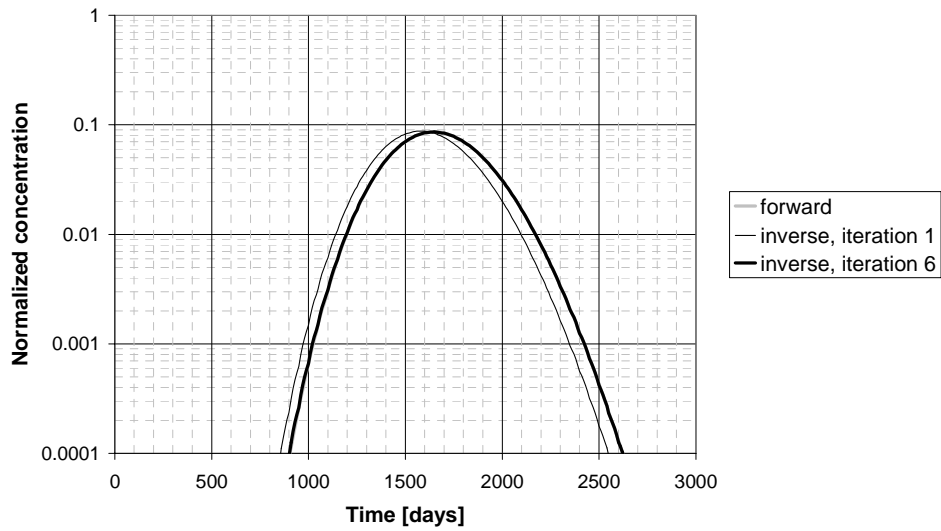


Figure 4.150: Match of the forward model tracer response from layer 1 by iteration 1 and 6 of inverse model in Run INV07-511

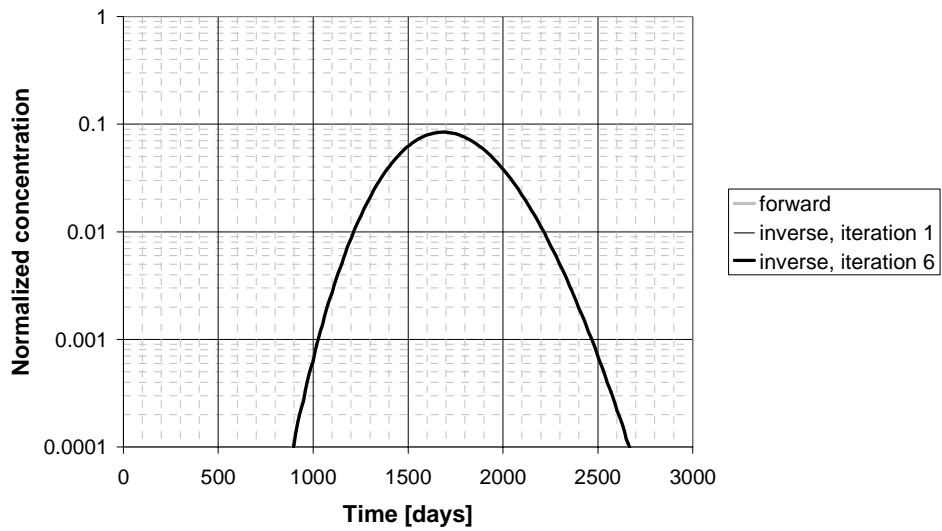


Figure 4.151: Match of the forward model tracer response from layer 2 by iteration 1 and 6 of inverse model in Run Inv07-511

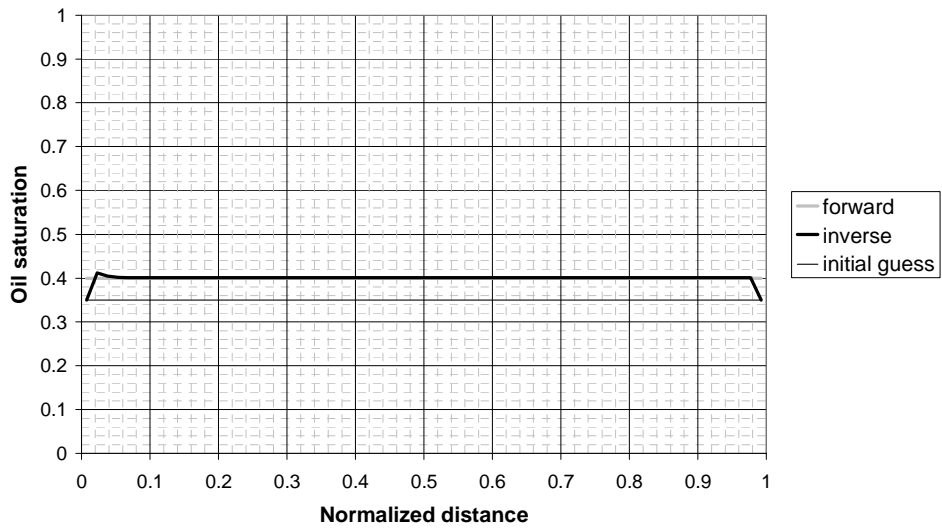


Figure 4.152: Inverse model oil saturation estimate in layer 1 in Run INV07-511

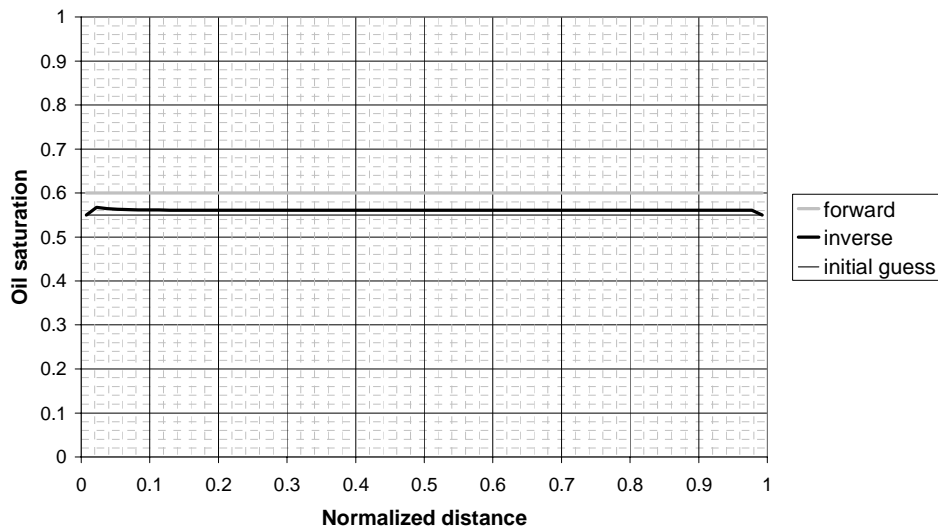


Figure 4.153: Inverse model oil saturation estimate in layer 2 in Run INV07-511

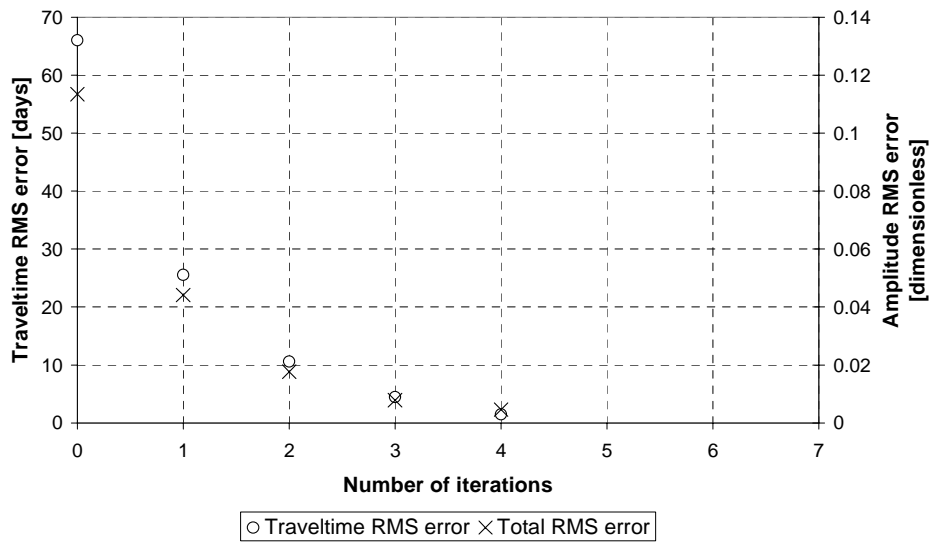


Figure 4.154: RMS change on travel time and amplitude in Run INV07-512

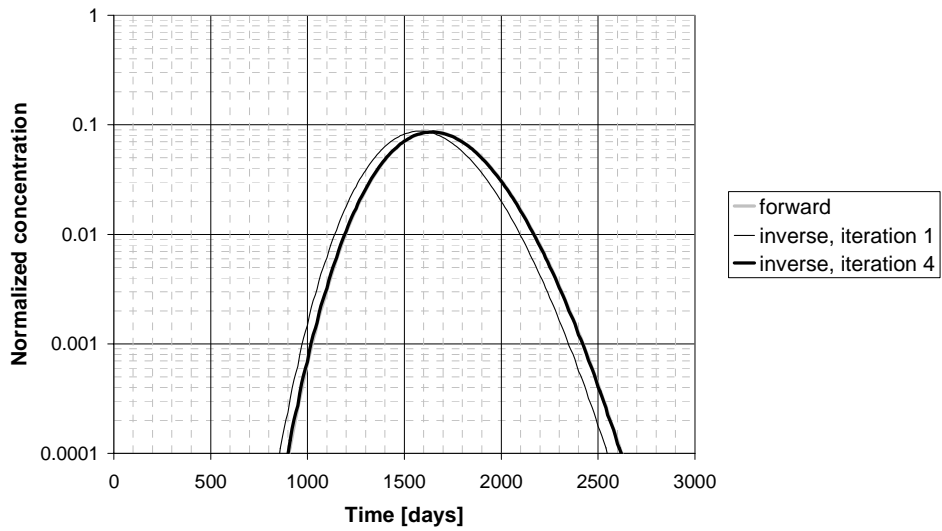


Figure 4.155: Match of the forward model tracer response from layer 1 by iterations 1 and 4 in Run INV07-512

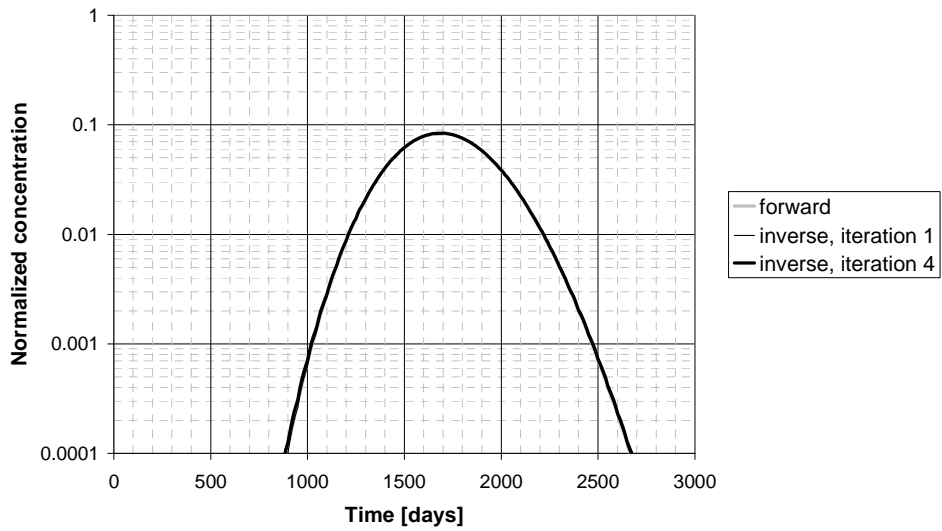


Figure 4.156: Match of the forward model tracer response from layer 2 by iteration 1 and 4 in Run INV07-512

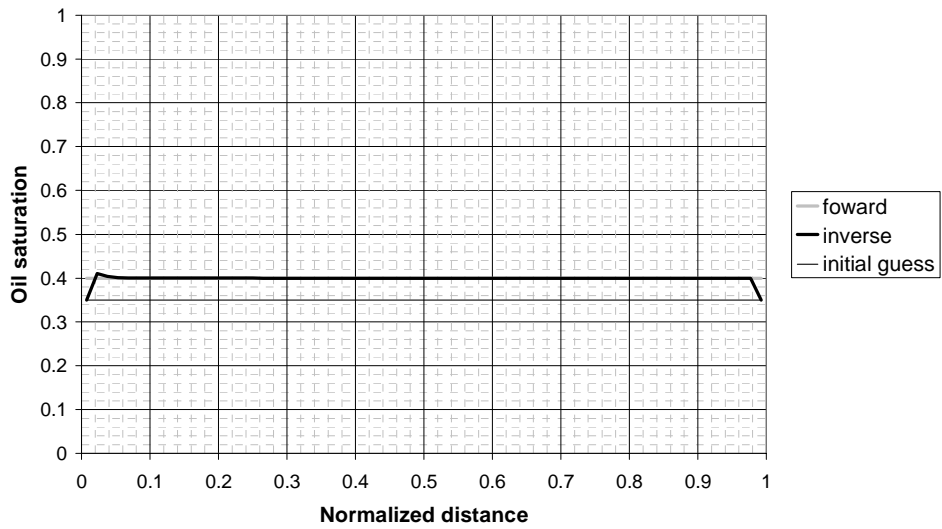


Figure 4.157: Oil saturation comparison in layer 1 in Run INV07-512

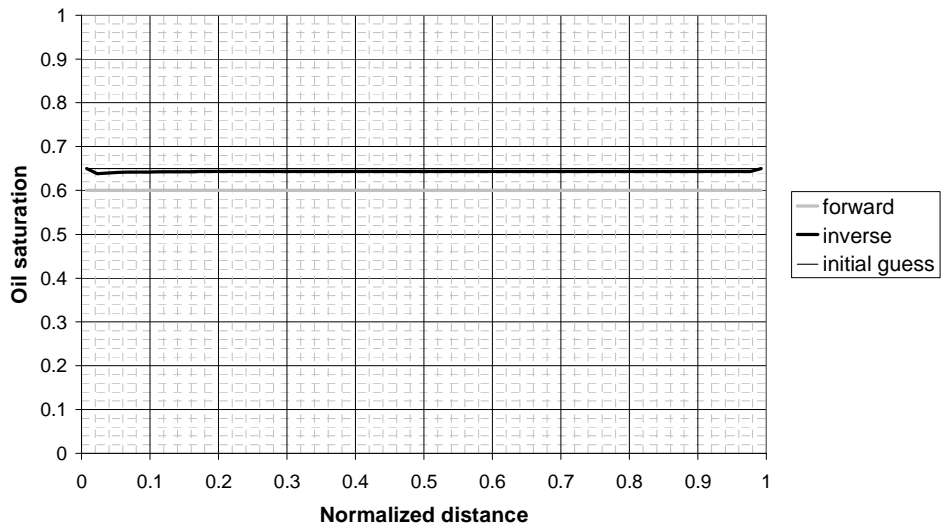


Figure 4.158: Oil saturation comparison in layer 2 in Run INV07-512

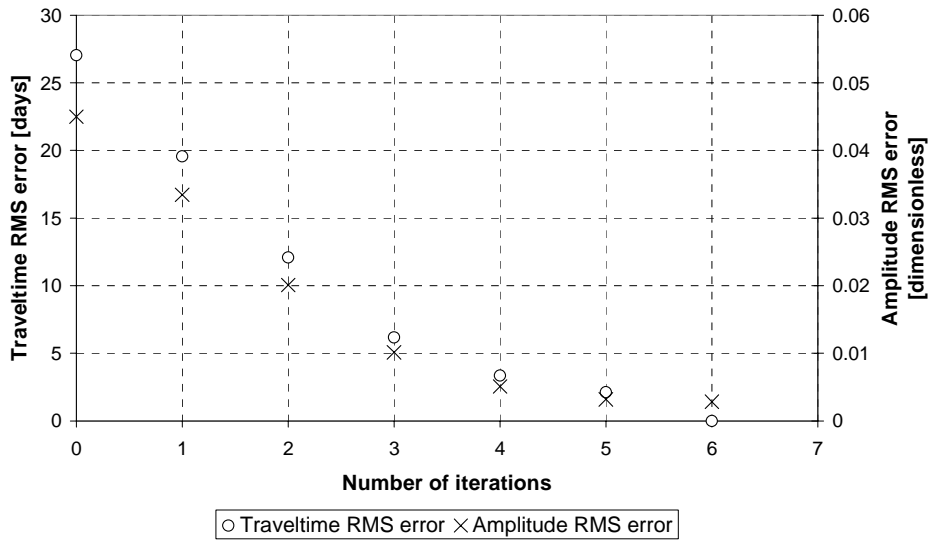


Figure 4.159: RMS change on travel time and amplitude in Run INV07-513

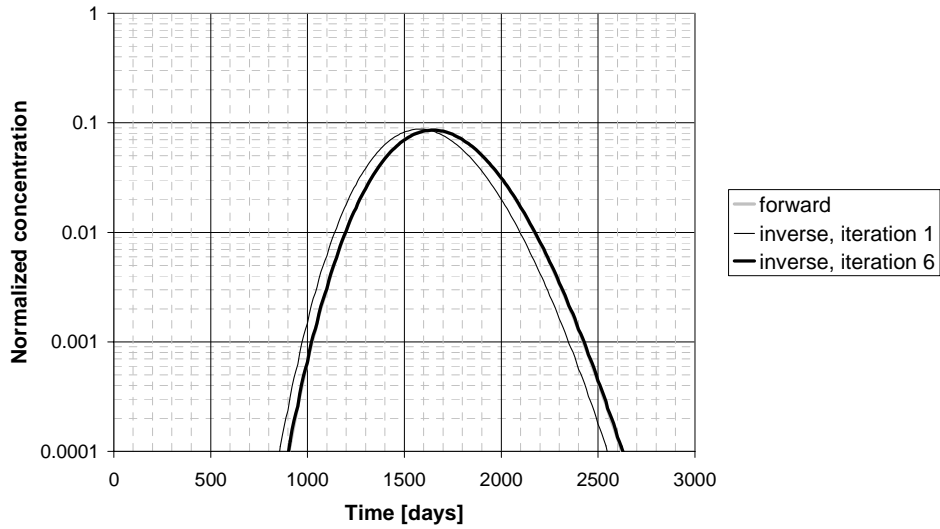


Figure 4.160: Match of the forward model tracer response from layer 1 by iterations 1 and 6 of in Run INV07-513

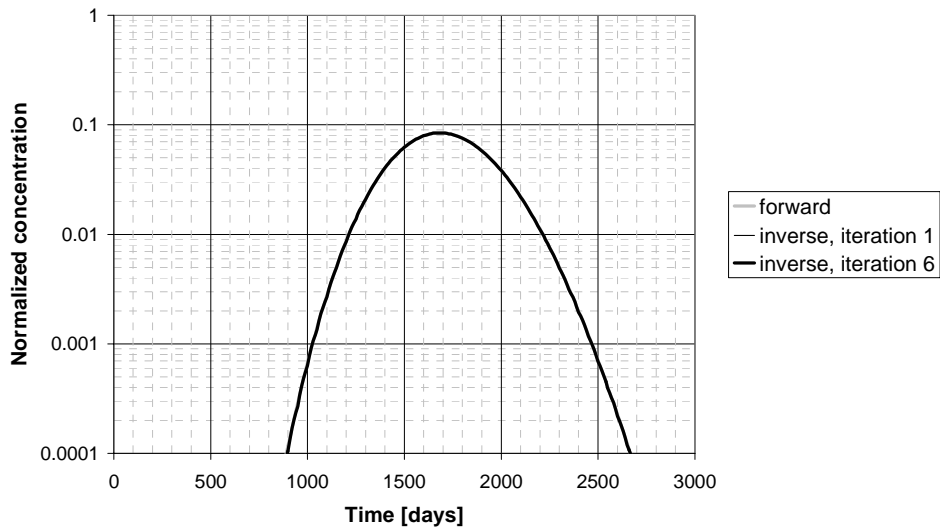


Figure 4.161: Match of the forward model tracer response from layer 1 by iterations 1 and 6 in Run INV07-513

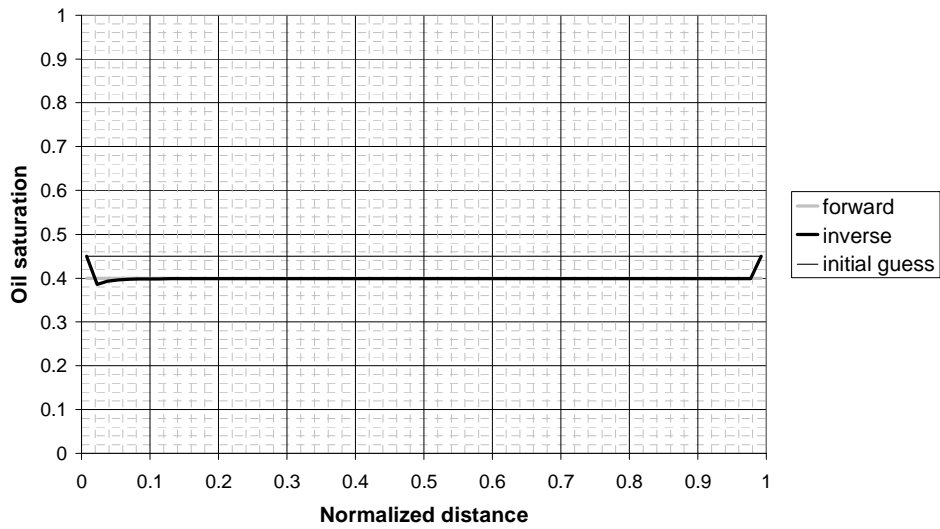


Figure 4.162: Oil saturation comparison in layer 1 in Run INV07-513

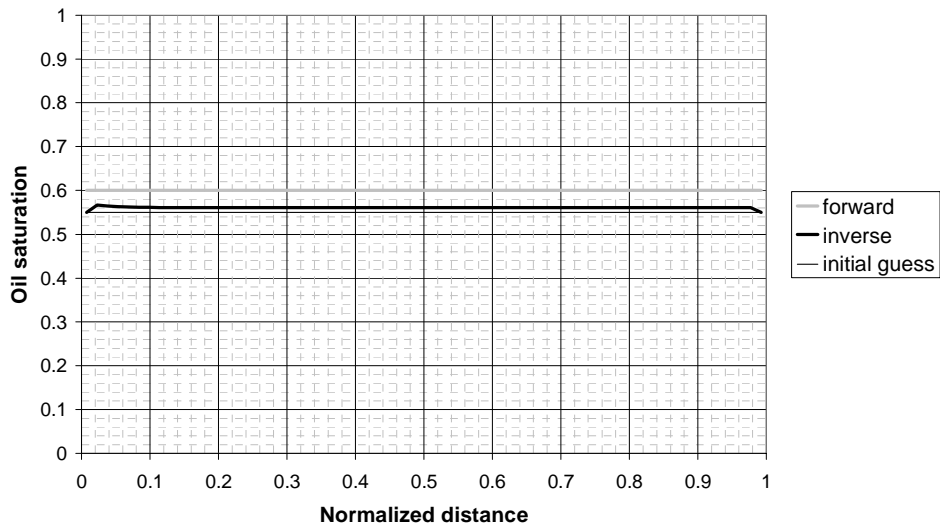


Figure 4.163: Oil saturation comparison in layer 2 in Run INV07-513

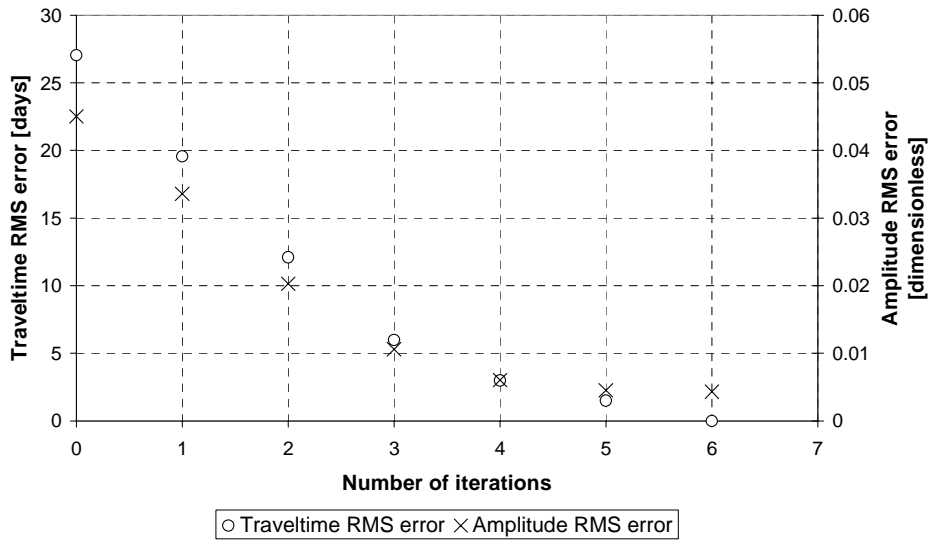


Figure 4.164: RMS change in travel time and amplitude in Run INV07-514

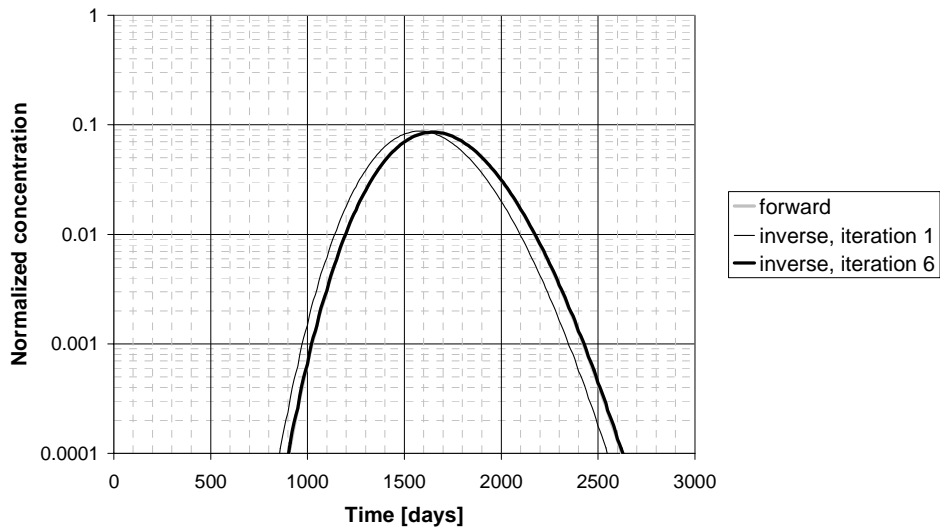


Figure 4.165: Match of the forward model tracer response from layer 1 by iterations 1 and 6 in Run INV07-514

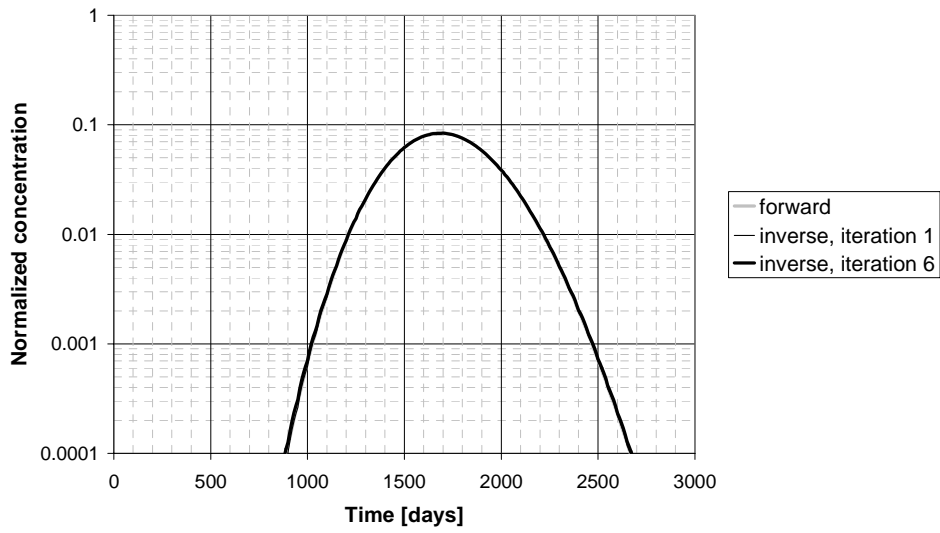


Figure 4.166: Match of the forward model tracer response from layer 2 by iterations 1 and 6 in Run INV07-514

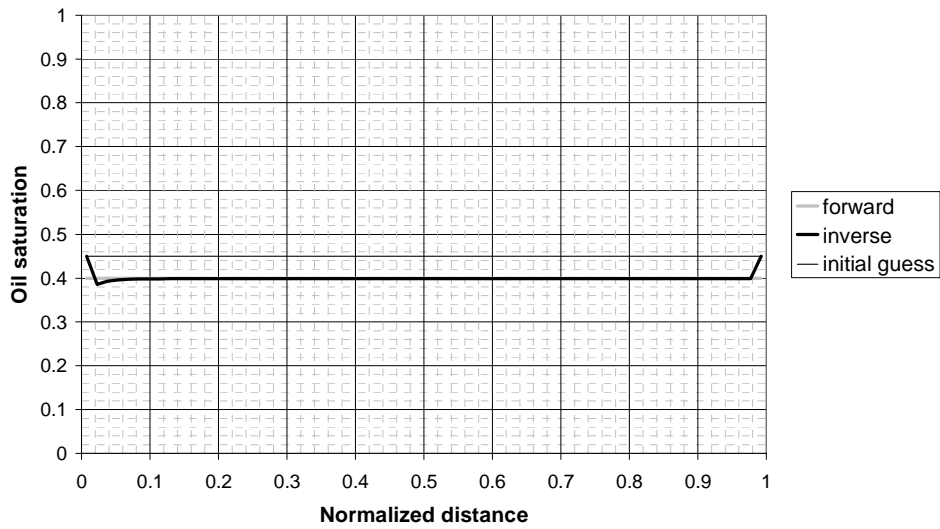


Figure 4.167: Oil saturation comparison in layer 1 in Run INV07-514

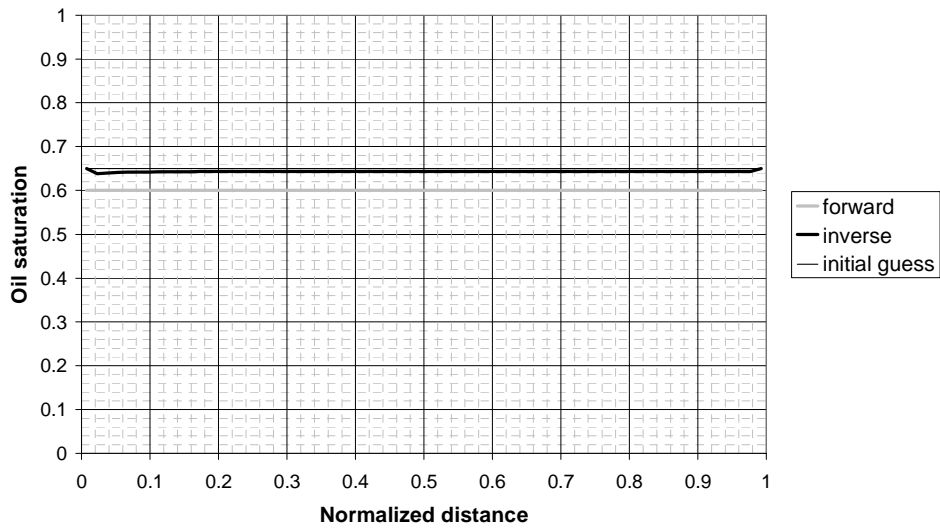


Figure 4.168: Oil saturation comparison in layer 2 in Run INV07-514

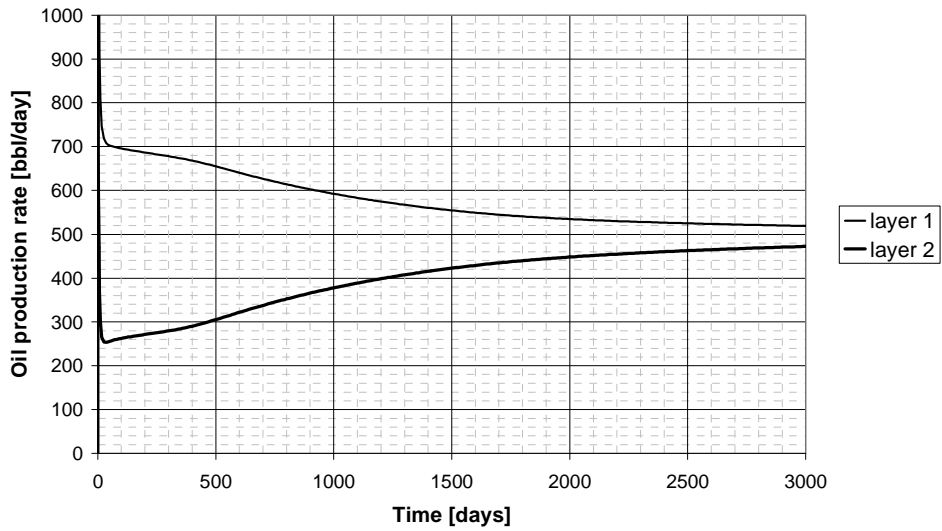


Figure 4.169: Injection rate change in Run INV07-513-b

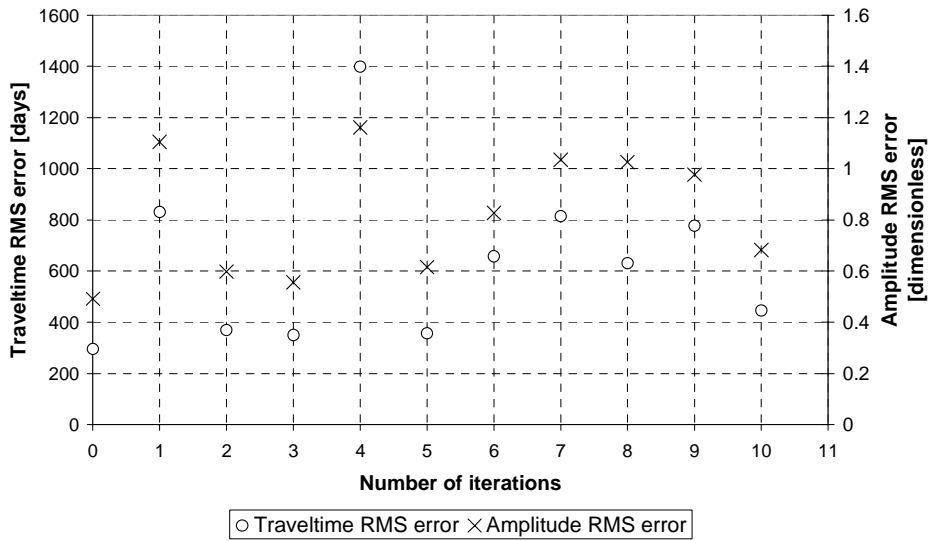


Figure 4.170: RMS change on travel time and amplitude in Run INV07-513-b with changing flow rate in each layer

Chapter 5: Summary, Conclusions, and Recommendations

5-1 SUMMARY AND CONCLUSIONS

The method of moments for calculating swept pore volume and oil volume and/or saturation has been derived for very general reservoir conditions. The method has been generalized so that it can be applied under two-phase flow conditions with mobile oil saturation rather than just residual oil saturation. The derivation is for general heterogeneity including even naturally fractured reservoirs. Both tracer slug injection and continuous injection cases were derived. The method was also extended to natural tracers (organic components that partition from the oil to the water). Equations were also derived to show how sweep efficiency is calculated from tracer concentration data from an injected tracer slug by integrating the data to equivalent continuous concentration data.

The generalized equations for the method of moments were applied to a variety of reservoir conditions with different permeability and saturation distributions to test the accuracy of the estimated oil volume or saturation. Synthetic tracer production data were generated by numerical simulation using the UTCHEM simulator for some cases and the ECLIPSE simulator for other cases so that the method could be evaluated under precisely known reservoir conditions. Both single porosity and dual porosity models were used. The method of Tang based upon a chromatographic transformation of the mass transport equations for partitioning tracers flowing at residual oil saturation was compared to the method of moments for some special cases.

The test cases indicate that the generalized method of moments is valid for calculating oil saturation for both mobile oil and residual oil saturation conditions. However, most of the mobile oil was produced before the tracers were produced, so the average oil saturation estimated from the PITT was not very much higher than the

residual oil saturation for the particular cases that were simulated. A more complete test of the theory with mobile oil is therefore needed.

When data are available for different layers in the reservoir, the oil saturation can be estimated for each layer with good accuracy. Tests based upon data simulated with a dual porosity simulator show the validity of the method for naturally fractured reservoirs. When a conventional partitioning interwell tracer test is done in naturally fractured reservoirs with large fracture spacing and/or large well spacing, the time required for a sufficiently high fraction of the tracer data to be produced is typically too large to be practical. However, it might be practical in some cases to use natural tracers analyzed using the method of moments to get useful estimates of oil saturation in a reasonable time. Preliminary results indicate that converting slug data to continuous data is also helpful for getting better estimates at early times.

Integrating tracer concentration data from tracer slugs to get equivalent continuous concentration data seems to have several advantages. First, swept pore volumes and/or sweep efficiency can be calculated for very general conditions of heterogeneity. Second, the volume of oil and/or oil saturation in the swept pore volume can be estimated at early times. This simple idea emerged late in this study so it has not been systematically investigated, but the preliminary favorable results suggest a more complete analysis would be justified.

The distribution of oil saturation was also calculated from synthetic partitioning tracer data using inverse modeling with a program developed at TAMU and coupled to the numerical reservoir simulator ECLIPSE as the forward model. The convergence and accuracy of the inverse model was evaluated for a range of initial oil saturation guesses and for a wide range of assumed tracer concentration detection limits. For most cases, the inverse modeling program converged very fast with good matches of the tracer

concentration data. The TAMU program coupled with ECLIPSE is extremely fast, so it can be used on much larger problems than possible in the past.

The inverse model program performed much better when the initial guess of the average oil saturation was close to the actual value. The method of moments can be used to obtain a value very close to the actual average oil saturation, so a good strategy is to use the inverse model with the initial guess from the method of moments. Tang's method using tracer recovery curves could also be used to obtain a good initial guess under some conditions such as uniform residual oil saturation. The inverse model does a good job of extrapolating the tracer tails beyond the tracer detection limit and is thus a good alternative to exponential extrapolation. However, the results become less reliable if the match of the data with the inverse model is not based upon a sufficiently complete tracer tail down to a low tracer concentration.

Even when performing well, the inverse model appears to have limited capability to estimate the three-dimensional distribution of oil if the only data are tracer data from the entire well. Data by layer could be used just as for the method of moments, but the complexity and cost of using inverse modeling is much greater than for the method of moments. Even more significant, the inverse model requires an accurate reservoir description whereas the method of moments does not. The permeability distribution can be estimated from the conservative tracer data using inverse modeling and then the oil saturation calculated from the partitioning tracer data, but this was not done in this study and requires even more time and effort and introduces even more uncertainty.

Distributions of oil saturation in the reservoir when the initial oil saturation was mobile were not accurately calculated with the inverse model program when the only data available were the tracer concentrations from the entire well. The reasons for this

failure are not clear at this time, but the problem might be ill posed due to inadequate data. More investigation is needed.

5-2 RECOMMENDATIONS

One of the most interesting observations that emerged late in this study was the advantage of Tang's method using tracer recovery curves in terms of providing good estimates of oil saturation at much early times than the method of moments. Tang's method does not take into account spatially or temporally variable oil saturation, so it also has some limitations. However, it would be very useful to systematically investigate its usefulness under a wide a variety of reservoir conditions and compare the results with the method of moments. Perhaps the best strategy is to combine the methods somehow.

More research is needed on the idea of using natural tracers to fully develop this approach and determine its advantages and limitations. Before field application, suitable components of the crude oil would need to be identified and measurement methods developed among other practical steps that would be needed.

More research is needed on applying the method of moments to estimate mobile oil saturation. More realistic and interesting cases of mobile oil should be used to test the generalized method of moments for this case.

More research is needed on the inverse modeling. The TAMU program is capable of matching production data and pressure data as well as tracer data, so it would be useful to investigate the accuracy of oil saturations when a combined data set is used. The benefits of additional data from different sampling points such as from different layers should be further investigated.

The idea of converting tracer slug data to continuous data and then calculating sweep efficiency is a potentially very useful idea that should be further investigated under

a very wide range of conditions. The shape of the continuous tracer curves (or Tang's recovery curves) might contain useful information about the distribution of the oil saturation since the retardation will tend to either increase or decrease in proportion to the oil saturation as the tracers flow along streamlines in the reservoir. Thus, the shape of these curves should be investigated with this in mind.

Appendix A

• Tracer flood input file for Run 2DHT04

```

CC*****
CC
CC   BRIEF DESCRIPTION OF DATA SET: UTCHEM (VERSION 10.0)
CC
CC*****
CC
CC   TRACER IN 5-SPOT, 30X30X1
CC
CC   LENGTH (FT) : 165                PROCESS : TRACER
CC   THICKNESS (FT) : 5                INJ. RATE (FT3/DAY) : 375
CC   WIDTH (FT) : 165                 COORDINATES : CARTESIAN
CC   POROSITY : 0.25
CC   GRID BLOCKS : 30x30x1
CC   DATE :
CC
CC*****
CC
CC*****
CC
CC   RESERVOIR DESCRIPTION
CC
CC*****
CC
CC Run number
*---- RUNNO
2DHT04
CC
CC Title and run description
*---- title(i)
2d TRACER TEST, qurater of five spot (areal simulation)
USING UTCHEM VERSION 10.0
IDISPC=3 , Dvp=0.80
CC
CC SIMULATION FLAGS
*---- IMODE IMES IDISPC ICWM ICAP IREACT IBIO ICOORD ITREAC ITC IGAS IENG
      1   1   3   0   0   0   0   1   0   0   0   0 0 0
CC
CC no. of gridblocks,flag specifies constant or variable grid size,unit
*---- NX   NY   NZ   IDXYZ IUNIT
      30   30   1   0   0
CC
CC constant grid block size in x,y,and z
*---- dx1       dy1       dz1
      5.5       5.5       5
CC
CC total no. of components,no. of tracers,no. of gel components
*----n   no   ntw   nta   ngc   ng   noth
      10   0   2   0   0   0   0
CC
CC Name of the components
*----spname(i) for i=1 to n
Water
Oil
Surf.
Polymer
Chloride
Calcium
Alcohol 1
Alcohol 2

```

```

tracer1
tracer2
CC
CC flag indicating if the component is included in calculations or not
*----icf(kc) for kc=1,n
      1 0 0 0 0 0 0 0 1 1
CC
CC*****
CC
CC      OUTPUT OPTIONS
CC
CC*****
CC
CC
CC FLAG TO WRITE TO UNIT 3,FLAG FOR PV OR DAYS TO PRINT OR TO STOP THE RUN
*---- ICUTM  ISTOP  IOUTGMS
      0      0      0
CC
CC FLAG INDICATING IF THE PROFILE OF KCTH COMPONENT SHOULD BE WRITTEN
*---- IPRFLG(KC),KC=1,N
      1 0 0 0 0 0 0 0 1 1
CC
CC FLAG FOR PRES.,SAT.,TOTAL CONC.,TRACER CONC.,CAP.,GEL, ALKALINE PROFILES
*---- IPPRES IPSAT IPCTOT IPBIO IPCAP IPGEL IPALK IPTEMP IPOBS
      0      0      1      0      0      0      0      0      0
CC
CC FLAG FOR WRITING SEVERAL PROPERTIES TO UNIT 4 (Prof)
*---- ICKL IVIS IPER ICNM ICSE IHYSTP IFOAMP INONEQ
      0      0      0      0      0      0      0      0
CC
CC FLAG for variables to PROF output file
*---- IADS IVEL IRKF IPHSE
      0      0      0      0
CC
CC*****
CC
CC      RESERVOIR PROPERTIES
CC
CC*****
CC
CC
CC MAX. SIMULATION TIME ( DAYS)
*---- TMAX
      1370
CC
CC ROCK COMPRESSIBILITY (1/PSI), STAND. PRESSURE(Psia)
*---- COMPR          PSTAND
      0              14.7
CC
CC FLAGS INDICATING CONSTANT OR VARIABLE POROSITY, X,Y,AND Z PERMEABILITY
*---- IPOR1  IPERMx  IPERMy  IPERmZ  IMOD
      0      2      3      3      0
CC
CC CONSTANT POROSITY FOR WHOLE RESERVOIR
*---- PORC1
      0.25
CC
CC CONSTANT X-PERMEABILITY FOR WHOLE RESERVOIR
*---- PERMXC
3899.99 1351.53  79.15  715.72 1017.68  208.30  620.41  383.49 2138.09 654.11
 317.86 1204.33  30.79  11.09 192.96  554.04  188.80  76.09  83.64 244.71
 101.45  118.49  38.27  11.56 686.92  309.78  719.80 3127.41 198.52 274.75
8405.21 2599.19 2826.49 583.59 1138.88  370.45 2533.08 4140.48 239.50 525.04
 16.53  22.51  28.76 113.98  60.63  694.83  115.09 107.33  60.97  65.02

```

47.35	37.96	1.86	99.44	1431.35	742.50	313.14	1323.14	283.39	304.27
9156.00	8244.04	456.99	272.30	922.94	2467.37	630.79	1059.48	199.02	73.37
39.96	78.00	446.50	629.49	93.13	200.72	1022.41	231.86	7.24	29.03
114.32	19.79	59.02	47.96	277.15	77.65	334.22	129.80	1351.99	285.79
4041.65	991.86	123.65	781.52	442.26	1506.29	324.68	772.99	1131.39	218.30
199.69	211.37	99.74	141.06	135.66	44.53	106.91	665.01	787.58	1628.63
187.94	310.37	96.32	251.09	109.08	23.86	28.55	552.97	938.29	253.20
162.89	230.32	92.39	180.24	49.47	170.27	276.37	819.72	285.03	27.34
44.04	146.01	10.03	48.37	262.22	83.96	283.17	253.12	374.78	754.28
78.50	57.37	88.55	544.91	218.86	200.00	71.67	234.59	1240.47	298.62
39.02	104.45	82.97	7.56	19.92	21.44	63.93	2011.08	227.90	17.30
14.55	26.74	9.61	108.68	303.89	769.48	175.05	343.79	65.68	151.35
536.47	47.30	54.59	122.51	135.42	18.85	28.43	77.93	683.19	53.22
24.09	7.15	3.86	22.20	10.62	15.78	70.15	4143.41	853.19	275.55
44.20	33.86	58.14	137.07	72.38	203.50	345.09	402.68	99.39	45.35
295.03	590.44	103.28	489.02	956.97	42.07	104.75	194.18	1045.02	26.92
12.78	18.42	339.13	51.72	36.12	19.77	25.39	2088.97	2598.94	61.07
168.99	38.06	253.94	31.20	160.82	6.56	111.26	100.55	23.39	786.59
850.36	17496.75	2658.81	143.28	347.60	86.96	257.78	173.62	238.04	132.37
74.26	150.02	78.78	224.88	32.53	173.67	1740.90	2202.95	609.86	86.05
184.12	42.46	22.16	32.34	24.74	10.51	51.10	149.98	35.48	853.86
6795.83	6253.65	4763.25	414.02	182.97	176.82	21.85	43.10	299.93	27.00
845.78	380.93	570.16	328.61	19.48	23.82	559.24	66.92	243.06	40.42
414.54	27.24	99.13	7.91	47.42	15.49	54.80	72.64	480.50	92.68
1887.61	761.46	507.99	1600.16	31.19	37.92	32.55	7.47	22.23	120.02
241.86	252.77	72.50	26.10	89.02	184.19	29.82	52.12	77.50	60.23
179.21	194.78	126.84	10.91	36.13	158.55	31.24	138.65	386.05	159.93
617.35	530.21	221.49	245.37	249.95	172.97	10.92	1.77	29.82	582.15
101.10	337.21	859.55	40.86	433.32	604.31	45.72	33.98	86.89	31.41
47.92	52.24	30.21	34.62	94.32	119.86	45.85	153.58	638.16	1081.31
2405.42	1049.15	633.16	2192.48	392.79	35.50	114.36	31.99	242.57	136.67
204.13	619.48	208.86	266.47	333.94	152.59	219.04	302.74	37.98	57.95
20.46	63.71	9.87	46.18	179.69	177.72	344.59	142.14	711.15	536.63
140.90	744.46	1360.04	1331.90	45.85	30.65	52.68	739.80	771.83	929.80
1095.51	129.42	783.08	53.93	66.23	122.25	231.84	19.31	78.41	39.61
22.01	21.10	118.86	133.16	111.14	139.06	24.09	24.51	59.48	281.97
131.62	716.54	169.42	687.68	9.33	33.20	175.96	261.27	207.02	1378.09
1770.60	362.53	52.14	25.68	120.74	42.40	22.27	5.02	16.30	10.99
137.28	49.85	237.31	234.67	204.72	74.34	128.11	108.38	121.52	171.87
200.33	625.19	426.95	21.41	106.01	79.28	21.04	27.87	71.19	5851.96
1793.14	199.18	64.35	70.29	306.40	60.53	259.51	25.03	27.16	30.64
29.04	73.75	245.42	239.52	777.65	327.75	211.10	44.80	1897.99	2524.33
131.13	363.86	866.01	76.43	282.64	70.93	13.60	5.60	12.16	375.09
444.02	336.59	251.86	127.79	135.72	369.49	1576.43	51.29	61.10	51.87

72.99	79.42	215.00	336.21	1573.95	3683.41	942.37	1835.30	465.49	902.93
385.54	1182.45	393.38	89.94	825.54	225.76	40.57	13.97	20.13	105.21
683.34	93.49	38.17	613.17	43.73	116.02	158.70	31.55	260.44	29.89
175.28	340.63	321.66	214.59	939.24	797.00	9246.33	6155.59	727.82	753.69
181.21	821.59	4703.60	1877.85	479.43	24.97	6.74	3.38	12.79	33.18
5187.72	1763.92	272.15	146.77	400.93	114.01	169.24	374.64	234.79	92.81
422.80	477.60	731.28	533.90	1189.48	4691.27	10752.22	6028.14	3985.07	1210.24
984.63	345.95	1077.10	770.61	619.07	1181.16	65.87	12.12	63.25	142.21
16741.66	253.18	310.70	744.13	7438.70	320.63	286.77	41.33	75.27	503.15
277.60	1931.74	1563.87	3101.50	1535.10	702.93	112.13	2233.91	15818.56	1040.27
396.58	1437.00	952.26	425.01	1336.05	7320.17	215.86	22.13	135.16	244.01
2485.30	442.39	2061.78	291.07	313.05	24.81	38.18	63.50	380.63	1391.97
1147.32	1128.33	8862.41	35364.54	6595.62	278.79	647.08	3802.98	484.56	1313.51
784.04	732.09	1685.13	595.06	341.35	154.10	30.76	184.05	176.00	461.68
1297.12	634.94	3566.79	1962.70	936.04	154.23	568.44	224.54	737.38	1323.48
685.59	2021.66	2061.35	12681.90	2380.88	3754.69	4416.23	16678.46	238.01	1093.40
145.57	2387.87	1261.59	493.54	345.87	80.80	113.83	830.25	118.34	1715.37
254.09	198.43	852.63	1030.95	294.01	60.71	905.24	373.72	295.79	519.65
2954.31	4054.62	25517.08	1008.32	584.17	333.50	1169.17	7955.58	1384.00	730.80
179.41	1157.47	144.17	115.68	42.39	271.12	281.84	61.50	63.24	325.51
70.21	58.56	59.98	79.19	86.28	327.21	578.52	663.21	45.94	815.15
516.36	927.65	9846.26	4223.60	2257.15	56.84	5172.30	2999.49	819.23	2120.61
178.03	1161.95	821.28	109.35	1535.66	1208.17	14801.76	256.89	171.68	79.26
56.75	200.60	94.12	385.94	546.02	395.16	56.71	453.15	712.73	780.45
260.22	377.06	346.95	211.58	117.16	234.00	628.60	7766.82	676.42	144.41
38.40	309.54	398.36	3442.65	736.47	1674.56	2846.12	1412.44	501.29	81.24
52.80	207.01	433.07	955.64	31.19	72.72	202.07	76.89	423.87	187.39
221.18	54.88	82.38	72.19	79.90	128.13	92.15	521.15	159.54	74.53
90.62	49.85	2086.65	3914.64	3832.66	833.50	300.80	302.78	49.16	5.19
265.00	37.80	269.79	160.99	161.92	237.49	163.59	201.90	89.42	390.42
523.79	147.59	55.66	36.81	53.58	181.18	306.24	511.65	365.27	252.66
654.69	72.43	962.67	3461.99	315.17	11471.98	582.84	95.74	94.27	153.65
105.43	42.68	19.83	208.99	398.76	401.03	305.57	54.41	71.59	76.33
324.64	159.46	39.53	11.13	19.71	431.63	180.29	1596.45	929.67	44.92
49.69	308.77	1266.39	424.16	2158.90	2161.16	1326.55	51.44	134.75	571.28
348.72	146.16	237.50	572.10	808.01	64.70	218.30	433.00	118.25	47.23
37.13	85.06	53.60	13.38	22.75	128.56	418.13	447.21	224.08	64.51
57.73	72.68	105.21	635.85	1422.50	176.11	1707.99	151.36	151.32	832.62
1304.72	9864.50	887.83	1099.12	669.42	468.54	187.78	213.97	68.53	182.44
8.54	128.44	60.97	279.52	107.14	70.73	108.05	111.83	219.73	152.68
207.76	12.90	11.59	126.06	358.33	49.45	235.27	96.55	134.40	301.81

CC
 CC CONSTANT Y-PERMEABILITY FOR WHOLE RESERVOIR
 *---- PERMYC

1

CC

```

CC CONSTANT Z-PERMEABILITY FOR WHOLE RESERVOIR
*---- PERMZC
      1
CC
CC FLAG FOR CONSTANT/VARIABLE DEPTH, PRES., WATER SAT., INITIAL AQUEOUS COMPOSITIONS
*---- IDEPTH  IPRESS  ISWI  ICWI
      0      0      0      -1
CC
CC CONSTANT DEPTH (FT)
*---- D111
      0
CC
CC CONSTANT PRESSURE (PSIA)
*---- PRESS1
      14.7
CC
CC CONSTANT INITIAL WATER SATURATION
*---- SWI
      1
CC
CC BRINE SALINITY AND DIVALENT CATION CONCENTRATION (MEQ/ML)
*---- C50      C60
      0      0
CC
CC*****
CC*****
CC      PHYSICAL PROPERTY DATA
CC*****
CC*****
CC
CC OIL CONC. AT PLAIT POINT FOR TYPE II(+)AND TYPE II(-), CMC
*---- c2plc  c2prc  epsme  ihand
      0      1      0.0001  0
CC
CC flag indicating type of phase behavior parameters
*---- ifghbn
      0
CC SLOPE AND INTERCEPT OF BINODAL CURVE AT ZERO, OPT., AND 2XOPT SALINITY
CC FOR ALCOHOL 1
*---- hbns70  hbnc70  hbns71  hbnc71  hbns72  hbnc72
      0.131  0.1      0.191  0.026  0.363  0.028
CC SLOPE AND INTERCEPT OF BINODAL CURVE AT ZERO, OPT., AND 2XOPT SALINITY
CC FOR ALCOHOL 2
*---- hbns80  hbnc80  hbns81  hbnc81  hbns82  hbnc82
      0      0      0      0      0      0
CC
CC LOWER AND UPPER EFFECTIVE SALINITY FOR ALCOHOL 1 AND ALCOHOL 2
*---- csel7  cseu7  csel8  cseu8
      0.177  0.344  0      0
CC
CC THE CSE SLOPE PARAMETER FOR CALCIUM AND ALCOHOL 1 AND ALCOHOL 2
*---- beta6  beta7  beta8
      0.8      -2      0
CC
CC FLAG FOR ALCOHOL PART. MODEL AND PARTITION COEFFICIENTS
*---- ialc  opsk7o  opsk7s  opsk8o  opsk8s
      1      0      0      0      0
CC
CC NO. OF ITERATIONS, AND TOLERANCE
*---- nalmax  epsalc
      20      0.0001
CC
CC ALCOHOL 1 PARTITIONING PARAMETERS IF IALC=1
*---- akwc7  akws7  akm7  ak7  pt7
      4.671  1.79  48  35.31  0.222

```

```

CC
CC ALCOHOL 2 PARTITIONING PARAMETERS IF IALC=1
*---- akwc8      akws8      akm8      ak8      pt8
          0          0          0          0          0

CC
CC ift model flag
*---- ift
          0

CC
CC INTERFACIAL TENSION PARAMETERS
*---- g11      g12      g13      g21      g22      g23
          13     -14.8     0.007     13      -14.5     0.01

CC
CC LOG10 OF OIL/WATER INTERFACIAL TENSION
*---- xiftw
          1.3

CC
CC ORGANIC MASS TRANSFER FLAG
*---- imass icor
          0          0

CC
CC CAPILLARY DESATURATION PARAMETERS FOR PHASE 1, 2, AND 3
*---- itrapp      t11      t22      t33
          0         1865     59074     364.2

CC
CC FLAG FOR RELATIVE PERMEABILITY AND CAPILLARY PRESSURE MODEL
*---- iperm
          0

CC
CC FLAG FOR CONSTANT OR VARIABLE REL. PERM. PARAMETERS
*---- isrw      iprw      iew
          0          0          0

CC
CC CONSTANT RES. SATURATION OF PHASES 1,2,AND 3 AT LOW CAPILLARY NO.
*---- slrwc      s2rwc      s3rwc
          0          0          0

CC
CC CONSTANT ENDPOINT REL. PERM. OF PHASES 1,2,AND 3 AT LOW CAPILLARY NO.
*---- plrwc      p2rwc      p3rwc
          1          1          1

CC
CC CONSTANT REL. PERM. EXPONENT OF PHASES 1,2,AND 3 AT LOW CAPILLARY NO.
*---- elwc      e2wc      e3wc
          2          2          2

CC
CC WATER AND OIL VISCOSITY , RESERVOIR TEMPERATURE
*---- VIS1      VIS2      TSTAND
          1          1          0

CC
CC COMPOSITIONAL PHASE VISCOSITY PARAMETERS
*---- ALPHAV1    ALPHAV2    ALPHAV3    ALPHAV4    ALPHAV5
          4          5          0          0.9        0.7

CC
CC PARAMETERS TO CALCULATE POLYMER VISCOSITY AT ZERO SHEAR RATE
*---- AP1      AP2      AP3
          0          0          0

CC
CC PARAMETER TO COMPUTE CSEP,MIN. CSEP, AND SLOPE OF LOG VIS. VS. LOG CSEP
*---- BETAP    CSE1      SSLOPE
          10         0.01     0

CC
CC PARAMETER FOR SHEAR RATE DEPENDENCE OF POLYMER VISCOSITY
*---- GAMMAC    GAMHF    POWN
          0          13         1.645

CC
CC CC FLAG FOR POLYMER PARTITIONING, PERM. REDUCTION PARAMETERS

```

```

*---- IPOLYM      EPHI3      EPHI4      BRK      CRK
          0          1          1          0      0
CC
CC SPECIFIC WEIGHT FOR COMPONENTS 1,2,3,7,8 ,Coefficient of oil and GRAVITY FLAG
*---- DEN1      DEN2      DEN23      DEN3      DEN7      DEN8      IDEN
          0.4291      0.3491      0.3491      0.42      0.346      0          1
CC
CC FLAG FOR CHOICE OF UNITS ( 0:BOTTOMHOLE CONDITION , 1: STOCK TANK)
*----- ISTB
          0
CC
CC COMPRESSIBILITY FOR VOL. OCCUPYING COMPONENTS 1,2,3,7,AND 8
*---- COMPC(1)  COMPC(2)  COMPC(3)  COMPC(7)  COMPC(8)
          0          0          0          0          0
CC
CC CONSTANT OR VARIABLE PC PARAM., WATER-WET OR OIL-WET PC CURVE FLAG
*---- ICPC      IEPC      IOW
          0          0          0
CC
CC CAPILLARY PRESSURE PARAMETER, CPC0
*---- CPC0
          0
CC
CC CAPILLARY PRESSURE PARAMETER, EPC0
*---- EPC0
          2
CC
CC MOLECULAR DIFFUSION COEF. KCTH COMPONENT IN PHASE 1
*---- D(KC,1),KC=1,N
          0          0          0          0          0          0          0          0          0
CC
CC MOLECULAR DIFFUSION COEF. KCTH COMPONENT IN PHASE 2
*---- D(KC,2),KC=1,N
          0          0          0          0          0          0          0          0          0
CC
CC MOLECULAR DIFFUSION COEF. KCTH COMPONENT IN PHASE 3
*---- D(KC,3),KC=1,N
          0          0          0          0          0          0          0          0          0
CC
CC LONGITUDINAL AND TRANSVERSE DISPERSIVITY OF PHASE 1
*---- ALPHAL(1)      ALPHAT(1)
          0.66          0
CC
CC LONGITUDINAL AND TRANSVERSE DISPERSIVITY OF PHASE 2
*---- ALPHAL(2)      ALPHAT(2)
          0.66          0
CC
CC LONGITUDINAL AND TRANSVERSE DISPERSIVITY OF PHASE 3
*---- ALPHAL(3)      ALPHAT(3)
          0.66          0
CC
CC flag to specify organic adsorption calculation
*---- iadso
          0
CC
CC SURFACTANT AND POLYMER ADSORPTION PARAMETERS
*---- AD31      AD32      B3D      AD41      AD42      B4D      IADK      IADS1      FADS      REFK
          1          0.5      1000      0          0          100      0          0          0          0
CC
CC PARAMETERS FOR CATION EXCHANGE OF CLAY AND SURFACTANT
*---- QV      XKC      XKS      EQW
          0          0.25      0.2          419
CC
CC TRACER PARTITIONING COEFFICIENT
*---- TK(I),I=1,NTW + NTA
          0          0

```

```

CC
CC TRACER PARTITION COEFFICIENT SALINITY PARAMETER (1/MEQ/ML)
*---- TKS(I) ,I=1 TO NTW C5INI
      0          0          0
CC
CC RADIOACTIVE DECAY COEFFICIENT
*---- RDC(I),I=1,NTW + NTA
      0          0
CC
CC TRACER ADSORPTION PARAMETER
*---- RET(I),I=1,NTW + NTA
      0          0
CC
CC*****
CC
CC WELL DATA
CC
CC*****
CC
CC FLAG FOR SPECIFIED BOUNDARY AND ZONE IS MODELED
*---- IBOUND IZONE
      0          0
CC
CC TOTAL NUMBER OF WELLS, WELL RADIUS FLAG, FLAG FOR TIME OR COURANT NO.
*---- NWELL IRO ITIME NWREL
      2          2          0          2
CC
CC WELL ID,LOCATIONS,AND FLAG FOR SPECIFYING WELL TYPE, WELL RADIUS, SKIN
*---- IDW IW JW IFLAG RW SWELL IDIR IFIRST ILAST IPRF
      1          1          1          1          0.05          0          3          1          1          0
CC
CC WELL NAME
*---- WELNAM
INJECTOR
CC
CC ICHEK , MAX. AND MIN. ALLOWABLE BOTTOMHOLE PRESSURE AND RATE
*---- ICHEK PWFMIN PWFMAX QTMIN QTMAX
      0          0          5000          0          1000
CC
CC WELL ID,LOCATIONS,AND FLAG FOR SPECIFYING WELL TYPE, WELL RADIUS, SKIN
*---- IDW IW JW IFLAG RW SWELL IDIR IFIRST ILAST IPRF
      2          30          30          2          0.05          0          3          1          1          0
CC
CC WELL NAME
*---- WELNAM
PRODUCER
CC
CC ICHEK , MAX. AND MIN. ALLOWABLE BOTTOMHOLE PRESSURE AND RATE
*---- ICHEK PWFMIN PWFMAX QTMIN QTMAX
      0          0          5000          0          50000
CC
CC ID,INJ. RATE AND INJ. COMP. FOR RATE CONS. WELLS FOR EACH PHASE (L=1,3)
*---- ID QI (M,L) C (M,KC,L)
      1          375          1          0          0          0          0          0          0          0          0          0
      1          0          0          0          0          0          0          0          0          0          0          0
      1          0          0          0          0          0          0          0          0          0          0          0
CC
CC ID, BOTTOM HOLE PRESSURE FOR PRESSURE CONSTRAINT WELL (IFLAG=2 OR 3)
*---- ID PWF
      2          14.7
CC
CC CUM. INJ. TIME , AND INTERVALS (PV OR DAY) FOR WRITING TO OUTPUT FILES
*---- TINJ CUMPR1 CUMHI1 WRHPV WRPRF RSTC
      100          50          50          1          50          50
CC

```

```

CC TIME STEP SIZE FOR CONSTANT TIME STEP OPTION
*----- DT
      0.002

CC
CC FLAG FOR INDICATING BOUNDARY CHANGE
*----- IEMOD
      0

CC
CC IRO, ITIME, NEW FLAGS FOR ALL THE WELLS
*----- IRO   ITIME   IFLAG
      2       0       1       2

CC
CC NUMBER OF WELLS CHANGES IN LOCATION OR SKIN OR PWF
*----- NWEL1
      0

CC
CC NUMBER OF WELLS WITH RATE CHANGES, ID
*----- NWEL2   ID
      1         1

CC
CC ID, INJ. RATE AND INJ. COMP. FOR RATE CONS. WELLS FOR EACH PHASE (L=1,3)
*----- ID      QI (M,L)      C (M,KC,L)
      1         375          1      0      0      0      0      0      0      0      1      1
      1         0           0      0      0      0      0      0      0      0      0      0
      1         0           0      0      0      0      0      0      0      0      0      0

CC
CC CUM. INJ. TIME , AND INTERVALS (PV) FOR WRITING TO OUTPUT FILES
*----- TINJ    CUMPR1    CUMHI1    WRHPV    WRPRF    RSTC
      101.815    1.815    1.815    0.1     0.9     25

CC
CC
*-----
0.002
CC
CC FLAG FOR INDICATING BOUNDARY CHANGE
*----- IEMOD
      0

CC
CC IRO, ITIME, NEW FLAGS FOR ALL THE WELLS
*----- IRO   ITIME   IFLAG
      2       0       1       2

CC
CC NUMBER OF WELLS CHANGES IN LOCATION OR SKIN OR PWF
*----- NWEL1
      0

CC
CC NUMBER OF WELLS WITH RATE CHANGES, ID
*----- NWEL2   ID
      1         1

CC
CC ID, INJ. RATE AND INJ. COMP. FOR RATE CONS. WELLS FOR EACH PHASE (L=1,3)
*----- ID      QI (M,L)      C (M,KC,L)
      1         375          1      0      0      0      0      0      0      0      0      1
      1         0           0      0      0      0      0      0      0      0      0      0
      1         0           0      0      0      0      0      0      0      0      0      0

CC
CC CUM. INJ. TIME , AND INTERVALS (PV) FOR WRITING TO OUTPUT FILES
*----- TINJ    CUMPR1    CUMHI1    WRHPV    WRPRF    RSTC
      1400       65       70       1       40      150

CC
CC
*-----
0.002

```

Appendix B

• Tracer flood input file for Run KVTR48

```
-- Lawyer Canyon cycle 1 grainstone Simulations
-- Eclipse input file
--   * regular grid
--   * tracer simulation
--   * partitioning tracers added
--   * residual oil
--   * constant flow rate injection
-- *****
-- *****

NOECHO

RUNSPEC

TITLE
Lawyer Canyon, cycle 1

oil
water
field

-- Dimensions and options for tracers
TRACERS
  0 4 0 0 DIFF /
-- Dimensions for the partitioned tracer option
PARTTRAC
  4 4 2 /

start -- start date
1 'JAN' 2000 /

dimens -- nx ny nz
      300 30 30 /

eqldims -- ntequl ndprvd ndrxdv nttrvd nstrvd
         1 100 10 1 20 /

endscale -- directional reversible tables nodes
          'NODIR' 'REVERS' 2 5 /

tabdims -- ntsfun ntpvt nssfuns nppvts ntfips nrpvts
         1 1 101 12 1 12 /

welldims -- wells connect per well groups wells per group
          60 75 2 30 /

nstack -- linear solver stack size
100 /

-- Indicates that output files are unified
UNIFOUT

-- Indicates that input files are unified
UNIFIN

-- *****
-- ***** End RUNSPEC section *****
-- *****
-- ***** Begin GRID section *****
```

```

-- *****
GRID
-- PSEUDOS    -- Write binary files for input to Pseudo
-- RPTGRID
-- 'TRANX' 'TRANZ' 'NNC' 'PORV' /
DX
  270000*0.5 /
DY
  270000*5.0 /
DZ
  270000*0.5 /
BOX    - ix1 ix2 jy1 jy2 kz1 kz2
        1 300  1  30  1  1 /
TOPS
  9000*20.0 /
ENDBOX
PORO
  270000*0.15 /
PERMX
  270000*1.0 /
PERMY
  270000*1.0 /
PERMZ
  270000*1.0 /
INCLUDE - X transmissibility multipliers
'kvtr.tx' /
INCLUDE - Y transmissibility multipliers
'kvtr.ty' /
INCLUDE - Z transmissibility multipliers
'kvtr.tz' /
GRIDFILE
  2
/
INIT
-- *****
-- ***** End    GRID *****
-- *****
-- ***** Begin  PROPS *****
-- *****
PROPS
include - relative permeability
'swof.txt' /
swl    -- connate water end point saturations
270000*0.40 /

```

```

swcr      -- critical water end point saturations
270000*0.40 /

swu       -- maximum water end point saturations
270000*0.70 /

sowcr     -- critical oil-in-water end point saturations
270000*0.30 /

pvtw      -- pref fvf compressibility viscosity viscosibility
           1000 1.0          0.0          0.8          0.0 /

rock      -- reference pressure (psia) compressibility (1/psi)
           1000          1.0e-8 /

density   -- oil water gas (lb/ft^3)
           65.1  65.1  1e-4 /

pvdo      -- poil fvfo viso
           100  1.0001  3.2
           10000 1.0    3.2 /

-- Set up tracers
TRACER
  CT1 WAT '' OIL 1 /
  PT1 WAT '' OIL 1 /
  PT2 WAT '' OIL 1 /
  PT3 WAT '' OIL 1 /
/

-- Specifies the K(P) tables for the partitioned tracer option
TRACERKP
  3000. 0.
  4000. 0.
/
  3000. .5
  4000. .5
/
  3000. 1.
  4000. 1.
/
  3000. 2.
  4000. 2.
/

-- Requests flux limited transport for tracers
TRACTVD

rptprops
'swfn' 'pvtw' 'pvdo' 'rock' /

REGIONS  =====

-- Defines tracer partitioning regions
TRKPFCT1
  270000*1 /
TRKPFPT1
  270000*2 /
TRKPFPT2
  270000*3 /
TRKPFPT3
  270000*4 /

SOLUTION =====

PRESSURE
  270000*1500 /

```

```

SWAT
    270000*0.70
/

-- Initial tracer concentrations
TBLKFCT1
    270000*0.0 /
TBLKFPT1
    270000*0.0 /
TBLKFPT2
    270000*0.0 /
TBLKFPT3
    270000*0.0 /

RPTSOL
'FIP' 'SWAT' /

RPTRST -- Controls restart file
'BASIC=2' -- keep all restarts, output every FREQth reporting period
'FREQ=10'
'NORST=1' -- 0=full restart, 1=graphics only, 2= no well arrays
/

summary =====

tcpu

fwit
foip
fwip
fopt
fwpt
fwir
fwct

FTPCCT1
FTPCPT1
FTPCPT2
FTPCPT3

RUNSUM
SEPARATE

SCHEDULE =====

RPTSCHED
'wells'
'summary=2'
'welspecs'
/

RPTRST -- Controls restart file
'BASIC=2' -- keep all restarts, output every FREQth reporting period
'FREQ=10'
'NORST=1' -- 0=full restart, 1=graphics only, 2= no well arrays
/

WELSPECS -- Name      Group    I      J      Datum    Phase
-----
'Left1'   'L'      1      1      20.0     'OIL' /
'Rght30'  'R'     300    30     20.0     'WAT' /
/

```

```

COMPDAT  -- Name      I      J      K1     K2  Status   SatTab   Tfac    Dia    Kh
          'Left1'    1      1      1     30  'OPEN'    0        1000.0  0.0    0.0 /
          'Rght30' 300    30     1     30  'OPEN'    0        1000.0  0.0    0.0 /
          /

WCONINJE -- Name      Phase      Status      Mode   Qsurf  Qres  BHP    THP  VFP  VOL
          -----
          'Left1'  'WATER'  'OPEN'      'BHP'  1*     1*    4000   1*   1*   1* /
          /

WCONPROD -- NAME      Status      Mode      Qo  Qe  Qg  Ql  Qr  BHP
          -----
          'Rght30' 'OPEN'      'BHP'      1*  1*  1*  1*  1*  1000 /
          /

-- Sets tracer concentrations for injection wells
WTRACER
  Left1  CT1  1.0e9 /

  Left1  PT1  1.0e9 /

  Left1  PT2  1.0e9 /

  Left1  PT3  1.0e9 /

  /

MESSAGES  -- Message  Comment  Warning  Problem  Error  Bug  -- Message Type
           1*         1*         1*         1*         1*         1*  1* -- Print limits
           1*         1*         1*         5          1*         1*  1* -- Stop limits

           /

tuning  -- Numerical controls
--      Time stepping controls
--      tsinit   tsmx     tsmn     tsmchp  tsfmax
--      1*      1*      0.001   0.0015  1*
--      tsfmin   tsfconv  tfdiff   thrupt
--      1*      1*      1*      1*
           /
--      Time Truncation and convergence controls
--      trgtte   trgcnv   trgmbe   trglcv   xxxtte   xxxcnv
--      1*      1*      1*      1*      1*      1*
--      xxxmbe   xxxlcv   xxwfl   trgfip   trgsft
--      1*      1*      1*      1*      1*
           /
--      Newton and linear solver controls
--      newtmx   newtmn   litmax   litmin   mxwsit   mxpwit
--      1*      1*      250     1*      1*      1*
--      ddplim   ddslim   trgdpr   xxxdpr
--      1*      1*      1*      1*
           /

-- 0days
tstep
10*1. /
-- 10days

-- Sets tracer concentrations for injection wells
WTRACER
  Left1  CT1  0.0 /

```

```

Left1  PT1  0.0 /

Left1  PT2  0.0 /

Left1  PT3  0.0 /

/
tuning -- Numerical controls
-- Time stepping controls
--   tsinit  tsmx   tsmi   tsmchp  tsfmax
--   1*      1*    0.001  0.0015  1*
--   tsfmin  tsfcon  tfdiff  thrupt
--   1*      1*    1*     1*
/
-- Time Truncation and convergence controls
--   trgtte  trgcnv  trgmbe  trglcv  xxxtte  xxxcnv
--   1*      1*    1*     1*     1*     1*
--   xxxmbe  xxxlcv  xxwfl  trgfip  trgsft
--   1*      1*    1*     1*     1*
/
-- Newton and linear solver controls
--   newtmx  newtmn  litmax  litmin  mxwsit  mxpwit
--   1*      1*    250    1*     1*     1*
--   ddplim  ddslim  trgdpr  xxxdpr
--   1*      1*    1*     1*
/

tstep
40*1. /

tstep
50*1. /

-- 100days
tstep
50*1. /

tstep
50*1. /

-- 200days
tstep
30*10. /
-- 500days
tstep
50*10. /
tstep
40*100. /
-- 5000days

END

```

Appendix C

• Natural tracer simulation input file for Run TZ5857

```

CC*****
CC
CC   BRIEF DESCRIPTION OF DATA SET : UTCHEM d10.0
CC
CC*****
CC
CC   WATER FLOOD TEST, 5X5X5
CC
CC   LENGTH (FT) : 500.                PROCESS : WATER FLOOD
CC   THICKNESS (FT) : 50.              INJ. RATE (FT3/DAY) : 2807.5
CC   WIDTH (FT) : 500.                COORDINATES : CARTESIAN
CC   POROSITY : 0.01 FRACTURE, .24 MATRIX
CC   GRID BLOCKS : 5X5X5 FRACTURE, 4X4 MATRIX
CC   DATE : 10/25/01
CC
CC*****
CC
CC*****
CC
CC   RESERVOIR DESCRIPTION
CC
CC*****
CC
CC
CC   *---RUNNO
CC   TZ9857
CC
CC
CC   *---HEADER
CC   '5 oil compnents used; res. size increased' case // TD5610 base (5x5x1 gridblocks used)
CC   dual porosity model // 10x10x1 matrix/fracture
CC   5000-day water flood // no oil in fracture; residual oil in matrix; molecular diffusion
CC   coefficient corrected; flow rate increased; 5x5x5 gridblocks used
CC
CC   CC SIMULATION FLAGS
CC   *---- IMODE IMES IDISPC ICWM ICAP IREACT IBIO ICOORD ITREAC ITC IGAS IENG IDUAL ITEN
CC           1   4   3   0   0   0   0   0   1   0   0   0   0   1   0
CC
CC   CC NO. OF GRIDBLOCKS, FLAG SPECIFIES CONSTANT OR VARIABLE GRID SIZE, UNIT
CC   *----NX  NY  NZ  IDXYZ  IUNIT
CC           5   5   5   0      0
CC
CC   CC GRID BLOCK SIZE IN X, Y, & Z
CC   *----DX  DY  DZ
CC           100. 100. 10.
CC
CC   CC TOTAL NO. OF COMPONENTS, NO. OF TRACERS, NO. OF GEL COMPONENTS
CC   *----N  no NTw nta  NGc  ng  noth
CC           13  5  0  0  0  0  0
CC
CC   CC NAME OF THE SPECIES
CC   *---- SPNAME(IT) FOR IT=1,N
CC   water
CC   oil
CC   surf. (no)
CC   polymer (no)
CC   anion
CC   calcium
CC   alcohol (no)

```

```

gas (no)
oil1
oil2
oil3
oil4
oil5
CC
CC FLAG INDICATING IF THE COMPONENT IS INCLUDED IN CALCULATIONS OR NOT
*----ICF(KC) FOR KC=1,N
      1 1 0 0 1 1 0 0 1 1 1 1 1
CC
CC*****
CC
CC      OUTPUT OPTIONS
CC
CC*****
CC
CC
CC FLAG FOR PV OR DAYS TO PRINT OR TO STOP THE RUN
*---- ICUMTM  ISTOP  IOUTGMS
      0          0      0
CC
CC FLAG INDICATING IF THE PROFILE OF KCTH COMPONENT SHOULD BE WRITTEN
*----IPRFLG(KC),KC=1,N
      1 1 0 0 0 0 0 0 1 1 1 1 1
CC
CC FLAG FOR PRES,SAT.,TOTAL CONC.,TRACER CONC.,CAP.,GEL, ALKALINE PROFILES
*----IPPRES IPSAT IPCTOT IPBIO IPCAP IPGEL IPALK IPTEMP ipobs ipbr
      1      1      1      0      0      0      0      0      0      0
CC
CC FLAG FOR WRITING SEVERAL PROPERTIES TO UNIT 4 (PROFIL)
*----ICKL IVIS IPER ICNM ICSE IHYST IFOAM INONEQ
      1      0      0      1      1      0      0      0
CC
CC FLAG FOR WRITING SEVERAL PROPERTIES PROFIL
*----IADS IVEL IRKF IPHSE
      0      0      0      1
cc
cc
*----nobsm
      0
CC
CC*****
CC
CC      RESERVOIR PROPERTIES
CC
CC*****
CC
CC
CC MAX. SIMULATION TIME ( DAYS)
*---- TMAX
      10000.
CCaad
CC ROCK COMPRESSIBILITY (1/PSI), STAND. PRESSURE(PSIA)
*----COMPR PSTAND 3.D-06
      0.      14.7
CC
CC FLAGS INDICATING CONSTANT OR VARIABLE POROSITY, X,Y,AND Z PERMEABILITY
*----IPOR1 IPERMX IPERMY IPERMZ imod
      0      0      3      3      0
CC
CC POROSITY
*----POR
      .01
CC
CC X-PERMEABILITY (MILIDARCY)

```

```

*----PERMX(1)
      100.
CC
CC Y-PERMEABILITY
*----FACTY
      1.
CC
CC Z-PERMEABILITY
*----FACTZ
      .1
CC
CC FLAG FOR CONSTANT OR VARIABLE DEPTH, PRESSURE, WATER SATURATION
*----IDEPH  IPRESS  ISWI  ICWI
      0          0          0      -1
CC
CC CONSTANT DEPTH (FT)
*----D111
      0.
CC
CC CONSTANT PRESSURE (PSIA)
*----PRESS1
      14.7
CC
CC INITIAL WATER SATURATION
*----S
      0.999
cc
cc
*----icoi
      0
cc
cc
*----coil
      0.999993899
cc
cc
*----coi2
      0.000000001
cc
cc
*----coi3
      0.0000001
cc
cc
*----coi4
      0.000001
cc
cc
*----coi5
      0.000005
CC
CC CONSTANT CHLORIDE AND CALCIUM CONCENTRATIONS (MEQ/ML)
*----C50      C60  0.4      .003
      0.15      .003
CC
CC*****
CC
CC      PHYSICAL PROPERTY DATA
CC
CC*****
CC
CC OIL CONC. AT PLAIT POINT FOR TYPE II(+)AND TYPE II(-), CMC
*---- C2PLC  C2PRC  EPSME  ihand
      0.      1.      .0001  0
CC

```

```

CC FLAG INDICATING TYPE OF PHASE BEHAVIOR PARAMETERS
*---- IFGHBN
    0
CC SLOPE AND INTERCEPT OF BINODAL CURVE AT ZERO, OPT., AND 2XOPT SALINITY
CC FOR ALCOHOL 1
*----HBNS70 HBNC70 HBNS71 HBNC71 HBNS72 HBNC72
    0.131  .1  .191  .026  .363  .028
CC SLOPE AND INTERCEPT OF BINODAL CURVE AT ZERO, OPT., AND 2XOPT SALINITY
CC FOR ALCOHOL 2
*----HBNS80 HBNC80 HBNS81 HBNC81 HBNS82 HBNC82
    0.    0.    0.    0.    0.    0.
CC
CC LOWER AND UPPER EFFECTIVE SALINITY FOR ALCOHOL 1 AND ALCOHOL 2
*----CSEL7  CSEU7  CSEL8  CSEU8
    .177  .344  0.    0.
CC
CC THE CSE SLOPE PARAMETER FOR CALCIUM AND ALCOHOL 1 AND ALCOHOL 2
*----BETA6  BETA7  BETA8
    .8    -2.    0.
CC
CC FLAG FOR ALCOHOL PART. MODEL AND PARTITION COEFFICIENTS
*----IALC  OPSK7O  OPSK7S  OPSK8O  OPSK8S
    1    0.    0.    0.    0.
CC
CC NO. OF ITERATIONS, AND TOLERANCE
*----NALMAX  EPSALC
    20    .0001
CC
CC ALCOHOL 1 PARTITIONING PARAMETERS IF IALC=1
*----AKWC7  AKWS7  AKM7  AK7  PT7
    4.671  1.79  48.  35.31  .222
CC
CC ALCOHOL 2 PARTITIONING PARAMETERS IF IALC=1
*----AKWC8  AKWS8  AKM8  AK8  PT8
    0.    0.    0.    0.    0.
CC
CC
*---- IFT MODEL FLAG
    0
CC
CC INTERFACIAL TENSION PARAMETERS
*----G11  G12  G13  G21  G22  G23
    13.  -14.8  .007  13.  -14.5  .010
CC
CC LOG10 OF OIL/WATER INTERFACIAL TENSION
*----XIFTW
    1.3
CC
CC MASS TRANSFER FLAG
*----IMASS  ICOR
    1    0
CC
cc
*----wsol
    0.0  1000.  10.0  1.0  0.2
CC
CC CAPILLARY DESATURATION PARAMETERS FOR PHASE 1, 2, AND 3
*----ITRAP  T11  T22  T33
    0  1865.  59074  364.2
CC
CC RELATIVE PERM. FLAG (0:IMBIBITION COREY,1:FIRST DRAINAGE COREY)
*----IPERM
    0
CC
CC FLAG FOR CONSTANT OR VARIABLE REL. PERM. PARAMETERS
*----ISRW  IPRW  IEW

```

```

0      0      0
CC
CC RES. SATURATION OF PHASES 1, 2, & 3 AT LOW CAPILLARY NO.
*----S1RW   S2RW   S3RW
      0.099  0.00   0.10
CC
CC ENDPOINT REL. PERM. OF PHASES 1, 2, & 3 AT LOW CAPILLARY NO.
*----P1RW   P2RW   P3RW
      1.00   1.00   1.00
CC
CC REL. PERM. EXPONENT OF PHASES 1, 2, & 3 AT LOW CAPILLARY NO.
*----E1W    E2W    E3W
      1.46   2.15   1.00
CC
CC WATER AND OIL VISCOSITY , RESERVOIR TEMPERATURE
*----VIS1   VIS2   TEMPV
      .5     2.0    0.
cc
cc
*----iovis
      0
CC
CC VISCOSITY PARAMETERS
*----ALPHA1 ALPHA2 ALPHA3 ALPHA4 ALPHA5
      4.     5.     0.     .9     .7
CC
CC PARAMETERS TO CALCULATE POLYMER VISCOSITY AT ZERO SHEAR RATE
*----AP1    AP2    AP3
      52.    2430.  40000.
CC
CC PARAMETER TO COMPUTE CSEP,MIN. CSEP, AND SLOPE OF LOG VIS. VS. LOG CSEP
*----BETAP CSE1  SSLOPE
      2.     .01   .175
CC
CC PARAMETER FOR SHEAR RATE DEPENDENCE OF POLYMER VISCOSITY
*----GAMMAC GAMHF  POWN
      4.     20.    1.1
CC
CC FLAG FOR POLYMER PARTITIONING, PERM. REDUCTION PARAMETERS
*----IPOLYM EPHI3 EPHI4 BRK   CRK
      1     1.    1.    1000.  0.0186
CC
CC SPECIFIC WEIGHT FOR COMPONENTS 1,2,3,7,AND 8 , AND GRAVITY FLAG
*----DEN1   DEN2           DEN3 DEN7 DEN8 IDEN IODEN
      .433   .368           .42  .346  0.  2    0
CC
CC FLAG FOR CHOICE OF UNITS ( 0:BOTTOMHOLE CONDITION , 1: STOCK TANK)
*----ISTB
      0
CC
CC COMPRESSIBILITY FOR VOL. OCCUPYING COMPONENTS 1,2,3,7,AND 8
*----COMPC(1) COMPC(2) COMPC(3) COMPC(7) COMPC(8) 3.03D-6 1.0D-5
      0.     0.     0.     0.     0.
cc
cc
*----icompo
      0
CC
CC CONSTANT OR VARIABLE PC PARAM., WATER-WET OR OIL-WET PC CURVE FLAG
*----ICPC   IEPC  IOW
      0     0     0
CC
CC CAPILLARY PRESSURE PARAMETERS, CPC
*----CPC    28.28
      0.
CC

```

```

CC CAPILLARY PRESSURE PARAMETERS, EPC
*---- EPC
    6.67
CC
CC MOLECULAR DIFFUSIVITY OF KCTH COMPONENT IN PHASE 1 (D(KC),KC=1,N)
*----D(1) D(2) D(3) D(4) D(5) D(6) D(7) D(8)
    2*9.30e-4 0.    0.    0.    0.    0.    0.    5*9.30e-4
CC
CC MOLECULAR DIFFUSIVITY OF KCTH COMPONENT IN PHASE 2 (D(KC),KC=1,N)
*----D(1) D(2) D(3) D(4) D(5) D(6) D(7) D(8)
    0.    0.    0.    0.    0.    0.    0.    5*0.
CC
CC MOLECULAR DIFFUSIVITY OF KCTH COMPONENT IN PHASE 3 (D(KC),KC=1,N)
*----D(1) D(2) D(3) D(4) D(5) D(6) D(7) D(8)
    0.    0.    0.    0.    0.    0.    0.    5*0.
CC
CC LONGITUDINAL AND TRANSVERSE DISPERSIVITY OF PHASE 1
*----ALPHAL(1)    ALPHAT(1)
    3.0          0.3
CC
CC LONGITUDINAL AND TRANSVERSE DISPERSIVITY OF PHASE 2
*----ALPHAL(2)    ALPHAT(2)
    3.          0.3
CC
CC LONGITUDINAL AND TRANSVERSE DISPERSIVITY OF PHASE 3
*----ALPHAL(3)    ALPHAT(3)
    3.          0.3
CC
CC
*---- IADSO
    0
CC
CC SURFACTANT AND POLYMER ADSORPTION PARAMETERS
*----AD31 AD32 B3D  AD41  AD42  B4D  iadk  iads1  fads  refk
    1.    .5  1000.  0.7  0.    100.  0    0    0    500.
CC
CC PARAMETERS FOR CATION EXCHANGE OF CLAY AND SURFACTANT
*----QV    XKC  XKS  EQW
    0.0    .0   .0   419.
cc
aad  subgrid system
*----nsubh nsubv isub isubeq ishape shpfac isubld isealt isealb iseals mgrav
    1     1     0     0           0     0.    0     0     0     0     0     1
cc
cc  matrix dimensions
*----  xl     yl     zl
    1.0    1.0    1.0
cc
cc  flags of matrix porosity, saturation and permeability
*----  kph    kswi kxx  kky  kkz  kbndry
    0     0    0    0    0    0
cc
cc  matrix porosity distribution
*----  phic
    0.24
cc
cc  matrix swi
*----  swi
    0.699
cc
cc  matrix permx
*----  kx
    1.0
cc
cc  matrix permy
*----  ky

```

```

1.0
cc
cc matrix permz
*---- kz
0.1
cc
cc thickness fraction of subgrids in vertical direction
*---- vfracm 9*5.25E-03      2*4.53E-01      9*5.25E-03
1
CC (SUBGRID SECTION)
CC CAPILLARY DESATURATION PARAMETERS FOR PHASE 1, 2, AND 3
*----ITRAPM T11M T22M T33M
0 1865. 59074 364.2
CC
CC FLAG FOR CONSTANT OR VARIABLE REL. PERM. PARAMETERS
*----ISRWM IPRWM IEWM
0 0 0
CC
CC CONSTANT RES. SATURATION OF PHASES 1,2,AND 3 AT LOW CAPILLARY NO.
*----S1RWCM S2RWCM S3RWCM
.249 .30 .25
CC
CC CONSTANT ENDPOINT REL. PERM. OF PHASES 1,2,AND 3 AT LOW CAPILLARY NO.
*----P1RWM P2RWM P3RWM
.20 .92 .20
CC
CC CONSTANT REL. PERM. EXPONENT OF PHASES 1,2,AND 3 AT LOW CAPILLARY NO.
*----E1WM E2WM E3WM
1.18 1.80 1.18
CC
CC CONSTANT OR VARIABLE PC PARAM., WATER-WET OR OIL-WET PC CURVE FLAG
*----ICPCM IEPCM IOWM
0 0 0
CC
CC CAPILLARY PRESSURE PARAMETERS, CPC
*----CPCM 0.2902
0.2902
CC
CC CAPILLARY PRESSURE PARAMETERS, EPC
*---- EPCM
2.00
CC
CC MOLECULAR DIFFUSIVITY OF KCTH COMPONENT IN PHASE 1 (DM(KC),KC=1,N)
*----DM(1) DM(2) DM(3) DM(4) DM(5) DM(6) DM(7) DM(8)
2*9.30e-4 0. 0. 0. 0. 0 0. 5*9.30e-4
CC
CC MOLECULAR DIFFUSIVITY OF KCTH COMPONENT IN PHASE 2 (DM(KC),KC=1,N)
*----DM(1) DM(2) DM(3) DM(4) DM(5) DM(6) DM(7) DM(8)
0. 0. 0. 0. 0. 0. 0 0. 5*0.
CC
CC MOLECULAR DIFFUSIVITY OF KCTH COMPONENT IN PHASE 3 (DM(KC),KC=1,N)
*----DM(1) DM(2) DM(3) DM(4) DM(5) DM(6) DM(7) DM(8)
0. 0. 0. 0. 0. 0. 0 0. 5*0.
CC
CC LONGITUDINAL AND TRANSVERSE DISPERSIVITY OF PHASE 1
*----ALPHAL(1) ALPHAT(1)
3. 0.3
CC
CC LONGITUDINAL AND TRANSVERSE DISPERSIVITY OF PHASE 2
*----ALPHAL(2) ALPHAT(2)
3. 0.3
CC
CC LONGITUDINAL AND TRANSVERSE DISPERSIVITY OF PHASE 3
*----ALPHAL(3) ALPHAT(3)
3. 0.3
CC

```

```

CC*****
CC
CC WELL DATA
CC
CC*****
CC
CC
CC FLAG FOR RIGHT AND LEFT BOUNDARY
*---- IBOUND IZONE
      0      0
CC
CC TOTAL NUMBER OF WELLS, WELL RADIUS FLAG, FLAG FOR TIME OR COURANT NO.
*----NWELL IRO ITIME NWREL
      2      2      1      2
CC
CC WELL ID,LOCATIONS,AND FLAG FOR SPECIFYING WELL TYPE, WELL RADIUS, SKIN
*----IDW IW JW IFLAG RW SWELL IDIR IFIRST ILAST IPRF
      1  1  1  1 .0001 0. 3 1 5 0
CC
CC WELL NAME
*---- WELNAM
INJECTOR
CC
CC ICHEK, MAX. AND MIN. ALLOWABLE BOTTOMHOLE PRESSURE AND RATE
*----ICHEK PWFMIN PWFMAX QTMIN QTMAX
      0  0.0  5000.  0.0  1000.
CC
CC WELL ID,LOCATIONS,AND FLAG FOR SPECIFYING WELL TYPE, WELL RADIUS, SKIN
*----IDW IW JW IFLAG RW SWELL IDIR IFIRST ILAST IPRF
      2  5  5  2 .0001 0. 3 1 5 0
CC
CC WELL NAME
*---- WELNAM
PRODUCER
CC
CC ICHEK, MAX. AND MIN. ALLOWABLE BOTTOMHOLE PRESSURE AND RATE
*----ICHEK PWFMIN PWFMAX QTMIN QTMAX
      0  0.0  5000.  0.0  1000.
CC
CC id,INJ. RATE AND INJ. COMP. FOR RATE CONS. WELLS FOR EACH PHASE (L=1,3)
*----id QI(M,L) C(M,KC,L)
      1 2807.5 1.00 0. 0.00 0.0 0.15 0.003 0.00 0. 5*0.
      1 0. 8*0.0 5*0.
      1 0. 8*0.0 5*0.
CC
CC id, pressure (IFLAG=2)
*----id pwf
      2 14.7
CC
CC CUM. INJ. TIME , AND INTERVALS (PV OR DAY) FOR WRITING TO OUTPUT FILES
*----TINJ CUMPR1 CUMHI1 WRHPV WRPRF RSTC
      0.1 .010 .010 .001 .010 9999.
CC
CC FOR IMES=4 ,THE INI. TIME STEP,CONC. TOLERANCE,MAX.,MIN. TIME STEPS
*----DT DELC CNMAX CNMIN
      1.e-10 13*0.001 0.2 0.000002
CC
CC
*---- IBSMOD
      0
CC
CC IRO, ITIME, NEW FLAGS FOR ALL THE WELLS
*---- IRO ITIME IFLAG(1) IFLAG(2)
      2 1 1 2
CC
CC NUMBER OF WELLS CHANGES IN LOCATION OR SKIN OR PWF

```

```

*----NWEL1
  0
CC
CC NUMBER OF WELLS WITH RATE CHANGES, ID
*----NWEL2  ID
  0
CC
CC CUM. INJ. TIME , AND INTERVALS (PV OR DAY) FOR WRITING TO OUTPUT FILES
*----TINJ  CUMPR1  CUMHI1  WRHPV  WRPRF  RSTC
  1.0      .100    .100    .010   .100    9999.
CC
CC FOR IMES=4 ,THE INI. TIME STEP,CONC. TOLERANCE,MAX.,MIN. TIME STEPS
*----DT    DELC          CNMAX  CNMIN
  1.e-10  13*0.001      0.2    0.0000002
CC
CC
*----  IBMOD
  0
CC
CC IRO, ITIME, NEW FLAGS FOR ALL THE WELLS
*---- IRO ITIME IFLAG(1) IFLAG(2)
  2  1  1  2
CC
CC NUMBER OF WELLS CHANGES IN LOCATION OR SKIN OR PWF
*----NWEL1
  0
CC
CC NUMBER OF WELLS WITH RATE CHANGES, ID
*----NWEL2  ID
  0
CC
CC CUM. INJ. TIME , AND INTERVALS (PV OR DAY) FOR WRITING TO OUTPUT FILES
*----TINJ  CUMPR1  CUMHI1  WRHPV  WRPRF  RSTC
  10.0     1.00    1.00    .100   1.00    9999.
CC
CC FOR IMES=4 ,THE INI. TIME STEP,CONC. TOLERANCE,MAX.,MIN. TIME STEPS
*----DT    DELC          CNMAX  CNMIN
  1.e-10  13*0.001      0.2    0.0000002
CC
CC
*----  IBMOD
  0
CC
CC IRO, ITIME, NEW FLAGS FOR ALL THE WELLS
*---- IRO ITIME IFLAG(1) IFLAG(2)
  2  1  1  2
CC
CC NUMBER OF WELLS CHANGES IN LOCATION OR SKIN OR PWF
*----NWEL1
  0
CC
CC NUMBER OF WELLS WITH RATE CHANGES, ID
*----NWEL2  ID
  0
CC
CC CUM. INJ. TIME , AND INTERVALS (PV OR DAY) FOR WRITING TO OUTPUT FILES
*----TINJ  CUMPR1  CUMHI1  WRHPV  WRPRF  RSTC
  100.0    10.0    10.0    1.00   10.0    9999.
CC
CC FOR IMES=4 ,THE INI. TIME STEP,CONC. TOLERANCE,MAX.,MIN. TIME STEPS
*----DT    DELC          CNMAX  CNMIN
  1.e-10  13*0.001      0.2    0.0000002
CC
CC
*----  IBMOD
  0

```

```

CC
CC IRO, ITIME, NEW FLAGS FOR ALL THE WELLS
*---- IRO ITIME IFLAG(1) IFLAG(2)
      2   1   1   2
CC
CC NUMBER OF WELLS CHANGES IN LOCATION OR SKIN OR PWF
*----NWEL1
      0
CC
CC NUMBER OF WELLS WITH RATE CHANGES, ID
*----NWEL2   ID
      0
CC
CC CUM. INJ. TIME , AND INTERVALS (PV OR DAY) FOR WRITING TO OUTPUT FILES
*----TINJ   CUMPR1   CUMHI1   WRHPV   WRPRF   RSTC
      1000.0   100.     100.     10.0    100.     9999.
CC
CC FOR IMES=4 ,THE INI. TIME STEP,CONC. TOLERANCE,MAX.,MIN. TIME STEPS
*----DT     DELC           CNMAX   CNMIN
      1.e-10 13*0.001        0.2     0.0000002
CC
CC
*---- IBMOD
      0
CC
CC IRO, ITIME, NEW FLAGS FOR ALL THE WELLS
*---- IRO ITIME IFLAG(1) IFLAG(2)
      2   1   1   2
CC
CC NUMBER OF WELLS CHANGES IN LOCATION OR SKIN OR PWF
*----NWEL1
      0
CC
CC NUMBER OF WELLS WITH RATE CHANGES, ID
*----NWEL2   ID
      0
CC
CC CUM. INJ. TIME , AND INTERVALS (PV OR DAY) FOR WRITING TO OUTPUT FILES
*----TINJ   CUMPR1   CUMHI1   WRHPV   WRPRF   RSTC
      10000.0  1000.     1000.     100.    1000.     9999.
CC
CC FOR IMES=4 ,THE INI. TIME STEP,CONC. TOLERANCE,MAX.,MIN. TIME STEPS
*----DT     DELC           CNMAX   CNMIN
      1.e-10 13*0.001        0.2     0.0000002

```

Appendix D

• Inverse modeling program input files for Run INV04UP2#10

resinv.ans

```
Test Project: layered case /Job Title
tr.in /measurement (observational) data file
stream.dat /slfile (streamline input file names)
22 22 10 /nx ny nz (grid size)
11 /nwelp2 (number of wells to be integrated)
2 /i_peak (peak time match? 1/0 = y/n )
40 30 /LSQR: it_max1 it_max2
0.6 0.6 /LSQR: step1 step2
10 /# of initial iteration (arrival time inversion)
1e-4 1e+4 /perm_min perm_max
1.E-5 0.8 /poro_min poro_max
1.E-5 0.999 /satw_min satw_max
4840*100. /initial permeability
4840*0.20 /initial porosity
sw0.dat /initial water saturation
0 /window size for sensitivity smoothing, if i_inv_pr=1
1 /Ncoeffs number of parameter sets
0 /i_weight 0:user specified 1:auto 2:auto_iteration
2 /if i_weight!=0: idweight
0.90 /decfrac (fraction of decrease of weights)
0.0 0.03 0. 0.000 0.05 0. /Dam1, Hsm1, Vsm1, Dam2, Hsm2, Vsm2
```

stream.dat

```
input01.dat
input02.dat
input03.dat
input04.dat
input05.dat
output11.out
output12.out
output13.out
output14.out
output15.out
```

input01.dat

```
index
idxp idxa
1 1

nxyz
nx ny nz nphase
22 22 10 2

wprod
Maxp
11
nwelp
11
iwp jwp kwptop kwbot rwp rop qp i_constr pressure
22 22 1 1 0.25 10.0 0.001 0 2000. 1
```

22	22	2	2	0.25	10.0	0.001	0	2000.	2
22	22	3	3	0.25	10.0	0.001	0	2000.	3
22	22	4	4	0.25	10.0	0.001	0	2000.	4
22	22	5	5	0.25	10.0	0.001	0	2000.	5
22	22	6	6	0.25	10.0	0.001	0	2000.	6
22	22	7	7	0.25	10.0	0.001	0	2000.	7
22	22	8	8	0.25	10.0	0.001	0	2000.	8
22	22	9	9	0.25	10.0	0.001	0	2000.	9
22	22	10	10	0.25	10.0	0.001	0	2000.	10
22	22	1	10	0.25	10.0	0.001	1	14.7	11

```

winj
MaxI
1
nwelli
1
iwi jwi kwitop kwibot rwi   roi   qi   i_constraint Pressure i_miscible idwelli wellname
1      1      1      10     0.25  10   6000      0      500      0      1

```

```

solver
isolver
1

```

```

update
i_update
0                               /0->no pr_update 1->pr_update
i_pup_sol
0                               /0->analytical 1->numerical
update_time_total  n_pup  dtafrac delt_num  time_write
2004                0      0.25    2.0      500.0

```

```

infill
N_recurrent_total
0

```

```

tracer
itracer
1
ntrc
1
part diffus disp
  2 0.0 0.0 0.0 0.0 0.1 0.0

```

```

outfmt
dbg
1 1 0

```

inp02.dat

```

dx
22*30.

```

```

dy
22*30.

```

```

dz
4840*5.

```

```

depth
484*0
484*5
484*10
484*15
484*20

```

```

484*25
484*30
484*35
484*40
484*45

por
4840*0.20

permx
484*300
484*250
484*150
484*100
484*90
484*200
484*500
484*650
484*600
484*300

permy
ky=kx*1.0

permz
kz=kx*0.1

ngr
4840*1.0

pvm
index   pvminner  pvmouter
leftside
  0      1.    20.
rightside
  0      1.    20.
northside
  0      1.    20
southside
  0      1.     1.

rock
1
4840*1

sat
4840*0.75

relw
4840*1.0

```

inp03.dat

```

title
test run for 2d reservoir with residual oil

nline
number of streamlines
1000

time
number_steps  deltime  tcutoff
167    12      500

```

```
cinj
number of time steps for input of injection tracer
2
1 0 'Well 38 SCN
```

inpu04.dat

```
fluid
visw      Bo      Bw      viso
0.5      1.0      1.0      2.0
```

```
iterat
maximum no. of iteration
1
```

```
press
datum      dt.Pressure      woc
0      14.7      0.
```

```
omega
Acceleration parameter
0.3
```

```
trans
itrans      co      cw      rock cf      dt_init      dt_factor      tma
0      0.00001      0.0000002      1.0E-06      15      1.3      60
```

```
sides
index      pressure at boundary
left
0 150
right
0 150
north
0 150
south
0 150
top
0 150
bottom
0 150
```

```
twoph
itwo_ph,end_kro,end_krw,sor,swc,real_no,real_nw
1      1      1      0.5      0      2.15      1.46
```

```
miscible
visg      omega      sorm
0.0427      0.66      0.06
```

```
gravity
index_gravity      denw      deno      denmisc
0      62.4      53.0      10.0
```

inp05.dat

[blank file]

References

- Ağca, C. "Field Tracer Studies Using a Compositional Simulator," MS thesis. The University of Texas at Austin, 1987.
- Aldejain, A. A. "Implementation of a Dual Porosity Model in a Chemical Flooding Simulator," dissertation. The University of Texas at Austin, 1999.
- Allison, S. B., G. A. Pope, and K. Sepehrnoori. "Analysis of Field Tracers for Reservoir Description," *Journal of Petroleum Science and Engineering* Vol. 5 No. 2 (Feb. 1991): 173-186.
- Allison, S. B. "Analysis and Design of Field Tracers for Reservoir Description," dissertation. The University of Texas at Austin, 1998.
- Altinay, E. I. "Application of Inverse Modeling to Partitioning Interwell Tracer Tests for Estimating Oil Saturation," MS thesis. The University of Texas at Austin, 2005.
- Garmeh, G. "Simulation of Interwell Gas Tracer Test in Naturally Fractured Reservoirs," MS thesis. The University of Texas at Austin, 2005.
- Lalehrokh, F. "Simulating Water Tracer Test in Naturally Fractured Reservoirs Using Discrete Fracture and Dual Porosity Models," MS thesis. The University of Texas at Austin, 2005.
- Bear, J. *Hydraulics of Groundwater*. New York: McGraw-Hill International, 1979.
- Cheng, H., A. Datta-Gupta, and Z. He. "A Comparison of Travel-Time and Amplitude Matching for Field-Scale Production-Data Integration: Sensitivity, Nonlinearity, and Practical Implications," *SPE 84570, SPE Journal* Vol. 10 No. 1 (Mar. 2005): 75-90.
- Cooke, C. E., Jr. Method of Determining Fluid Saturations in Reservoirs. Patent 3,590,923. 6 July 1971.
- Deans, H. A. "Using Chemical Tracers to Measure Fractional Flow and Saturation In-Situ," *SPE 7076, Proc. of the Fifth Symposium on Improved Methods for Oil Recovery of the Society of Petroleum Engineers of AIME*, 1978.
- Deeds, N. E., G. A. Pope, and D. C. McKinney. "Vadose Zone Characterization at a Contaminated Field Site Using Partitioning Interwell Tracer Technology," *Environmental Science & Technology* Vol. 33 No. 16 (Aug. 1999): 2745-2751.
- Deeds, N. E. "Development and Evaluation of Partitioning Interwell Tracer Test Technology for Detection of Non-Aqueous Phase Liquids in Fractured Media," dissertation. The University of Texas at Austin, 1999.

Delshad, M., G. A. Pope, and K. Sepehrnoori. "A Compositional Simulator for Modeling Surfactant Enhanced Aquifer Remediation, 1 Formulation," *Journal of Contaminant Hydrology* Vol. 23 No. 4 (Aug. 1996): 303-327.

Dwarakanath, V., N. Deeds, and G. A. Pope. "Analysis of Partitioning Interwell Tracer Tests," *Environmental Science & Technology* Vol. 33 No. 21 (Sept. 1999): 3829-3836.

Himmelblau, D. M., and K. B. Bischoff. *Process Analysis and Simulation: Deterministic Systems*. New York: John Wiley & Sons, 1968.

Illiassov, P. A., and A. Datta-Gupta. "Field-Scale Characterization of Permeability and Saturation Distribution Using Partitioning Tracer Tests: The Ranger Field, Texas," SPE 81198, *SPE Journal* Vol. 7 No. 4 (Dec. 2002): 409-422.

Jayanti, S. "Modeling Tracers and Contaminant Flux in Heterogeneous Aquifers," dissertation. The University of Texas at Austin, 2003.

Jennings, J. W., Jr., S. C. Ruppel, and W. B. Ward. "Geostatistical Analysis of Permeability Data and Modeling of Fluid-Flow Effects in Carbonate Outcrops," SPE 65370, *SPE Reservoir Evaluation & Engineering* Vol. 3 No. 4 (Aug. 2000): 292-303.

Jennings, J. W., Jr., F. J. Lucia, and S.C. Ruppel. "3D Modeling of Stratigraphically Controlled Petrophysical Variability in the South Wasson Clear Fork Reservoir," SPE 77592, *Proc. of the SPE Annual Technical Conference and Exhibition*, 2002.

Jin, M., M. Delshad, V. Dwarakanath, D. C. McKinney, G. A. Pope, K. Sepehrnoori, and C. E. Tilburg. "Partitioning Tracer Test for Detection, Estimation, and Remediation Performance Assessment of Subsurface Nonaqueous Phase Liquids," *Water Resources Research* Vol. 31 No. 5 (May 1995): 1201-1211.

Lichtenberger, G. J. "Field Application of Interwell Tracers for Reservoir Characterization of Enhanced Oil Recovery Pilot Areas," SPE 21652, *Proc. of the Production Operations Symposium*, 1991.

Lucia, F. J., J. W. Jennings, Jr., and S. C. Ruppel. "South Wasson Clear Fork Reservoir Model: Outcrop to Subsurface via Rock-Fabric Method," SPE 70063, *Proc. of the SPE Permian Basin Oil and Gas Recovery Conference*, 2001.

Lucia, F. J., C. Kerans, and J. W. Jennings, Jr. "Carbonate Reservoir Characterization," SPE 82071, *Journal of Petroleum Technology* Vol. 55 No. 6 (June 2003): 70-72.

Maroongroge, V. "Modeling and Application of Tracers for Reservoir Characterization," dissertation. The University of Texas at Austin, 1994.

Oyerinde, A. S. "A Composite Tracer Analysis Approach to Reservoir Characterization," MS thesis. Texas A&M University, 2004.

“Volume II: Technical Documentation for UTCHEM-9.0 A Three-Dimensional Chemical Flood Simulator.” Reservoir Engineering Research Program, Center for Petroleum and Geosystems Engineering, The University of Texas at Austin.

Sinha, R. “Simulation of Natural and Partitioning Interwell Tracers to Calculate Saturation and Swept Volumes in Oil Reservoirs,” MS thesis. The University of Texas at Austin, 2003.

Tang, J. S. “Analytical Methods for Determining Residual Oil Saturation from Interwell Partitioning Tracer Tests,” Proc. of the Petroleum Society's Canadian International Petroleum Conference 2002, 2002.

Tang, J. S., and B. Harker. “Interwell Tracer Test to Determine Residual Oil Saturation in a Gas-Saturated Reservoir. Part I: Theory and Design,” The Journal of Canadian Petroleum Technology Vol. 30 No. 3 (May-June 1991): 76-85.

Tang, J. S., and B. Harker. “Interwell Tracer Test to Determine Residual Oil Saturation in a Gas-Saturated Reservoir. Part II: Field Applications,” The Journal of Canadian Petroleum Technology 30.4 (July-Aug. 1991): 34-42.

Tang, J. S. “Partitioning Tracers and In-Situ Fluid-Saturation Measurements,” SPE 22344, SPE Formation Evaluation Vol. 10 No. 1 (Mar. 1995): 33-39.

Tang, J. S., and P-X. Zhang. “Effect of Mobile Oil on Residual Oil Saturation Measurement by Interwell Tracing Method,” SPE 64627, Proc. of the SPE International Oil and Gas Conference and Exhibition, 2000.

Tang, J. S., and P-X. Zhang. “Extended Brigham Model for Residual Oil Saturation Measurement by Partitioning Tracer Tests,” SPE 84874, Proc. of the SPE International Improved Oil Recovery Conference in Asia Pacific, 2003.

Vasco, D. W., S. Yoon, and A. Datta-Gupta. “Integrating Dynamic Data into High-Resolution Reservoir Models Using Streamline-Based Analytic Sensitivity Coefficients,” SPE 49002, Proc. of the SPE Annual Technical Conference and Exhibition, 1998.

Wood, K. N., J. S. Tang, and R. J. Luckasavitch. “Interwell Residual Oil Saturation at Leduc Miscible Pilot,” SPE 20543, Proc. of the 65th Annual Technical Conference and Exhibition of the Society of Petroleum Engineers, 1990.

Wu, X., G. A. Pope, G. M. Shook, and S. Srinivasan. “A Method of Analyzing tracer Data to Calculate Swept Pore Volume and Thermal Breakthrough in Fractured Geothermal Reservoirs under Two-Phase Flow Conditions,” Proc. of Thirtieth Workshop on Geothermal Reservoir Engineering, 2005.

Yoon, S., I. Barman, A. Datta-Gupta, and G. A. Pope. “In-Situ Characterization of Residual NAPL Distribution Using Streamline-Based Inversion of Partitioning Tracer

Tests,” SPE 52729, Proc. of the 1999 SPE/EPA Exploration and Production Environmental Conference, 1999.

Zemel, B. *Tracers in the Oil Field*. Amsterdam, NL: Elsevier Science, 1995.

Vita

Kazuhiro Asakawa was born on August 24, 1971 in Tokyo, Japan, the son of Koji Asakawa and Yoshie Asakawa. After graduating from Tokyo Gakugei University Senior High School in Tokyo, Japan, in 1990, he entered Waseda University in Tokyo, Japan. He received the degree of Bachelor of Science in Engineering in 1995 and the degree of Master of Science in Engineering in 1997. In 1997 he entered the Department of Petroleum and Geosystems Engineering at the University of Texas at Austin in 1997.

Permanent address: 2-23-18 Kameari, Katsushika, Tokyo 125-0061, Japan

This dissertation was typed by the author.